ITERATIVE METHODS FOR ELECTROMAGNETIC IMAGING OF DIELECTRIC OBJECTS

by

Yonghua Liu

A thesis submitted to the Faculty of Graduate Studies of the University of Manitoba in partial fulfillment of the requirements for the degree of

DOCTOR OF PHILOSOPHY

Department of Electrical and Computer Engineering

University of Manitoba

Winnipeg, Manitoba, Canada.

ISBN 0-612-13307-9

Canada

Name _____

Dissertation Abstracts International is arranged by broad, general subject categories. Please select the one subject which most nearly describes the content of your dissertation. Enter the corresponding four-digit code in the spaces provided.

Electronics and Electrical
SUBJECT TERM

0544
SUBJECT CODE

UMI

Subject Categories

THE HUMANITIES AND SOCIAL SCIENCES

COMMUNICATIONS AND THE ARTS
Architecture 0729
Art History 0377
Cinema 0900
Dance 0378
Fine Arts 0357
Information Science 0723
Journalism 0391
Library Science 0399
Mass Communications 0708
Music 0413
Speech Communication 0459
Theater 0465

EDUCATION
General 0515
Administration 0514
Adult and Continuing 0516
Agricultural 0517
Art 0273
Bilingual and Multicultural 0282
Business 0688
Community College 0275
Curriculum and Instruction 0727
Early Childhood 0518
Elementary 0524
Finance 0277
Guidance and Counseling 0519
Health 0680
Higher 0745
History of 0520
Home Economics 0278
Industrial 0521
Language and Literature 0279
Mathematics 0280
Music 0522
Philosophy of 0998
Physical 0523
Psychology 0525
Reading 0535
Religious 0527
Sciences 0714
Secondary 0533
Social Sciences 0534
Sociology of 0340
Special 0529
Teacher Training 0530
Technology 0710
Tests and Measurements 0288
Vocational 0747

LANGUAGE, LITERATURE AND LINGUISTICS
Language
- General 0679
- Ancient 0289
- Linguistics 0290
- Modern 0291

Literature
- General 0401
- Classical 0294
- Comparative 0295
- Medieval 0297
- Modern 0298
- African 0316
- American 0591
- Asian 0305
- Canadian (English) 0352
- Canadian (French) 0355
- English 0593
- Germanic 0311
- Latin American 0312
- Middle Eastern 0315
- Romance 0313
- Slavic and East European 0314

PHILOSOPHY, RELIGION AND THEOLOGY
Philosophy 0422
Religion
- General 0318
- Biblical Studies 0321
- Clergy 0319
- History of 0320
- Philosophy of 0322

Theology 0469

SOCIAL SCIENCES
American Studies 0323
Anthropology
- Archaeology 0324
- Cultural 0326
- Physical 0327

Business Administration
- General 0310
- Accounting 0272
- Banking 0770
- Management 0454
- Marketing 0338

Canadian Studies 0385
Economics
- General 0501
- Agricultural 0503
- Commerce-Business 0505
- Finance 0508
- History 0509
- Labor 0510
- Theory 0511

Folklore 0358
Geography 0366
Gerontology 0351
History
- General 0578
- Ancient 0579
- Medieval 0581
- Modern 0582
- Black 0328
- African 0331
- Asia, Australia and Oceania 0332
- Canadian 0334
- European 0335
- Latin American 0336
- Middle Eastern 0333
- United States 0337

History of Science 0585
Law 0398
Political Science
- General 0615
- International Law and Relations 0616
- Public Administration 0617

Recreation 0814
Social Work 0452
Sociology
- General 0626
- Criminology and Penology 0627
- Demography 0938
- Ethnic and Racial Studies 0631
- Individual and Family Studies 0628
- Industrial and Labor Relations 0629
- Public and Social Welfare 0630
- Social Structure and Development 0700
- Theory and Methods 0344

Transportation 0709
Urban and Regional Planning 0999
Women's Studies 0453

THE SCIENCES AND ENGINEERING

BIOLOGICAL SCIENCES
Agriculture
- General 0473
- Agronomy 0285
- Animal Culture and Nutrition 0475
- Animal Pathology 0476
- Food Science and Technology 0359
- Forestry and Wildlife 0478
- Plant Culture 0479
- Plant Pathology 0480
- Plant Physiology 0817
- Range Management 0777
- Wood Technology 0746

Biology
- General 0306
- Anatomy 0287
- Biostatistics 0308
- Botany 0309
- Cell 0379
- Ecology 0329
- Entomology 0353
- Genetics 0369
- Limnology 0793
- Microbiology 0410
- Molecular 0307
- Neuroscience 0317
- Oceanography 0416
- Physiology 0433
- Radiation 0821
- Veterinary Science 0778
- Zoology 0472

Biophysics
- General 0786
- Medical 0760

EARTH SCIENCES
Biogeochemistry 0425
Geochemistry 0996
Geodesy 0370
Geology 0372
Geophysics 0373
Hydrology 0388
Mineralogy 0411
Paleobotany 0345
Paleoecology 0426
Paleontology 0418
Paleozoology 0985
Palynology 0427
Physical Geography 0368
Physical Oceanography 0415

HEALTH AND ENVIRONMENTAL SCIENCES
Environmental Sciences 0768
Health Sciences
- General 0566
- Audiology 0300
- Chemotherapy 0992
- Dentistry 0567
- Education 0350
- Hospital Management 0769
- Human Development 0758
- Immunology 0982
- Medicine and Surgery 0564
- Mental Health 0347
- Nursing 0569
- Nutrition 0570
- Obstetrics and Gynecology 0380
- Occupational Health and Therapy 0354
- Ophthalmology 0381
- Pathology 0571
- Pharmacology 0419
- Pharmacy 0572
- Physical Therapy 0382
- Public Health 0573
- Radiology 0574
- Recreation 0575
- Speech Pathology 0460
- Toxicology 0383

Home Economics 0386

PHYSICAL SCIENCES
Pure Sciences
Chemistry
- General 0485
- Agricultural 0749
- Analytical 0486
- Biochemistry 0487
- Inorganic 0488
- Nuclear 0738
- Organic 0490
- Pharmaceutical 0491
- Physical 0494
- Polymer 0495
- Radiation 0754

Mathematics 0405
Physics
- General 0605
- Acoustics 0986
- Astronomy and Astrophysics 0606
- Atmospheric Science 0608
- Atomic 0748
- Electronics and Electricity 0607
- Elementary Particles and High Energy 0798
- Fluid and Plasma 0759
- Molecular 0609
- Nuclear 0610
- Optics 0752
- Radiation 0756
- Solid State 0611

Statistics 0463

Applied Sciences
Applied Mechanics 0346
Computer Science 0984
Engineering
- General 0537
- Aerospace 0538
- Agricultural 0539
- Automotive 0540
- Biomedical 0541
- Chemical 0542
- Civil 0543
- Electronics and Electrical 0544
- Heat and Thermodynamics 0348
- Hydraulic 0545
- Industrial 0546
- Marine 0547
- Materials Science 0794
- Mechanical 0548
- Metallurgy 0743
- Mining 0551
- Nuclear 0552
- Packaging 0549
- Petroleum 0765
- Sanitary and Municipal 0554
- System Science 0790

Geotechnology 0428
Operations Research 0796
Plastics Technology 0795
Textile Technology 0994

PSYCHOLOGY
General 0621
Behavioral 0384
Clinical 0622
Developmental 0620
Experimental 0623
Industrial 0624
Personality 0625
Physiological 0989
Psychobiology 0349
Psychometrics 0632
Social 0451

ITERATIVE METHODS FOR ELECTROMAGNETIC IMAGING ON DIELECTRIC OBJECTS

BY

YONGHUA LIU

A Thesis submitted to the Faculty of Graduate Studies of the University of Manitoba in partial fulfillment of the requirements of the degree of

DOCTOR OF PHILOSOPHY

To my parents and my family

Abstract

In this thesis, electromagnetic imaging is investigated as an application of inverse scattering with particular attention to the iterative algorithms used for numerical analysis.

The techniques of equivalent current refinement, prediction–correction and adaptive algorithm transference are developed to fulfil the numerical reconstruction of dielectric objects. The imaging of lossless and lossy dielectric objects is investigated in two– and three–dimensional cases. The involved nonlinear ill–posed problems are solved by using these techniques along with the Born and the Newton iterative technique. It is shown that the application of these techniques improves the numerical convergence, stability and flexibility of the iterative method. An efficient and better object reconstruction is achieved.

As the result of an analysis about the computational errors in the total electric field inside objects, a procedure of equivalent current refinement is presented. It improves the iteration results and the convergence of the iterative process. Since the refinement is applied after each iteration, it is applicable for different iterative algorithms. The added computation time for using this technique is comparatively negligible.

A prediction–correction algorithm is presented in the further investigation of the numerical algorithm for electromagnetic imaging. The numerical stability and fast convergence is achieved by using the full information obtained in the iteration process to make a prediction of the object function for each iteration. In the prediction procedure, the prediction of the solution for a nonlinear ill–posed problem consists of a linear prediction for an ill–posed linear problem and a prediction for a nonlinear well–posed problem. It avoids the difficulty in the direct prediction of the solution for a nonlinear ill–posed problem. The selection of the data used for making the prediction prevent the divergence of an iterative process. The prediction–correction technique presented in this algorithm is applicable with different iterative algorithms such as the Born and the Newton iterative methods. Its effectiveness is illustrated through solving the problems of electromagnetic imaging of lossless

and lossy dielectric objects.

In order to cope with the variety of the objects in electromagnetic imaging, an adaptive algorithm is presented. This proposed algorithm optimizes the iterative process by choosing the better algorithm for each iteration. A decreasing ratio of error in the computed scattered field is used as the criterion for selecting the more suitable algorithm for each iteration. This criterion allows that the performances of algorithms are compared in an efficient way. Because of the combination of the different algorithms, the adaptive algorithm is more flexible to different objects and capable to deal with more complex objects.

Numerical tests are carried out by using these techniques for lossless and lossy dielectric objects. The cases for the presence of noise in measured data are also considered and computed. The results are presented and discussed.

Acknowledgements

The author wishes to express his sincere gratitude to his thesis advisor, Professor I.R. Ciric, for providing support and continuous encouragement through this work. His expert guidance and valuable suggestions are greatly appreciated.

The author is specially thankful to Professor E. Bridges and Professor D.W. Trim for helpful suggestions and serving in the advisory committee.

The author deeply appreciates the support, encouragement and helpful comments of Dr. Y. Lin, Dr. Z. Mu, Mr. J. Carrie, Mr. J. Roy, Mr. T. Judge, Mr. M. Qin and Mr. M. Ouda.

Financial support in the form of a research assistantship from the NSERC research grant of Professor Ciric, a graduate fellowship from the university of Manitoba, and a teaching assistantship from the Department of Electrical & Computer Engineering enabled the author to pursue his graduate studies. They are gratefully acknowledged.

The author wishes to convey his sincere thanks to his wife, Li, his son Yi and his daughter Linda. Without their understanding and support, the author could not finish his study.

Finally, the author wishes to have a special thanks to his parents. Their great love supports the author in the whole course of this work.

Table of Contents

List of Principle Symbols

μ_o	Permeability of free space
ϵ_o	Permittivity of free space
$\epsilon(\mathbf{r})$	Permittivity of the objects
$\epsilon_r(\mathbf{r})$	Relative permittivity of the objects
$\sigma(\mathbf{r})$	Conductivity of the objects
ω	Angular Frequency
λ	Wavelength in free space
$\mathbf{B}$	The known column vector used in the global matrix equation for inverse problem
c	Arbitrary constant
$[D]$	The matrix used in the global matrix equation for the inverse problem
$\mathbf{E}^i(\mathbf{r})$	External incident electric field
$\mathbf{E}^i$	The column vector of external incident electric field
$\mathbf{E}^i_l$	The column vector of external incident electric field for the l–th illumination
$\mathbf{E}^s(\mathbf{r})$	Scattered electric field
$\mathbf{E}^s$	The column vector of scattered electric field
$\mathbf{E}^s_l$	The column vector of scattered electric field for the l–th illumination
$\mathbf{E}^s_T$	The column vector consisting of all $\mathbf{E}^s_l$
$\mathbf{E}^t(\mathbf{r})$	Total electric field in the object
$\mathbf{E}^t$	The column vector of total electric field
$\mathbf{E}^t_l$	The column vector of the total electric field for the l–th illumination
$\mathbf{E}^t_{lp}$	The column vector of the predicted total electric field for the l–th illumination

$[E_l^t]$ The diagonal matrix consisting of the elements of $\mathbf{E}_l^t$

$[\tilde{E}_l^t]$ The computed $[E_l^t]$ from the solution of the direct problem

$\mathbf{E}_T^t$ The column vector consisting of all $\mathbf{E}_l^t$

$\mathbf{E}_{Tp}^t$ The column vector consisting of all $\mathbf{E}_{lp}^t$

$[E_T^t]$ The diagonal matrix consisting of the elements of $\mathbf{E}_T^t$

$\overline{\overline{\mathbf{G}}}(\mathbf{r}, \mathbf{r}')$ Dyadic Green's function defined in (2–20)

$[G^i]$ The matrix of the Green's function for the direct problem

$[G^o]$ The matrix of the Green's function for the inverse problem

$[G_l^o]$ The matrix of the Green's function associated with l–th illumination for the inverse problem

$[G_{x_p x_q}^{\ i}]$ Submatrices of the matrix $[G^i]$ for the three dimensional case

$[G_{x_p x_q}^{\ o}]$ Submatrices of the matrix $[G^o]$ for the three dimensional case

g Regularization parameter

$H_0^{(2)}$ Hankel function of the second kind and zero order

$\overline{\overline{\mathbf{I}}}$ Unit dyadic function

$[I]$ Unit matrix

$\mathbf{J}(\mathbf{r})$ Equivalent current induced in the object

$\mathbf{J}_1(\mathbf{r})$ Radiating equivalent current

$\mathbf{J'}_1(\mathbf{r})$ The highly oscillatory part of $\mathbf{J}_1(\mathbf{r})$

$\mathbf{J}_2(\mathbf{r})$ Nonradiating equivalent current

$\mathbf{J}$ The column vector of equivalent current induced in the object

$\mathbf{J}_1$ The column vector of radiating equivalent current

$\mathbf{J'}_1$ The column vector representing the highly oscillatory part of $\mathbf{J}_1$

$\mathbf{J}_2$	The column vector of nonradiating equivalent current
$\mathbf{J}_l$	The column vector of the equivalent current for the l–th illumination
$\mathbf{J}_{lp}$	The column vector of the predicted equivalent current for the l–th illumination
$\mathbf{J}_T$	The column vector consisting of all $\mathbf{J}_l$
$\mathbf{J}_{Tp}$	The column vector consisting of all $\mathbf{J}_{lp}$
N_m	Maximum number used in the adaptive algorithm
k	Wavenumber in free space
k_e	Wavenumber inside objects
$\mathbf{O}(\mathbf{r})$	Object function
$\mathbf{O}$	The column vector of the object function $\mathbf{O}(\mathbf{r})$
$\mathbf{O}_p$	The predicted $\mathbf{O}$
$[O]$	The diagonal matrix consisting of the elements of $\mathbf{O}$
$[\tilde{O}]$	The computed $[O]$ from the solution of the direct problem
P	Probability of a stochastic event
r	Relative least square error of reconstructed object function
R	Criterion for algorithm comparison
s	Relative least square error of the computed scattered field
$\mathbf{x}$	The column vector of weight coefficients for equivalent current prediction
$\hat{\mathbf{x}}_p$	Unit vectors of Cardison coordinate components
$\mathbf{X}$	The unknown column vector used in the global matrix equation for inverse problem
$[W]$	The matrix used for the determination of $\mathbf{x}$ in the equivalent current prediction
[0]	The matrix consisting zero elements

List of Figures

Chapter 1

Introduction

1.1 General

Electromagnetic imaging of dielectric objects belongs to the class of inverse problem. It is an important research field and has been attracting the interests of many scientific researchers. Its applications can be found in various engineering fields such as geophysics, radar, remote sensing and nondestructive diagnosis and are associated with different physical means such as transient or single frequency electromagnetic waves and static electric or magnetic fields. The earliest engineering application is found in geophysics, in which the information of geologic structure is determined by inversion of measured electromagnetic sounding data [1]. In industry, an application is nondestructive detection, although there are other nondestructive means for nondestructive detection such as ultrasound and x–ray detection. The different physical mechanisms of electromagnetic imaging make it a potentially attractive means for nondestructive detection [2–3]. Electromagnetic radar imaging is applied for underground object identification [4–5]. In remote sensing, synthesized aperture radar is used for geophysical exploration or weather monitoring [6]. In medical diagnostics, except acoustic tomography [7–8], inverse scattering methods are used in electric impedance tomography [9] and microwave tomography [10–13] to image human body and determine the electric parameters of tissues.

The analysis of electromagnetic imaging is different from the methods used in electromagnetic scattering or diffraction, although it requires the theory of electromagnetic scattering and diffraction. When an electromagnetic field of any type is incident upon an object, a scattered electric field is generated by the electric current induced in the object. The determination of the scattered electromagnetic field when the incident field as well as the electromagnetic properties of the object are known is called the direct problem of scattering or diffraction and is solved by using the

theory of scattering or diffraction. Electromagnetic imaging is an inverse problem. It requires the determination of the electric parameters of the object from given data of the scattered electric field.

The theory of inverse scattering has been investigated extensively by many authors and various inverse scattering formulae have been derived [14–19]. In theoretical discussion, although the uniqueness of the solution in inverse scattering has been discussed for a long times [14–16], this problem still remains to be settled [20]. In engineering problems, the main difficulty is that inverse scattering is an ill–posed problem and the numerical solution is very sensitive to small error caused by measurement and numerical computation [20–24]. In different disciplines and in different cases, the mathematical expressions of the inverse problem are presented in various forms and thus, the methods for inverse scattering have been developed in very different ways. On the other hand, since inverse scattering covers many different disciplines, many methods applied in electromagnetic imaging can be found from their counterparts in other disciplines and some of the methods in electromagnetic imaging are brought from other disciplines such as seismic exploration, imaging process, X–ray and acoustic tomography.

In electromagnetic imaging, objects to be imaged can be divided into two categories. One category consists of perfectly conducting objects and the other category consists of lossless or lossy dielectric objects. For a conducting object, electromagnetic imaging is used to determine its shape from its scattering of the incident signal and for a dielectric object, the distribution of electric parameters in an object must be determined. However, these two categories are not entirely separated. When the conductivity of a dielectric object is very high, it can be taken as a perfectly conducting object.

1.2 Inverse Scattering Methods for Object Reconstruction

In inverse scattering, the simplest case is one–dimensional inverse scattering. One of the methods for the one–dimensional case of inverse scattering of dielectric objects is impediography [25]. In this method, the well known Wentzel–Kramers–Brillouin (WKB) approximation is used

to simplify the equation into a simple integral expression for the impedance spatial distribution. Since the WKB approximation is a first order approximation of the solution for the wave equation, impediography is valid only for media with sufficiently small spatial variations, such that the magnitude of the reflection wave is of an order smaller than that of the transmission wave. Another method is the Gaupillaud method [26] which is based on the discrete analysis of wave scattering in a layered medium. The medium is divided into special layers in which the travel time in each layer is the same. The reflection and transmission coefficients in each layer is obtained by recurrence. For a layered medium, this method is exact. For a continuous medium, the approximation is better as the slab division becomes fine. Because it incorporates both first and higher order reflections, this method can handle the case of large impedance variations. In geophysics, the methods for the mapping of layered media from the reflection of pulsed RF signal have been developed [27–29]. In the seismic exploration industry, the technique of dynamic decomposition is routinely applied with considerable success [30]. However, weak scattering is assumed and they subject the same limitation as the one for the impediography method.

Since the concept of plane wave propagation used in the one–dimensional case does not hold for the two– and three– dimensional cases, the equivalent radiating current source is widely used. The methods for the two– and three–dimensional cases that have been proposed are various and many of them can be also found in other descriptions such as quantum physics, optical holography, x–ray tomography, acoustic tomography, radar image processing.

A possible approach to the problem in the two– and three–dimensional cases, the ray–based algebraic reconstruction technique(ART) has been discussed by many authors. This approach has been applied to microwave imaging [31], but the images are seriously faulted by inaccurate reconstruction. For example, solid cylinders of uniform loss are reconstructed as nearly tubular in cross section. Some experiments have been performed with water–loaded and coupled waveguide antennas with low contrast targets in transmission tomography. The reconstruction from the experimented data lacked acceptable accuracy because of the use of the assumption of straight line propagation. Some modifications of ART have been proposed [32–33]. These approaches

use numerical damping factors and weighting to ensure convergence of ART solutions in the presence of the noise modeling of departures from ray optics. In ART, a serious defect is that a single, linear ray path can not be reasonably assumed to connect the transmitter and receiver. Neither can a single curved ray path be assumed to connect the transmitter and receiver. Minor changes in launch angle of a ray have a dramatic effect upon the receiver site where the ray is terminated.

The inverse scattering method proposed by Bojarski [14],[33] is exact and does not share the limitations of the Born and Rytov approximations applied to the description of the total electric field. Bojarski deduced a description of the total electric field that makes no assumptions with respect to weak scattering. Also minor assumptions with respect to the uniqueness of the inversion are necessary. The source must be limited in extent and have finite energy. It is also assumed that all source components must radiate [34–35]. The numerical solution of the integral equation derived by Bojarski is ill–posed and the theory has not been widely applied to the electromagnetic imaging of dielectric objects [19].

Another method is Diffraction Tomography (DT) [10–13] and it has received a lot of attention in the past decade. The method is quite similar to the x–ray tomography. The object is illuminated by a set of plane waves. For each illumination, the forward scattered fields are sampled along a straight line (or a plane in three–dimensional cases). With Born or Rytov approximations, the distribution of the electric parameters in the object are assumed to be linearly related with the scattered field. The implementation of fast Fourier transformation(FFT) of the data supplies the value along an arc in the spectrum of the object. The radius of the arc is $2k_o$, where k_o is the wavenumber of the incident field in the surrounding medium. The Fourier spectrum space is filled by the arcs obtained from multiple illuminations. The object is recovered from the band–limited Fourier spectrum. Because the FFT is employed in this algorithm, the speed of data processing can be fast enough to make real time imaging possible. The bandwidth of the Fourier spectrum limits the resolution of reconstruction. DT is also subject to various limitations, such as the creation of artifacts due to diffraction effects of strong contrasts and the need for a large

amount of sampling. It has been shown that with Born approximation, the total phase difference in phase shift through the surrounding medium and through the target must be less than 90 degree for reasonable numerical accuracy [12],[36]. In the case of Rytov approximation, larger total phase shifts are admissible, but the phase shift per wavelength must be small. As an example, a 5% deviation in index of refraction in a cylinder only one wavelength in diameter will ruin the reconstruction. Therefore, DT is generally applied to weaker scatterers. Numerical simulation for the case of lossy media has been performed by Slaney *et al* [36]. Loss in either the surrounding media or the object introduces some problems in the sense of signal–to–noise ratio (especially for the the higher spatial frequencies), but it offers the advantage that multiple scattering effects are reduced [37]. Lossy media have a distinct advantage to the Born approximation in comparison to the Rytov approximation with respect to the range of variation in the complex index refraction over which reasonable numerical accuracy may be obtained.

The Method of Moments has also been used in the spectral domain by Lee, Kim *et al* [38–39]. Although they get satisfactory results, the calculation is done only for objects of weak contrasts with one–dimensional plate in two dimensional space. The measurement spectrum is also assumed to be ideal although practical measurement is discrete in space. The errors between the ideal continuous spectrum and the actual discrete spectrum obtained from the FFT of measurement data are difficult to eliminate. Different basis functions have been tested and modified basis functions are proposed to improve the numerical results. Numerical tests show that this method is very sensitive to noise and regularization has to be applied to stabilize the reconstruction.

Since the methods in the space domain can deal with high contrast dielectric objects, these methods have received more attention in recent years. Compared with the methods in the spectral domain, these methods also have the advantage that there are fewer limitations on the positions of the radiators and receivers. In these methods, Richmond's procedure [40] is widely applied for the discretization of the integral equations for the electromagnetic imaging. This is because this procedure is easy to implement and has good accuracy. The discretization of integral equations converts the integral equations to matrix equations. To the equivalent current induced in the ob-

ject, the inverse scattering problem is a linear problem because the scattered field is linear to the equivalent current. For the distribution of electric parameters in the object, the problem of determining the distribution from the scattered field is nonlinear because the distribution is not linear to the equivalent current. The Born or Rytov approximation can be applied to simplify the problem by making the relation linear, if the objects are weak scatters.

Ney *et al* [21], [41] proposed the method of pseudoinverse transformation to electromagnetic imaging. The equivalent current distribution is reconstructed by using the pseudoinverse transformation. The electric parameters are obtained from the reconstructed equivalent current. Pseudoinverse transformation is a very powerful method in dealing with ill–conditioned matrix equations. In this method, the solution obtained is not only a least square solution but also a solution with minimum norm. In the solution, the highly oscillatory nonradiating part in the equivalent current is eliminated and a filtered solution is obtained. Caorsi *et al* [21], [42–43] have applied this method in two– and three–dimensional electromagnetic imaging of dielectric objects. They discussed convergence, errors, measurement and illumination positions in this method and they introduce a threshold to circumvent the ill–conditioning difficulty. For single illumination, the nonradiating current discarded in pseudoinverse transformation is impossible to reconstruct, because no information about the nonradiating current can be obtained from the measured scattered field. However, for the multiple illumination case, the nonradiating equivalent current information for an individual illumination can be provided by other illuminations. This part can be determined from the information provided by the solution for other illuminations. The separated applications of pseudoinverse transformation for different illuminations make the nonradiating parts of equivalent currents for different illuminations unrecoverable. The equivalent currents obtained by pseudoinverse transformation are incompatible for a same permittivity distribution. Although Caorsi *et al*[43] has tried to solve the equivalent current distribution for different illuminations by using only one unified pseudoinverse transformation, the problem of recovering the information in the nonradiating current is still not solved.

Hagmann *et al* [44] and Weiyan *et al* [45] have solved this problem by inversion of the ma-

trices consisting of scattered fields or incident fields by using special receiving or illumination arrangements. Since there is no inversion of ill–conditioned matrices in their methods, the algorithms are numerically stable. In [44], the special illuminations make the column vectors representing the measured scattered fields for different illuminations linearly independent and the corresponding matrix is invertible. In [45], the special measurements are applied and the invertible matrix is the matrix consisting of the column vectors for all incident fields. Such special illumination or receiving arrangement requires that the transmitters and receivers have narrow beam widths. Although this requirement can be satisfied by an array with a large numerical aperture in the near field region, it may be difficult to realize in practice. In their numerical computation tests, the effect of noise is not counted in.

The iterative methods with regularization in the space domain have become popular in recent years. Wang and Chew proposed the Born iterative method in which the total electric field and the distribution of electric parameters are updated by solving the direct and inverse problem separately in each iteration [46]. When the computed electric field tends to the actual one, the computed distribution of the electric parameters (object function) tends to the actual one. Chew and Wang also proposed the distorted Born iterative method [47]. In this method, the Green's function for the computed distribution of the electric parameters is updated in each iteration. The distorted Born iterative method provides a faster convergence than the Born iterative method. On the other side, it is not as robust to the noise as the Born iterative method. Joachimowicz *et al* [23] applied a Newton iterative procedure with the Tikhonov regularization [24]. In their method, the first order variations of the expression of the equivalent current is applied. The regularization applied in these methods is not only to make the numerical calculation stable but also to filter out the noise coming from measurement. To optimize the regularization parameter, Joachimowicz *et al* proposed the determination of the regularization parameter by including the trace of the ill–conditioned matrix and the error in the computed scattered electric field in the regularization parameter [23].

Stochastic methods are another kind of iterative method. In these methods, either the iterative

process is considered as a random process or the distribution of the electric parameters of the object is considered as a random distribution. The methods derived from the probability and stochastic process theory are applied to solve the problems. A typical method is the Maximum Entropy method [48–50]. This method has been applied in various fields such as image processing, antenna design [51–52] and has a clear physical explanation. In the reconstruction of the equivalent current, the effect of noise in measured data is reduced by applying a constraint of maximizing the entropy of the equivalent current. Because the entropy function is a nonlinear function, the linear relation between the scattered fields and the equivalent current becomes complicated and the problem has to be solved by iterative methods. To avoid the iterative process being trapped at a local minimum, the simulate annealing iterative methods were applied in [53–54]. This kind of methods is based on random search of a better solution and the acceptance of results is determined by its probability function at each iteration step. It provides better results when no noise is added but the manner of random search makes the computation time quite large. The method of Markov random fields was proposed by Caorsi *et* a*l* [55] recently and it uses Markov random fields to model the distribution of the electric parameters. The *a priori* knowledge is used to construct the probability function of the distribution of the electric parameters. The simulate annealing algorithm is applied to carry out the reconstruction. Since the *a priori* knowledge of the object can be easily applied in the constructed probability distribution of Markov random fields, it can reconstruct the object from highly noised data using the Born approximation. However, in this method, a reasonable construction of the probability distribution is highly dependent on the knowledge of the object.

In the time domain, Tijhuis[56] proposed an iterative method to reconstruct a one–dimensional dielectric plate in the time domain. Moghaddam and Chew [57] proposed a method to solve a two–dimensional problem in the time domain. In their method, the time domain problem is transformed by using Fourier transformation. The integral equation obtained in time domain is transformed in a set of integral equations in spatial domain with different frequencies which are solved by Born–type iteration method. In the computation, the dielectric profile is assumed independent

of frequency. Batrakov and Zhuk [58] proposed an algorithm based on the Newton–Kantorovich iterative procedure and Tikhonov regularization for solving the two–dimensional inverse problem in the time domain. Within their work, a lot of calculations are given in explicit form, which significantly reduce the computer implementation and consequently make the algorithm suitable for real–time processing of the experimental data. However, their analysis requires the object to be a cylinder with the permittivity varying in the radial direction, which limits its application to complex objects. In another paper[59], they extend their work to the case of an object with arbitrary distribution of the permittivity. In this generalized solution, the calculations are not simplified as in their earlier paper. The advantage of the methods in time domain is that more information is available. At the same time, the computation cost is huge compared with the one in the space domain because the fields at different times, or its time spectrum, has to be calculated. Because the short–duration pulse is often used as the excitation in the application, the excitation signal covers a wide frequency range. At high frequencies, the conductivity and the permittivity of the object are generally functions of frequency, and the reconstruction of the electric parameters requires knowledge of the dispersion of the materials. This limits the application of electromagnetic imaging over wide frequency band. Therefore, in many applications such as underground object detection and biological imaging [60–64], radar techniques are used to image shape or reflection contrast, not the distribution of electric parameters of objects.

As a limiting case when the frequency is zero, electrical impedance tomography has also been investigated by many people. It utilizes the fact that static voltage applied to the regions of different conductivity conduct different current. From the current measurements, the impedance image of objects are reconstructed [65–66]. Different techniques have been proposed to suppress the effect of error in experiments and regularization is applied to stabilize the numerical solution.

1.3 Outline of Thesis Work

In this work, iterative methods are used to study the nonlinear ill–posed problem of electromagnetic imaging of dielectric objects in the spatial domain. By using the iterative methods, the nonlinear problem is converted into a sequence of linear problems and regularization is applied to overcome the difficulty inherent in the numerical stability of the inversion of the ill–conditioned matrices involved.

The purpose of this thesis is to present iterative techniques which can be used to more accurately, efficiently and flexibly solve the integral equations associated with electromagnetic imaging of dielectric objects.

The convergence, numerical stability and flexibility of different iterative algorithms are discussed and three techniques are presented to improve the performance of iterative methods. These techniques are compatible with each other. Therefore, they can be used in the same iterative process.

The first method is the equivalent current refinement. This technique is based on the consideration of the error in the computed total electric field at each iteration step and its application improves the iteration results with less computation cost. For different iterative algorithms such as the Born and Newton iterative methods, the mathematical expressions are different but the scattered field is a linear function of the product of total electric field inside the object and the object function or its first order variation. As a result, the deviation of the computed object function compensates the error in the computed total electric field when solving the inverse problem. The equivalent current refinement uses this compensation to achieve a better evaluation of the equivalent current. From this equivalent current, a better evaluation of the object function is obtained. The current refinement technique improves the numerical stability and convergence of the itera-

tive process. Since it is a post–treatment of the iteration results in each iteration, it may be used in different algorithms.

The second technique is the prediction–correction technique. In this technique, instead of using the newly computed object function, a predicted object function is used as the initial guess for the next iteration. In the prediction procedure, a set of results consisting of selected previous iteration results and newly obtained ones are used for making the prediction. The prediction consists of two steps. First, a predicted equivalent current is computed from a linear weighted combination of the equivalent currents obtained from the selected data. Those weight coefficients used in the equivalent current prediction are the solution of a minimization problem, in which the difference between the scattered electric field generated by the predicted equivalent current and measured data is minimized. Then, the predicted object function is computed from the predicted equivalent current. The next procedure is correction, in which the total electric field is obtained from the direct problem with the predicted object function and the object function from the inverse problem, which is a typical iteration of a general iterative algorithm. The advantage of making a prediction is that information obtained in the iterative process itself is fully used. Since better data are used for making the prediction, a better estimate of the object function can be obtained. Since the prediction is made from a set of selected data, the effect from individual data is reduced and the iterative process becomes numerically more stable. The selection of the data used for making prediction plays an important role in keeping the iteration process out of divergence. Even when the preceding iteration generates much poorer results, these results are only applied once and later they will be removed from of the set used for making prediction. If the equivalent current refinement can be taken as a simple prediction, the presented prediction technique is a further development of current refinement technique. This technique is a pre–treatment

of iteration and can be applied to different iterative algorithms.

The third technique is adaptive algorithm transference. This technique originates from the observation of the results in numerical simulation of electromagnetic imaging for different objects. It is found that the behavior of different algorithms are quite different in different situations and is related with the property of the permittivity distribution of the object under imaging. In the adaptive algorithm, the behavior of different iterative techniques are compared and the algorithm which has better performance than the other available algorithms is selected for the next iteration. To compare different algorithms, a decreasing ratio is introduced as the criterion for the algorithm comparison. This ratio is defined as the ratio of the error in the computed scattered electric fields to the measured data. Those fields are computed from the object functions used for iteration and obtained after iteration, respectively. Since the algorithm comparison is a complex problem, a maximum number for the continuous application of a single algorithm is introduced for more unbiased comparison. The setup of this number also has the effect of helping the solution escape from local minimums. This technique combines different iterative algorithms. Therefore, it optimizes the iterative process and makes the iterative algorithm more flexible to various objects. Numerical results show that it can deal with more complicated objects.

In chapter 2, the matrix formulation of the electrical integral equations for the direct and inverse problems are given. The discretization of the integral equations for the two–dimensional TM wave and three–dimensional problem is presented.

The problem of uniqueness and numerical stability of the solution of electromagnetic imaging, as an ill–posed problem, is discussed in chapter 3. As a powerful method to overcome the difficulties in the numerical stability and the uniqueness of the solution, regularization is discussed and various regularization techniques are presented. Noise representing the measurement error

and its effect on the numerical reconstruction of the object are discussed.

In chapter 4, the equivalent current refinement technique is presented. The effect of the computed electric field on numerical reconstruction is discussed and an improvement of the iterative methods is presented by introducing the equivalent current refinement technique. The numerical simulation results for different dielectric cylinders illuminated by multiple two–dimensional TM incident waves are presented. The results obtained by this technique associated with the Born and the Newton iterative methods are presented.

In chapter 5, the prediction–correction technique is discussed in detail. For a clear explanation of the idea, the mathematical formulation is carried out for the case of single illumination and then, extended to the case of multiple illuminations. The numerical results for the case of two–dimensional TM waves are presented. The numerical results for different examples by this method and other ones are compared.

The adaptive algorithm transference technique is presented in chapter 6. The behavior of different algorithms in different situations are compared by numerical tests. The different methods of comparing the performance of different algorithms in an iterative process are discussed and the decreasing ratio of the errors in the computed scattered field is introduced, which is used as the criterion for selecting the better algorithm for later iterations. The maximum iteration number is defined, after the discussion of imperfections in the criterion. To make a comparison, in numerical computation, a more complex object is considered.

In chapter 7, the three–dimensional case is considered. Although more electric field components have to be considered, the matrix equations can be expressed in the same form. The results of reconstruction by using different polarization components in the measured data are presented and discussed.

Finally, the conclusion of the study work in this thesis is drawn and future work is suggested in chapter 8.

Chapter 2

Integral Equations for Electromagnetic Imaging

2.1 Dyadic Green's Function

A dyadic function $\overline{\overline{\mathbf{A}}}(\mathbf{r}, \mathbf{r}')$ can be defined as

$$\overline{\overline{\mathbf{A}}}(\mathbf{r}, \mathbf{r}') = \mathbf{B}(\mathbf{r}, \mathbf{r}')\mathbf{C} \tag{2–1}$$

where $\mathbf{B}(\mathbf{r}, \mathbf{r}')$ and $\mathbf{C}$ are vectors. When $\overline{\overline{\mathbf{A}}}(\mathbf{r}, \mathbf{r}')$ acts on a vector,

$$\overline{\overline{\mathbf{A}}}(\mathbf{r}, \mathbf{r}') \cdot \mathbf{a} = \mathbf{B}(\mathbf{r}, \mathbf{r}')[\mathbf{C} \cdot \mathbf{a}] \tag{2–2}$$

The dyadic function linearly transforms a vector function into a new vector function and therefore, it plays a role similar to that played by a matrix in algebra. Since, in the analysis of electromagnetic fields, the transformation between two vectors is often encountered, the dyadic function is found to be very useful [67]. Considering the vector Green function $\mathbf{g}_x(\mathbf{r}, \mathbf{r}')$, $\mathbf{g}_y(\mathbf{r}, \mathbf{r}')$ and $\mathbf{g}_z(\mathbf{r}, \mathbf{r}')$ which represent the vector fields generated by a unit source vector at $\mathbf{r}'$ in directions $\mathbf{x}$, $\mathbf{y}$ and $\mathbf{z}$, respectively, a dyadic Green function is obtained from their linear combination

$$\overline{\overline{\mathbf{G}}}(\mathbf{r}, \mathbf{r}') = \mathbf{g}_x(\mathbf{r}, \mathbf{r}')\mathbf{x} + \mathbf{g}_y(\mathbf{r}, \mathbf{r}')\mathbf{y} + \mathbf{g}_z(\mathbf{r}, \mathbf{r}')\mathbf{z} \tag{2–3}$$

From it, the field $\mathbf{g}_a(\mathbf{r}, \mathbf{r}')$ generated by a unit source vector at $\mathbf{r}'$ in arbitrary direction $\mathbf{a}$ can be obtained $\mathbf{g}_a(\mathbf{r}, \mathbf{r}') = \overline{\overline{\mathbf{G}}}(\mathbf{r}, \mathbf{r}') \cdot \mathbf{a}$.

2.2 Electric Field Integral Equations

For time–harmonic excitation, where the fields vary in time according to $e^{j\omega t}$, the Maxwell's equations can be written as

$$\nabla \times \mathbf{E}(\mathbf{r}) = -j\omega\mu\mathbf{H}(\mathbf{r}) \tag{2–4}$$

$$\nabla \times \mathbf{H}(\mathbf{r}) = \mathbf{J}(\mathbf{r}) + (j\omega\epsilon(\mathbf{r}) + \sigma(\mathbf{r}))\mathbf{E}(\mathbf{r}) \tag{2–5}$$

In most cases, the magnetic permeability μ is a constant μ_o and the information of interest in electromagnetic imaging is the spatial distribution of the electric permittivity $\epsilon(\mathbf{r})$ and of the conductivity $\sigma(\mathbf{r})$. From (2–5) and the curl of (2–4), the expression for the Hemholtz vector wave equation for $\mathbf{E}(\mathbf{r})$ can be obtained

$$\nabla \times \nabla \times \mathbf{E}(\mathbf{r}) + j\omega\mu[j\omega\epsilon(\mathbf{r}) + \sigma((r)]\mathbf{E}(\mathbf{r}) = -j\omega\mu\mathbf{J}(\mathbf{r}) \ . \tag{2–6}$$

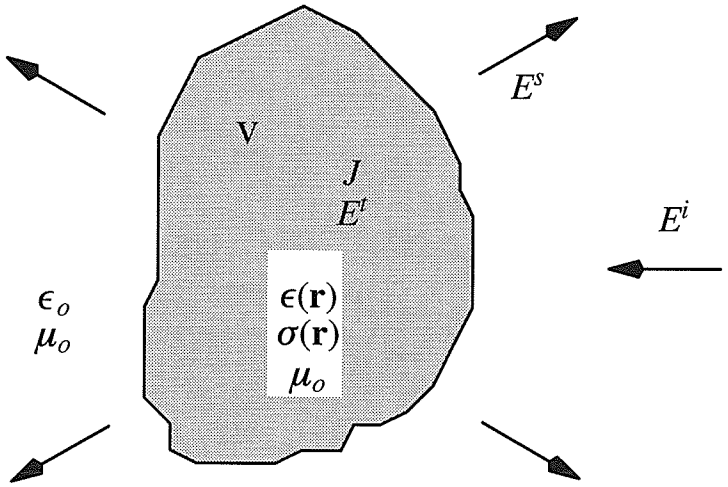

Fig. 2.1 : Illustration of electromagnetic scattering.

Consider a dielectric object with electric permittivity $\epsilon(\mathbf{r})$ and conductivity $\sigma(\mathbf{r})$ illuminated by an arbitrary electromagnetic field shown in Fig. 2.1. The electric field differential equation (2–6) outside the object can be written as

$$\nabla \times \nabla \times \mathbf{E}^t(\mathbf{r}) - k^2\mathbf{E}^t(\mathbf{r}) = 0 \qquad \mathbf{r} \notin V \tag{2–7}$$

where $k = \omega\sqrt{\epsilon_o\mu_o}$ is the wavenumber in free space with the permittivity ϵ_o and the permeabil-

ity μ_o in free space. $\mathbf{E}^t(\mathbf{r})$ represents the total electric field vector and is written as

$$\mathbf{E}^t(\mathbf{r}) = \mathbf{E}^i(\mathbf{r}) + \mathbf{E}^s(\mathbf{r}) \tag{2–8}$$

where $\mathbf{E}^i(\mathbf{r})$ and $\mathbf{E}^s(\mathbf{r})$ stand respectively for the incident and the scattered electric field vectors outside the object and satisfy (2–7) separately. Inside the object, the wavenumber becomes

$$k_e(\mathbf{r}) = \omega \sqrt{\epsilon(\mathbf{r})\ (1 + \frac{\sigma(\mathbf{r})}{j\omega\epsilon(\mathbf{r})})\mu_o}$$

$$= \omega \sqrt{\epsilon_o \mu_o \epsilon_r(\mathbf{r})} \tag{2–9}$$

where

$$\epsilon_r(\mathbf{r}) = \frac{\epsilon(\mathbf{r})}{\epsilon_o}(1 + \frac{\sigma(\mathbf{r})}{j\omega\epsilon(\mathbf{r})}) \tag{2–10}$$

and the differential equation for the electric field is

$$\nabla \times \nabla \times \mathbf{E}^t(\mathbf{r}) - k_e^2(\mathbf{r})\mathbf{E}^t(\mathbf{r}) = 0 \qquad \mathbf{r} \in V \tag{2–11}$$

which can be written as

$$\nabla \times \nabla \times \mathbf{E}^t(\mathbf{r}) - k^2\mathbf{E}^t(\mathbf{r}) = [k_e^2(\mathbf{r}) - k^2]\mathbf{E}^t(\mathbf{r}) \quad \mathbf{r} \in V \tag{2–12}$$

Since $\mathbf{E}^i(\mathbf{r})$ still satisfies (2–7), we can rewrite (2–12) with the help of (2–8) as

$$\nabla \times \nabla \times \mathbf{E}^s(\mathbf{r}) - k^2\mathbf{E}^s(\mathbf{r}) = [k_e^2(\mathbf{r}) - k^2]\mathbf{E}^t(\mathbf{r})$$

$$= -j\omega\mu\mathbf{J}(\mathbf{r}) \tag{2–13}$$

with an equivalent current called the polarization current, defined as

$$\mathbf{J}(\mathbf{r}) = j(\omega\mu)^{-1}[k_e^2(\mathbf{r}) - k^2]\mathbf{E}^t(\mathbf{r})$$

$$= \frac{jk^2}{\omega\mu} O(\mathbf{r})\mathbf{E}^t(\mathbf{r}) \tag{2–14}$$

where

$$O(\mathbf{r}) = \epsilon_r(\mathbf{r}) - 1 \tag{2–15}$$

is called the object function.

The solution of the total electric field inside the object with a known object function is called the direct problem and the electric field integral equation can be expressed as

$$\mathbf{E}^t(\mathbf{r}) = \int_v \overline{\overline{\mathbf{G}}}(\mathbf{r},\mathbf{r}') \cdot \mathbf{E}^t(\mathbf{r}')O(\mathbf{r}')\, d\mathbf{r}' + \mathbf{E}^i(\mathbf{r}) \tag{2–16}$$

The solution of the equivalent current or object function inside the object from the measured scattered electric field outside the object is called an inverse problem and the electric field integral equation can be expressed as

$$\mathbf{E}^s(\mathbf{r}) = \int_v \overline{\overline{\mathbf{G}}}(\mathbf{r},\mathbf{r}') \cdot \mathbf{J}(\mathbf{r}')\, d\mathbf{r}' \tag{2–17}$$

or

$$\mathbf{E}^s(\mathbf{r}) = \int_v \overline{\overline{\mathbf{G}}}(\mathbf{r},\mathbf{r}') \cdot \mathbf{E}^t(\mathbf{r}')O(\mathbf{r}')\, d\mathbf{r}' \tag{2–18}$$

In (2–17), to simplify the relation between the equivalent current and the object function, the equivalent current is normalized by the factor $\frac{jk^2}{\omega\mu}$ and the corresponding dyadic Green's function $\overline{\overline{\mathbf{G}}}(\mathbf{r},\mathbf{r}')$ satisfies the equation

$$\nabla \times \nabla \times \overline{\overline{\mathbf{G}}}(\mathbf{r},\mathbf{r}') - k^2\overline{\overline{\mathbf{G}}}(\mathbf{r},\mathbf{r}') = k^2\overline{\overline{\mathbf{I}}}\,\delta(\mathbf{r}-\mathbf{r}') \tag{2–19}$$

where $\overline{\overline{\mathbf{I}}} = \hat{\mathbf{x}}\hat{\mathbf{x}} + \hat{\mathbf{y}}\hat{\mathbf{y}} + \hat{\mathbf{z}}\hat{\mathbf{z}}$ is the unit dyadic function. In free space, the dyadic Green's function is defined as

$$\overline{\overline{\mathbf{G}}}(\mathbf{r},\mathbf{r}') = k^2 \begin{cases} \dfrac{-j}{4}H_0^{(2)}(k|\mathbf{r}-\mathbf{r}'|)\overline{\overline{\mathbf{I}}} & 2-D\ TM\ case \\ (\overline{\overline{\mathbf{I}}} + \dfrac{1}{k^2}\nabla\nabla\cdot)\left[\dfrac{-j}{4}H_0^{(2)}(k|\mathbf{r}-\mathbf{r}'|)\right] & 2-D\ TE\ case \\ (\overline{\overline{\mathbf{I}}} + \dfrac{1}{k^2}\nabla\nabla\cdot)\dfrac{e^{-jk|\mathbf{r}-\mathbf{r}'|}}{4\pi|\mathbf{r}-\mathbf{r}'|} & 3-D\ case \end{cases} \tag{2–20}$$

where $H_0^{(2)}$ is the Hankel function of the second kind and zero order.

2.3 Matrix Formulation of Discretized Electric Field Integral Equations

One of the most powerful numerical techniques for numerically solving an integral equation is the method of moments. It solves a linear operator equation by converting it to a system of linear equations. In the method of moments, the unknown quantity in the integrand such as the distribution of the equivalent current or the total electric field is expanded by a set of selected basis functions with unknown coefficients. Utilizing a set of testing functions, together with the evaluation of their moments, the integral equation is reduced to a system of linear equations. The unknown coefficients are determined by solving the corresponding matrix equation. By properly selecting the basis functions and testing functions, the computation in the discretization of the integral equation can be simplified greatly. The procedure proposed by Richmond [40] is widely used in solving the integral equations for the direct and inverse scattering problems. This procedure has the advantages of being convenient for numerical computation and having good accuracy.

2.3.1 Two–Dimensional TM Case

The electromagnetic scattering of a two–dimensional dielectric object by a TM incident wave can be simplified into a scalar integral equation. The electric field integral equation for the total electric field intensity is

$$E_z^t(x,y) + (jk^2/4)\int_s H_0^{(2)}(k\varrho)[\,\epsilon_r(x',y') - 1]E_z^t(x',y')ds' = E_z^i(x,y) \qquad (2\text{–}21)$$

where (x,y) and (x',y') are the Cartesian coordinates of the observation point and the source point, respectively, and

$$\varrho = \sqrt{(x-x')^2 + (y-y')^2} \qquad (2\text{–}22)$$

Using a point matching technique and a pulse function as the basis function, a system of discrete linear equations is obtained

$$\sum_{\substack{n=1 \\ n\neq m}}^{N} j\pi k a_j/2(\,\epsilon_n - 1)J_1(ka_n)H_0^{(2)}(k\varrho_{mn})E_n$$

$$+\left\{1+(\epsilon_m-1)(j/2)[\pi k a_m H_1^{(2)}(ka_m)-2j]\right\}E_m = E_m^i \quad m=1,2,\cdots,N \tag{2–23}$$

where

$$\varrho_{mn} = \sqrt{(x_m-x_n)^2+(y_m-y_n)^2} \tag{2–24}$$

For $n \neq m$, the matching point is not within the integrated region and the integration on the cell which the matching point is located in is approximated by the integral of the zero–order Hankel function over an equivalent circular region with the same area of the cell

$$(jk^2/4)\int_0^{2\pi}\int_0^{a_j} H_0^{(2)}(k\varrho)\varrho'\,d\varrho'\,d\phi'$$

$$= (j/2)\pi k a_n\ J_1(ka_n)H_0^{(2)}(k\varrho_{mn}) \qquad n \neq m$$

$$= (j/2)[\pi k a_m\ H_1^{(2)}(ka_m)-2j] \qquad n=m \tag{2–25}$$

Finally, the N equations in (2–23) can be written in a matrix form as

$$\mathbf{E}^i = ([I]-[G^i][O])\mathbf{E}^t \tag{2–26}$$

where $\mathbf{E}^t$, and $\mathbf{E}^i$ are the total electric field intensity and the incident electric field intensity, respectively. The elements of the matrix $[G^i]$ are defined as

$$G_{mn}^i = \begin{cases} (-j/2)\pi k a_n\ J_1(ka_n)H_0^{(2)}(k\varrho_{mn}) & n \neq m \\ (-j/2)[\pi k a_m\ H_1^{(2)}(ka_m)-2j] & n=m \end{cases} \tag{2–27}$$

and the diagonal matrix $[O]$ is obtained from the discretization of the object function.

For the inverse problem, the integral equation for the scattered electric field can be discretized as the matrix equation

$$\mathbf{E}^s = [G^o][O]\mathbf{E}^t = [G^o]\mathbf{J} \tag{2–28}$$

where $\mathbf{E}^s$ and $\mathbf{J}$ are the column vectors of the scattered electric field intensity and the equivalent current density, respectively. The elements of the matrix $[G^o]$ are defined as

$$G^{o}_{mn} = (-j/2)\pi k a_n \; J_1(k a_n) H_0^{(2)}(k\varrho_{mn}) \quad m = 1, 2, \cdots, M \;,\; n = 1, 2, \cdots, N \tag{2–29}$$

2.3.2 Three–Dimensional Case

The integral equation for the direct scattering problem can be expressed as

$$\mathbf{E}^t(\mathbf{r}) = \int_v \left[PV\overline{\overline{\mathbf{G}}}(\mathbf{r}, \mathbf{r}') - \frac{\overline{\overline{\mathbf{I}}}\delta(\mathbf{r} - \mathbf{r}')}{3j\omega\epsilon_o} \right] \mathbf{J}(\mathbf{r}')d\mathbf{r}' + \mathbf{E}^i(\mathbf{r}') \tag{2–30}$$

where PV stands for the principal value of the integral as defined by Van Bladel [68]. Implementing the integral of the delta function, (2–30) can be rewritten as

$$\left[1 + \frac{\epsilon_r(\mathbf{r}) - 1}{3} \right] \mathbf{E}^t(\mathbf{r}) - \int_v PV\overline{\overline{\mathbf{G}}}(\mathbf{r}, \mathbf{r}')\mathbf{J}(\mathbf{r}')d\mathbf{r}' = \mathbf{E}^i(\mathbf{r}') \tag{2–31}$$

For each scalar component x_p, the above equation may be expressed as

$$\left[1 + \frac{\epsilon_r(\mathbf{r}) - 1}{3} \right] E_{x_p}{}^t(\mathbf{r}) - PV \int_v [\epsilon_r(\mathbf{r}') - 1] \left[\sum_{q=1}^{3} G_{x_p x_q}(\mathbf{r}, \mathbf{r}') E_{x_q}(\mathbf{r}') \right] d\mathbf{r}' = E_{x_p}{}^i(\mathbf{r}') \tag{2–32}$$

where

$$G_{x_p x_q} = \delta_{pq} k^2 + \frac{\partial}{\partial x_p} \frac{\partial}{\partial x_q} \psi(\mathbf{x}_p, \mathbf{x}_q) \tag{2–33}$$

and

$$\psi(\mathbf{r}, \mathbf{r}') = \frac{\exp(-jk|\mathbf{r} - \mathbf{r}'|)}{4\pi|\mathbf{r} - \mathbf{r}'|} \tag{2–34}$$

By dividing the object into N cells and assuming that the distribution of the permittivity is constant in each cell, the moment method may be applied with a point matching technique and a pulse function as the basis function [69]. The equation for the m–th cell is

$$\left[1 + \frac{\epsilon_r(\mathbf{r}_m) - 1}{3} \right] E_{x_p}{}^t(\mathbf{r}_m) - \sum_{q=1}^{3} \sum_{n=1}^{N} E_{x_q}{}^t(\mathbf{r}_n)[\epsilon_r(\mathbf{r}_n) - 1] PV \int_{v_n} G_{x_p x_q}(\mathbf{r}_m, \mathbf{r}')d\mathbf{r}'$$

$$= E_{x_p}{}^i(\mathbf{r}_m) \tag{2–35}$$

where the equivalent current is expressed as

$$\mathbf{J} = \sum_{q=1}^{3}\sum_{n=1}^{N} E_{x_q}{}^{t}(\mathbf{r}_n)[\epsilon_r(\mathbf{r}_n) - 1]\hat{\mathbf{x}}_q \tag{2–36}$$

where $\hat{\mathbf{x}}_q$ are unit vectors of Cartesian coordinate components. The corresponding matrix equation is

$$\left\{\begin{bmatrix}[[I]\ [0]\ [0]]\\ [0]\ [I]\ [0]\\ [0]\ [0]\ [I]\end{bmatrix} - \begin{bmatrix}[G^i_{xx}]\ [G^i_{xy}]\ [G^i_{xz}]\\ [G^i_{yx}]\ [G^i_{yy}]\ [G^i_{yz}]\\ [G^i_{zx}]\ [G^i_{zy}]\ [G^i_{zz}]\end{bmatrix}\begin{bmatrix}[O]\ [0]\ [0]\\ [0]\ [O]\ [0]\\ [0]\ [0]\ [O]\end{bmatrix}\right\}\begin{bmatrix}\mathbf{E}^t_x\\ \mathbf{E}^t_y\\ \mathbf{E}^t_z\end{bmatrix} = \begin{bmatrix}\mathbf{E}^i_x\\ \mathbf{E}^i_y\\ \mathbf{E}^i_z\end{bmatrix} \tag{2–37}$$

The submatrices $[G^i_{x_px_q}]$ are $N \times N$ matrices and the the elements are defined by

$$(G^i_{x_px_q})_{mn} = \delta_{pq}\delta_{mn}\frac{-1}{3} + PV\int_{v_n} G_{x_px_q}(\mathbf{r}_m, \mathbf{r}')d\mathbf{r}' \tag{2–38}$$

For the off–diagonal elements of $[G^i_{x_px_q}]$, since there is no singularity in the Green's function when m is not equal to n, (2–38) is approximated as

$$\begin{aligned}(G^i_{x_px_q})_{mn} &= \int_{v_n} G_{x_px_q}(\mathbf{r}_m, \mathbf{r}')d\mathbf{r}'\\ &\approx \Delta v_n G_{x_px_q}(\mathbf{r}_m, \mathbf{r}_n) \qquad\qquad m \neq n\end{aligned} \tag{2–39}$$

In (2–39),

$$\begin{aligned}G_{x_px_q}(\mathbf{r}_m, \mathbf{r}_n) = \frac{k^3\exp(-j\alpha_{mn})}{4\pi\alpha^3_{mn}} \times\\ [(\alpha^2_{mn} - 1 - j\alpha_{mn})\delta_{pq} + \cos\theta_{x_p}{}^{mn}\cos\theta_{x_q}{}^{mn}(3 - \alpha^2_{mn} + 3j\alpha_{mn})]\end{aligned} \tag{2–40}$$

where

$$\alpha_{mn} = k\sqrt{\sum_{p=1}^{3}(x_p^m - x_p^n)^2}$$

$$\cos\theta_{x_p}{}^{mn} = \frac{(x_p{}^m - xp^n)}{|\mathbf{r}_m - \mathbf{r}_n|}$$

$$\cos\theta_{x_q}{}^{mn} = \frac{(x_q{}^m - xq^n)}{|\mathbf{r}_m - \mathbf{r}_n|} \tag{2–41}$$

For the diagonal elements of $[G^i_{x_p x_q}]$, after approximating v_n by a sphere of equal volume Δv_n centered at $\mathbf{r}_n$, we have

$$(G^i_{x_p x_q})_{nn} = \delta_{pq}\frac{-1}{3} + PV\int_{v_n} G_{x_p x_q}(\mathbf{r}_n, \mathbf{r}')d\mathbf{r}'$$

$$= \delta_{pq}\frac{-1}{3} + PV\int_{v_n} [\delta_{pq}k^2 + \frac{\partial^2}{\partial x_p{}'\partial x_q{}'}]\psi(\mathbf{r}_n, \mathbf{r}')d\mathbf{r}' \tag{2–42}$$

This integral can be determined analytically and the result is expressed as

$$(G^i_{x_p x_q})_{nn} = \delta_{pq}\frac{2}{3}[exp(-jka_n)(1+jka_n) - 1] - \delta_{pq}\frac{1}{3}$$

$$= \delta_{pq}[\frac{2}{3}\exp(-jka_n)(1+jka_n) - 1] \tag{2–43}$$

where

$$a_n = \left(\frac{3\Delta v_n}{4\pi}\right)^{1/3} \tag{2–44}$$

In the inverse problem, the electric field integral equation is expressed as

$$\mathbf{E}^s(\mathbf{r}) = \int_v \overline{\overline{\mathbf{G}}}(\mathbf{r}, \mathbf{r}')\mathbf{J}(\mathbf{r}')d\mathbf{r}' \tag{2–45}$$

The corresponding matrix equation obtained by applying the method of moments in (2–45) is expressed as

$$\begin{bmatrix} [G^o_{xx}] & [G^o_{xy}] & [G^o_{xz}] \\ [G^o_{yx}] & [G^o_{yy}] & [G^o_{yz}] \\ [G^o_{zx}] & [G^o_{zy}] & [G^o_{zz}] \end{bmatrix} \begin{bmatrix} [O]\mathbf{E}^t_x \\ [O]\mathbf{E}^t_y \\ [O]\mathbf{E}^t_z \end{bmatrix} = \begin{bmatrix} \mathbf{E}^s_x \\ \mathbf{E}^s_y \\ \mathbf{E}^s_z \end{bmatrix} \tag{2–46}$$

Since measurements are carried out outside the object ($|\mathbf{r} - \mathbf{r}'| \neq 0$), there is no singularity in the integrand. The principal value of the integral in (2–42) is zero and the expression for the matrix elements can be found as

$$(G^{o}_{x_p x_q})_{mn} = \int_{v_n} G_{x_p x_q}(\mathbf{r}_m, \mathbf{r}_n) d\mathbf{r}'$$

$$= \frac{k^3 \exp(-j\alpha_{mn})}{4\pi\alpha_{mn}^3} \times$$

$$[(\alpha_{mn}^2 - 1 - j\alpha_{mn})\delta_{pq} + \cos\theta_{x_p}{}^{mn} \cos\theta_{x_q}{}^{mn}(3 - \alpha_{mn}^2 + 3j\alpha_{mn})] \qquad (2\text{–}47)$$

In (2–46), each component at the measurement point is included in the expression. If only some of the components are measured, (2–46) can be simplified. For example, when only the x–component of the scattered electric field is considered, the corresponding matrix equation is

$$\left[\; [G^o_{xx}][G^o_{xy}][G^o_{xz}] \; \right] \begin{bmatrix} [O]\mathbf{E}^t_x \\ [O]\mathbf{E}^t_y \\ [O]\mathbf{E}^t_z \end{bmatrix} = \mathbf{E}^s_x \; . \qquad (2\text{–}48)$$

In the three–dimensional case, the equivalent current at each point inside the object has three independent polarization components and the scattered electric field at each receiving point also has three polarization components. For a discretization mesh of N elements, the size of the matrix equations for the direct scattering problems are $3N$ by $3N$ and the number of equations for the inverse problem is also larger than the number of measurement positions.

Chapter 3

Regularization of Ill–posed Problems

3.1 Introduction

In this chapter, we first discuss the uniqueness and the stability of the solution in electromagnetic imaging. This is because reconstruction of dielectric objects is an inverse scattering problem, which means the problem is often an ill–posed problem. Different from a well–posed problem, the uniqueness and stability of the solution are not guaranteed in an ill–posed problem. In this chapter, the uniqueness and stability of the solution of electromagnetic imaging, the associated 'nonradiating current' and the highly oscillated part in the radiating current are discussed from the points of view of mathematics and engineering practice. The noise coming from the errors in measurement also makes the solution deviate from the exact solution of the problem. To overcome these difficulties in solving an ill–posed problem with corrupted measured data, regularization has to be used. The application of regularization transforms an ill–posed problem into a well–posed problem. Associated with this transform, some information about the object is also lost. The regularization procedure can be obtained from many methods and different regularization techniques provide different solutions. In the third part of this chapter, various regularization techniques are discussed.

3.2 Uniqueness and Stability in Inverse Scattering

In mathematics, a problem is called well–posed [24] if the following three conditions are satisfied:

1) a solution can be found;

2) the solution is unique;

3) the solution is stable.

The problems that do not satisfy these three conditions are said to be ill–posed.

In electromagnetic imaging of dielectric objects, the following two integral equations

$$\mathbf{E}^t(\mathbf{r}) = \int_v \overline{\overline{\mathbf{G}}}(\mathbf{r}, \mathbf{r}')\mathbf{J}(\mathbf{r}')dv + \mathbf{E}^i(\mathbf{r}) \qquad \mathbf{r} \in v \tag{3–1}$$

and

$$\mathbf{E}^s(\mathbf{r}) = \int_v \overline{\overline{\mathbf{G}}}(\mathbf{r}, \mathbf{r}')\mathbf{J}(\mathbf{r}')dv \qquad \mathbf{r} \notin v \tag{3–2}$$

have to be solved, where the normalized equivalent current is

$$\mathbf{J}(\mathbf{r}) = \left[\frac{\epsilon(\mathbf{r})}{\epsilon_o}(1 + \frac{\sigma(\mathbf{r})}{j\omega\epsilon(\mathbf{r})}) - 1\right]\mathbf{E}^t(\mathbf{r}) \tag{3–3}$$

For the convenience of our discussion of physical meanings, we directly put the physical quantities in (3–3) instead of using the object function.

The uniqueness of the solution in electromagnetic imaging has been discussed for a long time. Here, it is divided in two parts:

1. if the ϵ, σ can be uniquely determined from the equivalent current.

2. if the equivalent current can be uniquely determined from the measured data.

Uniqueness of type 1 is not always achievable. For example, in the case of the object being a closed perfectly conducting shell filled with a dielectric medium shown in Fig. 3.1, the parameters inside the shell can never be determined regardless of the measurement or the illumination being used, because the field is always zero inside the shell. If this conducting shell is replaced by a thick shell of lossy material, then, the higher the conductivity of the shell, the more difficult

is the determination of the permittivity and conductivity distributions for the inner region.

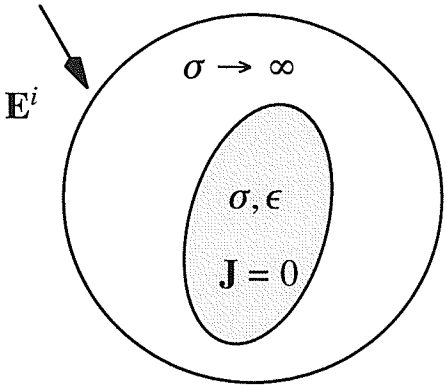

Fig. 3.1 : Uniqueness for a conducting shell filled with dielectric.

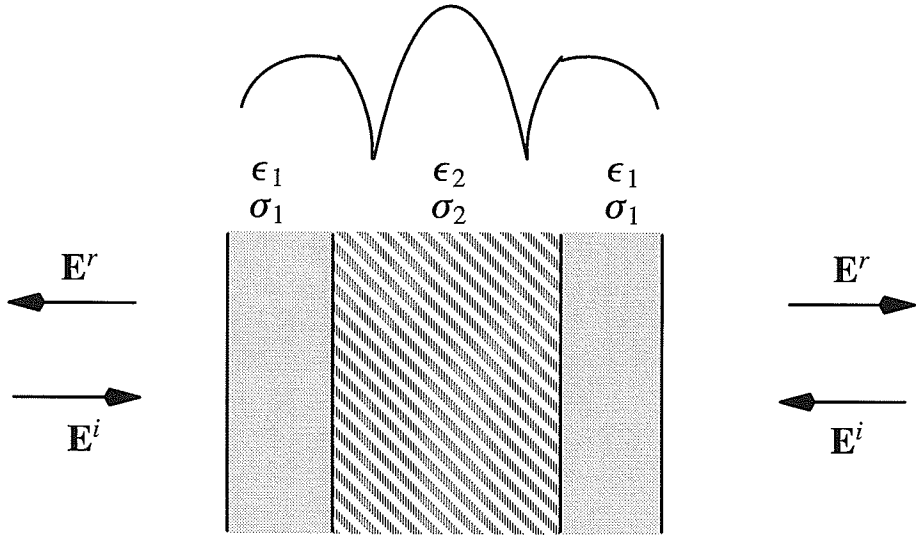

Fig. 3.2 : Uniqueness for a symmetric dielectric plate.

Another example is in the one–dimensional case as shown in Fig. 3.2. If the incident wave and the variation of the wave impedance of the layered medium is symmetric, there will be a standing

wave inside the medium and the impedance at points where the total field is zero can not be determined. This is because any change of the wave impedance at these points in the medium has no effect on the field distribution.

From these two examples, it can be seen that the nonuniqueness may come from the nature of the object to be imaged or the improper excitement. The effects of these factors greatly depend on the property of the individual problem and a generally theoretical discussion of it is quite difficult. In engineering applications, these effects have to be excluded or reduced by using *a priori* knowledge of the object and careful arrangement of the experiment. In the numerical analysis, what people are more concerned with is the second uniqueness.

The second form of uniqueness occurs if the equivalent current can be uniquely determined from the measured data. This uniqueness has been considered by many authors in the discussion of the inverse source problem [14–19]. This problem may be viewed from two aspects.

First, let us look at the electric field integral equation in (3–2). The solution of (3–2) for a known scattered field outside the object indicated by v can be divided in two parts,

$$\mathbf{J}(\mathbf{r}) = \mathbf{J}_1(\mathbf{r}) + \mathbf{J}_2(\mathbf{r}) \tag{3–4}$$

with

$$\mathbf{E}^s(\mathbf{r}) = \int_v \overline{\overline{\mathbf{G}}}(\mathbf{r}, \mathbf{r}')\mathbf{J}_1(\mathbf{r}')dv \tag{3–5}$$

$$0 = \int_v \overline{\overline{\mathbf{G}}}(\mathbf{r}, \mathbf{r}')\mathbf{J}_2(\mathbf{r}')dv \qquad \mathbf{r} \notin v \tag{3–6}$$

where $\mathbf{J}_1(\mathbf{r})$ generates the scattered field $\mathbf{E}^s(\mathbf{r})$ which is known outside the object and $\mathbf{J}_2(\mathbf{r})$ has no contribution to the part of $\mathbf{E}^s(\mathbf{r})$ outside the object. When the integral equation (3–2) has nontrivial solutions for the associated homogeneous integral equation, the solution of (3–2) is not unique. In this case, $\mathbf{J}_2(\mathbf{r}) \neq 0$ and the linear combination $\mathbf{J}_1(\mathbf{r}) + c\mathbf{J}_2(\mathbf{r})$ is the solution of equa-

tion (3–2), where c is an arbitrary constant. Therefore, even though $\mathbf{E}^s(\mathbf{r})$ outside the region v is known, the equivalent current inside v can not be uniquely determined. It has been proven by Porter and Devaney [17] that, in the scalar case, only the radiating source with minimum norm can be uniquely determined. The sources $\mathbf{J}_2(\mathbf{r})$ which generate the fields that vanish identically outside v are the solutions for the associated homogeneous integral equation (3–6) and are called nonradiating sources. Nonradiating components of a source are inherently unobservable from the field measurements performed outside the source region v. Detailed discussion of this uniqueness question can be found in [17–18].

The second aspect is the engineering consideration of uniqueness. In practical applications, the measurement is done at discrete points. Therefore, we only measure part of the information about the scattered electric field outside the object. The integral equations can be discretized in the form of matrix equations for discrete sampling positions. The matrix equation of the scattered electric field for the equivalent current distribution is

$$\mathbf{E}^s = [G^o]\mathbf{J} \tag{3–7}$$

where $\mathbf{E}^s$ and $\mathbf{J}$ are the column vectors representing the scattered field and the equivalent current distribution, and the matrix $[G^o]$ is obtained from the discretization of the Green's function. Similarly to the discussion of the integral equation of the scattered field, the column vector representing the actual radiating equivalent current can be divided into two parts: $\mathbf{J} = \mathbf{J}_1 + \mathbf{J}_2$, where $\mathbf{J}_1$ generates the scattered field $\mathbf{E}^s$, measured in the experiment,

$$\mathbf{E}^s = [G^o]\mathbf{J}_1 \tag{3–8}$$

and has the minimum norm and $\mathbf{J}_2$ generates the scattered field which just happens to be zero at precisely all of the receiving points.

$$0 = [G^o]\mathbf{J}_2 \tag{3–9}$$

Since the scattered field is measured at discrete points, the equivalent current $\mathbf{J}_2$ may actually generate a nonzero scattered field outside the object provided that the scattered field is zero at all receiving points. It can be seen that when (3–7) is an underdetermined matrix equation or $[G^o]$ is a singular square matrix, $\mathbf{J}_2$ is not a trivial solution of (3–9).

The nonuniqueness brought about here is different from the nonuniqueness in theoretical discussion. For example, in an inverse source problem, it has been proven in [13] that, for the scalar case, the source distribution has a minimum norm, i.e. $\mathbf{J}_2 = 0$, when the field outside the object is completely known. However, since the scattered field is measured at discrete points, the equivalent current $\mathbf{J}_2$ may actually radiate a scattered field which happens to be zero at precisely all the receiving points. The 'nonradiating' nature of the current $\mathbf{J}_2$ is only with respect to the measurement positions.

From an engineering point of view, Hanashy and Mittra [70], and also Fisher and Langenberg [71] have pointed out that, in many cases, the nonradiating sources are found to be highly oscillatory functions. In other words, the solution of the integral equation for the scattered field can be taken as a low–pass filtered solution. The contribution from the highly oscillatory part has been filtered by the integration operation. This is because the amplitude of the Green's function in (3–2) is inversely proportional to the distance between the source and the observation positions. When the observation position is far from the source, a small change is difficult to detect. Here, we can have a comparison between the inverse and direct scattering problem for the two–dimensional case with a TM incident wave. In a direct problem, the test (observation) points are inside the object. When the test point is near a line source of equivalent current, the argument of the Hankel function of the second kind and order zero in the Green's function tends to zero. When $x \to 0$, $H_2^{(0)}(x) \to 1/x$, the Hankel function becomes singular and the field becomes infinite.

Any small change in the amplitude of the source can be detected easily. In numerical analysis, because of this singularity in the integrand, the corresponding matrix $[G^i]$ is diagonally dominant and not ill–conditioned. In inverse scattering, the test or observation points are outside the object and the distance between the source and any observation point can never be zero. There is no singularity in the Green's function and the corresponding matrix $[G^o]$ generally is not diagonally dominant and may be quite ill–conditioned. The field outside the object is not as sensitive to small changes in the radiating current source as the field inside the object. Secondly, an integration operation is a summation operation and the contributions from different parts of a highly oscillated distribution in (3–2) may be eliminated by each other. For a simple example, consider the integral

$$\int G(x, x')a\sin(2\pi bx')dx \tag{3–10}$$

where a and b are constant. When $G(\ )$ is a nonsingular smooth function and b is a very large constant, the sine function is highly oscillatory which makes the value of the integral very small. Even when the amplitude a of this highly oscillatory function is large, provided b is large enough, the value of the integration is still very small. In inverse problems, the Green's function is a smooth function, because the observation points are located outside the object. Therefore the integration operation for the scattered field outside the object acts like a low–pass filter and suppresses the highly oscillatory part of the current distribution.

In solving (3–2), when some necessary information for reconstruction is hidden in $\mathbf{J}_2$, it is not possible to exactly recover the object from the measured scattered field as illustrated in Fig. 3–3. The existence of $\mathbf{J}_2$ makes the solution not unique.

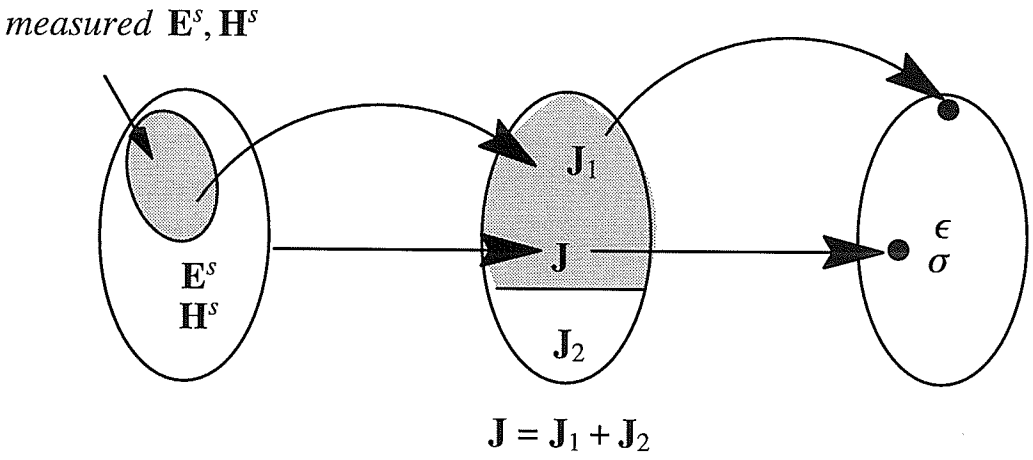

Fig. 3.3 : Reconstruction of an object without $\mathbf{J}_2$.

For the source $\mathbf{J}_1$, some part of $\mathbf{J}_1$ may have a very small contribution to the scattered field $\mathbf{E}^s$ and it can be considered as a linear combination of the eigenvectors of matrix $[G^o]$ with very small eigenvalues. We denote it as $\mathbf{J}'_1$. When $\mathbf{J}'_1$ exists and contains some necessary information for the object's recovery, there is another problem in that a small change in the error of measurement or numerical computation may cause a large change in $\mathbf{J}'_1$ and the associated change in permittivity and conductivity distribution of the object. In the above discussion, we have mentioned the equivalent current $\mathbf{J}_2$ may radiate the scattered field which just happen to be zero at all receiving points. We may take $\mathbf{J}'_1$ as a perturbation of this kind of source, which is illustrated in Fig. 3.4. Therefore, $\mathbf{J}'_1$ is also a highly oscillatory function. The existence of $\mathbf{J}'_1$ makes the solution unstable and very sensitive to any errors in numerical computation or measurement.

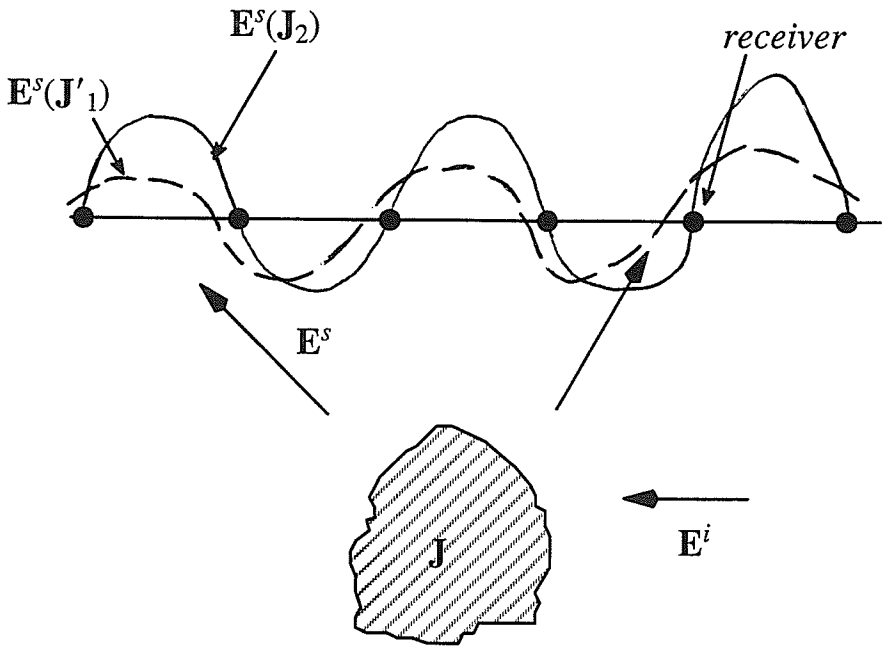

Fig. 3.4 : Scattered fields generated by $\mathbf{J}_2$ and $\mathbf{J}'_1$.

In numerical computation, the equivalent current is obtained by inverting the matrix $[G^o]$. Generally the matrix $[G^o]$ is not a square matrix and cannot be inverted directly. Its important solution is its least square solution and is related with the inverse of the matrix $[G^o]^H[G^o]$ where H stands for the conjugate transpose of a complex matrix. The existence of $\mathbf{J}_2$ or $\mathbf{J}'_1$ makes the matrix $[G^o]$ or $[G^o]^H[G^o]$ either singular or near singular. The nonradiating current $\mathbf{J}_2$ consists of the eigenvectors of $[G^o]$ or $[G^o]^H[G^o]$ which have zero eigenvalue. The equivalent current $\mathbf{J}'_1$ consists of the eigenvectors of $[G^o]$ or $[G^o]^H[G^o]$ with small eigenvalues. The numerical stability of inverting $[G^o]$ or $[G^o]^H[G^o]$ can be measured by its condition number. The condition number of a square matrix is defined as [72]

$$\gamma([A]) = \max \frac{\| [A]\mathbf{u} \|}{\| [A]\mathbf{v} \|} \tag{3–11}$$

where $\| \mathbf{u} \| = 1$ and $\| \mathbf{v} \| = 1$. This number has a simple interpretation. If $\lambda_1, \lambda_2, \ldots \lambda_n$ are the eigenvalues of $[A]$ arranged so that $|\lambda_1| \geq |\lambda_2| \geq \cdots \geq |\lambda_n|$, the condition number is the absolute value of the ratio of the maximum eigenvalue to the minimum eigenvalue

$$\gamma([A]) = |\frac{\lambda_1}{\lambda_n}| \tag{3–12}$$

When the condition number of a matrix is large, the numerical computation of its inverse is more unstable.

In the solution of (3–7), $\mathbf{J}_2$ and $\mathbf{J}'_1$ are closely related to the condition number of $[G^o]$ or $[G^o]^H[G^o]$. The infinite condition or large number of $[G^o]$ or $[G^o]^H[G^o]$ means that $\mathbf{J}_2$ or $\mathbf{J}'_1$ exists. The information about $\mathbf{J}_2$ can not be obtained and the information about $\mathbf{J}'_1$ is difficult to obtain from the solution of (3–7) by inverting $[G^o]$ or $[G^o]^H[G^o]$.

From the above discussion, the 'nonradiating' currents $\mathbf{J}_2$ and $\mathbf{J}'_1$ have these properties

a. The 'nonradiating' currents $\mathbf{J}_2$ and $\mathbf{J}'_1$ are generally highly oscillatory functions in the spatial domain;

b. They are related to the receiver positions during measurement and the ways illumination is applied;

c. The corresponding matrix $[G^o]$ or $[G^o]^H[G^o]$ may be singular or near singular and has a large condition number, when $\mathbf{J}_2$ or $\mathbf{J}'_1$ exists;

d. $\mathbf{J}'_1$ is very sensitive to any error either in numerical calculation or in experimental data;

e. $\mathbf{J}_2$ is in the null space of $[G^o]$ and can not be recovered directly from the solution of the matrix equation of $[G^o]$.

Since the existence of $\mathbf{J}_2$ violates condition 2 and the existence of $\mathbf{J}'_1$ violates condition 3 required by a well–posed problem which are defined at the beginning of this section, they indi-

cate that inverse scattering problems are ill–posed problems. For the solution of (3–9), if $\mathbf{J}_2$ is not zero, the solution is not unique. If $\mathbf{J}'_1$ exists, small errors in measurement and numerical calculation cause a large change in the solution and the solution is not numerically stable.

To overcome the difficulty brought by the existence of $\mathbf{J}_2$ and $\mathbf{J}'_1$, we can reduce the effect from $\mathbf{J}_2$ and $\mathbf{J}'_1$ by proper arrangement of the measurement system and object illumination in the experiment to make the problem not very ill–posed or by using multiple illuminations to get more information to recover $\mathbf{J}_2$ and $\mathbf{J}'_1$ in imaging. On the other hand, better algorithms have to be found to overcome the instability in the numerical computation and fully utilize the information for reconstruction. Accordingly, various methods have been proposed and all of these methods transform the ill–posed problem into a well–posed problem. This can be considered as the regularization of ill–posed problems.

3.3 Effect of Noise on Solution

In engineering practice, errors in measurement are almost inevitable [73]. The errors may come from the imperfection of instruments, mistakes in the operation of the instruments, or effects of the environment. For example, when a rectangular waveguide is used as a receiver or transmitter in microwave imaging, if the position and orientation of the waveguide are not accurately placed, the scattered field measured will be in error. In an experiment, the scattered waves from walls, ceiling or supporting structures blur the the field to be measured. In electromagnetic imaging, the receivers not only receive the scattered field but also receive the incident field. As a result, the improper arrangement of receivers can make the incident wave much larger than the scattered field at the receiving position, which affects the accuracy of the scattered field measurement. The dynamic noise in the measurement system also generates inherent noise in measure-

ment. All of these errors are generally taken as noise in measurement which corrupts the measured data. Since noise is randomly variant, it is highly oscillatory and makes the solution of the electromagnetic imaging problem numerically unstable. After discretization of the integral equation, if the obtained matrix equation (3–7) is overdetermined, the addition of noise may make the exact solution unattainable and one must settle for an approximate solution. An effective way to circumvent the difficulties coming from the noise is to us a proper regularization procedure to suppress the effects from noise.

3.4 Regularization Methods for Ill–posed Problems

Regularization methods are widely applied in solving ill–posed problems. The work of Tikhonov and Arsenine[24] set up a reliable theoretical framework for regularization. The regularization technique transforms an ill–posed problem into a well–posed one by using a constructed regularizing operator to replace the original one. The solution of the well–posed problem after regularization is an approximate solution of the original one. The regularization operator is constructed from the analysis of *a priori* knowledge to the ill–posed problem. After applying the regularization procedure, a stable solution with certain *a priori* requirements can be obtained from the associated well–posed problem. There are many ways to carry out the regularization. It can be done by changing the definition of the solution or the space in which the problem is posed, by introducing regularization operators or by using statistical techniques [74].

Pseudoinverse transformation is a typical regularization method [75],[21]. In this method, the pseudoinverse transformation is used to circumvent the ill–conditioning of the matrix equation in the equation (3–7). Instead of searching for the exact solution, this method generates an estimate $\hat{\mathbf{J}}$ such that $\min \| \mathbf{E}^s - [G^o]\hat{\mathbf{J}} \|$ is achieved with a $\min \| \hat{\mathbf{J}} \|$ where $\| \cdot \|$ indicates the least

square norm. The minimization of the norm of the current vector in this method has also the physical meaning of excluding the nonradiating current $\mathbf{J}_2$ and $\mathbf{J}_1'$ in the radiating current. In this method, what is looked for is $\mathbf{J}_1 - \mathbf{J}_1'$ which is determined from the solution of the minimum problem by using pseudoinverse transformation.

The current $\mathbf{J}_2$ belongs to the null space of $[G^o]$ and the scattered field generated by it is zero at the measurement points. When $[G^o]$ is a singular matrix, the nonradiating current $\mathbf{J}_2$ is not zero and the solution of the inverse scattering problem is not unique.

In the pseudoinverse transformation, $\mathbf{J}_2$ and $\mathbf{J}_1'$ are found by repeatedly using the Gram–Schmidt orthogonalization method. Consider a complex rectangular matrix $[G^o] \in C_{M\times N}$, the algorithm in the method of pseudoinversion transformation is as follows.

Let $\{ \mathbf{g}_1, \mathbf{g}_2, \cdots \mathbf{g}_N \}$ be the set of the vectors corresponding to the columns of $[G^o]$

i) Begin with the vector of the largest norm, say $\mathbf{g}_k$ (pivot vector).

ii) Make all other vectors orthogonal to the pivot vector by using the Gram–Schmidt orthogonalization method

$$\underline{\mathbf{g}}_i = \mathbf{g}_i - \frac{< \mathbf{g}_i , \mathbf{g}_k >}{\| \mathbf{g}_k \|^2} \mathbf{g}_k \qquad (3\text{–}13)$$

where $< \mathbf{g}_i , \mathbf{g}_k >= \mathbf{g}_k^H \mathbf{g}_i$ represents the vector inner product and $\| \mathbf{g}_k \| = \sqrt{\mathbf{g}_k^H \mathbf{g}_k}$ represents the vector norm.

iii) Among the modified vectors, choose the vector with the next largest norm, say , $\mathbf{g}_{i+q}$ (the second pivot vector).

iv) Make all other vectors (excluding all pivot vectors, $\mathbf{g}_k , \ldots \mathbf{g}_{i+q}$) orthogonal to it using (3–13).

v) Repeat iii) and iv) until the search for a new $\underline{\mathbf{g}}_l$ finds no vectors whose norm is above a certain threshold.

In order to keep a record of the operations on the columns of $[G^o]$, the transformation in (3–13) is applied at each step to the column vector of the identity matrix $[I]$ as well.

The matrices $[G^o]$ and $[I]$ are transformed into the new matrices $[P]$ and $[Q]$, respectively

$$\begin{Bmatrix} [G^o] \\ [\ I\ ] \end{Bmatrix} \xrightarrow{eq.(3-13)} \begin{Bmatrix} [\underline{\mathbf{g}}_1, \underline{\mathbf{g}}_2, \cdots \underline{\mathbf{g}}_m,\ 0,\ \cdots\ 0] \\ [\mathbf{q}_1, \mathbf{q}_2, \cdots \mathbf{q}_m, \mathbf{q}_{m+1} \cdots \mathbf{q}_N] \end{Bmatrix} = \begin{Bmatrix} [P] \\ [Q] \end{Bmatrix} \tag{3–14}$$

Since $[Q]$ records the operations performed on $[G^o]$, one gets

$$[G^o][Q] = [P] \tag{3–15}$$

Consequently, $\{\ \mathbf{q}_{m+1}, \mathbf{q}_{m+2} \cdots \mathbf{q}_N\ \}$ is a basis for the nullspace of $[G^o]$. It is then orthogonalized with the same procedure described before. In addition, the set $\{\ \mathbf{g}_1, \mathbf{g}_2 \cdots \mathbf{g}_m\ \}$ forms an orthogonal basis for the range of $[G^o]$. Consequently, the projection of $\mathbf{E}^s$ onto the range of $[G^o]$ can be written as

$$\mathbf{E}_p^s = [P]\mathbf{a} = [G^o][Q]\mathbf{a} \tag{3–16}$$

with

$$\begin{aligned} a_i &= \frac{< \mathbf{E}^s\ , \underline{\mathbf{g}}_i >}{\| \underline{\mathbf{g}}_i \|^2} \qquad i \le m \\ a_i &= 0 \qquad\qquad\quad i > m \end{aligned} \tag{3–17}$$

By virtue of (3–17), the solution of the equation

$$\mathbf{E}_p^s = [G^o]\mathbf{J}_p \tag{3–18}$$

is clearly

$$\mathbf{J}_p = [Q]\mathbf{a} \tag{3–19}$$

Only the orthogonal projection of the solutions of (3–18) onto the range of $[G^o]$ remains to be

carried out and this projection of $\mathbf{E}^s$ onto $\{ \mathbf{g}_1, \mathbf{g}_2 \cdots \mathbf{g}_m \}$ generates the least square solution of the matrix equation. The set of vectors $\{ \mathbf{q}_{m+1}, \mathbf{q}_{m+2} \cdots \mathbf{q}_N \}$ constitutes a basis for the orthogonal complement of the range of $[G^o]$ by virtue of the decomposition theorem. Consequently, the pseudoinverse solution is obtained as a vector orthogonal to the nullspace of $[G^o]$, which is given by

$$\hat{\mathbf{J}} = \mathbf{J}_p - \sum_{i=m+1}^{N} \frac{< \mathbf{J}_p, \mathbf{q}_i >}{\| \mathbf{q}_i \|^2} \mathbf{q}_i \tag{3–20}$$

The second term of the right–hand side of (3–17) represents the orthogonal projection of the vector given by (3–18) onto the nullspace of $[G^o]$. The projection of $\mathbf{J}_p$ onto $\{ \mathbf{q}_1, \mathbf{q}_2 \cdots \mathbf{q}_m \}$ generates the solution of the matrix equation with minimum norm.

In reality, the matrix $[G^o]$ is often nearly singular. That means that $\mathbf{J}_2 = 0$ and $\mathbf{J}_1'$ exists. In order to find the pseudoinverse solution of (3–7) and reduce the effect from $\mathbf{J}_1'$, one must set some of its column vectors to be linearly dependent. The Gram–Schmidt orthogonalization provides an indication about which column vectors of $[G^o]$ should be assumed to be dependent. Calculation examples prove that the selection of the number of linearly dependent columns has a great influence on the computation results.

In the case $M<N$, a more convenient and equivalent procedure is that of using the generalized right inverse $[G]^R$ to express the solution as

$$\hat{\mathbf{J}} = [G]^R \mathbf{E}^s \tag{3–21}$$

where

$$[G]^R = ([G^o][G^o]^H)^{-1}[G^o]^H \tag{3–22}$$

and where H indicates the conjugate transpose of a complex matrix. The solution obtained is also a least square solution with minimum norm. Once $\hat{\mathbf{J}}$ is obtained, an approximate estimate of the

object can be made from $\hat{\mathbf{J}}$.

In the pseudoinverse transformation the information in $\mathbf{J}_2$ and $\mathbf{J}'_1$ is lost. Although the application of pseudoinverse transformation stabilizes the numerical computation and suppresses the effect of noise which is highly oscillatory, the resolution of reconstruction is limited. When multiple illuminations are used, the information in $\mathbf{J}_2$ and $\mathbf{J}'_1$ for an individual illumination can be provided by other illuminations. $\mathbf{J}_2$ and $\mathbf{J}'_1$ can be determined from the information in the solution for other illuminations. The separated applications of pseudoinverse transformation for different illuminations cause the nonradiating parts of equivalent currents for different illuminations to be lost and those equivalent currents becomes incompatible for the same object.

Another way to convert an ill–posed electromagnetic imaging problem into a well–posed one is by using special measurement or illumination arrangements. Assuming that the object is divided into N cells, N different illuminations are applied and the scattered field is measured at N different points. The scattered field, the incident field and the current distribution are represented by square matrices and (3–7) becomes

$$[E^s] = [G^o][J] \tag{3–23}$$

If the measurement points and the incident fields are properly chosen, $[E^s]^{-1}$ may exist. Thus the object function can be obtained from the matrix equation for the forward problem

$$\begin{aligned}[O]^{-1} - [G^i] &= [E^i][J]^{-1} \\ &= [E^i][E^s]^{-1}[G^o]\end{aligned} \tag{3–24}$$

This matrix equation can be written as

$$[O]^{-1} = [E^i][E^s]^{-1}[G^o] + [G^i] \tag{3–25}$$

In this equation $[E^s]$, instead of $[G^o]$, is inverted so that the numerical instabilities in inverting

$[G^o]$ are avoided. Instead of inversion of $[E^s]$, another method using a group of special illuminations obtains an invertible matrix $[E^i]$. (3–25) is transformed into

$$[E^s][E^i]^{-1} = ([G^o] + [E^s][E^i]^{-1}[G^i])[O] \tag{3–26}$$

Since the arrangement of the incident field is independent of the object, an invertible $[E^i]$ is easier to obtain than an invertible $[E^s]$.

These methods present the chief advantage that they are numerically stable and are not prone to any loss of information. In practice, it is difficult to achieve the special measurement or illumination arrangements. These methods get rid of the difficulty in numerical implementation by raising the requirement for experiments.

In the discretization of the object, using large sized cells can also be considered as a regularization, since the matrix equation obtained from the discretization with large cell size generally is not very ill–conditioned. However, the most generally accepted method is that of the Lagrange multipliers to construct a new equation, the regularization operator. Consider an operator equation

$$Az = u \tag{3–27}$$

where A is a linear operator. By using the method of the Lagrange multipliers, a regularization of the above operator equation constructs a functional

$$M(z, u) = \varrho^2(Az, u) + g\Omega(z) \tag{3–28}$$

where $\varrho(\ ,\ )$ is the distance between two points in a metric space, $\Omega(\ )$ is a function called the stabilizing function and g is a constant called the regularization parameter. As a conditional extremum problem, the approximate solution of the original problem is determined from the minimum of functional $M(z, u)$.

Various constraints have been proposed for $\Omega(\ )$. For reasons of convenience in numerical computation, it is often written in the form of a quadratic function

$$\Omega(z) = \| f(z) \|^2 \tag{3–29}$$

where $f(\ )$ is a linear function. The stabilizing function is a constraint and generally comes from a physical requirement, a mathematical requirement or *a priori* information of the object. It may be the distribution of the equivalent current, its derivative or the distribution of the object function, or its derivative. For example, to filter the nonradiating current and the highly oscillated part in the radiating current, $\Omega(\ )$ may be the square of the norm of the equivalent current distribution. The functional for the matrix equation

$$\mathbf{E}^s = [G^o]\mathbf{J} \tag{3–30}$$

is constructed as

$$M(\mathbf{J}, \mathbf{E}^s) = \| [G^o]\mathbf{J} - \mathbf{E}^s \|^2 + g \| \mathbf{J} \|^2 \tag{3–31}$$

At the extremum of this functional, the derivative of the functional must be zero. A matrix equation is obtained

$$([G^o]^H[G^o] + g[I])\mathbf{J} = [G^o]^H\mathbf{E}^s \tag{3–32}$$

When the permittivity distribution in some region of the object is smooth such that its first or second order spatial derivative in this region is finite, the derivative in that region of the object function $O(\mathbf{r})$ can be chosen as $f(\ )$.

A very important parameter in regularization is the regularization parameter g. If g is set to be zero, what we obtain is a least square treatment of the original matrix equation

$$[G^o]^H[G^o]\mathbf{J} = [G^o]^H\mathbf{E}^s \tag{3–33}$$

A large g suppresses the highly oscillatory part in the solution and smooths the solution. A small

g makes the solution more accurate but the numerical stability of the solution is decreased. It has to be carefully chosen to meet both requirements. In an iterative process, g has to be changed according to the iteration results at each step in order to have a good reconstruction.

Other types of stabilizing functions come from stochastic iterative methods and many of them are borrowed from the methods used for image processing. In these methods, the distribution of equivalent current is considered as a random vector or a stochastic process. In information theory, the entropy is a measure of information. It is related to the probability density of random variables. In the Maximum Entropy Method (MEM) [50–52], the equivalent current in each cell, for example the i–th cell, is considered as consisting of two positive and independent random quantities, the real part J_i^{Re} and imaginary part J_i^{Im} of equivalent current J_i. The entropy of the equivalent current distribution is defined as

$$H(\mathbf{J}) = \sum_{i=1}^{N} \ln(J_i^{\mathrm{Re}}) + \sum_{i=1}^{N} \ln(j_i^{\mathrm{Im}}) \tag{3–34}$$

In MEM, the equivalent current is obtained from the maximum of the following function

$$S(\mathbf{J}) = H(\mathbf{J}) - gQ(\mathbf{J}) \tag{3–35}$$

where

$$Q(\mathbf{J}) = \| \mathbf{E}^s - [G^o]\mathbf{J} \|^2 \tag{3–36}$$

Maximizing $S(\mathbf{J})$ can be considered as both maximizing the entropy $H(\mathbf{J})$ and minimizing the least square error with a parameter given by the Lagrange multiplier g. In this formulation, $H(\mathbf{J})$ is a nonlinear function and $S(\mathbf{J})$ is a highly nonquadratic one. Conjugate gradient methods can be applied to solve the nonlinear problem. In MEM, the random quantities can not be negative which requires that the amplitudes of the real and imaginary parts of the equivalent current distribution can not be negative. By shifting the zeroes of the current amplitude for the real and

imaginary parts this requirement can be satisfied [50]. When the problem is expressed as minimizing the functional –S(J)/g, it comes back to the form expressed in (3–29).

In the Markov Random Field method [55], the object function distribution in space is considered as a stochastic process called the Markov Random Field. The Bayesian image restoration algorithm is used to obtain a model of the distributions of dielectric features in the scattering region. In this way, *a priori* knowledge of the object can be easily inserted in the imaging scheme. This stochastic approach requires a functional to be minimized. This minimization can be done by using the simulated annealing algorithm. It is said that this method seems better than those obtained by other imaging techniques in the space domain. The algorithm is also able to operate in a strongly noisy environment.

The aim of the algorithm is finding the maximum of the posterior conditional probability

$$P(\mathbf{O}/\mathbf{E}_T^s) \tag{3–37}$$

which can be understood as the probability of a stochastic distribution of the object function $\mathbf{O}$ when the measured scattered field is $\mathbf{E}_T^s$. Because the probabilities of $P(\mathbf{E}_T^s/\mathbf{O})$ and $P(\mathbf{O})$ are more easily constructed, the Bayes' rule

$$P(\mathbf{O}/\mathbf{E}_T^s) = \frac{P(\mathbf{E}_T^s/\mathbf{O})P(\mathbf{O})}{P(\mathbf{E}_T^s)} \tag{3–38}$$

is applied. $P(\mathbf{E}_T^s/\mathbf{O})$ is constructed as

$$P(\mathbf{E}_T^s/\mathbf{O}) = c\ e^{-\frac{1}{2\sigma^2}|\Delta\mathbf{E}_T^s|^2} \tag{3–39}$$

where c and σ are constants. $P(\mathbf{O})$ is the probability of the discrete random vector $\mathbf{O}$ called the Markov Random Field. To simplify the construction of $P(\mathbf{O})$, it is assumed that the value of the element O_n in $\mathbf{O}$ depends on the values of its neighbouring points indicated by the set χ_n or L_n and the probability of $\mathbf{O}$ is constructed as

$$P(\mathbf{O}) = c_0 e^{c_1 \sum_{n=1}^{N} \sum_{j \in \chi_n} (1-\alpha_{jn})|o_n - o_j|^2 + c_2 \sum_{n=1}^{N} \sum_{i \in L_n} L_i(o_n)} \tag{3–40}$$

where c_0, c_1, c_2 are constants. From the above expression, a total energy function is defined as

$$U(\mathbf{O}) = \beta \sum_{n=1}^{N} \sum_{j \in \chi_n} (1-\alpha_{jn})|o_n - o_j|^2 + \gamma \sum_{n=1}^{N} \sum_{i \in L_n} L_i(o_n) + |\Delta \mathbf{E}_T^s|^2 \tag{3–41}$$

where $\alpha_{jn}, \beta, \gamma$ are constants and L_i is a function related to the discontinuities in the object. Maximizing $P(\mathbf{O}/\mathbf{E}_T^s)$ is transformed into minimizing the total energy function. The most *a posterior* (MAP) estimate of the object function is obtained from the minimum of the total energy function. In the expression of the total energy function, the constant parameters $\alpha_{jn}, \beta, \gamma$ and the function L_i have to be determined from the knowledge of the object. In computation of $\Delta \mathbf{E}_T^s$, the difference between the measured data and the computed electric scattered field, the Born approximation is used to simplify the computation of the scattered electric field. The first term of $U(\mathbf{O})$ is the constraint to smooth the local part of the object function and the second term of $U(\mathbf{O})$ is the constraint to preserve the discontinuity of the object function. The information about the object has to be applied to determine the type of constraint for each point in the $U(\mathbf{O})$.

Although the deviation of this method is based on the theory of stochastic theory, the final equation to be solved is quite similar to iterative methods with regularization. The main difference is that the regularization is more carefully constructed from *a priori* knowledge of the object, such as the smoothness or discontinuity. Based on the knowledge of the object, the effect of noise in measurement is reduced. However, the construction of the probability expression is complicated and is not convenient in practice. Since the Born approximation is used in this method, the availability of this method to the case of an object with strong contrast has to be tested by

further investigation.

3.5 Conclusion

In this chapter, the uniqueness and the stability of the solution in electromagnetic imaging, as an ill–posed problem, is discussed. The nonradiating current and high spatial frequency components in the radiating current play important roles in the stability of numerical computation. In order to obtain a numerically stable reconstruction, various regularization techniques are discussed. In the later chapters, the regularization technique applied in the Born iterative method is used in our computation and several techniques used for improving the convergence, numerical stability and flexibility with weaker regularization are presented.

Chapter 4
Equivalent Current Refinement

4.1 Introduction

In this chapter, the Born and the Newton iterative methods are discussed and a procedure of equivalent current refinement is presented. In this procedure, the object function is reconstructed from the refined equivalent current. As shown in Section 5.3, this technique improves the numerical convergence and stability of the Born and the Newton iterative methods.

The Born and the Newton iterative methods have the advantage of faster convergence, compared to the stochastic iterative methods such as the Simulated Annealing and the Markov Random Field iterative methods. This is because, in stochastic iterative methods, the solution is searched randomly. In the Born and the Newton iterative methods, the object function is reconstructed by minimizing the difference between the measured data and the computed scattered field. At each iteration step, the total electric field used in solving the inverse problem is computed from the estimated object function. In these methods, the errors in the computed total electric field decrease the convergence of the iterative process. In this chapter, an analysis is performed in order to show that the errors in the computed total electric field are compensated by the errors in the object function, thus yielding a refined equivalent current. This refined equivalent current is used to obtain a better reconstructed object function. In the algorithm presented here, the object function obtained at each iteration is used to update the equivalent current. Then, from the refined equivalent current and the associated total electric field, a better estimate of the object function is computed. The introduction of this technique increases the convergence rate of an iterative process. Since no dense matrix equation has to be solved in this refinement, the increase in the computation time due to this technique is negligible. Numerical results prove that by using this technique, the iterative process is more numerically stable and a better reconstruction of the

object function is achieved.

4.2 Born and Newton Iterative Methods

The Born and the Newton iterative methods are typical methods used in solving the inverse scattering problem in electromagnetic imaging. In each step of the iterative processes, the direct problem and the inverse problem are solved in turn. The total electric field is updated from the solution of the direct problem with the estimated object function. Then, the object function is updated from the solution of the inverse problem by using the newly computed total electric field. Since the inverse problem is ill–posed, the Born and the Newton iterative methods suffer from numerical instability, and regularization is applied to overcome this difficulty. In the literature [23][46], the object contrast for the numerical experiments are less than 2.5.

4.2.1 Born Iterative Method

The Born iterative method was proposed by Wang and Chew [28]. In this method, the matrix equations for the direct problem and the inverse problem for the case of multiple illuminations are written in the form

$$\mathbf{E}_l^i = ([I] - [G^i][O])\mathbf{E}_l^t \tag{4–1}$$

$$\mathbf{E}_l^s = [G_l^o][E_l^t]\mathbf{O} \qquad l = 1, 2, \ldots, L \tag{4–2}$$

A global equation for all illuminations of (4–2) with the matrices $[E_l^t]$ solved from (4–1) can be written as

$$\mathbf{E}_T^s = [D]\mathbf{O} \tag{4–3}$$

where

$$[D] = \begin{bmatrix} [G_1^o][E_1^t] \\ [G_2^o][E_2^t] \\ \cdot \\ \cdot \\ \cdot \\ [G_L^o][E_L^t] \end{bmatrix} \qquad \mathbf{E}_T^s = \begin{bmatrix} \mathbf{E}_1^s \\ \mathbf{E}_2^s \\ \cdot \\ \cdot \\ \cdot \\ \mathbf{E}_L^s \end{bmatrix} \tag{4–4}$$

The least square solution of the object function is obtained from the matrix equation

$$[D]^H \mathbf{E}_T^s = [D]^H [D]\mathbf{O} \tag{4–5}$$

where H stands for the conjugate transpose of a matrix. Because of the ill–conditioning of the matrix $[D]^H[D]$, the matrix inversion involved in (4–5) is numerically unstable. A regularization is used to stabilize the solution of the matrix equation. A popular regularization is using the method of Lagrange multipliers with the norm square of the object function being used as the stabilizing function. After applying this regularization, (4–5) becomes

$$[D]^H \mathbf{E}_T^s = ([D]^H [D] + g[I])\mathbf{O} \tag{4–6}$$

where g is the regularization parameter. In (4–6), the matrix $[D]^H[D] + g[I]$ obtained after the regularization has a smaller condition number than $[D]^H[D]$.

At each step of the iteration, $\mathbf{E}_l^t$ is solved from (4–1) and can be expressed as

$$\mathbf{E}_l^t = ([I] - [G^i][O])^{-1}\mathbf{E}_l^i \tag{4–7}$$

where the matrix $[O]$ is determined from the object function obtained in the preceding iteration. By substituting the newly obtained $\mathbf{E}_l^t$ in (4–4), the matrix $[D]$ is computed. A new estimate of the object function $\mathbf{O}$ is solved from

$$([D]^H [D] + g[I])^{-1}[D]^H \mathbf{E}_T^s = \mathbf{O} \tag{4–8}$$

The updated object function is substituted back into (4–7) to start the next iteration. The iterative process ends when the difference between the computed scattered field and the measured data is within an acceptable level.

The matrices $[D]^H[D]$ obtained before the regularization and $[D]^H[D] + g[I]$ after the regularization have the same eigenvectors. For the i–th eigenvector, the eigenvalue is λ_i for matrix $[D]^H[D]$ and is $\lambda_i + g$ for matrix $[D]^H[D] + g[I]$. The regularization parameter g is a positive number and generally very small compared to the large eigenvalues. For $[D]^H[D] + g[I]$, all eigenvalues are obtained by adding a constant g. This has a great effect on the small eigenvalues

but has a very small effect on the larger eigenvalues. The introduction of the regularization factor g improves the matrix condition number by increasing the smallest eigenvalue of the matrix $[D]^H[D]$. The decrease of the condition number suppresses the high spatial frequency components in the solution. These high spatial frequency components are very sensitive to the noise in the measurement and round off error in the numerical calculation. On the other hand, a strong regularization process may remove useful information and decrease the spatial resolution of the image. As a consequence, the regularization parameter g must be chosen in order to accommodate a compromise between a convenient spatial resolution and a desired level of stability.

4.2.2 Newton Iterative Method

This iterative method is proposed in [19] by Joachimowicz *et al.* Considering small variations of (4–1) and (4–2) with fixed $\mathbf{E}_l^i$, two set of matrix equations are obtained. These matrix equations can be expressed as

$$\Delta\mathbf{E}_l^t = [G^i]\Delta([O]\mathbf{E}_l^t) \tag{4–9}$$

$$\Delta\mathbf{E}_l^s = [G_l^o]\Delta([O]\mathbf{E}_l^t) \qquad l = 1, 2, \ldots, L \tag{4–10}$$

With the first order approximation, it can be shown that

$$\Delta([O]\mathbf{E}_l^t) \approx \Delta[O]\mathbf{E}_l^t + [O]\Delta\mathbf{E}_l^t \tag{4–11}$$

Substituting (4–11) in (4–9) and (4–10) yields

$$\Delta\mathbf{E}_l^s = [G_l^o]([I] - [O][G^i])^{-1}\Delta[O]\mathbf{E}_l^t \tag{4–12}$$

For the convenience of discussion, the product of the diagonal matrix $[O]$ and the column vector $\mathbf{E}_l^t$ in (4–12) is rewritten as

$$\Delta[O]\mathbf{E}_l^t = [E_l^t]\Delta\mathbf{O} \tag{4–13}$$

where $[E_l^t]$ is a diagonal matrix consisting of the elements of the total field column vector, $\mathbf{E}_l^t$. By using (4–13), (4–12) can be expressed as

$$\Delta\mathbf{E}_l^s = [G_l^o]([I] - [O][G^i])^{-1}[E_l^t]\Delta\mathbf{O}$$

$$= [D_l]\Delta\mathbf{O} \tag{4–14}$$

A least square solution of the global matrix equation of (4–14) for all illuminations is obtained by solving the matrix equation

$$\Delta\mathbf{O} = ([D]^H[D])^{-1}[D]^H\Delta\mathbf{E}_T^s \tag{4–15}$$

where

$$[D] = \begin{bmatrix} [D_1] \\ [D_2] \\ \cdot \\ \cdot \\ \cdot \\ [D_L] \end{bmatrix} \qquad \Delta\mathbf{E}_T^s = \begin{bmatrix} \Delta\mathbf{E}_1^s \\ \Delta\mathbf{E}_2^s \\ \cdot \\ \cdot \\ \cdot \\ \Delta\mathbf{E}_L^s \end{bmatrix} \tag{4–16}$$

By using the above equations in an iterative procedure, the initial nonlinear relation characterizing the inverse scattering problem is transformed into a sequence of linear ones. Hence, starting with an initial guess O_o, a succession of intermediate functions O_k are generated by minimizing the difference between the computed scattered field and the measured scattered field. This procedure is summarized as follows:

1) Compute the total internal field $\mathbf{E}_l^t$ by solving (4–1).

2) Estimate the scattered field at the receiver locations from (4–2).

3) Compute the error $\Delta\mathbf{E}_l^s$ from $\mathbf{E}_l^s$, the scattered field computed in 2), and the measured field.

4) Compute $\Delta\mathbf{O}$, the first–order estimation of the error in the object function by solving (4–15).

5) Update the object function $\mathbf{O} + \Delta\mathbf{O} \rightarrow \mathbf{O}$.

6) Go to 1) as long as $\Delta\mathbf{E}_T^s$ is larger than an acceptable error.

The highly ill–posed inverse problem is very sensitive to small errors in the numerical calculation. This numerical instability in the inverse problem is related to the large condition number of the matrix $[D]^H[D]$. The larger the condition number of $[D]$, the more sensitive to error are the eigenvectors of small eigenvalues. Due to this instability, a regularization procedure is employed

to stabilize the numerical process. Instead of solving (4–15), $\Delta\mathbf{O}$ is computed from

$$\Delta\mathbf{O} = ([D]^H[D] + g[I])^{-1}[D]^H\Delta\mathbf{E}^s \tag{4–17}$$

The regularization used in (4–17) is the same as the one used in the Born iterative method. The regularization parameter g is determined from [19]

$$g = c\frac{trace\ of\ [D]^H[D]}{N}\frac{\| \Delta\mathbf{E}_T^s \|}{\| \mathbf{E}_T^s \|} \tag{4–18}$$

where N is the matrix dimension. In the expression (4–18),

1) the parameter c is determined empirically, according to the convergence of the process;
2) the trace of the matrix $[D]^H[D]$ is used to reduced the gap between its higher and lower eigenvalues and thus, to improve its condition number;
3) the relative mean square error of the scattered field is used to decrease g during the iterative process.

It has been found that the regularization determined in this way allows for an easy insertion of *a priori* information that can be used to remove unphysical solutions or to recover the components which were filtered out during the regularization procedure. The typical *a priori* information includes the knowledge of the external contour and of the extremum values of complex permittivity.

The distorted Born iterative method is also a very important iterative method proposed by Chew and Wang [47]. In this method, the Green's function for a given permittivity distribution is used in solving the direct and the inverse problems. In the iterative process, the Green's function is updated by using the newly computed object function in the preceding iteration. At each step of iteration, the updated Green's function is used in the solution of the direct and the inverse problems. The correction of the object function is obtained from the solution of the inverse problem. Numerical results show that the distorted Born iterative method converges faster than the Born iterative method. However, the Born iterative method is more robust in the presence of noise than

the Distorted Born iterative method. In later sections and chapters, the Born and the Newton iterative methods are used for numerical computation.

4.3 Errors in the Computed Total Electric Field

In the Born and the Newton iterative methods, at each step of iteration, the object function is obtained from the solution of the matrix equations for the inverse problem. These matrix equations for the inverse problem can be expressed in a unified form as

$$\mathbf{B} = [D]\mathbf{X} \tag{4–19}$$

In the Born iterative method, $\mathbf{X}$ is $\mathbf{O}$, $[D]$ consists of submatrices $[G_l^o][E_l^t]$ and $\mathbf{B}$ consists of column vectors $\mathbf{E}_l^s$, respectively. In the Newton iterative method, $\mathbf{X}$ is $\Delta\mathbf{O}$, $[D]$ consists of submatrices $[G_l^o]([I]-[O][G^i])^{-1}[E_l^t]$ and $\mathbf{B}$ consists of $\Delta\mathbf{E}_l^s$, respectively. The matrix $[D]$ is generally a rectangular one and the least square solution of (4–19) is obtained from the matrix equation

$$[D]^H\mathbf{B} = [D]^H[D]\mathbf{X} \tag{4–20}$$

To overcome the numerical instability in solving the ill–conditioned matrix equation (4–20), a regularization technique is applied. The equation to be solved for the least square solution becomes

$$[D]^H\mathbf{B} = ([D]^H[D] + g[I])\mathbf{X} \tag{4–21}$$

At each step of iteration, the vectors $\mathbf{E}_l^t$ are solved from the direct problem by using the object function updated from the preceding iteration. These $\mathbf{E}_l^t$ are used in the computation of the matrix $[D]$. The errors in $\mathbf{E}_l^t$ yield inherently errors in the reconstruction of $\mathbf{O}$ and $\Delta\mathbf{O}$. In the Born iterative method, the errors in $[D]$ come from the errors in the matrices $[E_l^t]$. In the Newton iterative method, since the variation $\Delta([O]\mathbf{E}_l^t)$ is replaced by its first order approximation $\Delta[O]\mathbf{E}_l^t + [O]\Delta\mathbf{E}_l^t$, the errors in $[D]$ are not obvious. By denoting the computed object function

and the total electric field as $[\tilde{O}]$ and $\tilde{\mathbf{E}}_l^t$ and the actual ones as $[O]$ and $\mathbf{E}_l^t$, respectively, the exact variation expression of $[O]\mathbf{E}_l^t$ is

$$\begin{aligned}\Delta([O]\mathbf{E}_l^t) &= [O]\mathbf{E}_l^t - [\tilde{O}]\tilde{\mathbf{E}}_l^t \\ &= ([O] - [\tilde{O}])\mathbf{E}_l^t + [\tilde{O}](\mathbf{E}_l^t - \tilde{\mathbf{E}}_l^t) \\ &= \Delta[O]\mathbf{E}_l^t + [\tilde{O}]\Delta\mathbf{E}_l^t \ . \end{aligned} \tag{4–22}$$

Following the derivation of the Newton iterative method, we obtain

$$\Delta\mathbf{E}_l^s = [G_l^o]([I] - [\tilde{O}][G^i])^{-1}[E_l^t]\Delta\mathbf{O} \tag{4–23}$$

After using the first order approximation, the unknown $[E_l^t]$ is replaced by the computed matrix, $[\tilde{E}_l^t]$. In the Newton iterative method, the errors in $[D]$ also come from the computed $[E_l^t]$. Obviously, the errors have a negative impact on the convergence of the iteration process.

By denoting the change generated by the errors in the computed total electric field in the matrix $[D]$ as $[\Delta D]$, (4–19) can be written as

$$\mathbf{B} = [D + \Delta D]\tilde{\mathbf{X}} \tag{4–24}$$

and $\tilde{\mathbf{X}} = \mathbf{X} + \Delta\mathbf{X}$ becomes the solution for (4–24) rather than $\mathbf{X}$. Therefore, the actual $\mathbf{O}$ or $\Delta\mathbf{O}$ cannot be solved from (4–24). Consider the difference between (4–19) and (4–24), with fixed $\mathbf{B}$,

$$0 = [\Delta D]\tilde{\mathbf{X}} + [D]\Delta\mathbf{X} \ . \tag{4–25}$$

The errors in $\tilde{\mathbf{X}}$ generated by $[\Delta D]$ can be calculated from

$$\Delta\mathbf{X} = -([D]^H[D])^{-1}[D]^H[\Delta D]\tilde{\mathbf{X}} \ . \tag{4–26}$$

Because of the existence of $[\Delta D]$, the solution becomes $\mathbf{X} + \Delta\mathbf{X}$ rather than $\mathbf{X}$. From (4–25) and the negative sign in (4–26), it can be seen that the effect of $\Delta\mathbf{X}$ is always against the deviation generated from $[\Delta D]$. In other words, considering the expression $[D]$, the computed $\mathbf{O}$ has to eliminate the errors of $[E_l^t]$ in $[E_l^t]\mathbf{O}$ for the Born iterative method or $\Delta\mathbf{O}$ has to eliminate

the errors of $[E_l^t]$ in $[E_l^t]\Delta\mathbf{O}$ for the Newton iterative method, respectively.

4.4 Equivalent Current Refinement

From the above discussion, it can be seen that more consideration should be given to the errors in the computed electric field when solving (4–19).

An immediate way is to replace $[E_l^t]\mathbf{O}$ in (4–2) by $\mathbf{J}_l$ or replace $([I]-[O][G^i])^{-1}[E_l^t]\Delta\mathbf{O}$ in (4–14) by $\Delta\mathbf{J}_l$. Thus the inverse problem becomes a linear one for the reconstruction of the equivalent current. But this replacement breaks the global equation (4–19). The equivalent currents $\mathbf{J}_l$ or their variations $\Delta\mathbf{J}_l$ for different illuminations can only be solved separately from their corresponding matrix equations, because $\mathbf{J}_l$ or $\Delta\mathbf{J}_l$ are different for different illuminations. For an individual illumination, the corresponding equivalent current is difficult to fully recover from the measured data, especially the highly oscillatory part of the equivalent current. Caorsi *et al* have used the pseudoinverse transformation method to solve the equivalent currents for different illuminations separately. However, in the pseudoinverse transformation, the nonradiating current cannot be determined and is excluded from the solution in order to get a unique solution for each illumination. Since the nonradiating current is lost in the pseudoinverse transformation solution, there are large errors in the reconstructed equivalent currents and object functions for different illuminations.

In contrast, the Born and Newton iterative methods combine the information from different illuminations to obtain a global solution of the object function. In these methods, the global equation (4–19) is solved to update the object function. Because of the errors in $[E_l^t]$, the global equation at each step of iteration is the distorted matrix equation (4–24). In the iterative process, the differences between (4–19) and (4–24) become smaller as the errors in the computed electric field $[E_l^t]$ decrease. However, in the Born and Newton iterative methods, at each step of iteration, how the distorted solution $\mathbf{X}+\Delta\mathbf{X}$ as obtained from (4–24) can be used to compute a better eval-

uation of $\mathbf{X}$ for (4–19) is not considered.

As discussed in the preceding section, the errors in $[E_l^t]$ and $\mathbf{O}$ for (4–2) or $\Delta\mathbf{O}$ for (4–14) are opposite to each other as shown in (4–26). The total errors in their product are reduced by this relation. By using the inaccurate solution $\mathbf{X}+\Delta\mathbf{X}$ for $\mathbf{O}$ or $\Delta\mathbf{O}$, we can find a better evaluation of $\mathbf{J}_l$ from

$$\mathbf{J}_l = [E_l^t]\mathbf{O} \tag{4–27}$$

or a better evaluation of the difference between the actual equivalent current distribution and the computed one, $\Delta\mathbf{J}_l$, from

$$\Delta\mathbf{J}_l = ([I]-[O][G^i])^{-1}[E_l^t]\Delta\mathbf{O} \ . \tag{4–28}$$

The error in computed $[E_l^t]$ and the error in computed $\mathbf{O}$ or $\Delta\mathbf{O}$ are opposite to each other and the contribution of these errors to the equivalent current is reduced.

To provide a simple illustration, we consider the case of a single illumination. For simplification, we assume that the receiving arrangement makes $[G^o]$ a square matrix. In each iteration step, the matrix equations for the Born and the Newton iterative methods are

$$\mathbf{E}^s = [G^o][\tilde{E}^t]\tilde{\mathbf{O}} \tag{4–29}$$

and

$$\Delta\mathbf{E}^s = [G^o]([I]-[\tilde{O}][G^i])^{-1}[\tilde{E}^t]\Delta\tilde{\mathbf{O}} \tag{4–30}$$

respectively, where the quantities with the tilde sign are the computed ones. The errors in the computed electric field make the solutions become

$$\tilde{\mathbf{O}} = [\tilde{E}^t]^{-1}[E^t]\mathbf{O} \tag{4–31}$$

and, compared with (4–23),

$$\Delta\tilde{\mathbf{O}} = [\tilde{E}^t]^{-1}[E^t]\Delta\mathbf{O} \ . \tag{4–32}$$

Only when

$$[\tilde{E}^t]^{-1}[E^t] = [I] \tag{4–33}$$

can the actual object function be solved from (4–29) or (4–30). However, by using these incorrect quantities, the correct $\mathbf{J}$ and $\Delta\mathbf{J}$ can still be obtained from

$$\mathbf{J} = [\tilde{E}^t]\tilde{\mathbf{O}} \tag{4–34}$$

and

$$\Delta\mathbf{J} = ([I] - [\tilde{O}][G^i])^{-1}[\tilde{E}^t]\Delta\tilde{\mathbf{O}} \tag{4–35}$$

respectively. By using $\mathbf{J}$ as obtained from (4–34) or (4–35), it is not difficult to compute the object function. The relationship between the scattered electric fields and the object function or the one between their corresponding differences is not linear because $[E_l^t]$ is a function of $\mathbf{O}$. But the relationship between the scattered electric fields and the equivalent currents or the one between their corresponding difference quantities is linear. $\mathbf{O}$ or $\Delta\mathbf{O}$ cannot be directly solved from (4–29) or (4–30), respectively. However, the equivalent currents $\mathbf{J}$ or $\Delta\mathbf{J}$ can be better evaluated from $\tilde{\mathbf{O}}$ or $\Delta\tilde{\mathbf{O}}$ and can be used to reconstruct $\mathbf{O}$ or $\Delta\mathbf{O}$, respectively.

4.5 The Procedure of Reconstruction with Equivalent Current Refinement

The idea behind the procedure of reconstruction with equivalent current refinement is based on reconstructing $\mathbf{O}$ or $\Delta\mathbf{O}$ at each iteration by using the refined $\mathbf{J}_l$ or $\Delta\mathbf{J}_l$. These updated $\mathbf{J}_l$ and $\Delta\mathbf{J}_l$ currents are computed from (4–27) or (4–28) after substitution of newly obtained $\mathbf{O}$ or $\Delta\mathbf{O}$, respectively. The updated $\mathbf{J}_l$ is then used to improve the evaluation of $\mathbf{E}_l^t$ as

$$\mathbf{E}_l^t = [G^i]\mathbf{J}_l + \mathbf{E}_l^i \ . \tag{4–36}$$

Using updated $\mathbf{J}_l$ and $\mathbf{E}_l^t$ in (4–27) yields an improved object function at each iteration step. Since for different illuminations, (4–27) gives different results, a least square treatment to (4–27) is applied and the object function is obtained from

$$\mathbf{O} = ([E_T^t]^H[E_T^t])^{-1}[E_T^t]^H\mathbf{J}_T \tag{4–37}$$

where $[E_T^t]$ is a matrix consisting of all the matrices $[E_l^t]$ and $\mathbf{J}_T$ is a column vector consisting

of all the vectors $\mathbf{J}_l$,

$$[E_T^t] = \begin{bmatrix} [E_1^t] \\ [E_2^t] \\ \cdot \\ \cdot \\ \cdot \\ [E_L^t] \end{bmatrix}, \qquad \mathbf{J}_T = \begin{bmatrix} \mathbf{J}_1 \\ \mathbf{J}_2 \\ \cdot \\ \cdot \\ \cdot \\ \mathbf{J}_L \end{bmatrix}. \tag{4–38}$$

This better evaluated object function is used in the next iteration. Once the scattered electric field is computed with a desired accuracy, the process is terminated and the permittivity distribution is obtained from the object function.

The algorithm of reconstruction from equivalent current can be described as follows:

1) Take the incident field as the initial guess of the total electric field inside the region investigated, $\mathbf{E}_l^t = \mathbf{E}_l^i$;

2) Calculate matrix $[D]$ from

$$[G_l^o][E_l^t] \tag{4–39}$$

if the Born iterative method is used, or

$$[G_l^o]([I] - [O][G^i])^{-1}[E_l^t] \tag{4–40}$$

if the Newton iterative method is used, and then solve the matrix equation

$$[D]^H\mathbf{B} = ([D]^H[D] + g[I])\mathbf{X} \tag{4–41}$$

to obtain $\mathbf{O}$ or $\Delta\mathbf{O}$;

3) Obtain the refined equivalent current $\mathbf{J}_l$ from

$$\mathbf{J}_l = [E_l^t]\mathbf{O} \tag{4–42}$$

or $\Delta\mathbf{J}_l$ from

$$\Delta\mathbf{J}_l = ([I] - [O][G^i])^{-1}[E_l^t]\Delta\mathbf{O} \tag{4–43}$$

and then the refined total electric field $\mathbf{E}_l^t$ from

$$\mathbf{E}_l^t = \mathbf{E}_l^i + [G^i]\mathbf{J}_l \; ; \tag{4–44}$$

4) Calculate the least square solution of $\mathbf{O}$ from

$$[E_T^t]^H[E_T^t]\mathbf{O} = [E_T^t]\mathbf{J}_T \; ; \tag{4–45}$$

5) Substitute the updated $\mathbf{O}$ in the direct problem to obtain the total electric field $\mathbf{E}^t$, and $[I] - [O][G^i]$ if the Newton iterative method is used, and calculate the scattered field at the receivers as

$$\mathbf{E}^s = [G^o][O]\mathbf{E}^t \; ; \tag{4–46}$$

6) Compare the scattered field with the measured ones. If the difference is less than an acceptable level, terminate the iteration, otherwise go back to step 2.

In this procedure, there is no matrix inversion involved in updating the equivalent current density distribution and the total electric field. Since the matrix $[E_T^t]$ consists of diagonal matrices, the matrix $[E_T^t]^H[E_T^t]$ to be inverted is also a diagonal matrix, which simplifies the solution of (4–37) greatly. As a consequence, the extra computation time required in the new procedure is negligible with respect to the computation time of the original methods.

4.6 Numerical Results

In this section, the electromagnetic imaging of two–dimensional dielectric objects with multiple TM wave illuminations are considered. The current refinement technique along with either the Born or the Newton iterative technique is applied to reconstruct three different examples of dielectric cylinders and the numerical results for these three examples are presented [76–78].

Example 1 – A lossless dielectric cylinder of square cross section with continuous permittivity distribution as shown in Fig. 4.1(a). The distribution of the permittivity is $\epsilon_r(x, y) = 2.2 - 2[(x/\lambda - 0.45)^2 + (y/\lambda - 0.45)^2]$ where λ is the wavelength in free

space. The maximum and the minimum of ϵ_r are 2.2 and 1.2, respectively. The cross section is discretized into 100 cells (cell size $0.1\lambda \times 0.1\lambda$) as shown in Fig. 4.1(b). The illumination is provided by a line source parallel to the cylinder placed successively at different positions, equally spaced around the cylinder at a distance of six wavelengths from its center. The z component of scattered electric field is measured by equidistant receivers on a $1.67\lambda \times 1.67\lambda$ square contour as indicated in Fig. 4.1(b).

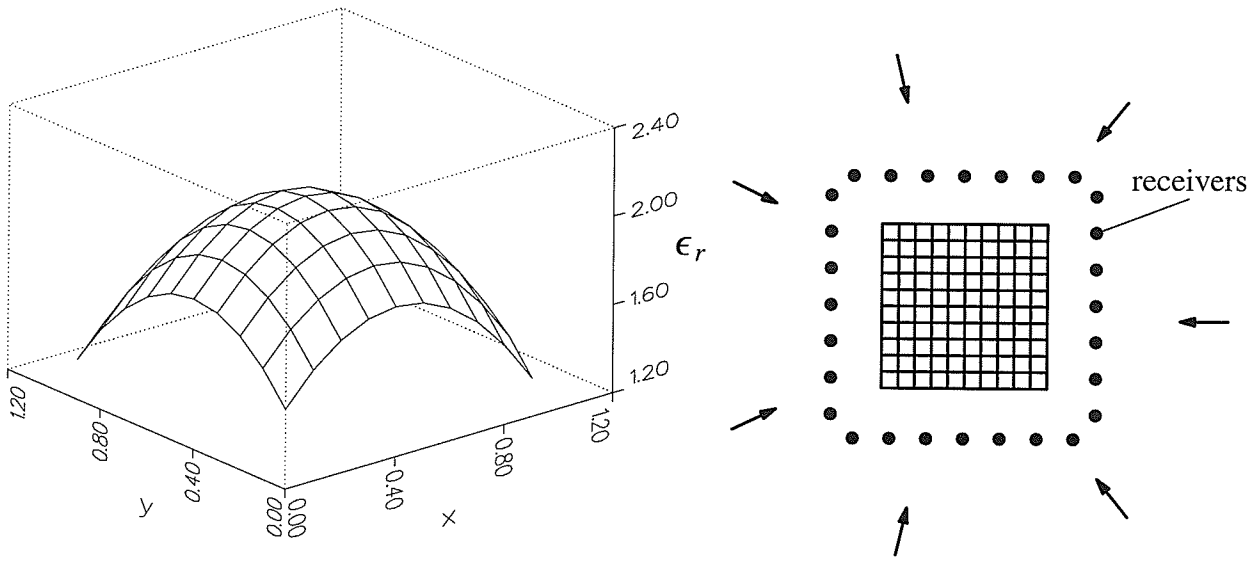

(a) permittivity profile. (b) discretization grid.

Fig. 4.1 : The grid and the permittivity distribution of example 1.

Example 2 – Two dielectric cylinders of different square cross sections are placed inside a square region of investigation. The region is divided into 36 cells (cell size $0.2\lambda \times 0.2\lambda$), as shown in Fig. 4.2. The permittivity of one cylinder is $\epsilon_r = 2$ and that of the other one is $\epsilon_r = 2 - j2.5$. The illumination is provided by a line

source parallel to the cylinders. The line source is placed successively at different positions which are equally spaced around the region at a distance of 2.7λ from the center of the region. The scattered field is measured by using a number of receivers equally spaced on a circular cylinder of diameter 2.2λ, coaxial with the investigation region.

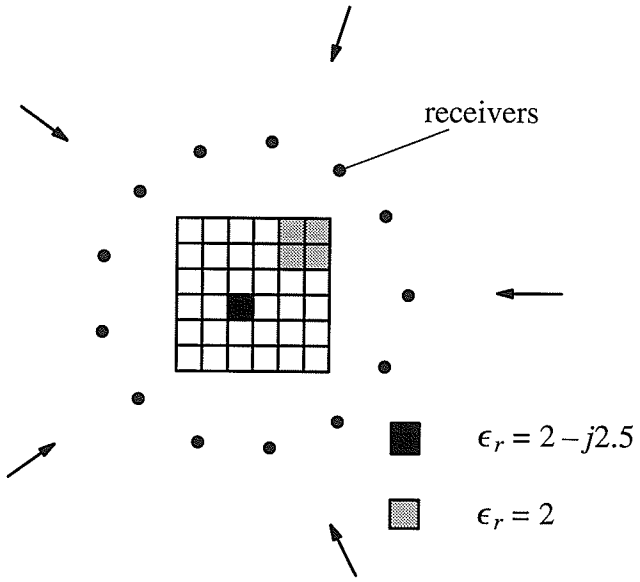

Fig. 4.2 : The grid and the permittivity distribution of example 2.

Example 3 – A dielectric cylinder with a step discontinuity in its permittivity distribution is placed inside a square region of investigation. The region is divided into 36 cells (cell size $0.2\lambda \times 0.2\lambda$) and the dielectric permittivity distribution are shown in Fig. 4.3. The illumination is provided by a line source parallel to the cylinders. The line source is placed successively at different positions which are equally spaced around the region at a distance of 2.7λ from the center of the region. The scattered field is measured by using a number of receivers equally spaced on a cir-

cular cylinder of diameter 2.2λ , coaxial with the investigation region.

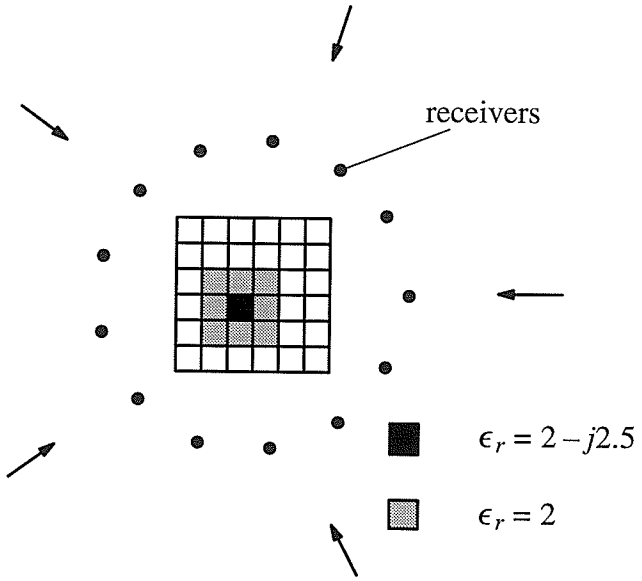

Fig. 4.3 : The grid and the permittivity distribution of example 3.

A parameter s of the relative error in the computed scattered electric field at each iteration step is defined as

$$s = \sqrt{\sum_{l=1} \| \Delta \mathbf{E}_l^s \|^2 / \sum_{l=1} \| \mathbf{E}_l^s \|^2} \tag{4–47}$$

where the summations run over all applied illuminations. A relative error of reconstruction r for the permittivity ϵ is defined as

$$r = \sqrt{\sum_{k} |\Delta \epsilon_k|^2 / \sum_{k} |\epsilon_k|^2} \tag{4–48}$$

where the summations run over all the cells in the investigation region. The computed values of s and r at each iteration step are used to show the numerical convergence and the stability of the iterative process. The regularization parameter g is determined by numerical experiment. Gener-

ally it is big at the beginning of the iterative process and then decreases to smaller values. The numerical computation is performed on a SPARC station 2/SUN–UNIX system.

For the first example, the current refinement algorithm with the Born iterative technique is used in computation and the results are presented in Fig. 4.4. Seven illuminations and 28 receivers are used in the experiment. For the current refinement algorithm, in order to speed up the convergence, a larger regularization parameter $g = 6 \times 10^{-3}$ is used in the 2nd to 9th iterations, except 6×10^{-4} for the first iteration. The regularization parameter g is reduced to 2.7×10^{-3} after the 9th iteration and to 2.3×10^{-3} after the 13th iteration. The results obtained by the Born iterative method are also presented in Fig. 4.4. The regularization parameter used in the Born iterative method is 6.5×10^{-3} except 6×10^{-4} for the first iteration. The regularization used in the current refinement algorithm is weaker than the one used in the Born iterative method. To make a comparison, the regularization parameter used in the current refinement method is also used in the Born iterative method and the results are shown Fig. 4.5. When the smaller regularization is employed with the Born iterative method, the iterative process becomes divergent. From these two numerical simulation results, it can be seen that the current refinement technique improves the convergence rate of the iterative process and has better numerical stability.

The case of the addition of noise in the measured data is also computed by using the same algorithms. In the computation, a Gaussian noise with a signal–to–noise ratio of 20 dB is added to the scattered field. Due to the effect of noise, a stronger regularization has to be applied to suppress the effect of noise. The reconstruction results obtained by using the current refinement algorithm with the Born iterative technique and the Born iterative method are shown in Fig. 4.6 and Fig. 4.7. For the results shown in Fig. 4.6, the regularization parameter is 6×10^{-4} at the first iteration, and reduced to 5×10^{-3} from the 2nd iteration. The results shown in Fig. 4.7 are obtained by using the same regularization as the one corresponding to Fig. 4.6 in the first seven iterations and then, the regularization parameter g is reduced to 3×10^{-3} after the 7th iteration. These two results show that the current iterative technique improves the convergence rate of the

iterative process and provides a better reconstruction.

For the second and the third examples, the current refinement procedure with the Newton iterative technique is used in the numerical experiment. Five illuminations and 13 receivers are used. For the second example, without noise in the measured data, the results obtained by the current refinement algorithm with the Newton iterative technique and the Newton iterative method are presented in Figures 4.8 – 4.10. Except 6×10^{-4} for the first iteration, the regularization parameter is 10^{-9}, 10^{-11} and 10^{-13} for Figures 4.8, 4.9 and 4.10, respectively. Although the regularization parameter varies in a wide range, the current refinement algorithm provides a better reconstruction and a better convergence rate. For the third example, without noise in the measured data, the results obtained by these two algorithms are presented in Fig. 4.11 and Fig. 4.12. For the results shown Fig. 4.11, the regularization parameter is 6×10^{-4} for the first iteration, 2×10^{-3} after the first iteration, 10^{-4} after 4th iteration, and 10^{-5} after 7th iteration. For the results shown Fig. 4.12, the regularization parameter is 6×10^{-4} for the first iteration, 10^{-6} after the first iteration and 10^{-11} after 9th iteration. In Fig. 4.11, the results of object function reconstruction obtained by the current refinement algorithm with the Newton iterative technique is slightly better than those by the Newton iterative method. Once the regularization parameter g is reduced, the iterative process for the Newton iterative method is divergent as indicated in Fig. 4.12. In contrast, the iterative process for the current refinement algorithm becomes more convergent. The better numerical stability of the current refinement algorithm permits the employment of a weaker regularization to obtain a higher convergence rate. From these results, it can be seen that the current refinement technique improves not only the results of the object reconstruction but also the numerical stability of the iterative process.

The presence of noise in the scattered electric field is also considered. In the computation, a Gaussian noise with a signal–to–noise ratio of 20 dB is added in the scattered field. In contrast to example one, the permittivity distributions of the second and third examples are discontinuous. Therefore, a larger number of high spatial frequency components of the object function have to be

reconstructed.

To investigate the computational behavior of the current refinement algorithm for example two, three different regularizations and two different measurement arrangements are used. The reconstruction results for 5 illuminations and 13 receivers are shown in Figures 4.13 – 4.15 and the results for 22 illuminations and 23 receivers are shown in Figures 4.16 – 4.18. Except 6×10^{-4} for the first iteration, the regularization parameter is 10^{-3} for Fig. 4.13 and Fig. 4.16, 10^{-7} for Fig. 4.14 and Fig. 4.17, and 10^{-11} for Fig. 4.15 and Fig. 4.18. The results obtained by the current refinement algorithm are better than those by the Newton iterative method as shown in figures 4.13 – 4.15. Owing to the presence of noise in the measured data, the reconstruction errors with different regularization values are high. Increasing the number of the illuminations and measurements provide more information about the object. It improves the results of the reconstruction greatly. In Fig. 4.16, the difference between the two methods in terms of the convergence of the iterative process and the resolution of image are obvious and the current refinement algorithm is still better. From Fig. 4.17 and Fig. 4.18, it can be seen that the current refinement algorithm is faster than the Newton iterative method.

For the third example, the current refinement procedure with the Newton iterative technique is used in the numerical computation. Two different illuminations and 13 receivers are used in the experiment. The reconstruction results for 5 illuminations are shown in figures 4.19 – 4.21. Except 6×10^{-4} for the first iteration, the regularization parameter is 2×10^{-3}, 10^{-3} and 10^{-4} for figures 4.19, 4.20 and 4.21, respectively. The current refinement algorithm is faster than the Newton iterative method as indicated in these figures. It also provides better images of the reconstructed object than the ones by the Newton iterative method even if values of the parameter s for both algorithms are almost the same at the final stage of the process. The errors of the final reconstruction by using the current refinement algorithm are about 13% for the three regularization cases and are too high to be accepted. This is the same as the case for the second example. It is due to less illuminations and measurements used. The situation is improved by increasing the illuminations and measurements to reduce the effect of noise present in the measured data. When

more illuminations and measurements are applied, a smaller regularization parameter can be employed in the computation and the solution is improved greatly. The numerical results for 22 illuminations and 13 receivers are presented in Fig. 4.22 and Fig. 4.23. Except 6×10^{-4} for the first iteration, the regularization parameter is 10^{-6} for Fig. 4.22, and 10^{-8} for Fig. 4.23. The errors in the final reconstruction by the current refinement algorithm are about 6% for these two regularization cases. The results for the Newton iterative method are divergent since the regularization is too weak for it. To find the best results that the Newton iterative method can provide, a set of regularization parameters are used in simulation and the results are presented in Fig. 4.24. Except 6×10^{-4} for the first iteration, the regularization parameter g is 0.05, 0.005, 0.001 and 0.0001, respectively, for the results shown in Fig. 4.24. Only when g is in the range 0.05 to 0.005, is the process using Newton iterative method convergent. Only when g equals 0.005, is the smallest error of reconstruction, i.e. 7%, obtained. Generally speaking, the value of regularization parameter is determined empirically, according to the convergence of the process. For the current refinement algorithm, fewer simulations are needed to determine the appropriate regularization parameter. At the same time, the construction of an appropriate regularization from the simulation results also becomes easier. Therefore, in practice, the equivalent current algorithms are numerically quite efficient.

4.7 Conclusion

In this chapter, the current refinement method is presented. The effect of the errors in the computed electric field on the the solution of the inverse problem is analyzed. From the relation between the errors in the matrix equation for the inverse problem and its solution, a better evaluation of the equivalent current method is found. It can be used to obtain a better estimate of the object function. Numerical simulation for different objects by using this technique, along with the Born and the Newton iterative methods, with different regularization parameters are carried out. The computations show that the application of this current refinement technique improves

the image resolution, the convergence rate and numerical stability of an iterative process. Its application also reduces the sensitivity of the Born and the Newton iterative methods to the change in the value of regularization parameter.

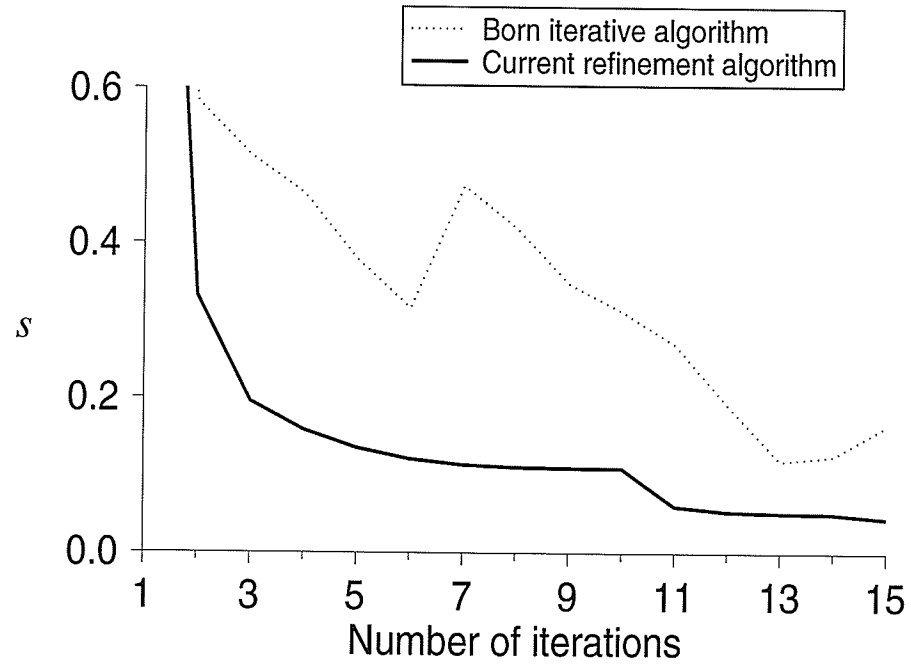

(a)

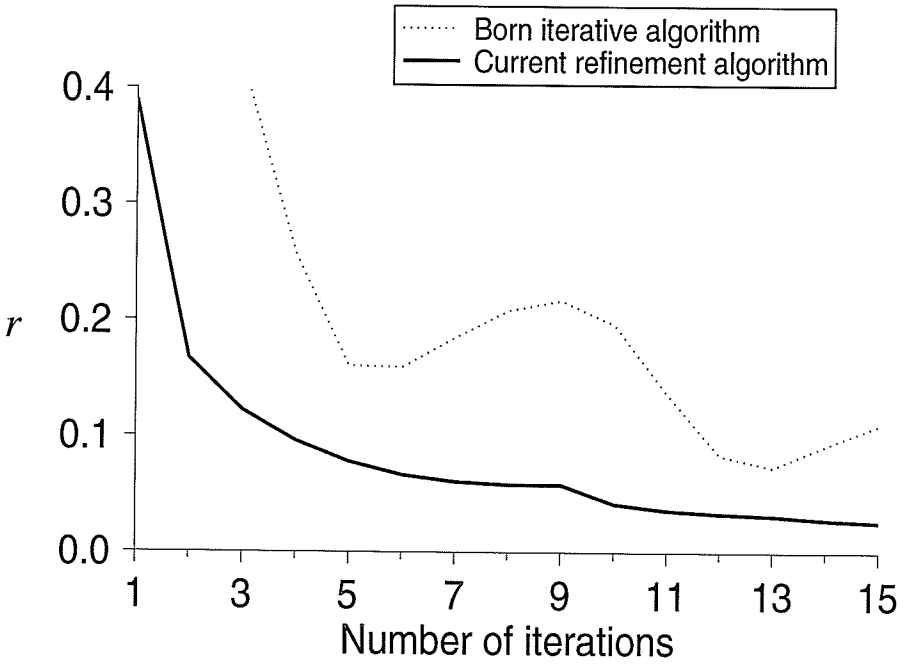

(b)

Fig. 4.4 : Errors s and r for example one with a weaker regularization used in the current refinement algorithm.

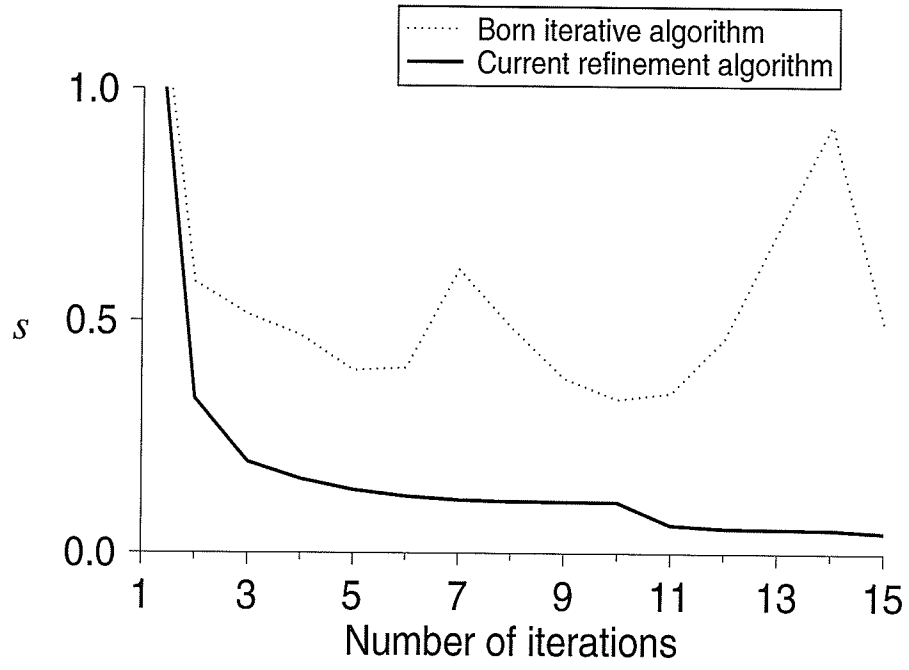

(a)

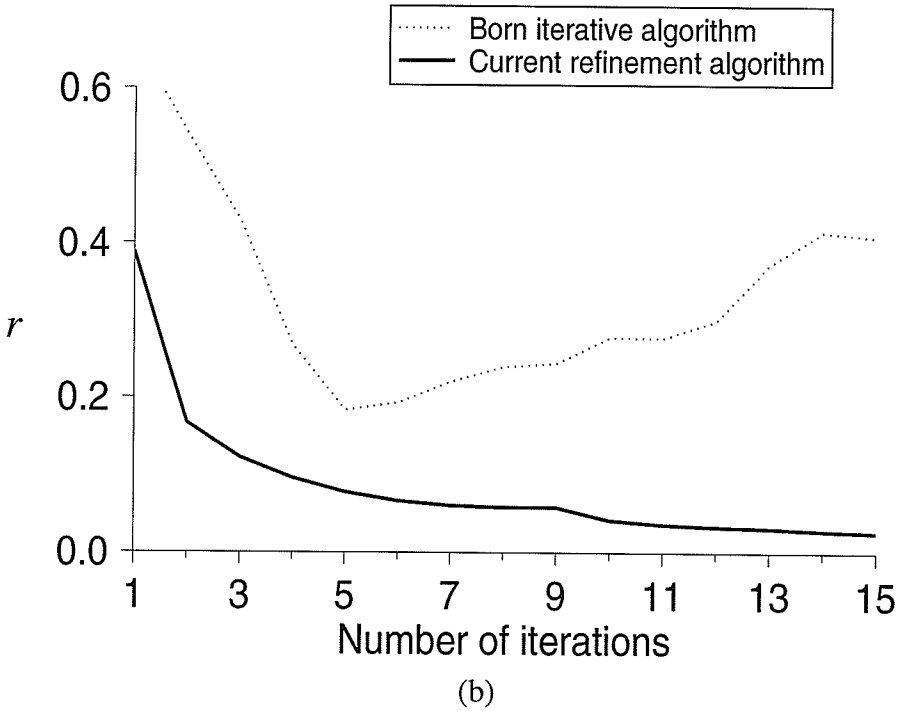

(b)

Fig. 4.5 : Errors s and r for example one with a weaker regularization used in all algorithms.

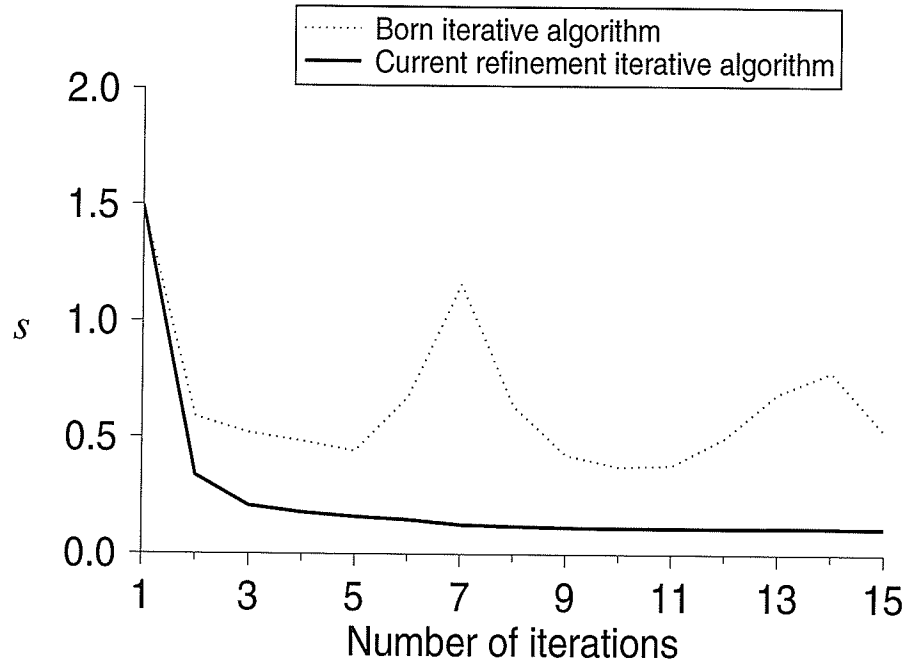

(a)

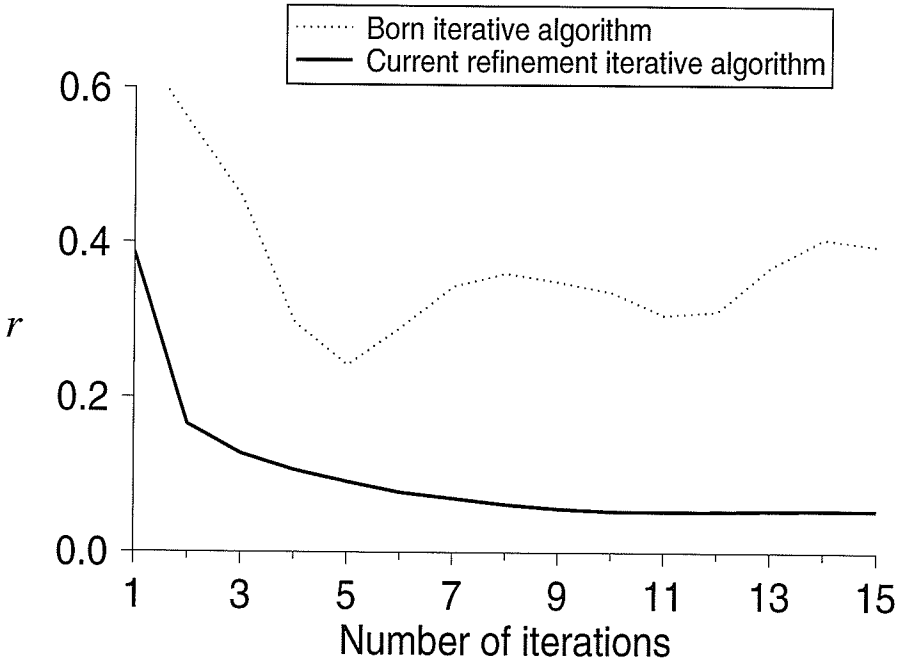

(b)

Fig. 4.6 : Errors s and r for example one in the presence of noise (20dB) in the measured data and $g = 5 \times 10^{-3}$ after the first iteration.

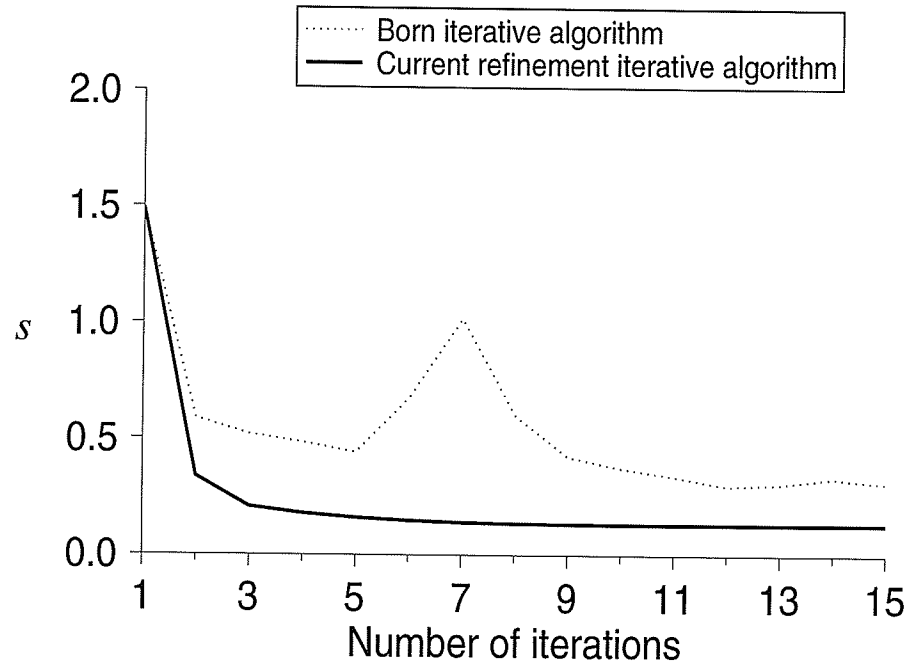

(a)

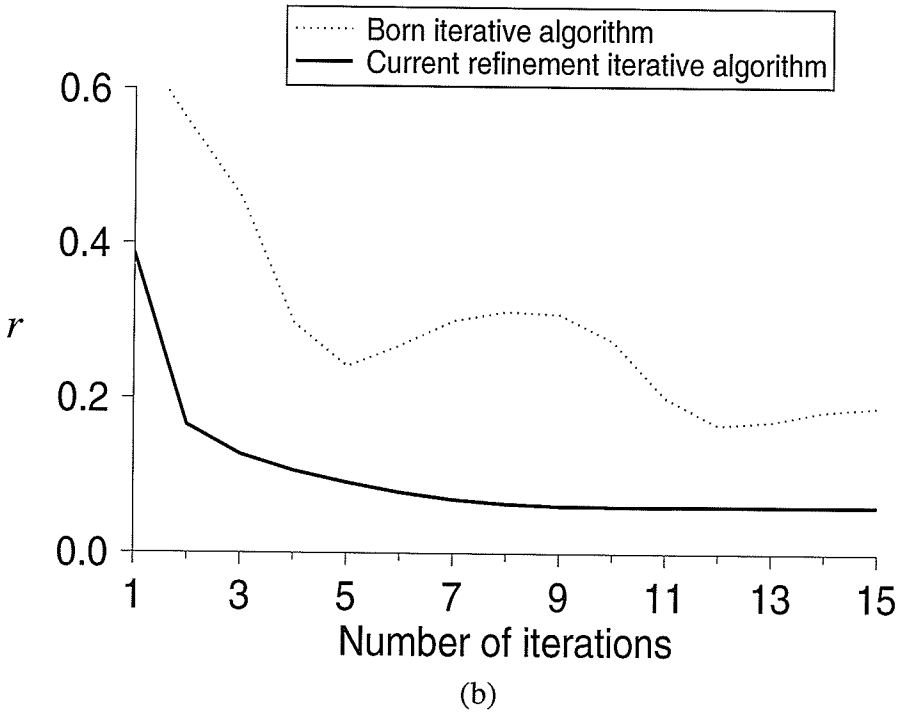

(b)

Fig. 4.7 : Errors s and r for example one in the presence of noise (20dB) in the measured data and $g = 3 \times 10^{-3}$ after the 7th iteration.

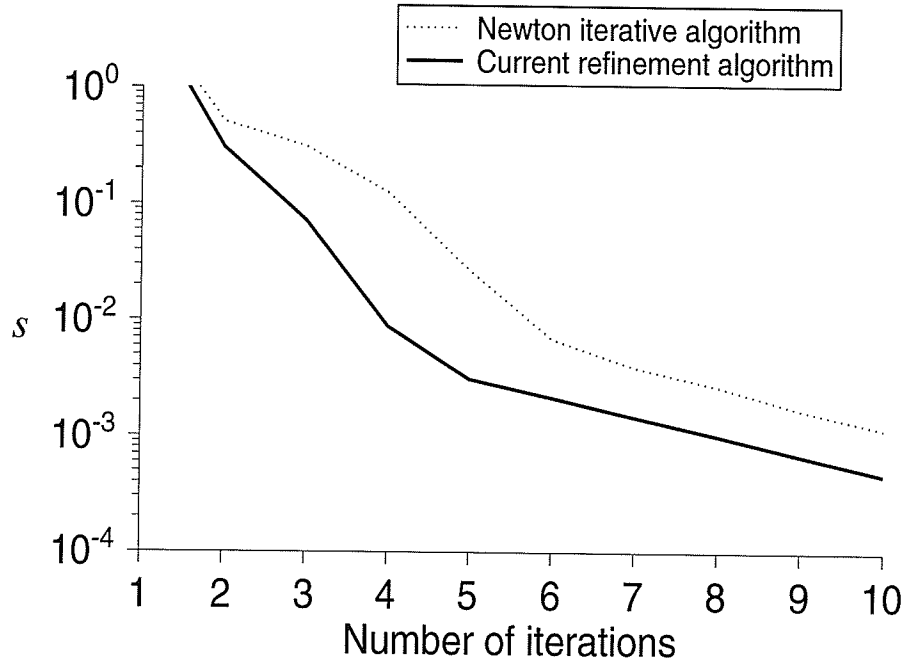

(a)

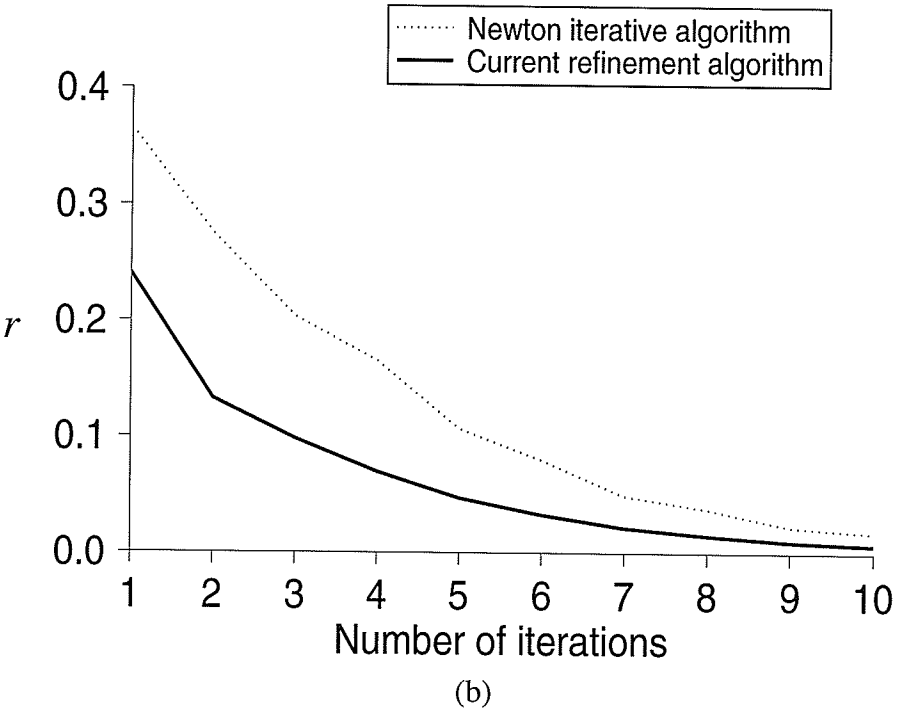

(b)

Fig. 4.8 : Errors s and r for example two with $g = 10^{-9}$ after the first iteration.

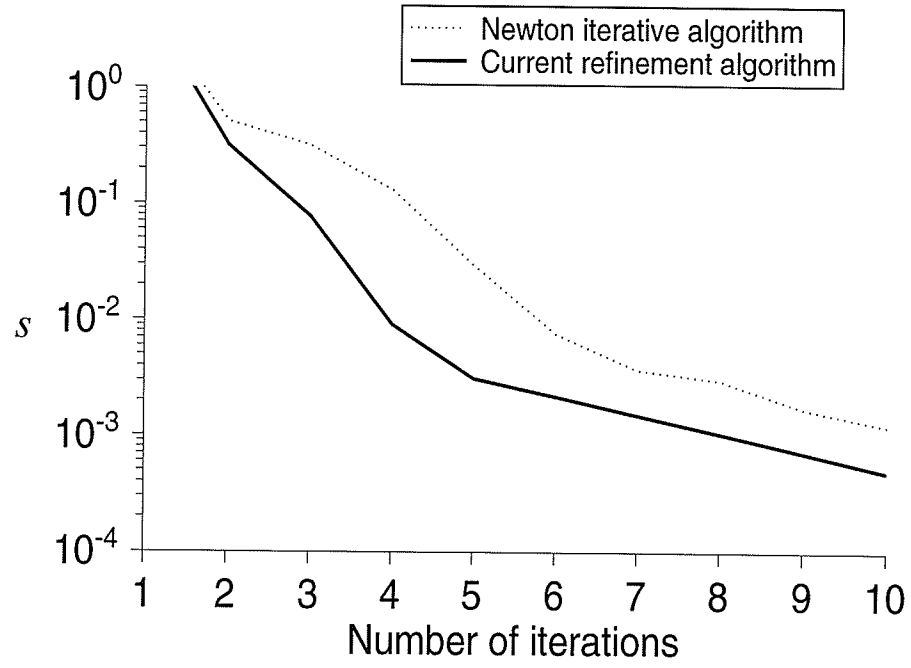

(a)

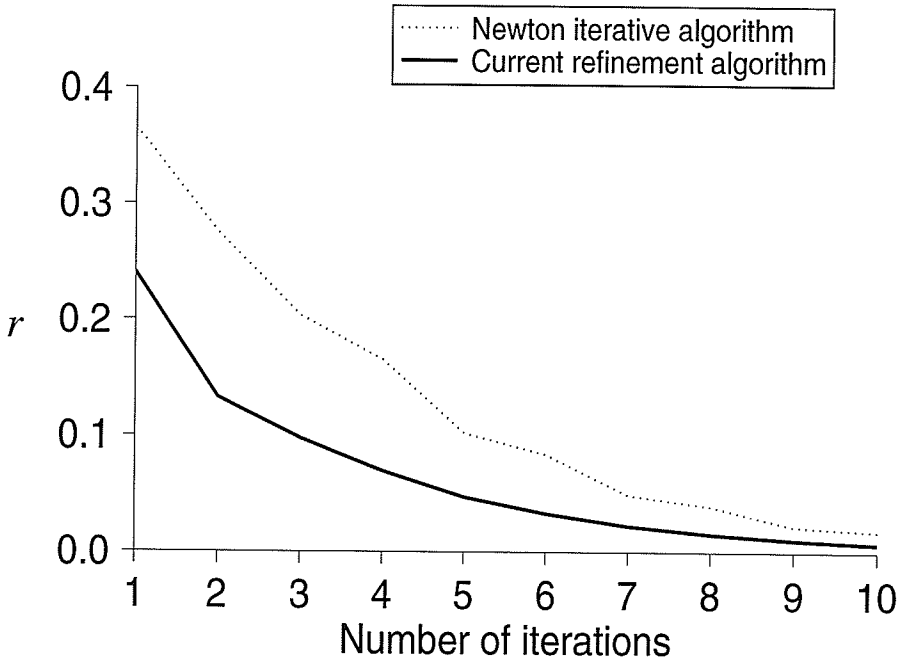

(b)

Fig. 4.9 : Errors s and r for example two with $g = 10^{-11}$ after the first iteration.

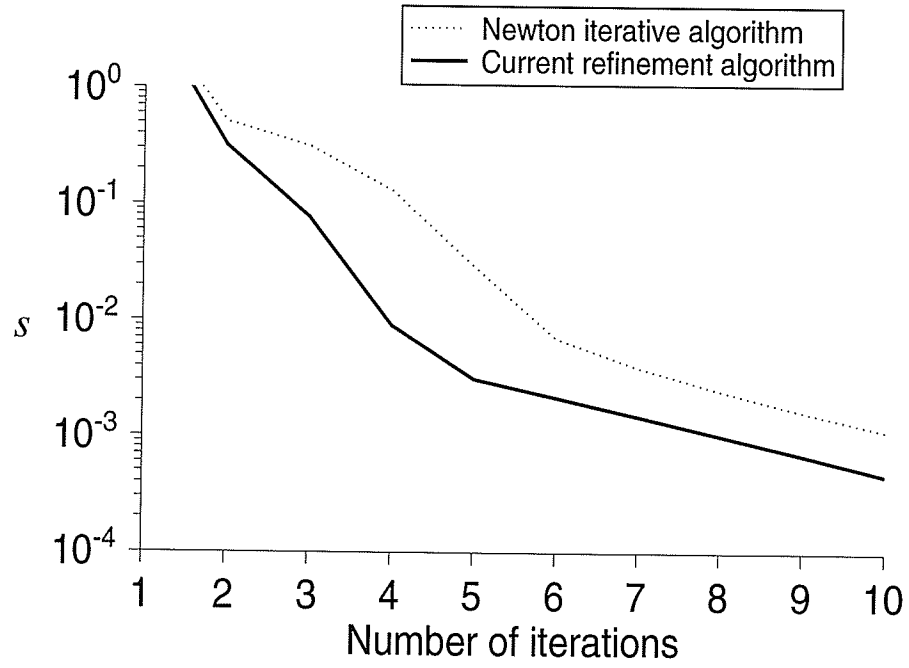

(a)

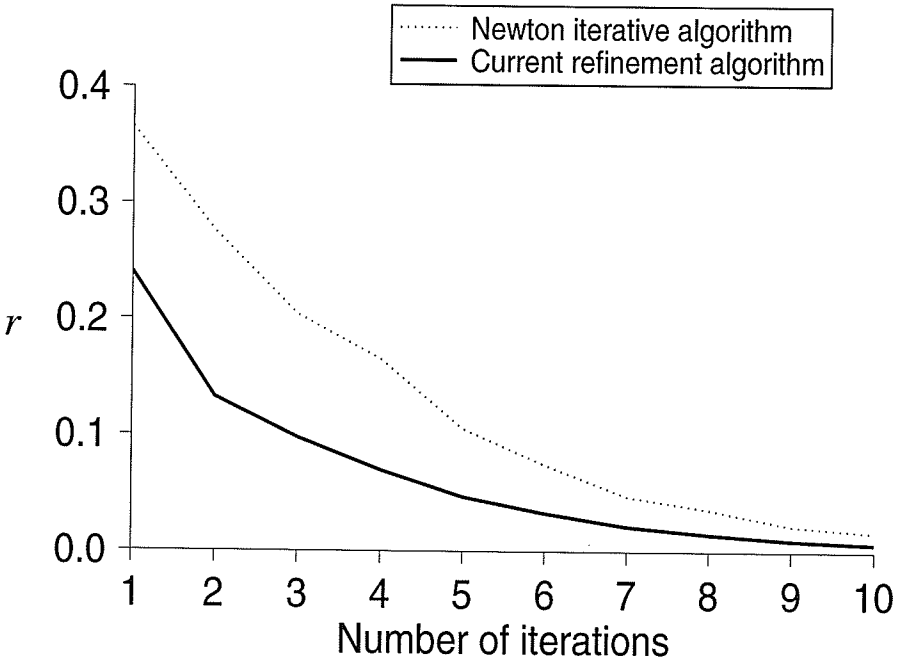

(b)

Fig. 4.10 : Errors s and r for example two with $g = 10^{-13}$ after the first iteration.

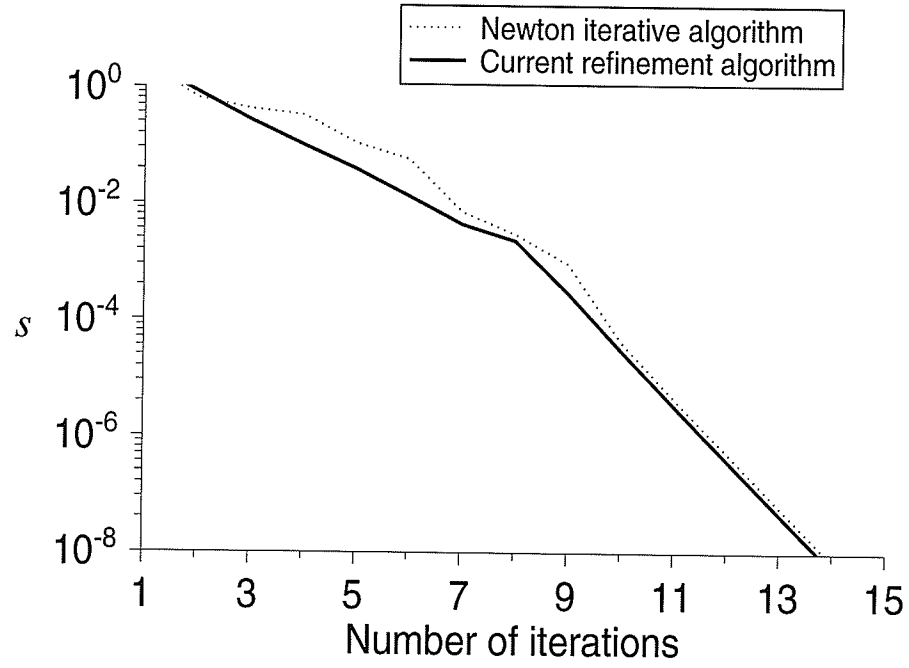

(a)

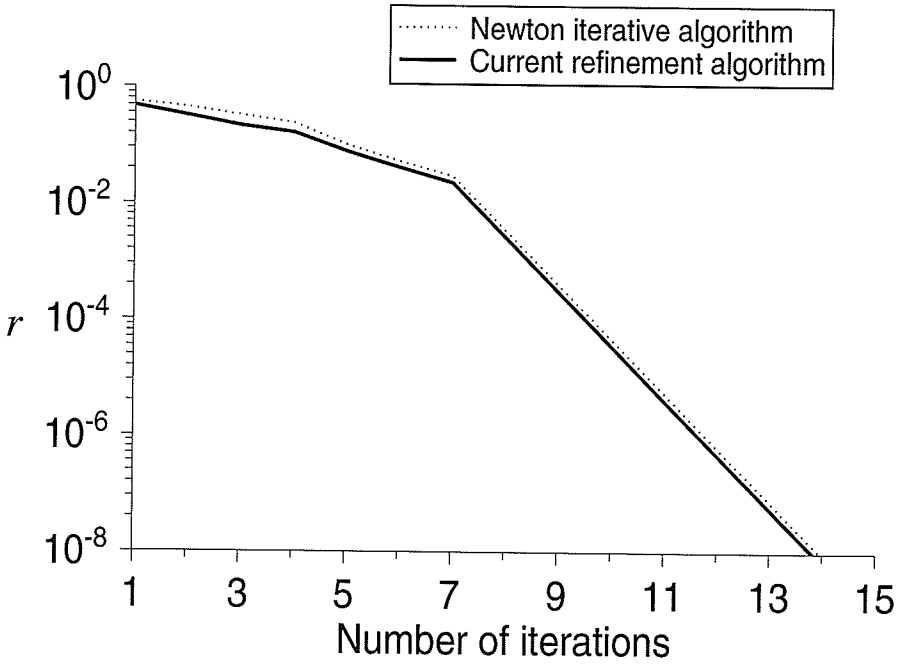

(b)

Fig. 4.11 : Errors s and r for example three with $g = 10^{-5}$ after 7th iteration.

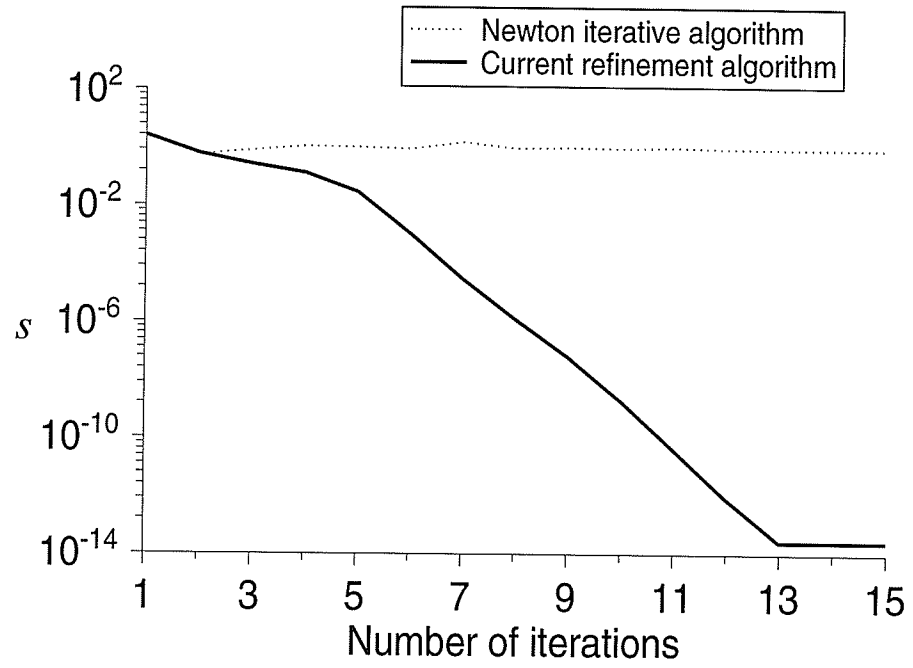

(a)

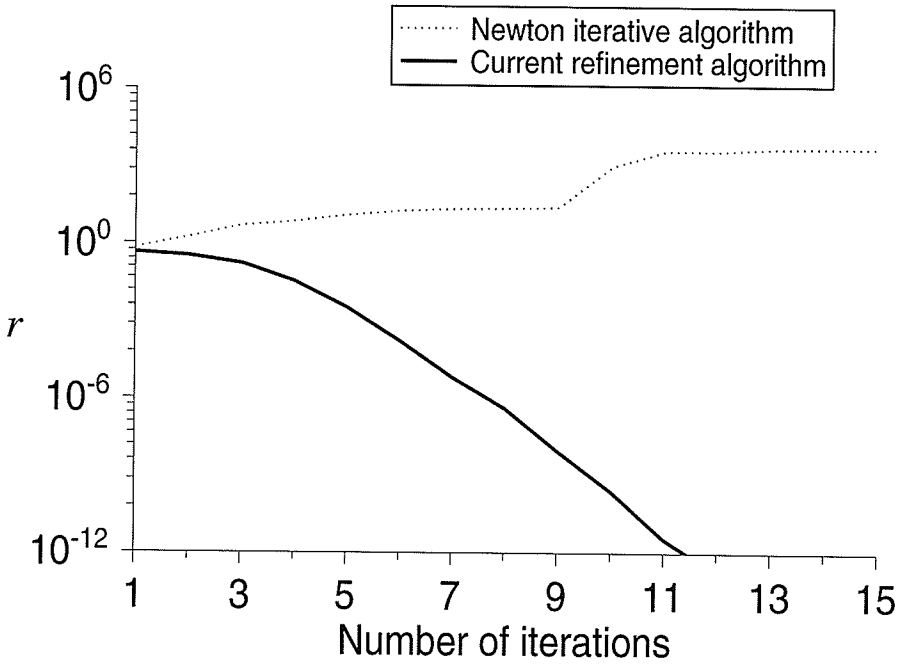

(b)

Fig. 4.12 : Errors s and r for example three with $g = 10^{-11}$ after 7th iteration.

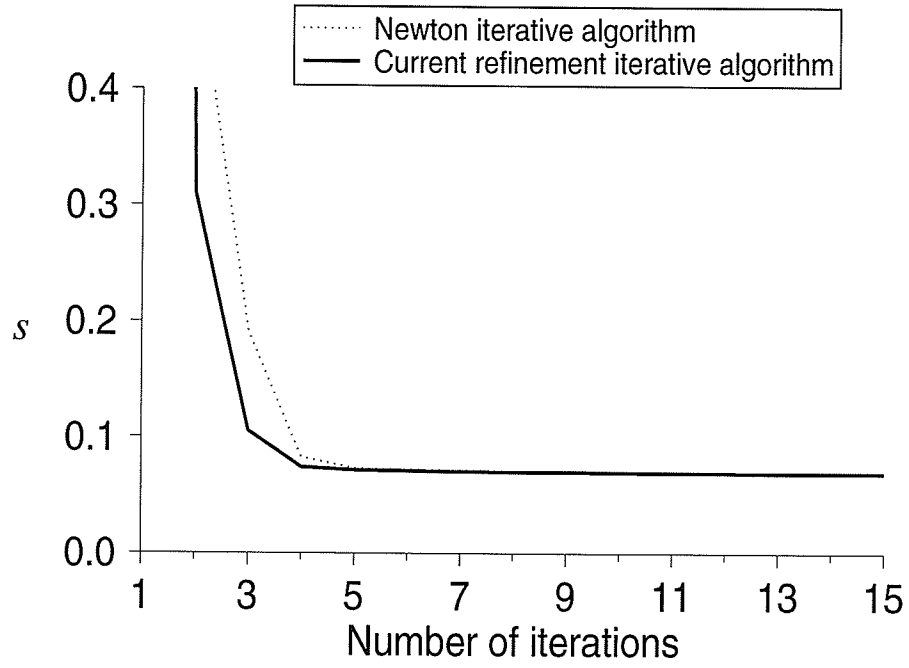

(a)

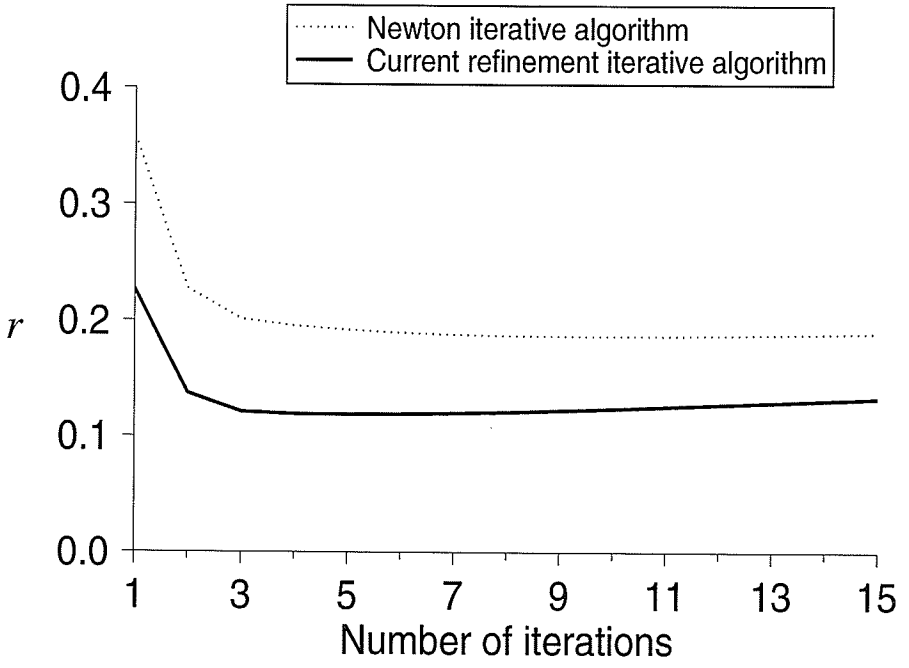

(b)

Fig. 4.13 : Errors s and r for example two in the presence of noise in the measured data: 5 illuminations, 13 receivers, and $g = 10^{-3}$ after the first iteration.

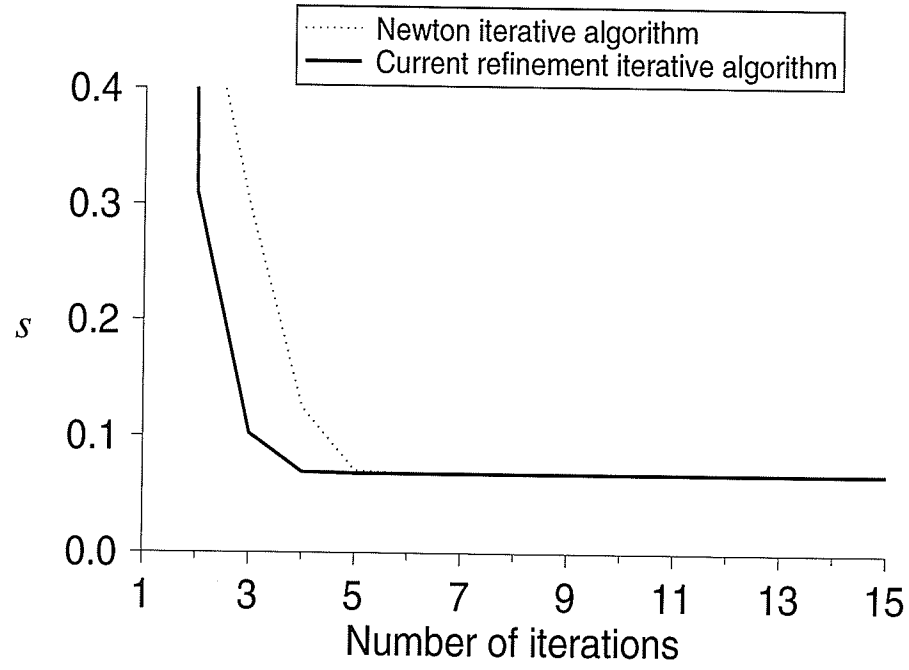

(a)

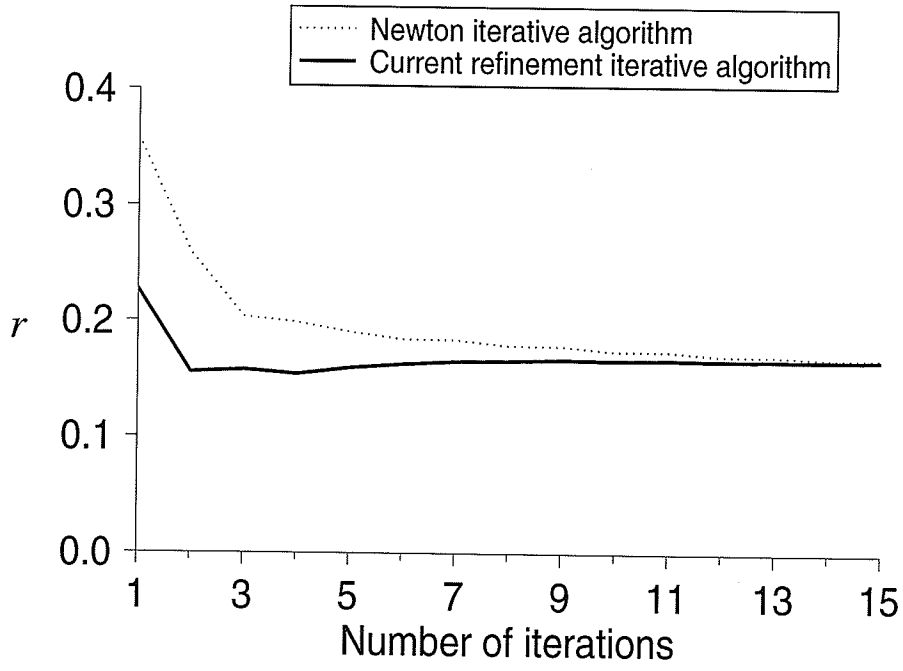

(b)

Fig. 4.14 : Errors s and r for example two in the presence of noise in the measured data: 5 illuminations, 13 receivers, and $g = 10^{-7}$ after the first iteration.

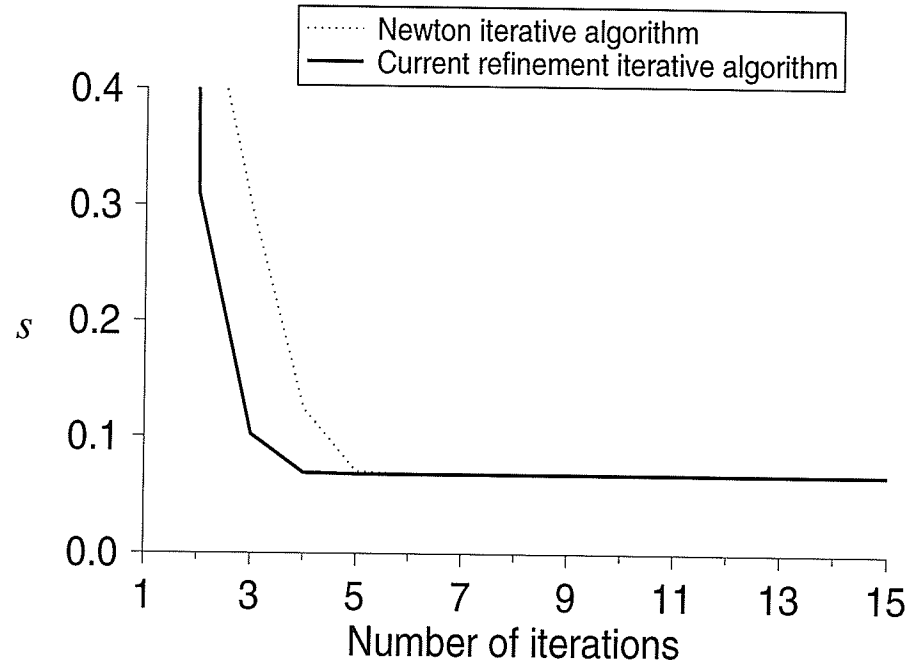

(a)

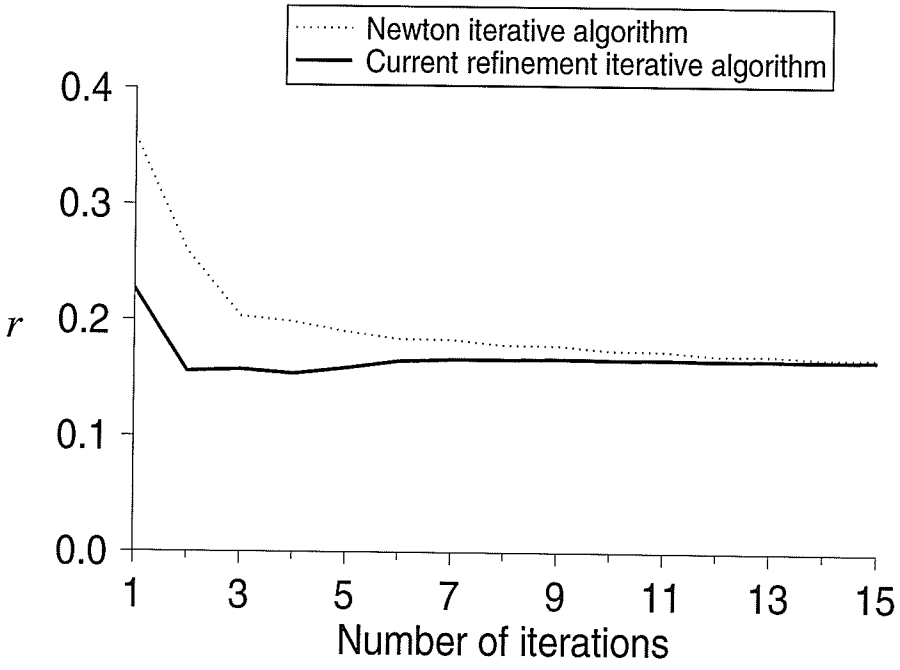

(b)

Fig. 4.15 : Errors s and r for example two in the presence of noise in the measured data: 5 illuminations, 13 receivers, and $g = 10^{-11}$ after the first iteration.

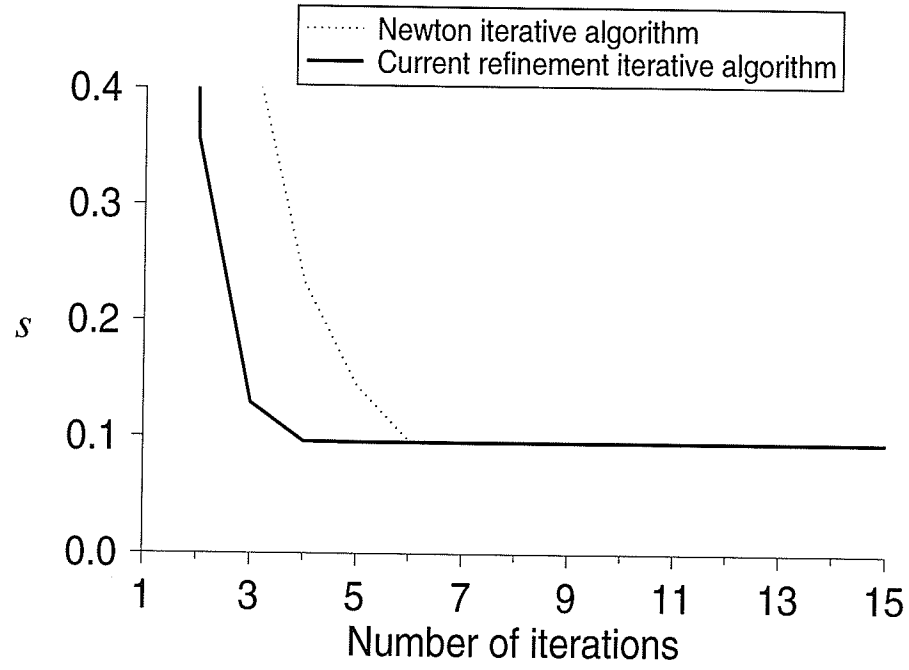

(a)

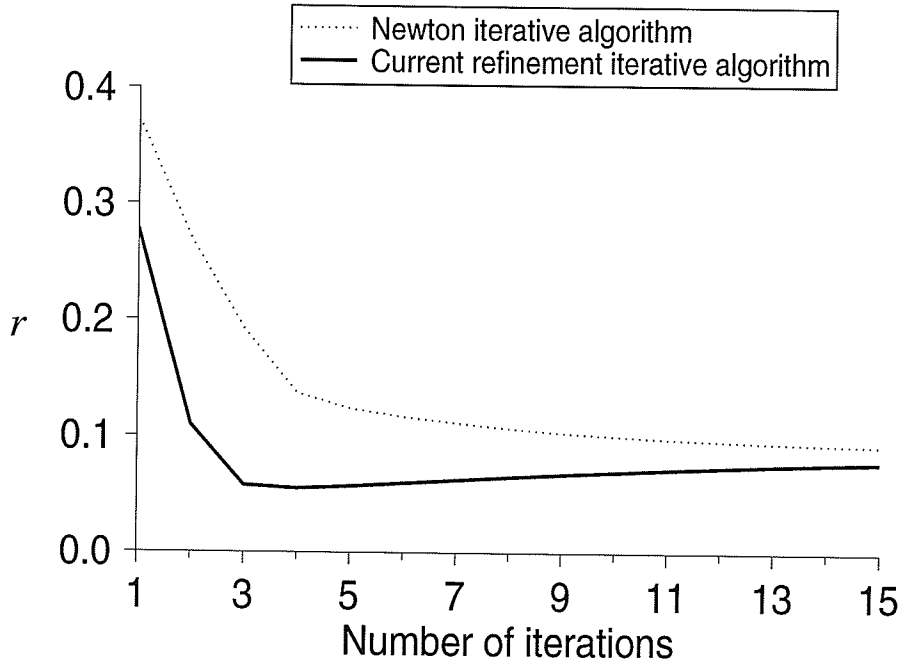

(b)

Fig. 4.16 : Errors s and r for example two in the presence of noise in the measured data: 22 illuminations, 23 receivers, and $g = 10^{-3}$ after the first iteration.

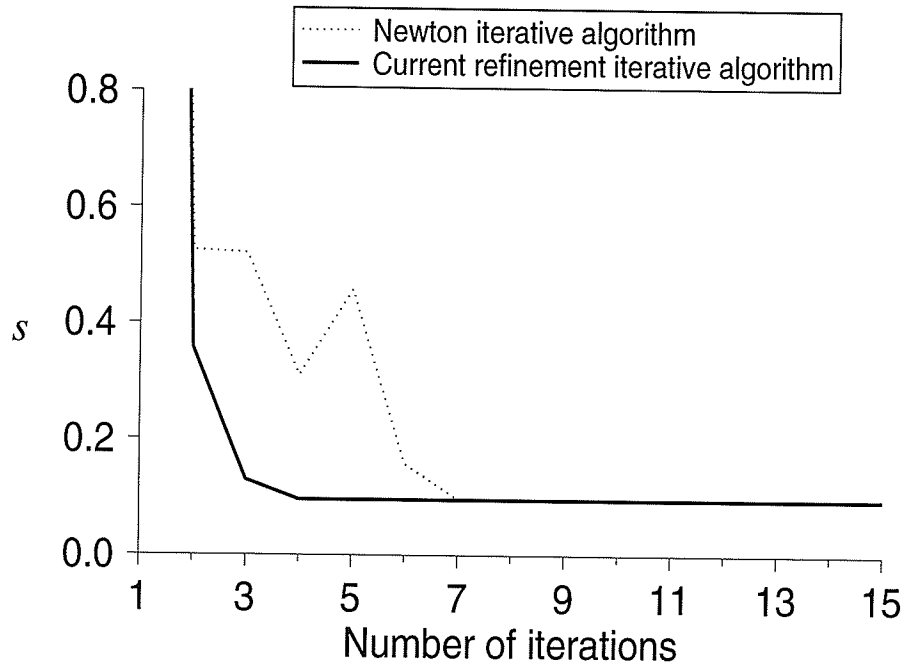

(a)

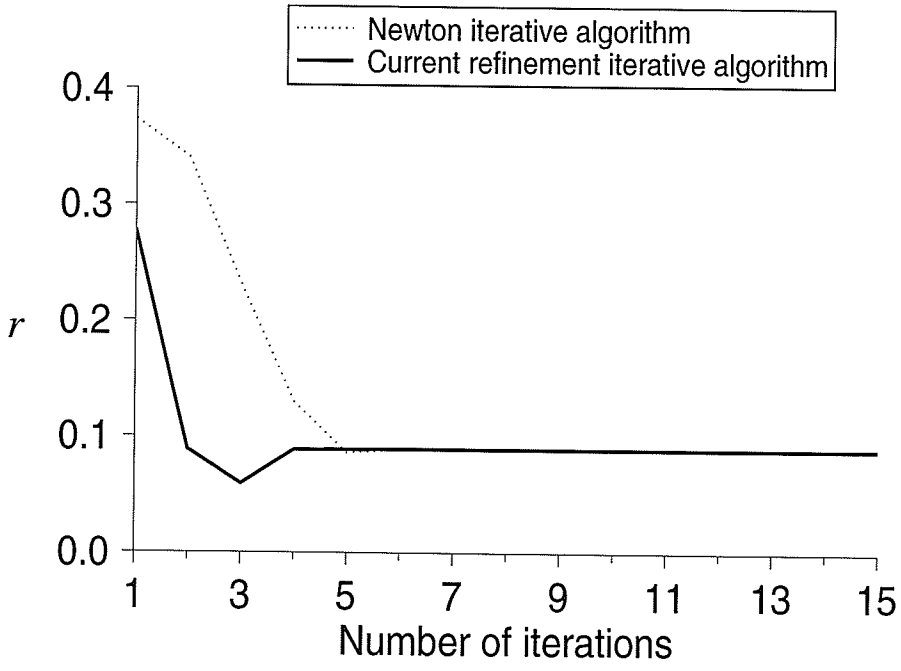

(b

Fig. 4.17 : Errors s and r for example two in the presence of noise in the measured data: 22 illuminations, 23 receivers, and $g = 10^{-7}$ after the first iteration.

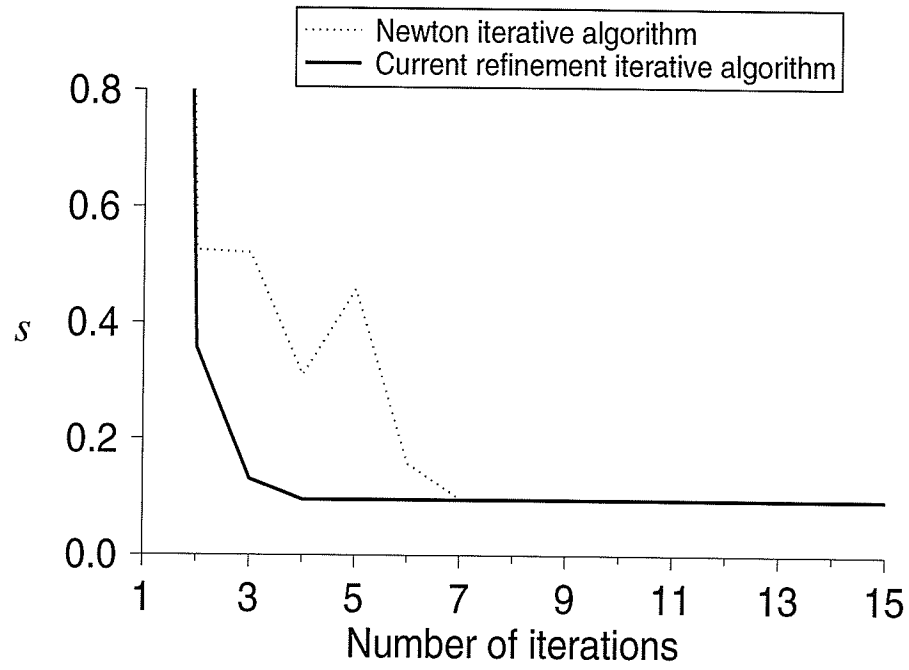

(a)

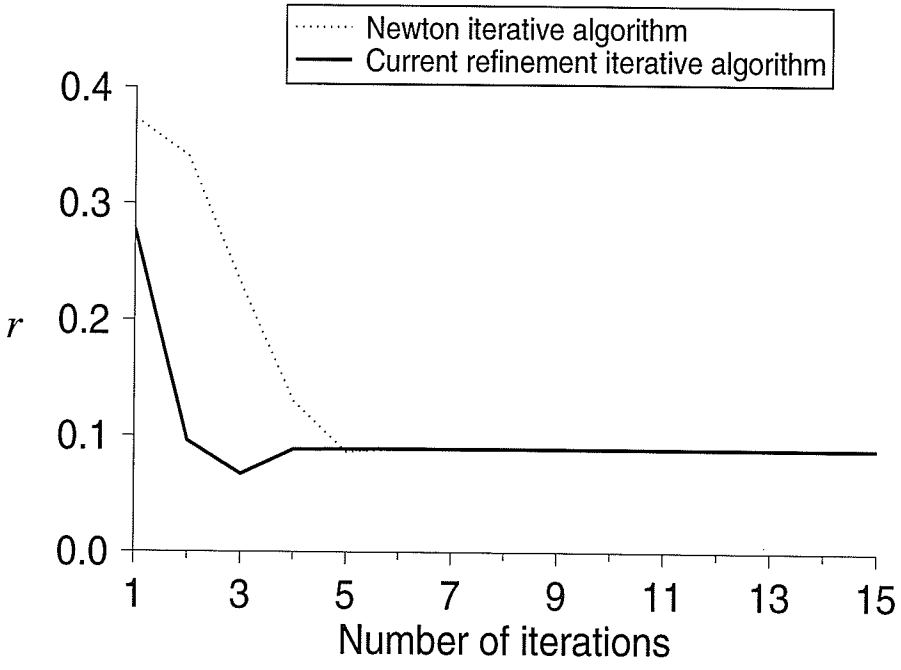

(b)

Fig. 4.18 : Errors s and r for example two in the presence of noise in the measured data: 22 illuminations, 23 receivers, and $g = 10^{-11}$ after the first iteration.

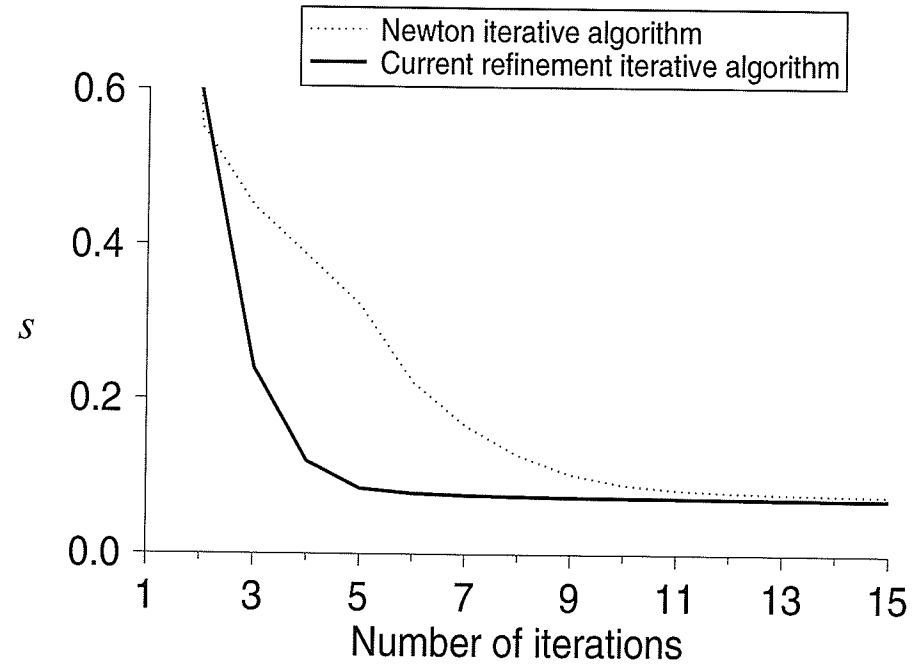

(a)

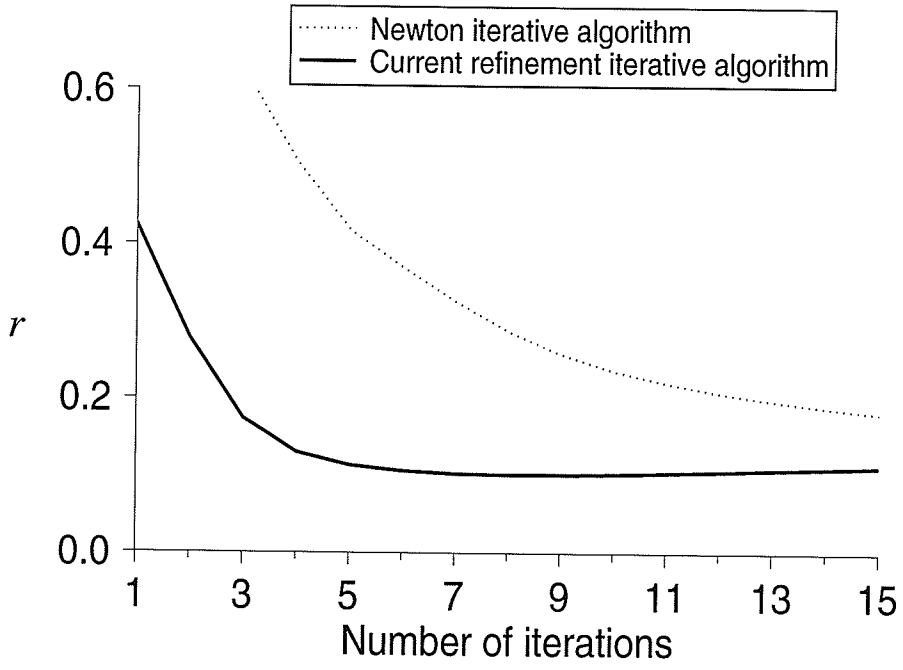

(b)

Fig. 4.19 : Errors s and r for example three in the presence of noise in the measured data: 5 illuminations, 13 receivers, and $g = 2 \times 10^{-3}$ after the first iteration.

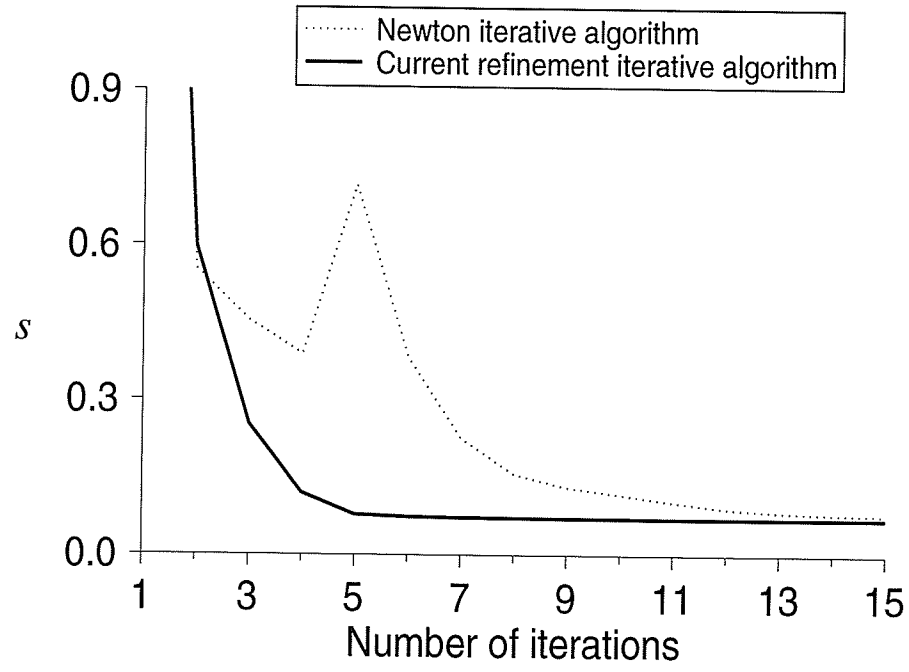

(a)

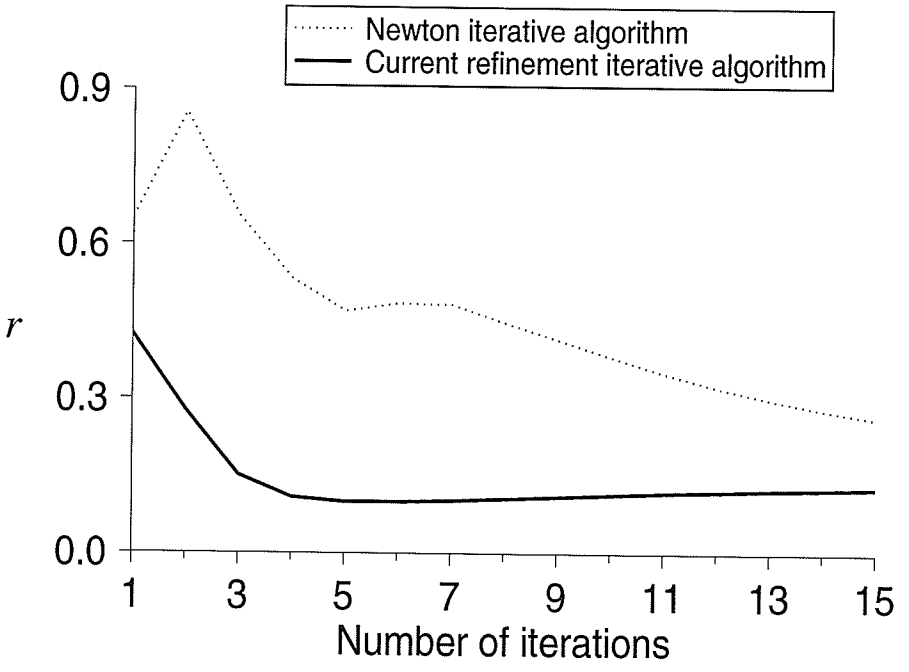

(b)

Fig. 4.20 : Errors s and r for example three in the presence of noise in the measured data: 5 illuminations, 13 receivers, and $g = 10^{-3}$ after the first iteration.

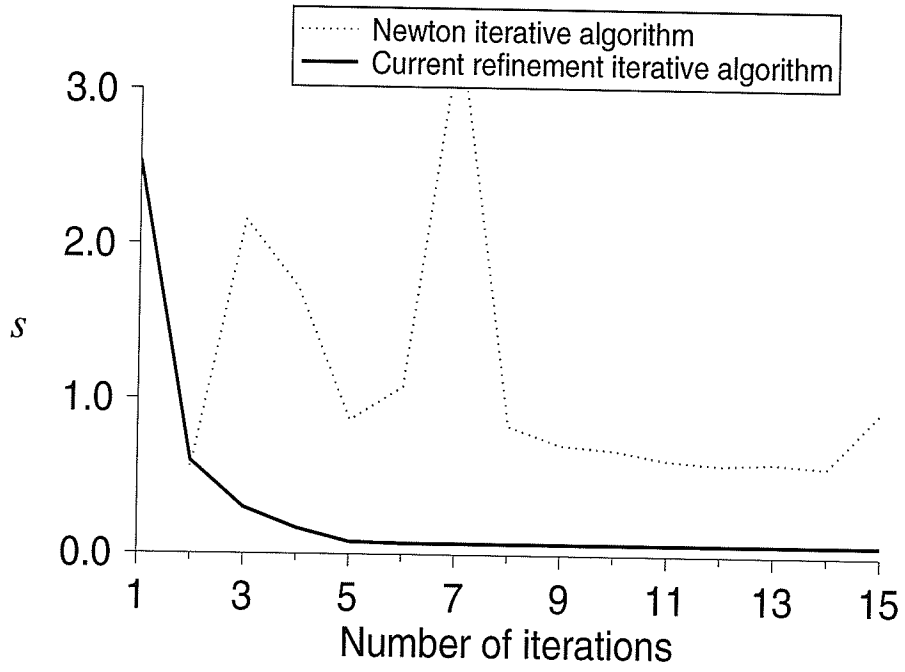

(a)

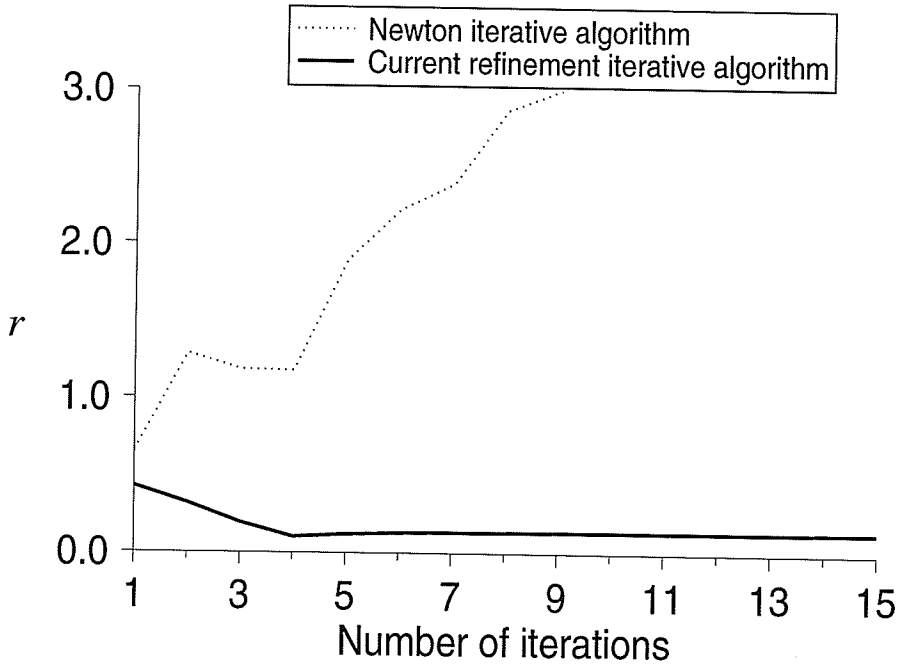

(b)

Fig. 4.21 : Errors s and r for example three in the presence of noise in the measured data: 5 illuminations, 13 receivers, and $g = 10^{-4}$ after the first iteration.

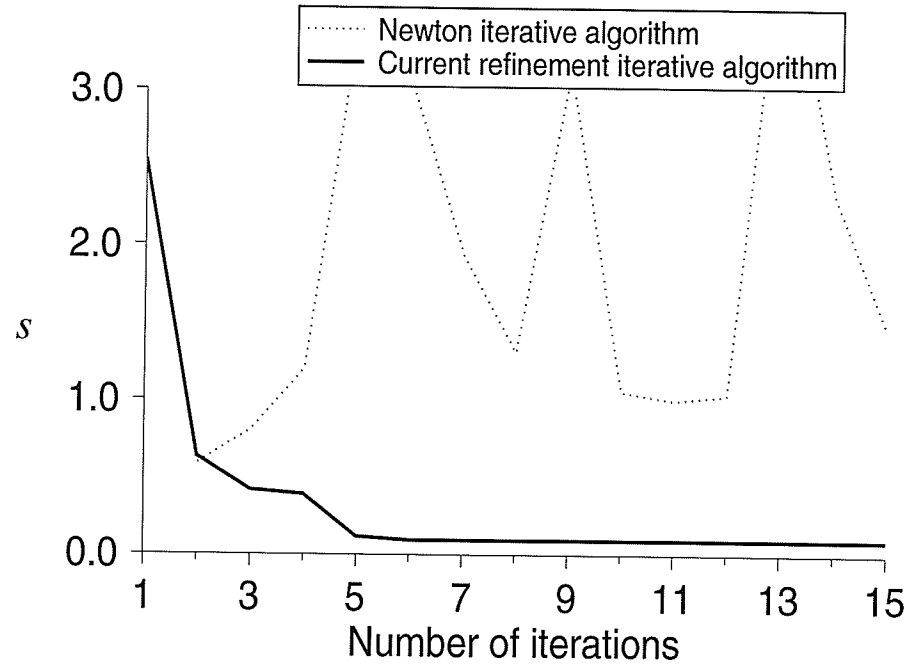

(a)

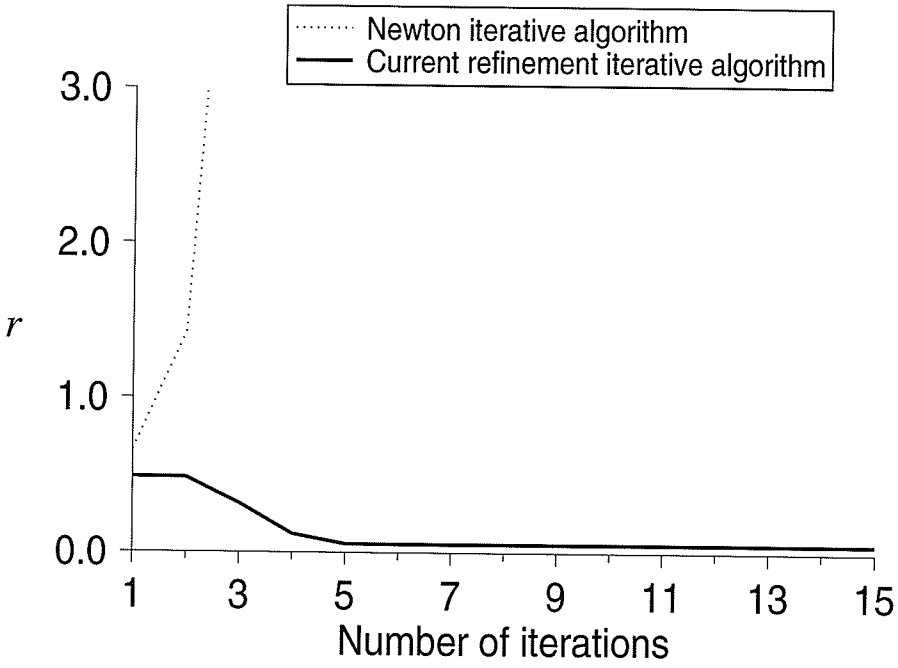

(b)

Fig. 4.22 : Errors s and r for example three in the presence of noise in the measured data: 22 illuminations, 13 receivers, and $g = 10^{-6}$ after the first iteration.

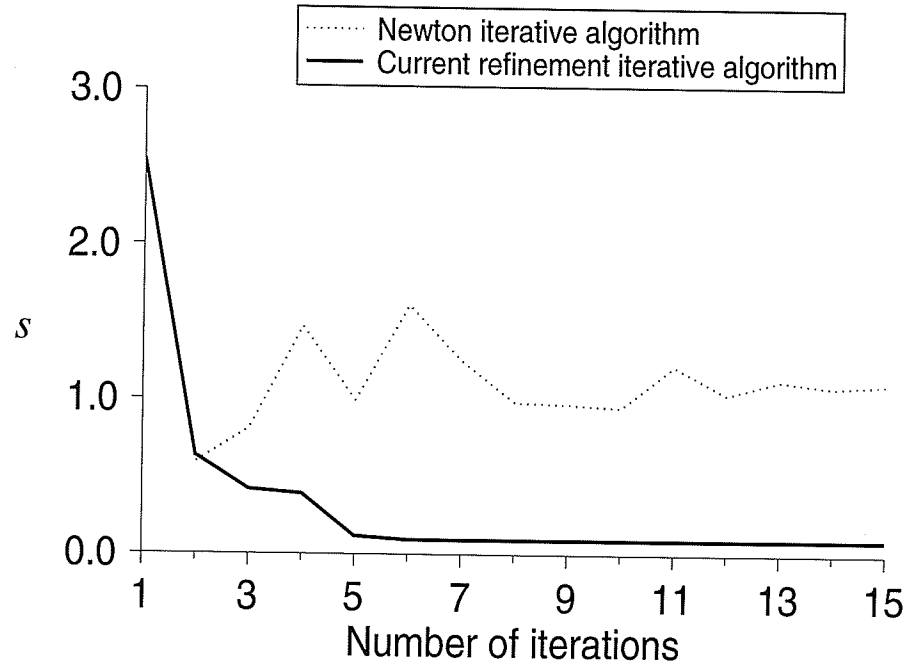

(a)

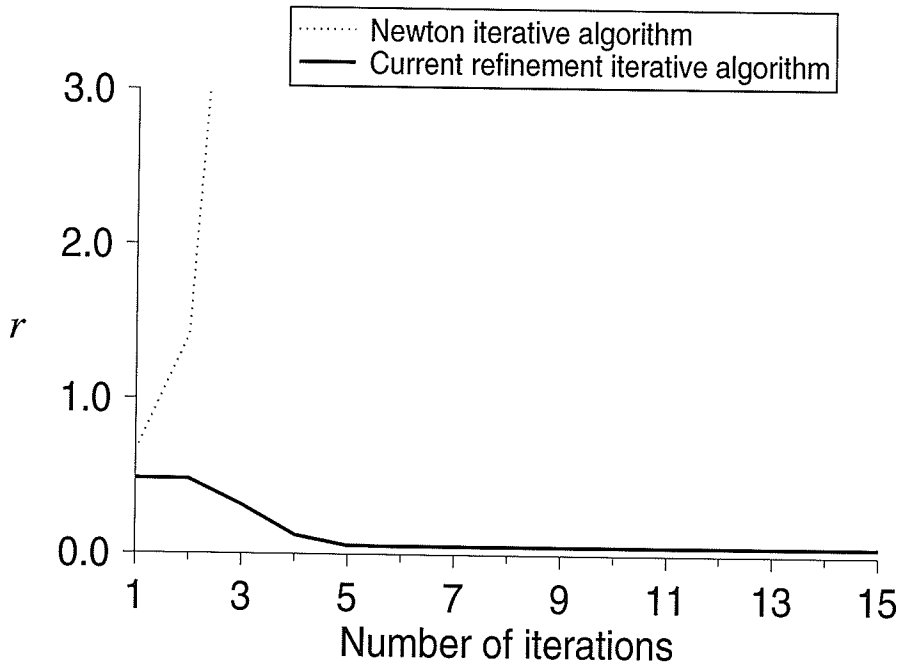

(b)

Fig. 4.23 : Errors s and r for example three in the presence of noise in the measured data: 22 illuminations, 13 receivers, and $g = 10^{-8}$ after the first iteration.

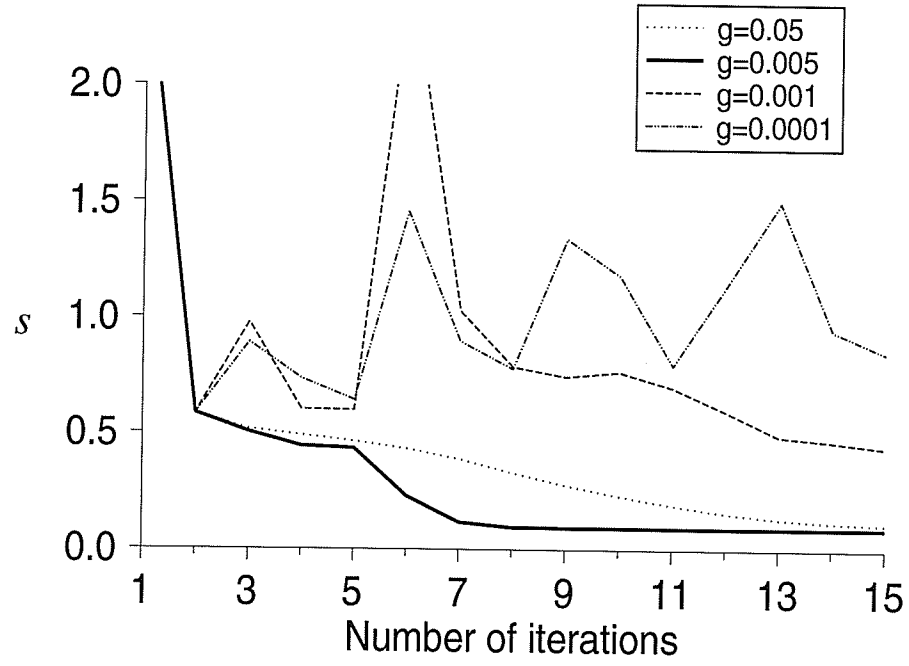

(a)

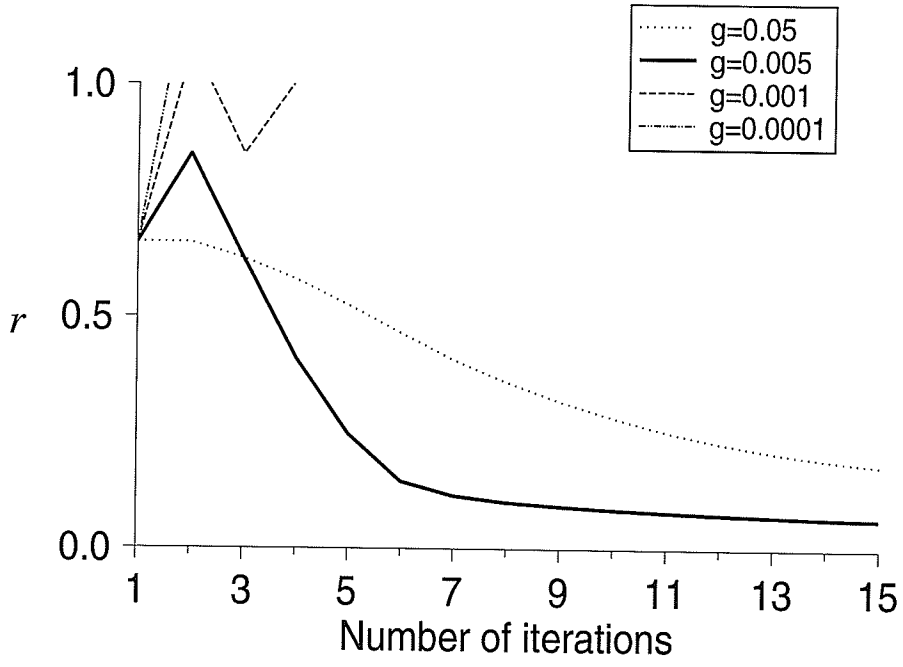

(b)

Fig. 4.24 : Errors s and r for example three in the presence of noise in the measured data: 22 illuminations, 13 receivers, and using the Newton iterative method.

Chapter 5
Prediction–correction Algorithm

5.1 Introduction

In the iterative methods for the electromagnetic imaging, a succession of ill–conditioned linear matrix equations have to be solved. The accuracy of reconstruction in each iteration is decided by the method used for solving the ill–posed inverse problem and the estimate of the object function used in the direct problem. Because of the numerical difficulty in inverting an ill–conditioned matrix equation, regularization is applied to stabilize the computation. The regularization can stabilize the iteration process and suppress the effect of the noise present in the data. On the other hand, a strong regularization filters out useful information present in the high spatial frequency components and decreases the solution accuracy. Therefore, in engineering computation, an appropriate regularization parameter has to be chosen. It is generally a trade–off between the stabilization of the iteration process and the imaging accuracy. As for the estimate of the object function, it determines the accuracy of the total electric field inside the object. In the solution of the inverse problem, the degree of accuracy of the object function reconstruction is greatly dependent on the accuracy of the total electric field. In chapter 4, the algorithm based on the equivalent current refinement is presented to provide a better evaluation of the object function. The numerical experiments prove that it improves the resolution of the image and at the same time, the convergence of the iterative process. However, in that algorithm, the improvement is based on the preceding iteration results. The degree of improvement of the current refinement technique is limited. For a given iteration step, the convergence of the succeeding iterations depends on the results of that iteration regardless of the results obtained before. For the Born and Newton iterative methods, the convergence of the iterative process is also determined by the results of each iteration. The regularization used to stabilize the iterative process has to be strong enough to

make the iterative process numerically stable.

In this chapter, we present a prediction–correction algorithm in which the previous iteration results are used to make a prediction of the object function for the next iteration. It allows the iterative process to be carried out with a weaker regularization and provides a better estimate than the one obtained from other methods. It has the following two advantages.

First, it provides a better estimate for the initial estimate of the object function for each iteration. In the iterative process with the Born, the Newton or the current refinement iterative method, the object function obtained from the preceding iteration is directly used in the next iteration. A poor estimate of the object function affects strongly the whole iterative process. In the prediction–correction algorithm, the results acquired in the previous iterations are used to make a prediction of the object function for the next iteration. Since more information is used, a better estimate of the object function is obtained for the next iteration.

A second important advantage of the algorithm is that it can prevent the divergence of the iterative process. In a linear numerical problem, the solution generally is achievable by a numerically stable process. A typical example is the conjugate gradient iterative algorithm. In this algorithm, the solution can be obtained after a finite number of iterations by monotonically decreasing the residual error. The inverse scattering problem is a nonlinear problem. The iterative process is not numerically stable and the residual error obtained in the process is often not monotonically decreasing although a lot of algorithms are proposed for solving the nonlinear problem. When the Born, the Newton or the current refinement method is employed in an iterative process, poor results obtained at any iteration step may make later iterations divergent. In the prediction–correction algorithm, the information used in prediction is obtained from previous iterations and the effects coming from the results of individual iterations are reduced. Because the data used for making the prediction is selected, the divergence of the iterative process can be prevented.

Numerical computation results demonstrate that it has better numerical stability and better reconstruction can be achieved by using this algorithm.

5.2 Prediction–correction Algorithm

The inverse scattering problem formulated in chapter 2 is a nonlinear problem. The iteration process is not uniformly convergent and the error of reconstruction fluctuates in general from iteration to iteration, especially when a weaker regularization is applied. In the Born iterative method, the Newton iterative method and the current refinement algorithm presented in chapter 4, only the results obtained in the preceding iteration are considered for the next iteration. The numerical stability of these methods is sensitive to the reconstruction error at each iteration step, which has a strong effect on the convergence of the entire process.

In this chapter, we introduce a prediction–correction procedure into the iterative process. In this procedure, an appropriate linear combination of the equivalent currents obtained in the last iteration and in previous iterations is used to predict a new equivalent current density distribution, $\mathbf{J}_p$. The object function $\mathbf{O}_p$ obtained from this $\mathbf{J}_p$ is employed in the next iteration for its further correction. This prediction–correction technique is practically not sensitive to the error in individual iterations and can prevent the iterative process from diverging. It makes it possible to stabilize the iterative process with a weaker regularization and, thus, yields an improved accuracy.

First, consider an object illuminated by only one incident wave. At the k–th iteration, an equivalent current distribution $\mathbf{J}_k$ and the difference between the measured field and the field generated by $\mathbf{J}_k$,

$$\Delta\mathbf{E}_k^s = \mathbf{E}^s - [G^o]\mathbf{J}_k \tag{5–1}$$

is obtained. In order to reduce the effect of the individual iterations, all the previous results are taken into account to make a prediction of the object function for the next iteration. Namely, after K iterations, the predicted equivalent current $\mathbf{J}_p$ is taken to be of the form

$$\mathbf{J}_p = [J]\mathbf{x} \tag{5–2}$$

where $[J]$ is a rectangular matrix consisting of the column vectors $\mathbf{J}_k$,

$$[J] = [\mathbf{J}_1\ \mathbf{J}_2 \cdots \mathbf{J}_K]\ , \tag{5–3}$$

and $\mathbf{x}$ is an unknown coefficient column vector to be determined. The corresponding $\Delta\mathbf{E}_p^s$ is

$$\Delta\mathbf{E}_p^s = [\Delta E^s]\mathbf{x} \tag{5–4}$$

where $[\Delta E^s]$ consists of the column vectors $\Delta\mathbf{E}_k^s$,

$$[\Delta E^s] = [\Delta\mathbf{E}_1^s\ \Delta\mathbf{E}_2^s \cdots \Delta\mathbf{E}_K^s]\ . \tag{5–5}$$

By substituting the object function from

$$\mathbf{O} = [E^t]^{-1}\mathbf{J}\ , \tag{5–6}$$

into the equation for the direct problem

$$([I] - [G^i][O])\mathbf{E}^t = \mathbf{E}^i\ , \tag{5–7}$$

the following linear combination of equations (5–7) corresponding to the K iterations already performed

$$\sum_{k=1}^{K} x_k\mathbf{E}_k^t - [G^i]\sum_{k=1}^{K} x_k\mathbf{J}_k = \mathbf{E}^i\sum_{k=1}^{K} x_k \tag{5–8}$$

where x_k are the elements of $\mathbf{x}$, is constructed. By setting

$$\sum_{k=1}^{K} x_k = 1 \tag{5–9}$$

equation (5–8) can be written as

$$\mathbf{E}_p^t = [G^i]\mathbf{J}_p + \mathbf{E}^i \tag{5–10}$$

where $\mathbf{E}_p^t$ represents the total electric field corresponding to $\mathbf{J}_p$. Similar to (5–6), the predicted object function $\mathbf{O}_p$ is obtained from

$$\mathbf{O}_p = [E_p^t]^{-1}\mathbf{J}_p \tag{5–11}$$

with $[E_p^t]$ being a diagonal matrix consisting of the elements of $\mathbf{E}_p^t$. To obtain a good prediction for the next iteration, the unknown $\mathbf{x}$ is determined by minimizing $\| \Delta\mathbf{E}_p^s \|$ in (5–4), where $\| \cdot \|$

is the Euclidean norm of a complex column vector. Assuming that $\Delta\mathbf{E}^s_{k'}$, corresponding to $x_{k'}$, has the smallest norm in the set $\{\Delta\mathbf{E}^s_k\}$, the solution of this minimization problem is found as a least square approximation from the equation

$$[\Delta\tilde{E}^s]\tilde{\mathbf{x}} = -x_{k'}\Delta\mathbf{E}^s_{k'} \tag{5–12}$$

In the above equation (5–12), the matrix $[\Delta\tilde{E}^s]$ and the column vector $\tilde{\mathbf{x}}$ consist of the column vectors of $[\Delta E^s]$ and the elements of $\mathbf{x}$ except for $\Delta\mathbf{E}^s_{k'}$ and $x_{k'}$, respectively. Taking into account (5–9), this equation can be written as

$$([\Delta\tilde{E}^s] - [\Delta E^s_{k'}])\tilde{\mathbf{x}} = -\Delta\mathbf{E}^s_{k'} \tag{5–13}$$

where $[\Delta E^s_{k'}]$ is a rectangular matrix consisting of identical column vectors $\Delta\mathbf{E}^s_{k'}$. The least square solution of (5–13) is obtained from the equation

$$[W]^H[W]\tilde{\mathbf{x}} = -[W]^H\Delta\mathbf{E}^s_{k'} \tag{5–14}$$

with

$$[W] \equiv [\Delta\tilde{E}^s] - [\Delta E^s_{k'}] \ . \tag{5–15}$$

The solution of (5–14), with (5–15), yields $\mathbf{J}_p$ in (5–2). The predicted object function is computed from (5–11). It is obvious that, if the column vector $\Delta\mathbf{E}^s_{k'}$ is in the space spanned by the column vectors of $[W]$, $[E^t_p]$ and $\mathbf{O}_p$ computed from (5–10) and (5–11), respectively, by using $\mathbf{J}_p$ obtained from (5–2), give the solution of the matrix equation (5–7) for the direct problem and the matrix equation for the inverse problem

$$\mathbf{E}^s = [G^o][E^t]\mathbf{O} \tag{5–16}$$

For the case of multiple illuminations, $\mathbf{J}_k$ and $\Delta\mathbf{E}^s_k$ are replaced by $\mathbf{J}_{Tk}$ and $\Delta\mathbf{E}^s_{Tk}$ which consist of the corresponding column vectors for different illuminations, respectively,

$$\mathbf{J}_{Tk} = \begin{bmatrix} \mathbf{J}_{1k} \\ \mathbf{J}_{2k} \\ \cdot \\ \cdot \\ \cdot \\ \mathbf{J}_{Lk} \end{bmatrix}, \qquad \Delta\mathbf{E}^s_{Tk} = \begin{bmatrix} \Delta\mathbf{E}^s_{1k} \\ \Delta\mathbf{E}^s_{2k} \\ \cdot \\ \cdot \\ \cdot \\ \Delta\mathbf{E}^s_{Lk} \end{bmatrix} \tag{5–17}$$

where L is the number of illuminations used. $\mathbf{x}$ is determined by following the procedure presented in (5–12) to (5–15), from the minimization of $\| \Delta\mathbf{E}^s_{Tp} \|$. This $\mathbf{x}$ yields a set of $\mathbf{J}_{lp}$ and $\mathbf{E}^t_{lp}$ for each illumination,

$$\mathbf{J}_{lp} = [J_l]\mathbf{x}\,, \tag{5–18}$$

$$\mathbf{E}^t_{lp} = [G^i]\mathbf{J}_{lp} + \mathbf{E}^i_l\,, \qquad l = 1, 2, \ldots, L\,. \tag{5–19}$$

Since (5–11) gives different object functions for different illuminations, a least square treatment is applied to the equations associated with all illuminations to obtain

$$\mathbf{O}_p = ([E^t_{Tp}]^H[E^t_{Tp}])^{-1}[E^t_{Tp}]^H\mathbf{J}_{Tp} \tag{5–20}$$

where the matrix $[E^t_{Tp}]$ consists of the diagonal matrices $[E^t_{lp}]$, which represent the column vectors $\mathbf{E}^t_{lp}$, and the vector $\mathbf{J}_{Tp}$ of the column vectors $\mathbf{J}_{lp}$ for all the illuminations, respectively,

$$[E^t_{Tp}] = \begin{bmatrix} [E^t_{1p}] \\ [E^t_{2p}] \\ \cdot \\ \cdot \\ \cdot \\ [E^t_{Lp}] \end{bmatrix}, \qquad \mathbf{J}_{Tp} = \begin{bmatrix} \mathbf{J}_{1p} \\ \mathbf{J}_{2p} \\ \cdot \\ \cdot \\ \cdot \\ \mathbf{J}_{Lp} \end{bmatrix}. \tag{5–21}$$

The predicted object function $\mathbf{O}_p$ in (5–20) is applied to the next iteration for its further correction.

From (5–2) and (5–4), it can be seen that the elements in the set $\{ \mathbf{J}_k \}$ corresponding to large $\| \Delta\mathbf{E}^s_k \|$ have a smaller contribution to the predicted current $\mathbf{J}_p$. At the same time, it is not necessary to use all the equivalent current distributions obtained in the previous iterations to make the prediction for the next iteration. Therefore, only those elements of the set which are asso-

ciated with smaller norms $\| \Delta \mathbf{E}_k^s \|$ are selected to make the prediction.

Practically, the computation starts without implementing the process just described. Then, after several iterations, the prediction–correction technique is applied with the elements in the sets $\{ \mathbf{J}_k \}$ and $\{ \Delta \mathbf{E}_k^s \}$ being those from the iterations already performed. These elements are updated at each subsequent iteration step by replacing the entries from the iteration corresponding to the largest $\| \Delta \mathbf{E}_{Tk}^s \|$ with the ones newly computed. Consequently, the worst data are discarded successively and only the better previous iteration results and the results in the new iteration are used to make the prediction. If the new results have a larger $\| \Delta \mathbf{E}_T^s \|$ than the other one used in making prediction, they will be discarded in the next prediction. Thus, the divergence of the iteration process is prevented. This procedure makes the process stable and capable of converging with a weaker regularization.

The proposed algorithm can be summarized as follows:

1) correction:

a) solve the direct scattering problem in (5–7) for all illuminations to obtain the column vectors $\mathbf{E}_{Tk}^t$, $\mathbf{J}_{Tk}$, and $\Delta \mathbf{E}_{Tk}^s$;

b) compute the object function by the Born or the Newton iterative technique;

c) compute the improved object function by equivalent current refinement;

2) if the number of iterations is smaller than or equal to a chosen integer K, go to 1).

3) prediction:

a) solve the direct scattering problem in (5–7) for all illuminations and compute the column vectors $\mathbf{J}_{Tk}$ from

$$\mathbf{J}_l = [E_l^t]\mathbf{O} , \tag{5–22}$$

and $\Delta \mathbf{E}_{Tk}^s$ from

$$\Delta \mathbf{E}_l^s = \mathbf{E}_l^s - [G_l^o][E_l^t]\mathbf{O} \ ; \tag{5–23}$$

b) update the sets $\{ \mathbf{J}_{Tk} \}$ and $\{ \Delta\mathbf{E}^s_{Tk} \}$ used for making the prediction;

c) determine $\mathbf{x}$ from (5–14) (with (5–17)) and compute the predicted $\mathbf{J}_{Tp}$ and $\mathbf{E}^t_{Tp}$;

d) compute the predicted object function $\mathbf{O}_p$ from (5–20);

e) if $\| \Delta\mathbf{E}^s_{Tk} \|$ stays smaller than a specified error or the number of iterations reaches an imposed number, stop the iteration process; otherwise go to 1).

In the prediction–correction algorithm presented in this chapter, only better results, selected from all previous iterations, are used for making the successive predictions. Moreover, a least square treatment is applied to a linear equation in the prediction procedure, since the relationship between the measured scattered field and the equivalent current density is linear. The relationship between the measured data and the estimated object function for all illuminations is nonlinear. The advantage of using equivalent currents consists in the fact that the prediction of the solution of a nonlinear and ill–posed problem is separated into a least square estimation of the solution of an ill–posed linear problem for these equivalent currents and of a well–posed nonlinear problem for the object function. Thus, the difficulties in the direct, nonlinear problem for the prediction of the object function are circumvented by applying the prediction procedure to a linear problem for the equivalent currents, which prevents the divergence of the iterative process.

This prediction–correction algorithm is quite similar to the predictor–corrector algorithms used in the numerical solution of nonlinear differential equations [79–80]. In the predictor–corrector algorithm, the method of data selection and the weight coefficients are fixed in prediction and the effect from the worst data cannot be reduced. The problem of divergence is not solved [79]. The autoregressive method is a method used for solving linear problems related to radar imaging [81] and cannot be directly applied to solve the nonlinear problem. However, the linear prediction of the equivalent current used in the presented method is quite similar to the autoregressive method. The difference between them is the selection of the data used for making the prediction. The data selection in the prediction–correction algorithm filters the worst data and the linear prediction reduces the effect of individual iteration results, which keep the iterative

process from diverging. Since in the autoregressive method, the data for making prediction is taken from the results of previous iterations with a fixed formula, the worst data is not filtered out and the effect from the worse data cannot be reduced efficiently.

5.3 Numerical Results

In this section, the results for the three examples described in chapter 4 are discussed. The results by the prediction–correction algorithm, the current refinement algorithm and the iterative techniques associated with them are presented [82–83].

For the first example, 7 illuminations are applied and 28 receivers are used to measure the scattered field, which have been used in chapter 4 for the numerical computation. The prediction–correction algorithm with the current refinement and Born iterative techniques is used in the numerical test. In Fig. 5.1, the computation results by different algorithms are presented, along with those by the prediction–correction (P–C) algorithm with the current refinement and the Born iterative techniques and with the original dielectric permittivity distribution profile. To reconstruct the profile in Fig. 1(d), the prediction–correction technique was implemented from the 6th iteration, and six $\mathbf{J}_{Tk}$ and six $\Delta\mathbf{E}^s_{Tk}$ were selected to make the prediction at each subsequent iteration. The regularization parameter used in the prediction–correction algorithm is 6×10^{-4} for the first iteration, 6×10^{-3} after the first iteration and 10^{-4} after the 5th iteration. For the current refinement algorithm, the regularization parameter is 6×10^{-4} for the first iteration, 6×10^{-3} after the first iteration, reduced to 2.7×10^{-3} after the 9th iteration and reduced to 2.3×10^{-3} after the 13th iteration. The regularization parameter used in the Born iterative method is 6×10^{-4} for the first iteration, 1.2×10^{-2} after the first iteration, 9×10^{-3} after the 6th iteration and 6×10^{-3} after the 9th iteration.

The results by the prediction–correction method are more accurate than those computed by other methods. The relative error in the computed scattered electric field intensity and the relative error in the reconstructed permittivity are plotted in Fig. 5.2. The prediction–correction al-

gorithm provides faster convergence. At the same time, the regularization parameter used in the new method to stabilize the iteration process is smaller than the ones for the other two methods. This indicates that the new algorithm is numerically more stable. In the first five iterations, the same regularization parameter g is used in the current refinement algorithm and in the new method, which is smaller than the one for the Born iterative method. After the 5th iteration, the value of g used in the prediction–correction algorithm is reduced to ten times smaller than the ones for the current refinement algorithm and the Born iterative method. The plots obtained by the Born iterative method show a fluctuation during the iteration process in spite of a larger g used in it. To see the effect of a weaker regularization on various methods, the same smaller regularization parameter used for the prediction–correction method in Fig. 5.2 has been employed for the other two methods. The computational errors in the scattered electric field and the relative error of the reconstructed object function are presented in Fig. 5.3. With this weaker regularization, the iterative process becomes divergent when the Born iterative method or the corresponding current refinement method are employed. In the iteration process associated with these methods, a stronger regularization should be used when $\| \Delta \mathbf{E}^s_{Tk} \|$ is comparatively large and as the error in the computed scattered electric field decreases, the regularization parameter should be correspondingly decreased. However, at present, there is no general rule available for selecting the regularization parameter at each iteration step. Practically, a better regularization is found by repeating the numerical simulation with different regularizations. The application of the prediction–correction technique from the 6th iteration improves substantially the situation and the iteration process converges more rapidly. This method allows for a weaker regularization to be used, which yields better numerical stability and solution accuracy, as well as faster convergence.

When a stronger regularization is used in the iteration process, the results obtained are shown in Fig. 5.4. The regularization parameter used in the prediction–correction algorithm and the current refinement algorithm is 6×10^{-4} for the first iteration, 6×10^{-3} after the first iteration, 3×10^{-3} after the 5th iteration and 2×10^{-3} after the 13th iteration. The prediction–correction algorithm still provides better results. Compared with the results for a weaker regularization, the

reconstruction error is slightly increased. This is because the high spatial frequency components are filtered too much by the stronger regularization and the image resolution is reduced.

The case when a Gaussian noise of 20 dB level is added to the measured data of the scattered field is also considered. The data is obtained by using the same illumination and measurement arrangements as above. The numerical tests are carried out with two regularizations. For the results shown in Fig. 5.5 , the regularization parameter is 6×10^{-4} for the first iteration, 6×10^{-3} after the first iteration and 3×10^{-3} after the 5th iteration. For the results shown in Fig. 5.6, the difference in regularization is that g is reduced to 10^{-3} after the 5th iteration. It can be seen that the prediction–correction algorithm is less sensitive to the change in the regularization parameter than the current refinement algorithm and has better numerical stability. The errors in the object function reconstructed by the prediction–correction algorithm are smaller than the ones corresponding to the current refinement algorithm.

For the second and the third examples, the prediction–correction algorithm with the current refinement and Newton iterative techniques is used in the numerical test. In the cases without noise in the measured data, 5 illuminations and 13 receivers are used. For the second example, the results obtained by the prediction–correction algorithm, the current refinement algorithm and the Newton iterative algorithm are presented in Fig. 5.7 to Fig. 5.8. Except 6×10^{-4} for the first iteration, the regularization parameter is 10^{-9} for Fig. 5.7, and 10^{-13} for Fig. 5.8. For Fig. 5.7, the reconstructed profile of permittivity by different algorithms are presented in Fig. 5.9. In the new algorithm, the prediction–correction procedure is applied from the 6th iteration and again six $\mathbf{J}_{Tk}$ and six $\Delta\mathbf{E}^s_{Tk}$ are selected to make the prediction. After applying the prediction–correction procedure, it can be seen that the convergence rate of the iteration process is much higher than the ones in the other methods with the same regularization. The prediction–correction algorithm has this advantage for a quite wide range of the regularization parameter.

The results obtained for the third example are presented in Fig. 5.10 and Fig. 5.11. For the results shown in Fig. 5.10, the regularization parameter is 6×10^{-4} for the first iteration,

2×10^{-3} after the first iteration, 10^{-4} after the 4th iteration and 10^{-5} after the 7th iteration. For the results shown in Fig. 5.11, the regularization parameter is 6×10^{-4} for the first iteration, 10^{-6} after the first iteration and 10^{-11} after the 9th iteration. In Fig. 5.10 and Fig. 5.11, the results by the new algorithm are the same or better than those by the other methods.

When a Gaussian noise with a signal–to–noise ratio of 20 dB is presented in the measured data, more receivers and illuminations have to be used to overcome the effect of the noise. For the second example, the results for the regularization parameter being 10^{-8} and 10^{-9} except 6×10^{-4} for the first iteration are shown in Fig. 5.12 and Fig. 5.13, respectively. Twenty three receivers and 22 illuminations are used and the prediction–correction procedure is applied from the 6th iteration. In this case, there is no obvious difference between the errors in the computed scattered electric field by the new method and by the other methods in the final stage of the iteration process, although the prediction–correction method provides faster convergence. However, the prediction–correction algorithm provides better reconstruction of the object function as indicated in those figures. For the third example, two different illumination and measurement arrangements are used. When 5 illuminations and 13 receivers are used, the results for the regularization parameter being 2×10^{-3}, 10^{-3} and 10^{-4}, except 6×10^{-4} for the first iteration, are shown in Fig. 5.14, Fig. 5.15 and Fig. 5.16, respectively. The results by the prediction–correction algorithm are better than the ones by the Newton iterative algorithm but not as good as the ones by current refinement algorithm. When 22 illuminations and 13 receivers are used for imaging, more information is obtained. The results are presented in Fig. 5.17 and Fig. 5.18 corresponding to the regularization parameter being 10^{-6} and 10^{-8} except 6×10^{-4} for the first iteration, respectively. With these weaker regularizations, the iterative process becomes divergent when the Newton iterative method is employed. The error of the object function reconstruction by the prediction–correction algorithm is about 5%. From these results, it can be seen that current refinement and prediction–correction algorithms provide better reconstructions than Born and Newton iterative algorithms, when noise is presented in the measured data. Whenever more measured

data are used, the results by these algorithms are improved. Therefore, to reduce the effect of noise, more samples of scattered field are required.

In regarding to the amount of computation involved in the prediction–correction algorithm, it should be noticed that the supplementary work for generating a predicted object function corresponds to an iteration without the inversion of the ill–conditioned matrix. Since the dimension of the matrix $[W]$ is much smaller than that of the ill–conditioned matrix involved in the inverse problem, the computation time needed for solving (5–14) is, correspondingly, much smaller than the total computation time. Figures 5.2 and 5.7 can be used as typical examples to compare the reconstruction results and computer CPU time. For Fig. 5.2, when the reconstruction error is about 5%, the CPU time is about 3.3 minutes for the Born iterative algorithm, 2.5 minutes for the current refinement algorithm and 2 minutes for the prediction–correction algorithm; for Fig. 5.7, when the reconstruction error is about 0.2%, the number of iterations is 14, 12 and 6 for these algorithms, respectively.

5.4 Conclusion

The prediction–correction algorithm is a numerically stable and efficient method. Compared to other iterative methods, such as the Born, the Newton and the current refinement methods, numerical tests show that this iterative method has better numerical stability and convergence. In this algorithm, selected results, which are obtained from previous iterations, are used to make prediction for the next iteration. Because more information of the object is used in the procedure of prediction, the effect of individual iteration to the iterative process is reduced and a good evaluation of object function is obtained. The proposed algorithm is numerically more stable and keeps the iteration process from diverging. At the same time, numerical results also show that this method provides results better than the ones obtained by the algorithms such as Born and Newton iterative algorithms when noise is presented in the measured data.

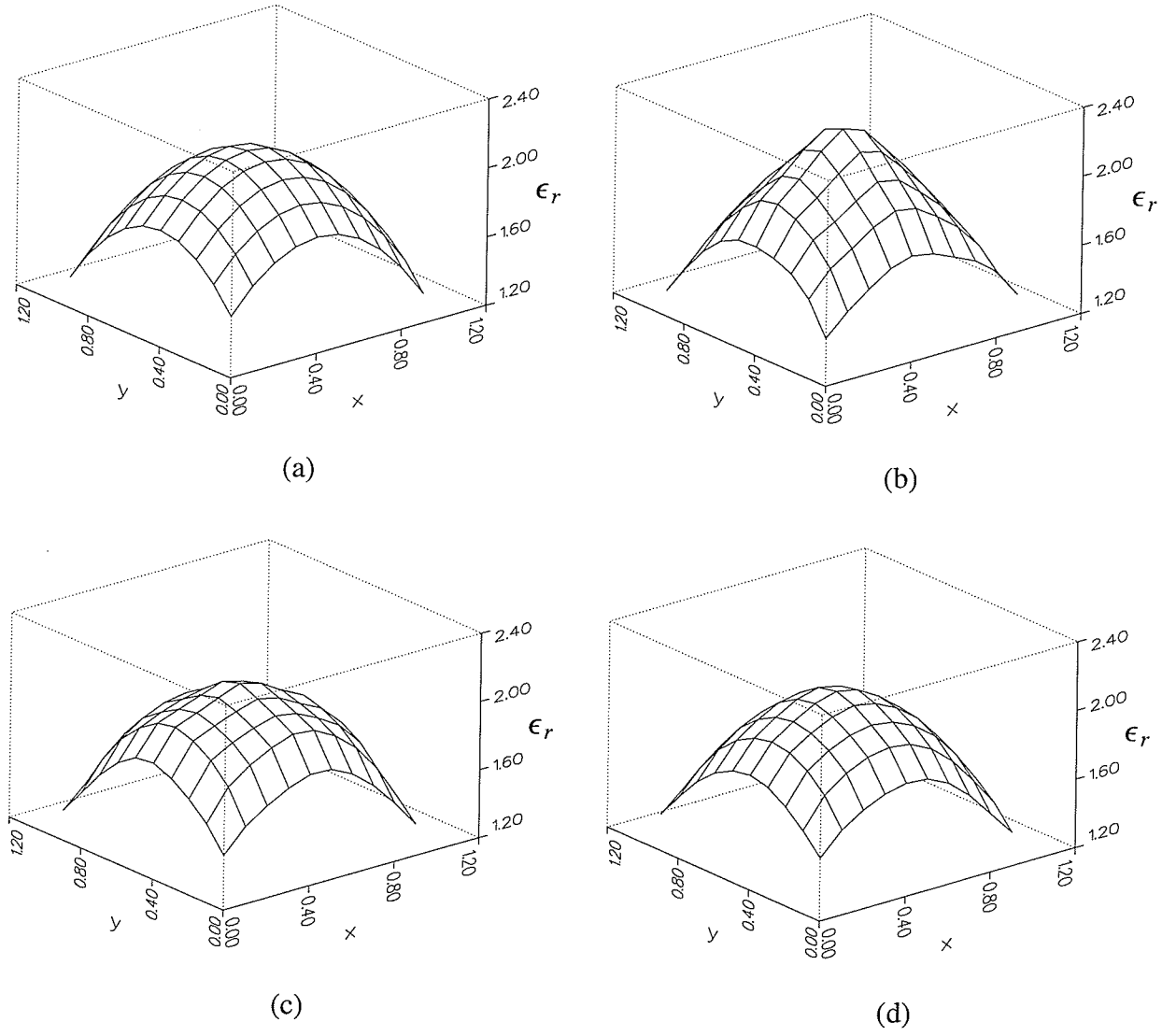

Fig. 5.1 : Comparison of reconstruction results: (a) Original profile, (b) Born iterative method after 18 iterations, (c) Current refinement method after 15 iterations, (d) Prediction–correction method after 15 iterations. Coordinates x and y are in wavelengths.

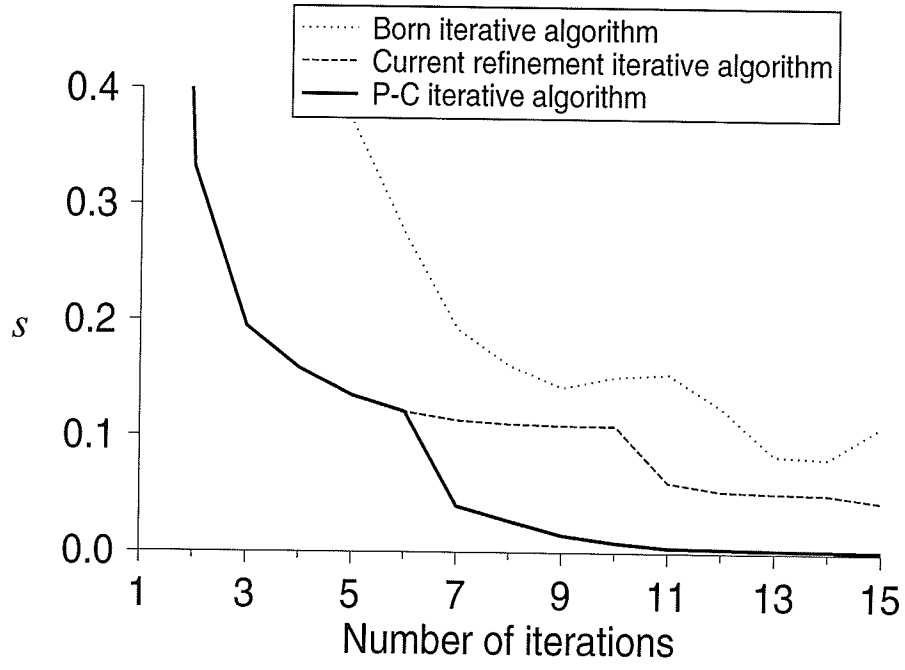

(a)

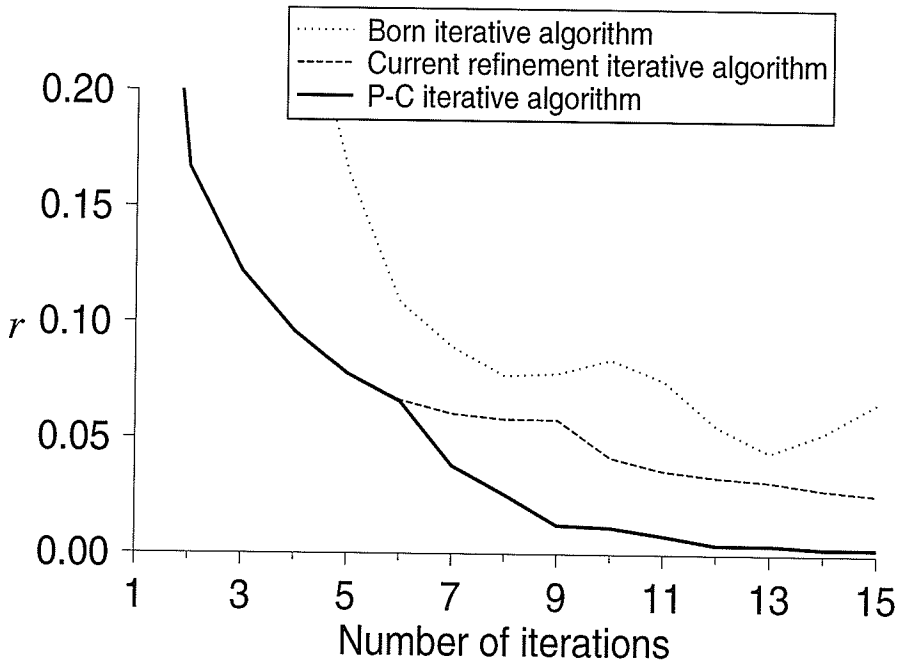

(b)

Fig. 5.2 : Errors s and r for example one with a weaker regularization used in the prediction–correction algorithm.

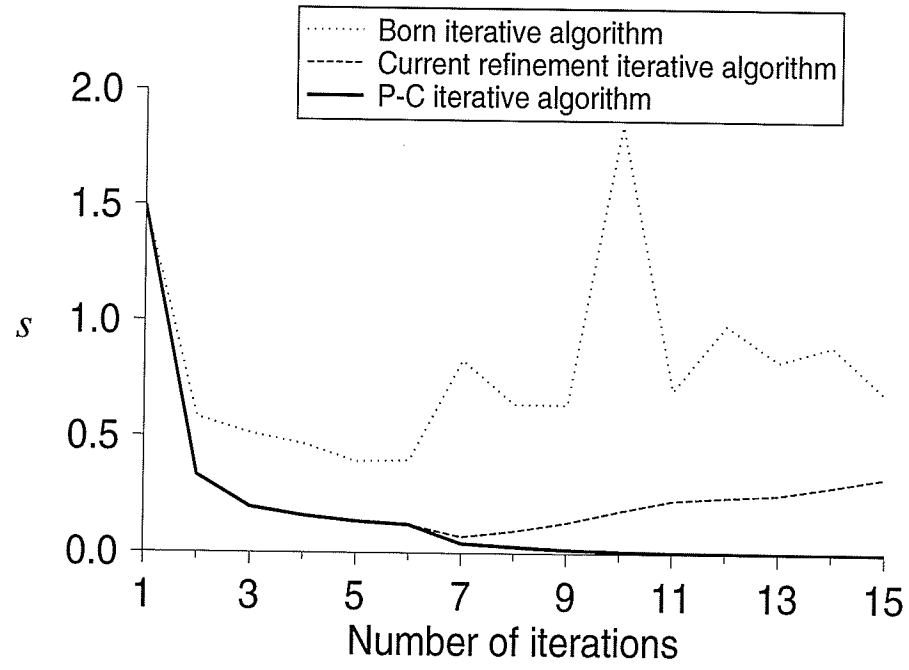

(a)

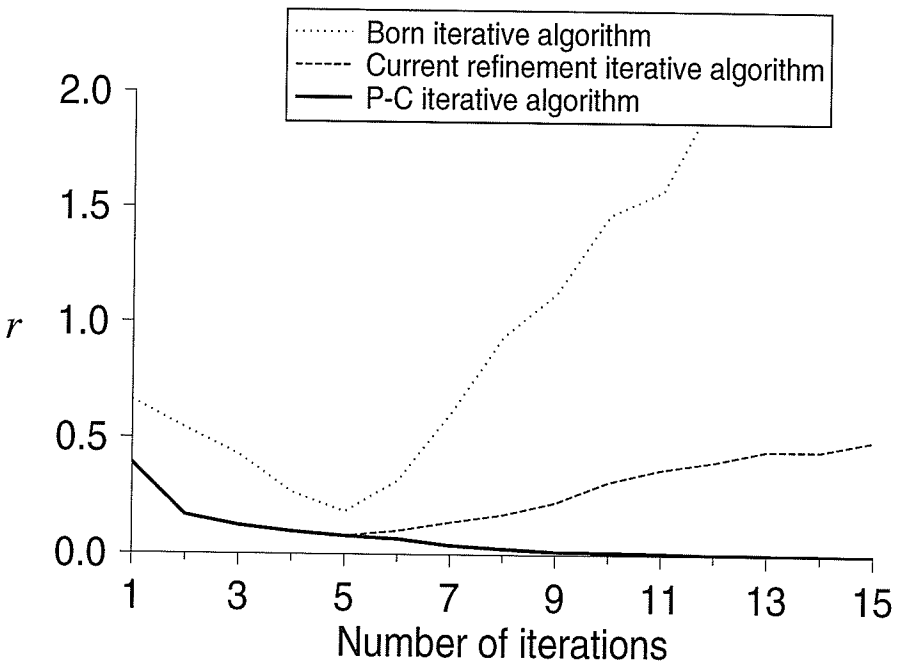

(b)

Fig. 5.3 : Errors s and r for example one with a weaker regularization used in all algorithms.

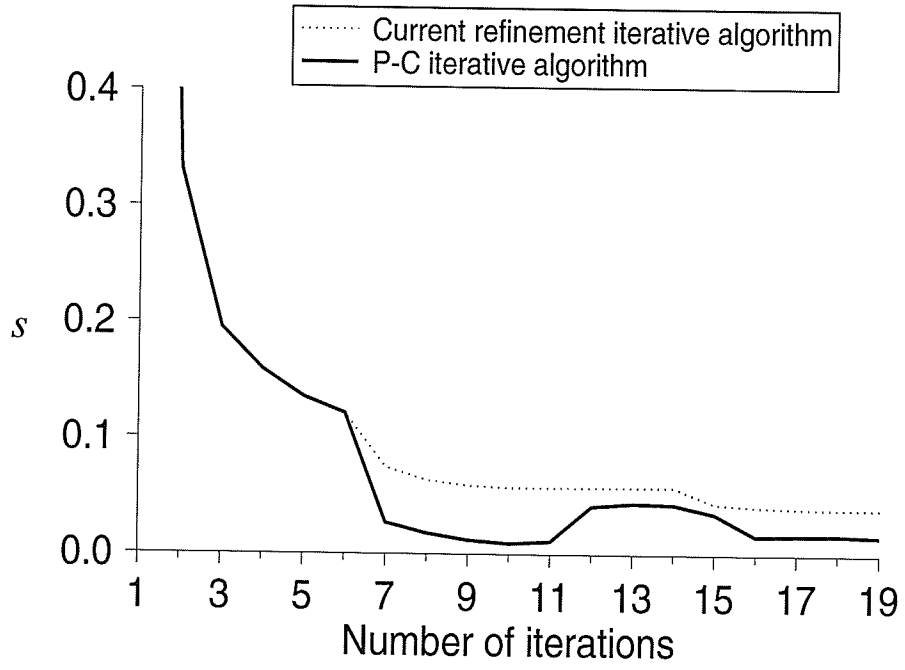

(a)

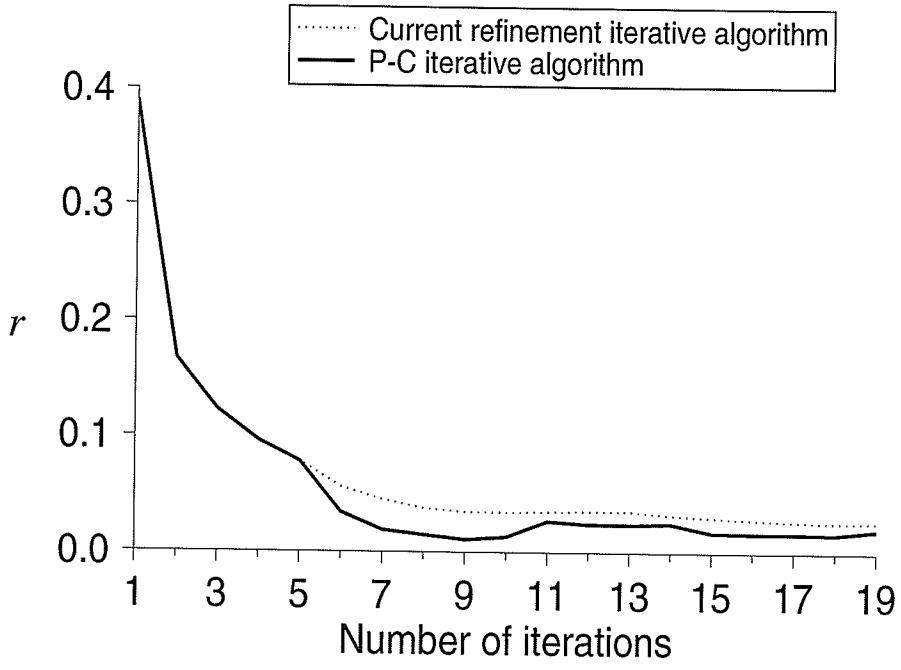

(b)

Fig. 5.4 : Errors s and r for example one with a stronger regularization used in all algorithms.

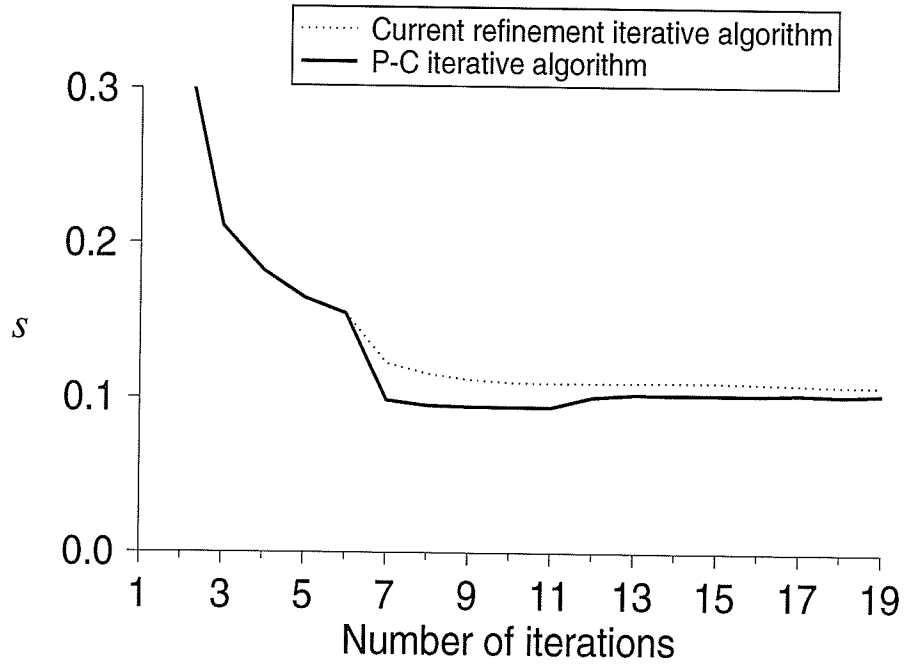

(a)

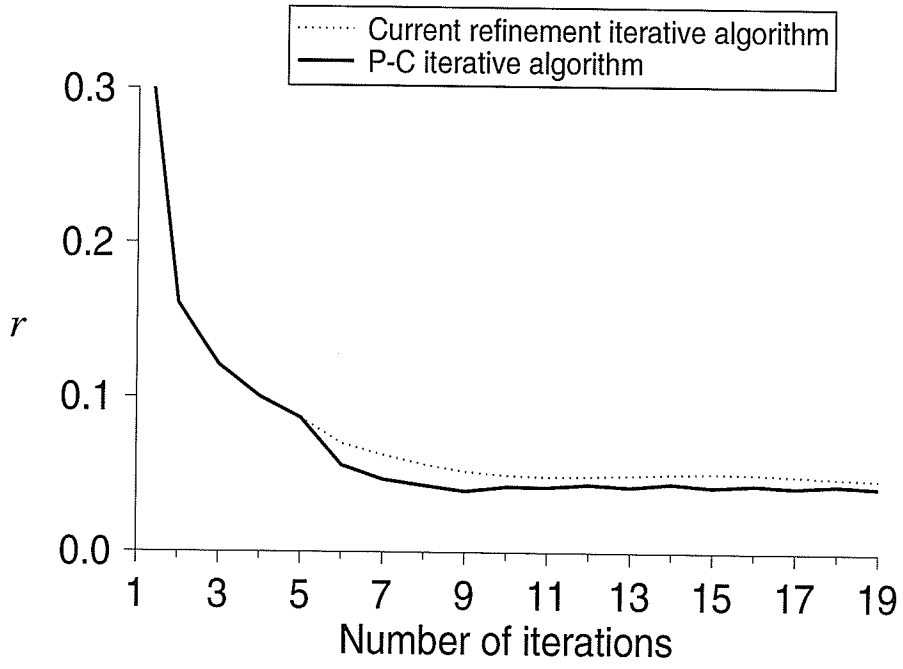

(b)

Fig. 5.5 : Errors s and r for example one in the presence of noise in the measured data and $g = 3 \times 10^{-3}$ after the 5th iteration.

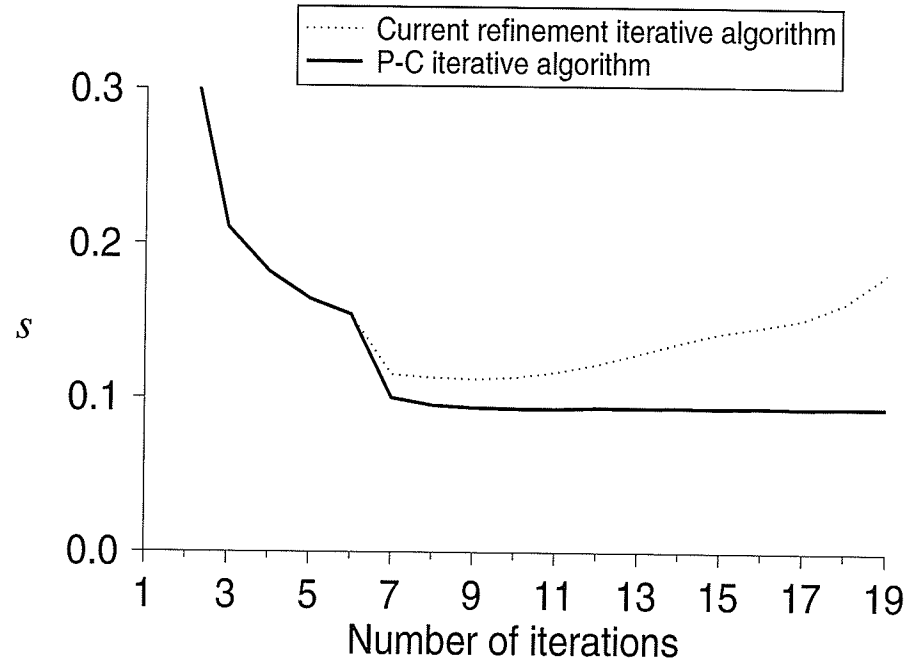

(a)

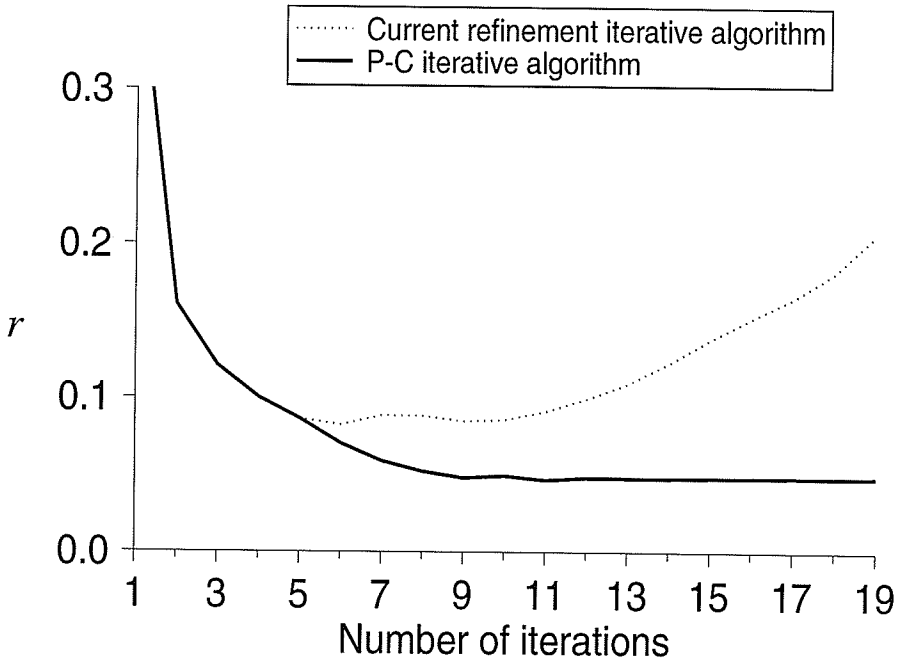

(b)

Fig. 5.6 : Errors s and r for example one in the presence of noise in the measured data and $g = 10^{-3}$ after the 5th iteration.

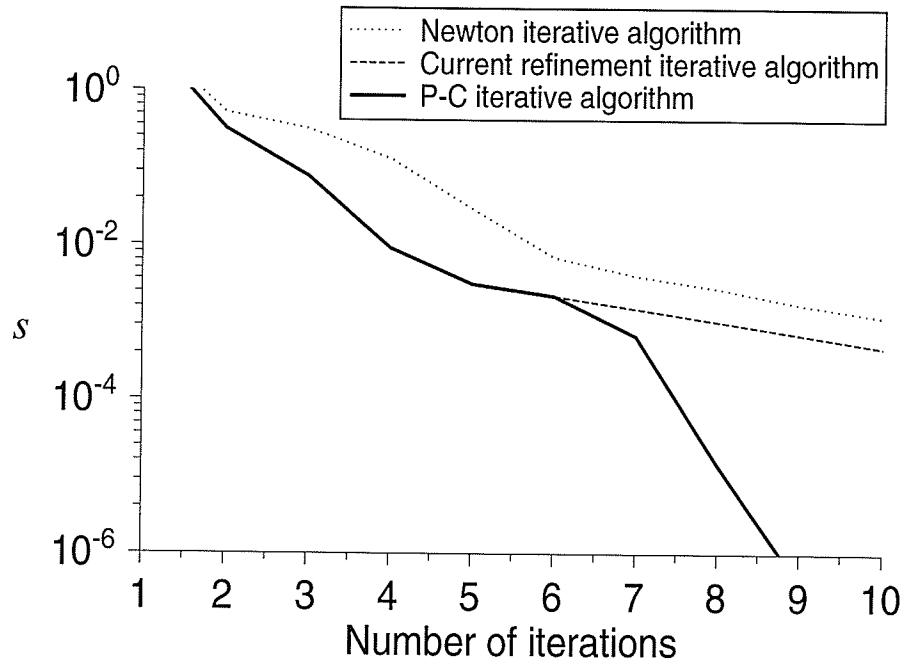

(a)

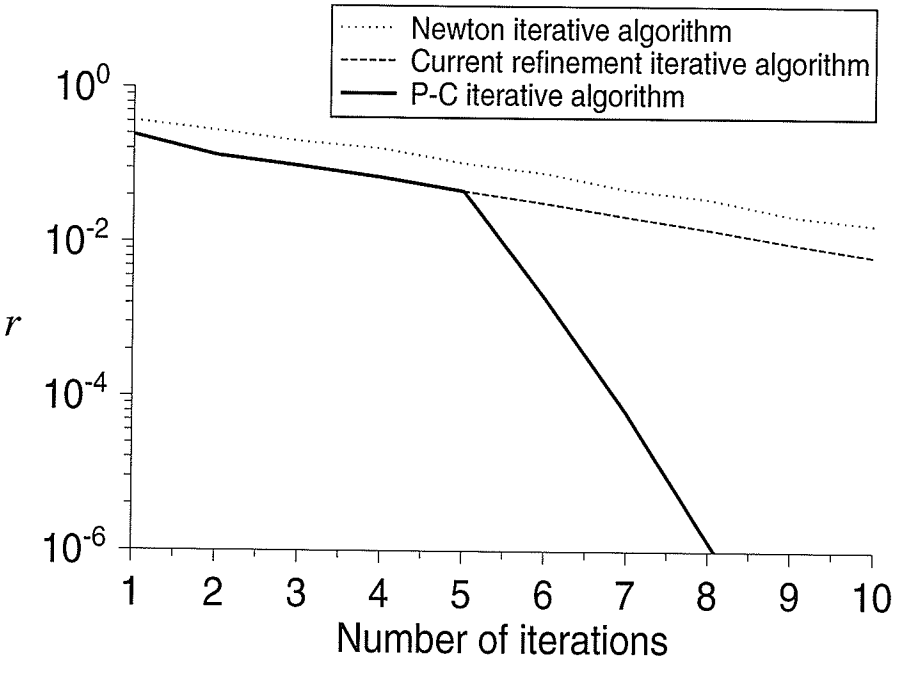

(b)

Fig. 5.7 : Errors s and r for example two with $g = 10^{-9}$ after the first iteration.

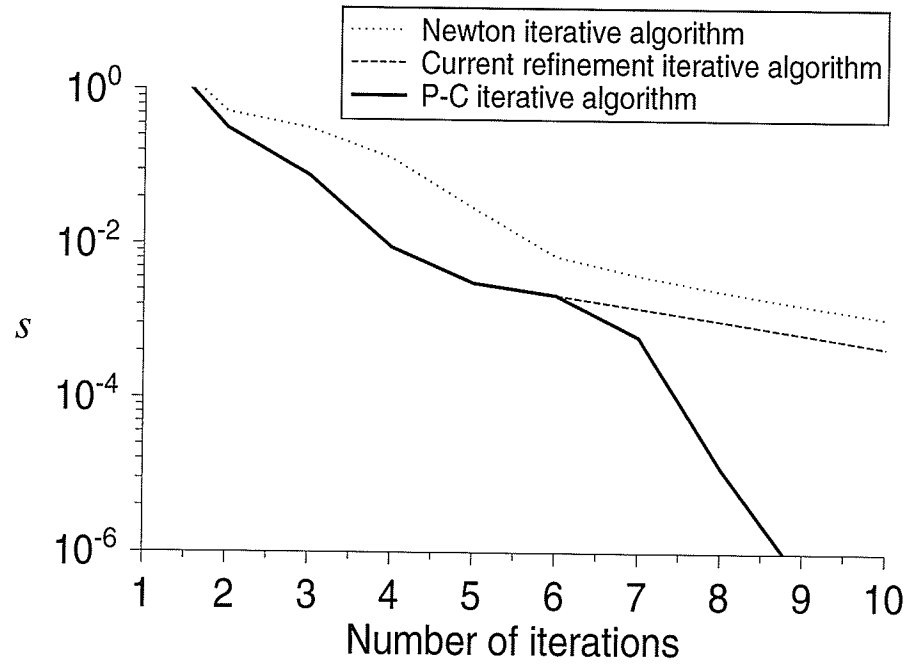

(a)

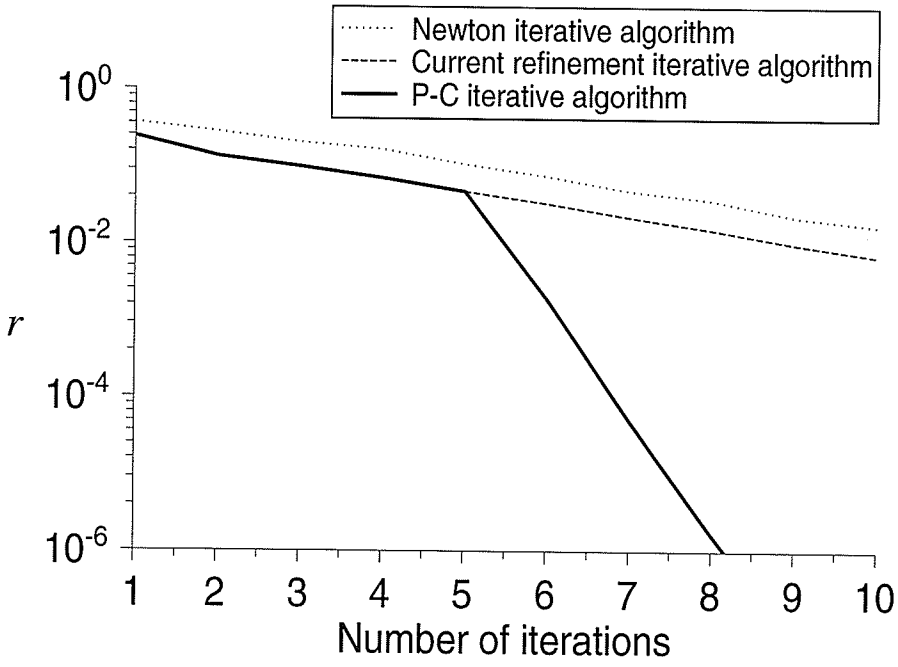

(b)

Fig. 5.8 : Errors s and r for example two with $g = 10^{-13}$ after the first iteration.

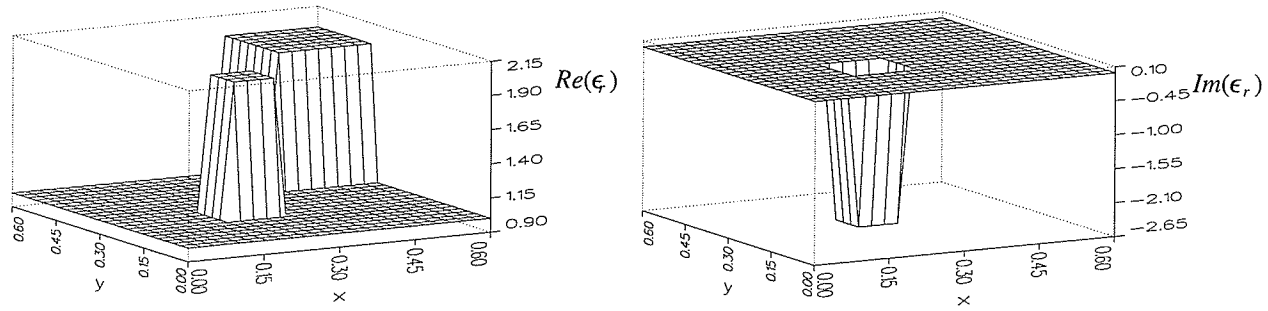

(a)

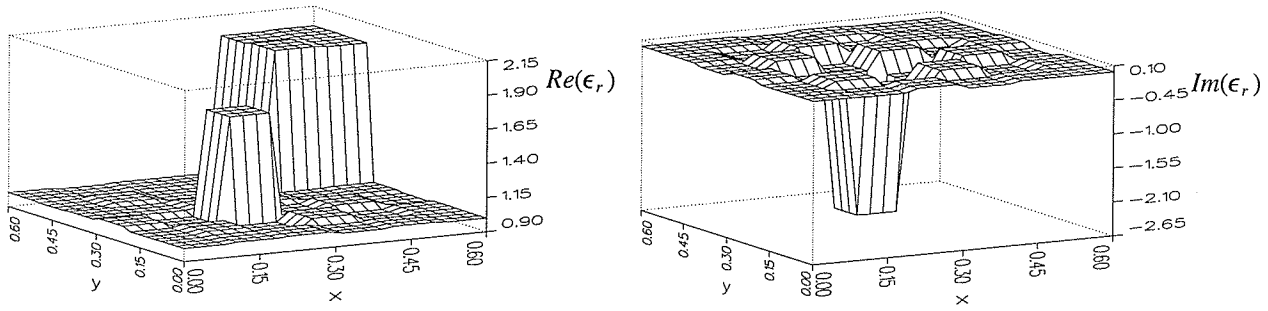

(b)

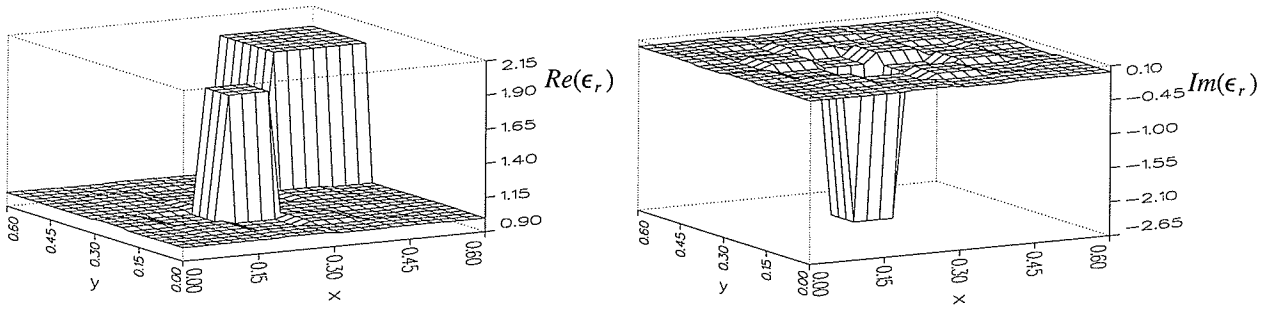

(c)

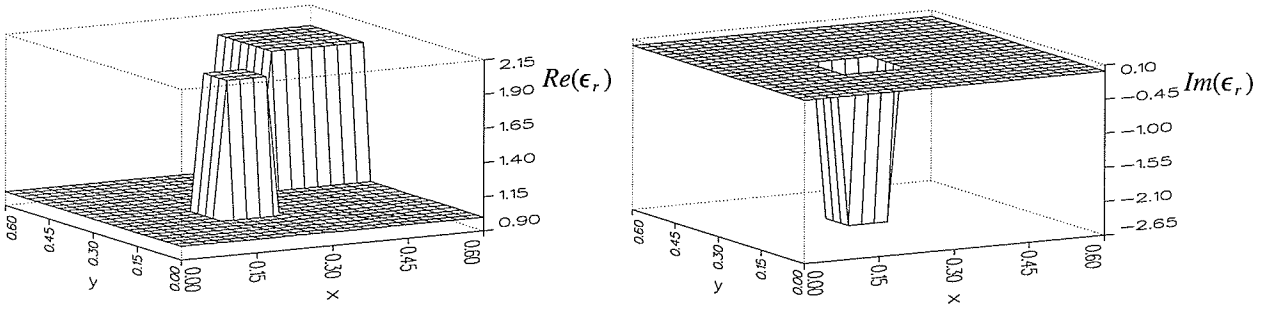

(d)

Fig. 5.9 : Comparison of reconstruction results after 6 iterations: (a) Original profile, (b) Newton iterative method, (c) Current refinement method, (d) Prediction–correction method. Coordinates x and y are normalized to two wavelengths.

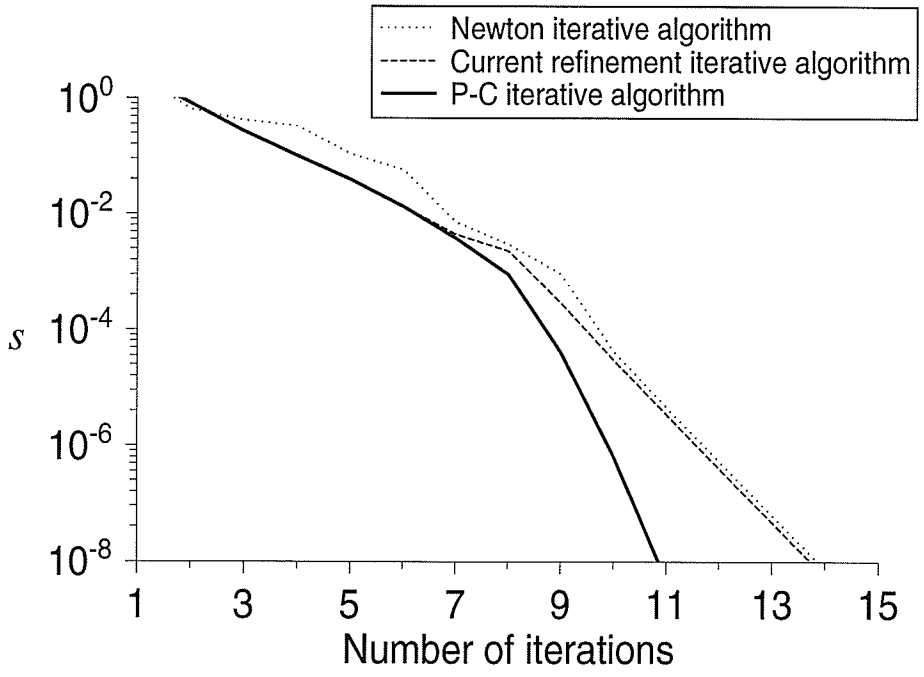

(a)

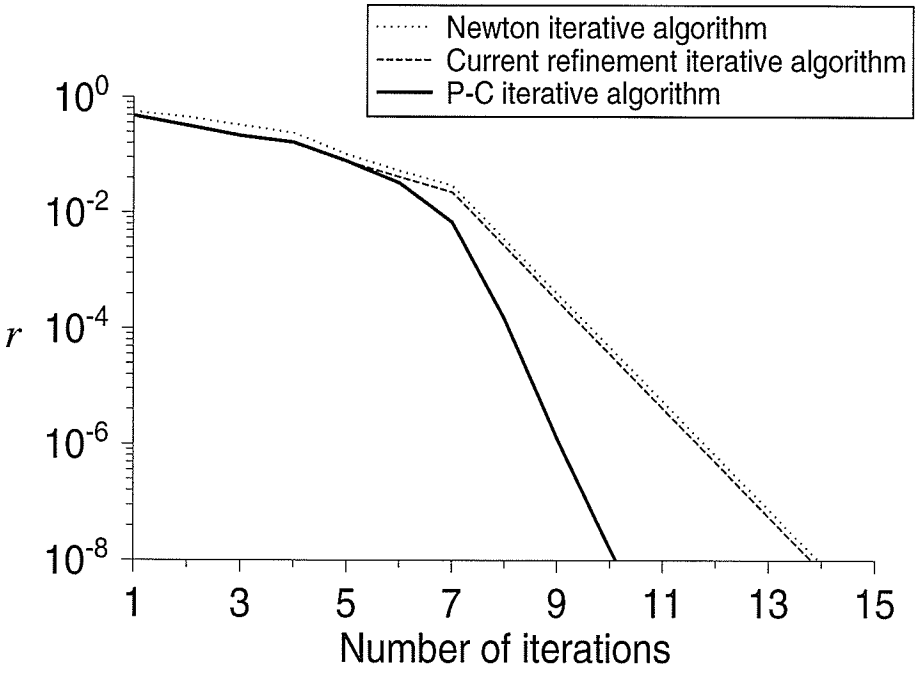

(b)

Fig. 5.10 : Errors s and r for example three with $g = 10^{-5}$ after the 7th iteration.

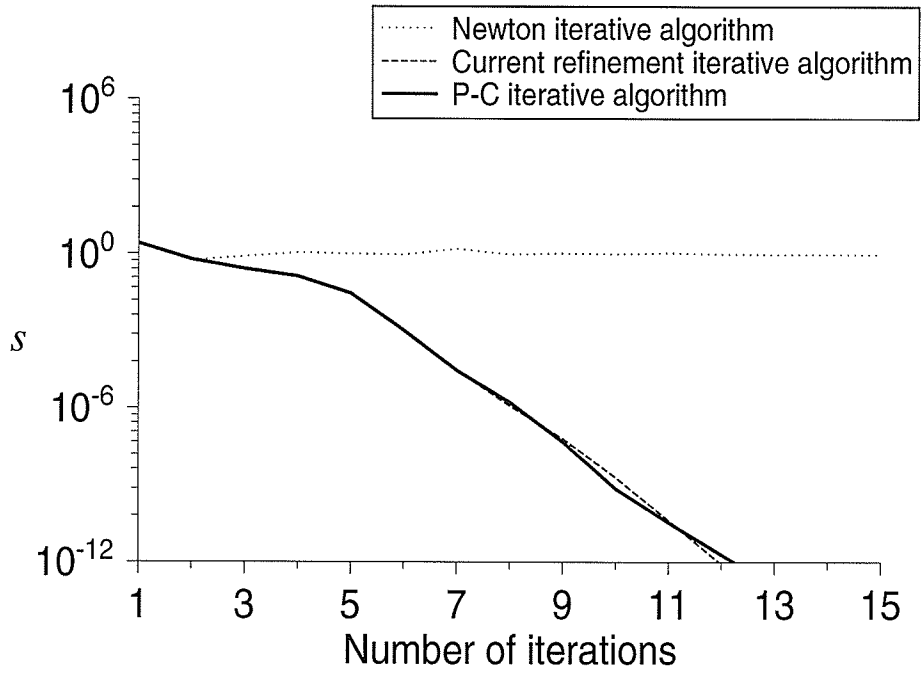

(a)

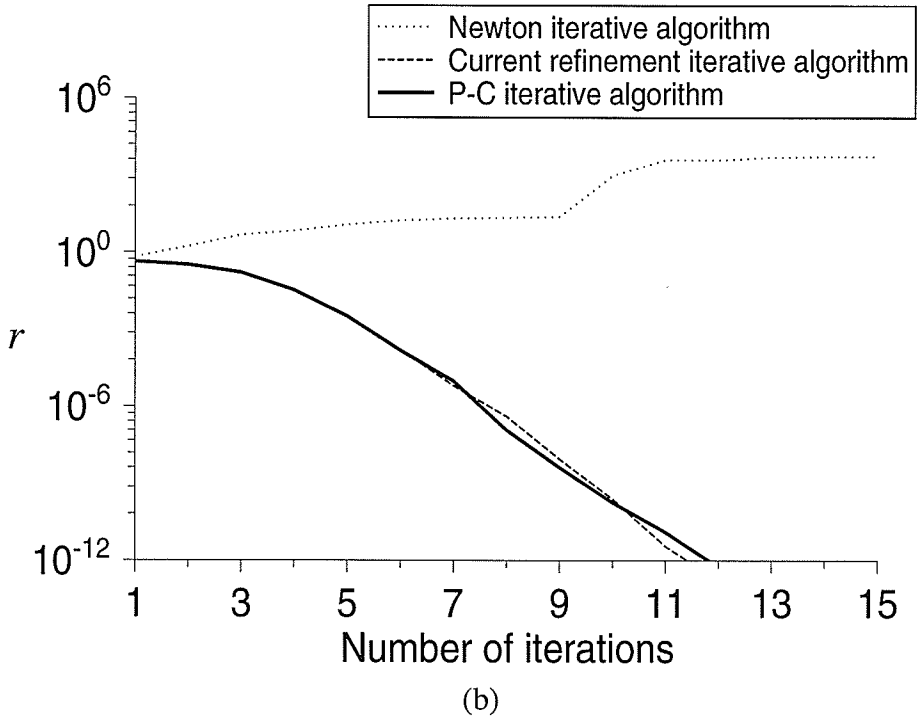

(b)

Fig. 5.11 : Errors s and r for example three with $g = 10^{-11}$ after the 9th iteration.

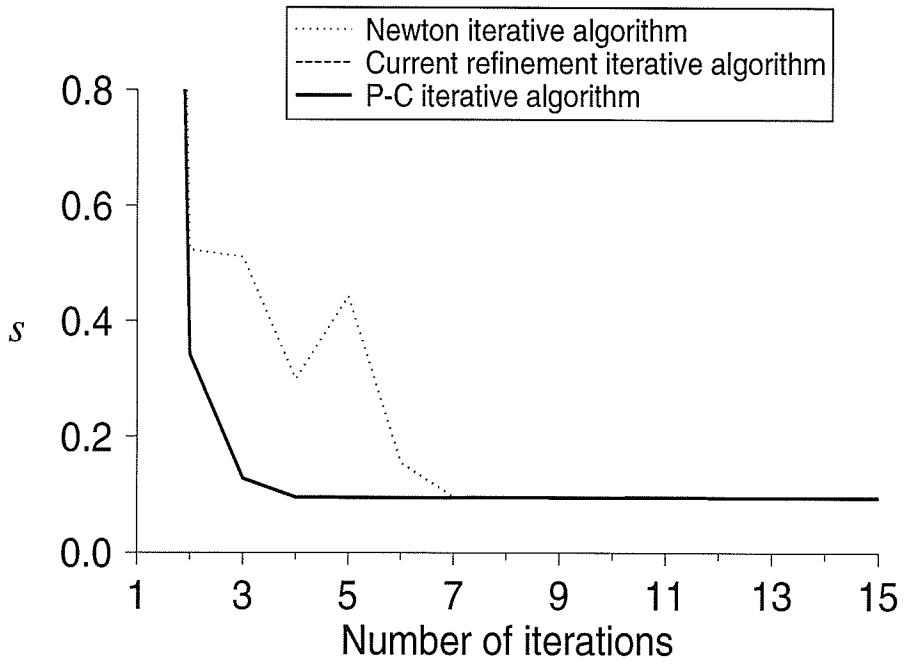

(a)

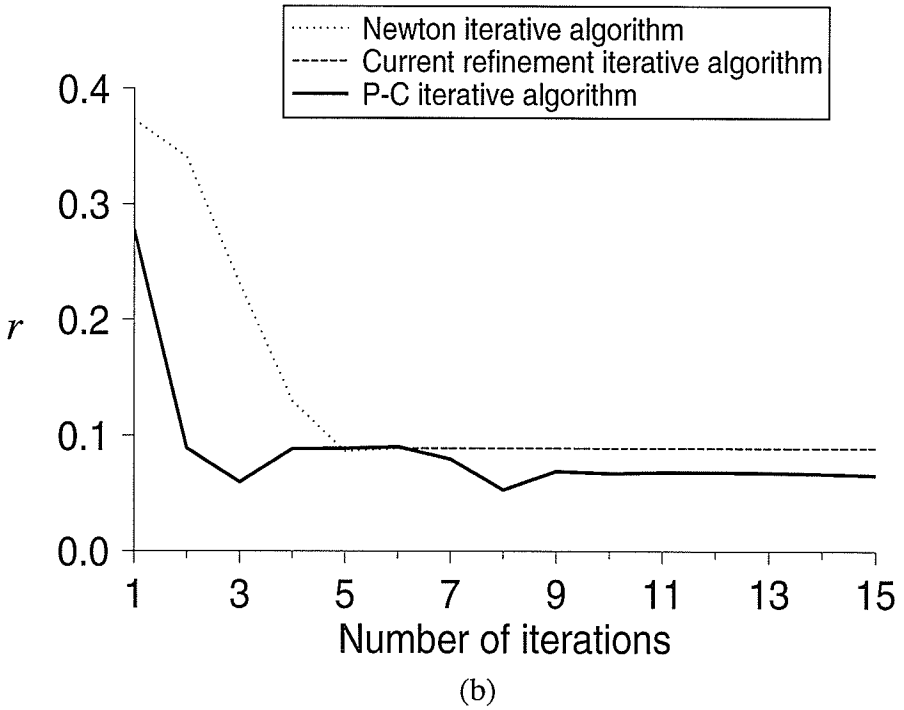

(b)

Fig. 5.12 : Errors s and r for example two in the presence of noise in the measured data: 22 illuminations, 23 receivers, and $g = 10^{-8}$ after the first iteration.

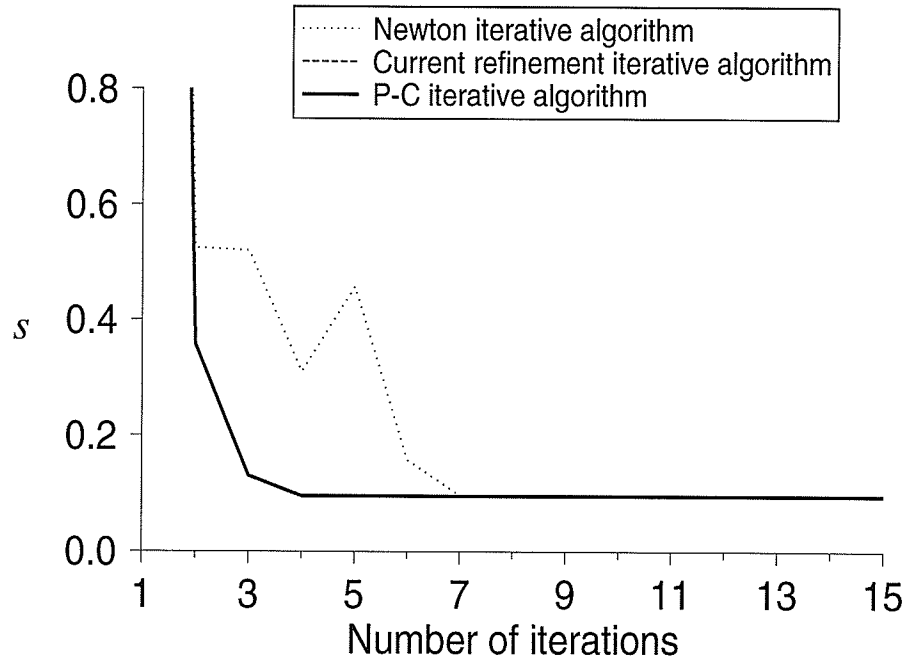

(a)

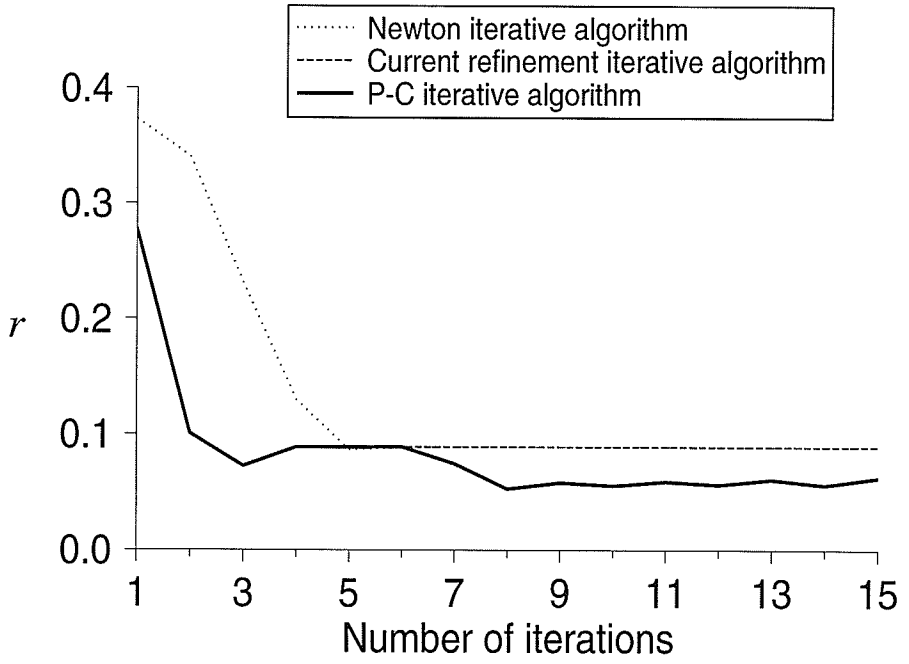

(b)

Fig. 5.13 : Errors s and r for example two in the presence of noise in the measured data: 22 illuminations, 23 receivers, and $g = 10^{-9}$ after the first iteration.

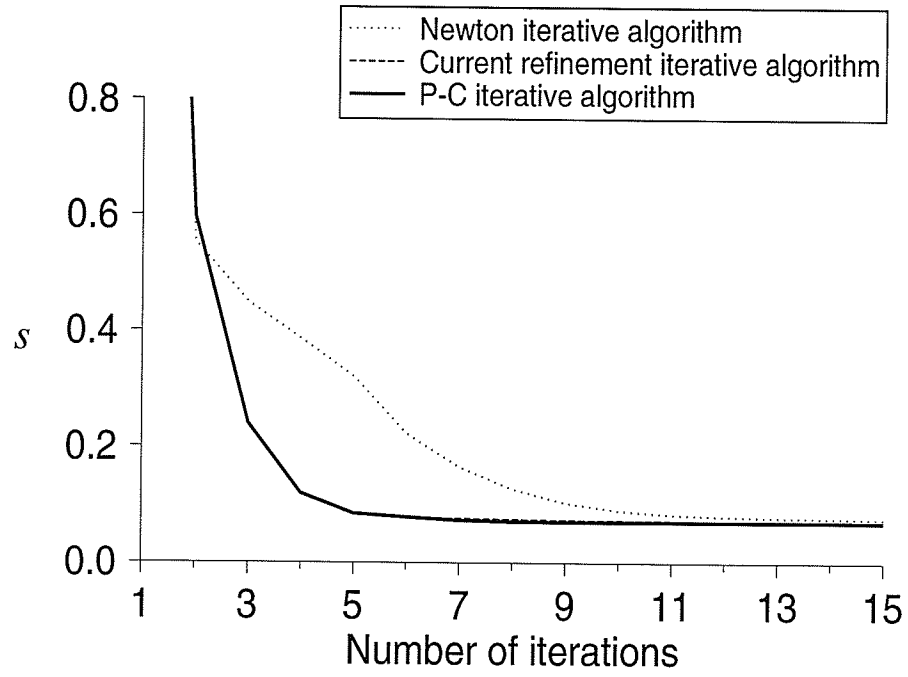

(a)

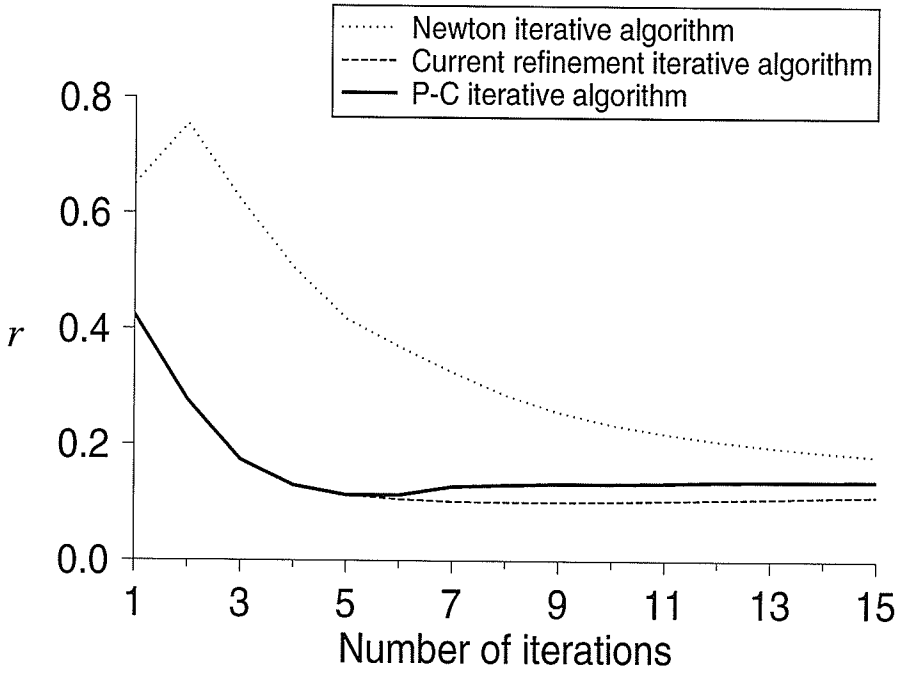

(b)

Fig. 5.14 : Errors s and r for example three in the presence of noise in the measured data: 5 illuminations, 13 receivers, and $g = 2 \times 10^{-3}$ after the first iteration.

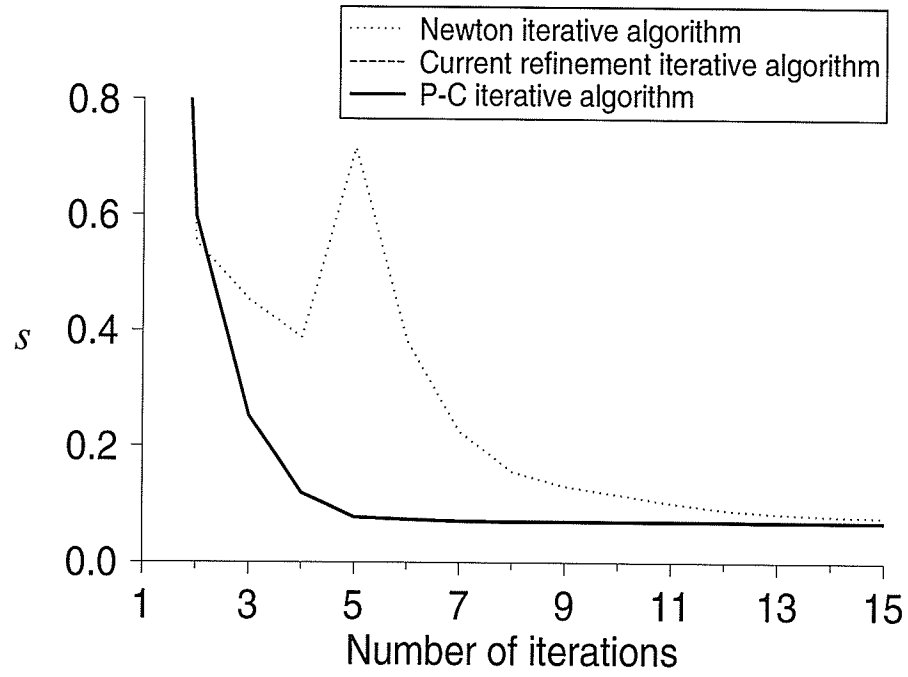

(a)

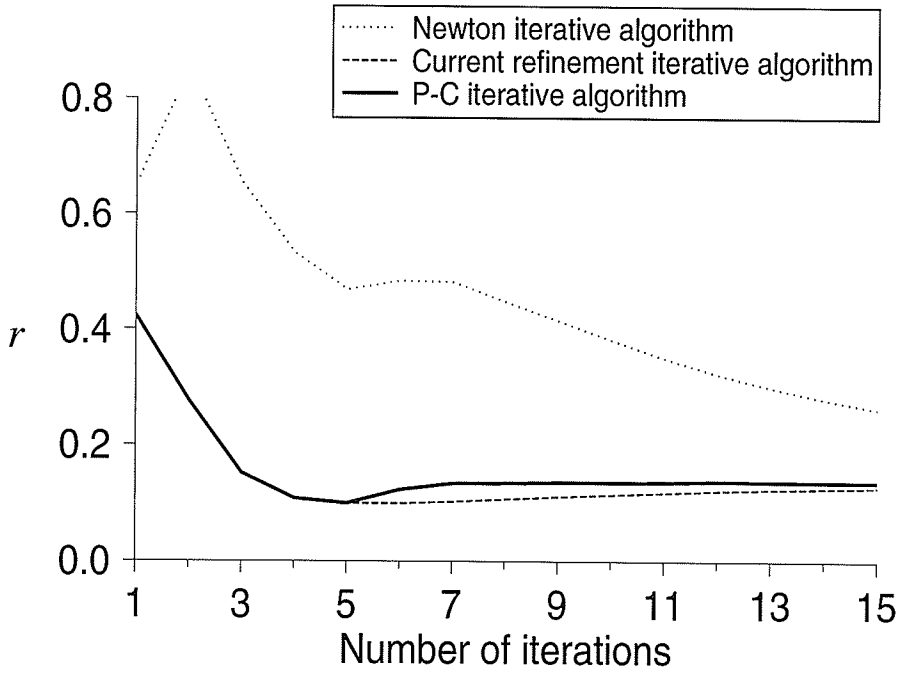

(b)

Fig. 5.15 : Errors s and r for example three in the presence of noise in the measured data: 5 illuminations, 13 receivers, and $g = 10^{-3}$ after the first iteration.

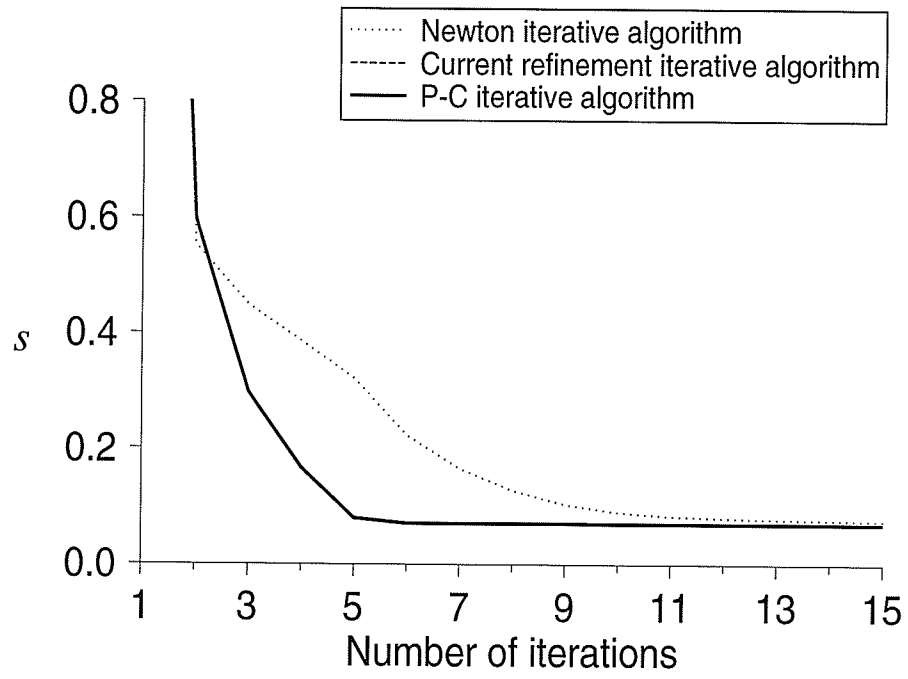

(a)

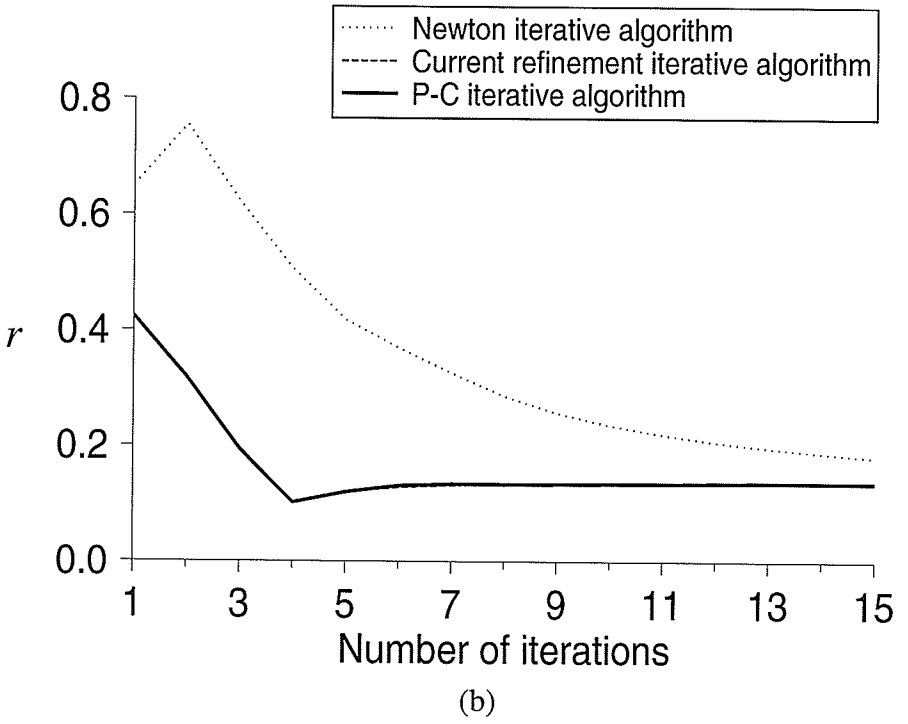

(b)

Fig. 5.16 : Errors s and r for example three in the presence of noise in the measured data: 5 illuminations, 13 receivers, and $g = 10^{-4}$ after the first iteration.

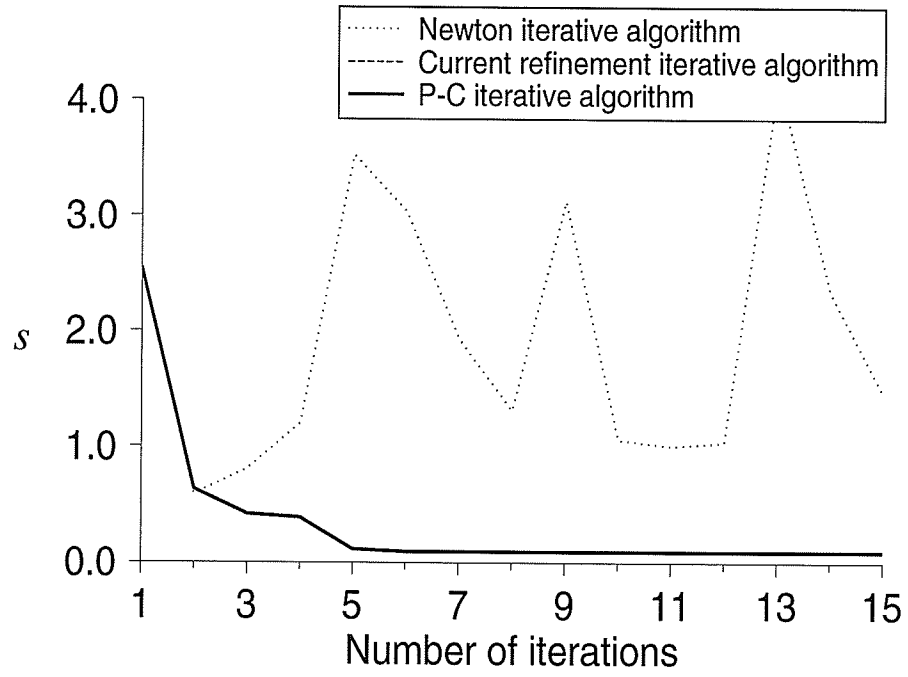

(a)

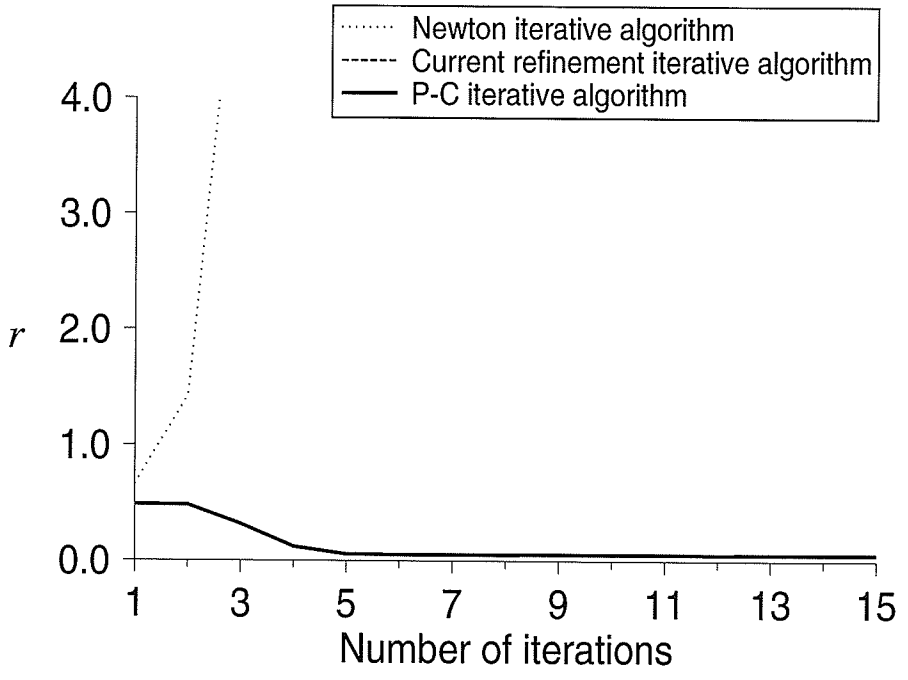

(b)

Fig. 5.17 : Errors s and r for example three in the presence of noise in the measured data: 22 illuminations, 13 receivers, and $g = 10^{-6}$ after the first iteration.

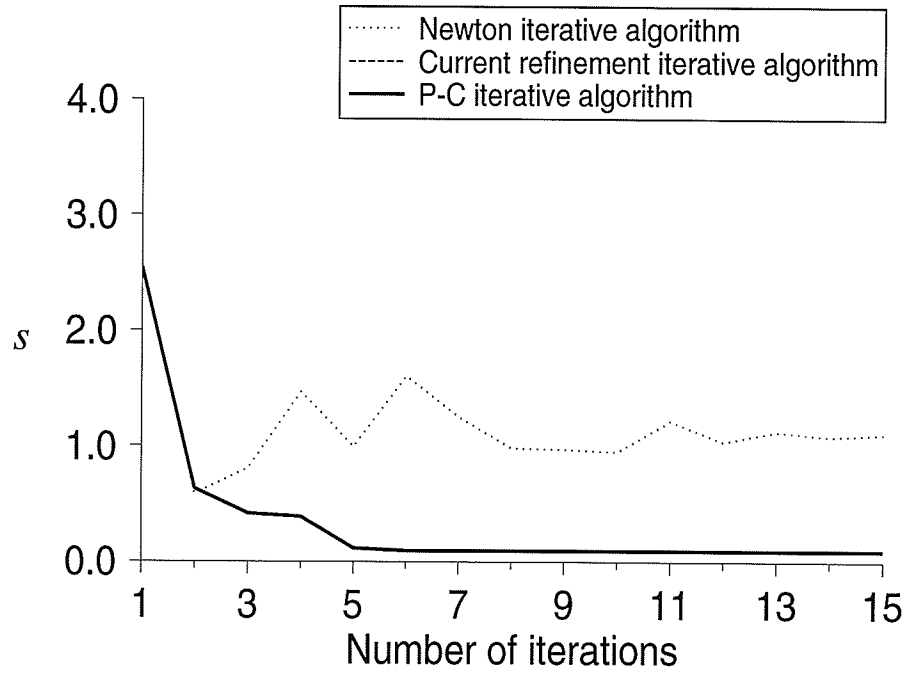

(a)

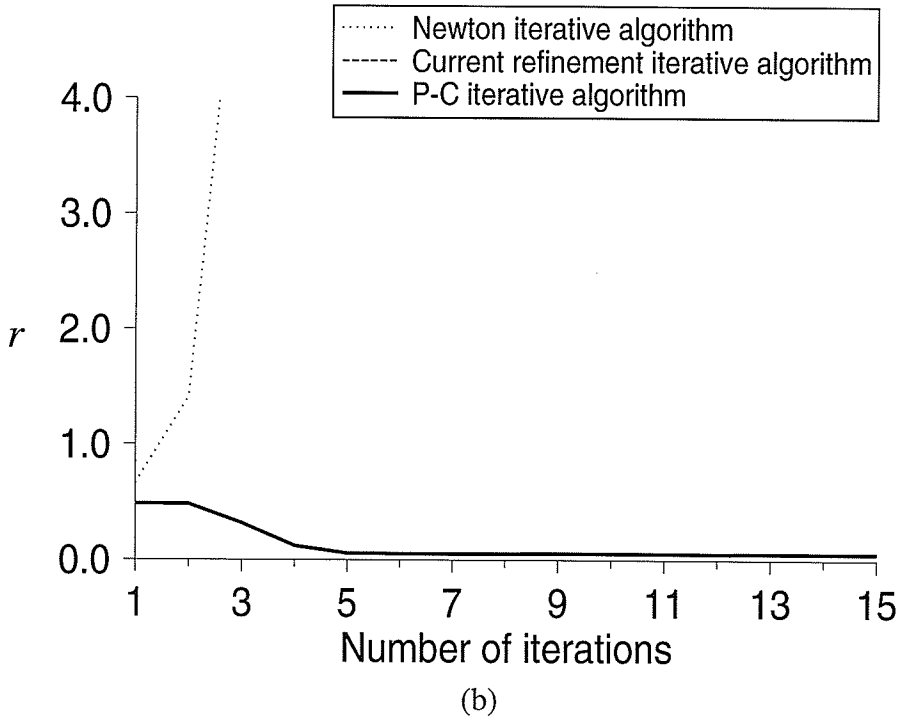

(b)

Fig. 5.18 : Errors s and r for example three in the presence of noise in the measured data: 22 illuminations, 13 receivers, and $g = 10^{-8}$ after the first iteration.

Chapter 6

Adaptive Algorithm for Optimization of the Iterative Process

6.1 Introduction

There are many iterative algorithms for electromagnetic imaging. For a given object to be imaged, before the numerical analysis, one has to select a algorithm to be used for numerical computation. Since the object is unknown or partly known, the decision is generally made by repeated numerical simulations. In the previous chapters, the current refinement and the prediction–correction algorithms are discussed. These algorithms improve the convergence and numerical stability of the iterative process. They can be applied with the Born or the Newton iterative techniques to solve the problems of electromagnetic imaging. However, the behavior of those algorithms are related to the technique used in the solution of the inverse problem and the distribution of the permittivity of the object. In this chapter, an adaptive algorithm is presented to optimize the iterative process by selectively using different iterative techniques. This adaptive algorithm is flexible in the sense that it can incorporate various available techniques and is capable to deal with a wider range of objects than existing methods.

In the next section, the current refinement algorithm with the Born and with the Newton iterative techniques are used to reconstruct different objects. The behavior of different current refinement algorithms are examined. Numerical tests show that for different objects, their behavior may be quite different and the optimum algorithm gives the better reconstruction results.

The adaptive algorithm is presented in section 6.3. In this algorithm, the performances of different algorithms are compared and the best one is selected for the next iteration. In order to fully utilize the results obtained in the iteration process itself, the results obtained by different iterative techniques in different iteration steps are used in an algorithm comparison. A ratio of decrease of the error in the computed scattered electric field is defined as the the criterion for the algorithm

selection. Compared with the determination of the optimum algorithm by separate numerical simulations, this method is numerically efficient. This algorithm is flexible for various unknown objects, since, in the iterative process, the suitable algorithm for the given object is found and applied. The combination of the strengths of different iterative techniques make this algorithm more powerful to deal with complex objects. The comparison of algorithms is a complex problem. The performance of different algorithms are affected by not only the numerical technique used for the inversion of an ill–conditioned matrix but also the the initial estimate of the object function at each iteration. Therefore, a maximum number for the continuous application of a single algorithm is set up to update the criteria used for algorithm comparison. This setup of the maximum number can also prevent the iteration process from becoming trapped at a local minimum.

In the numerical computation, a more complex example along with some of those described in chapter 4 are computed. Numerical results show that the adaptive algorithm optimizes the iterative process.

6.2 Comparison of Two Iterative Algorithms

The inverse scattering problem is a nonlinear and ill–posed problem. The application of iterative methods makes the solution of a nonlinear problem become the solution of a sequence of linear problems. In the Born and the Newton iteration technique, at each iteration, the direct problem is solved to obtain the total electric field and then, the ill–conditioned matrix equations for the inverse problem are solved to update the object function. The direct problem is a well–posed problem and the main concern is focused on the solution of the inverse scattering problem. Although in different algorithms, such as the Born and the Newton iterative methods, all ill–conditioned equations to be solved for updating the object function are linear, their structure is different and involves different eigenvectors. Thus, the errors in numerical results are different when applying different algorithms. The selection of an appropriate algorithm for a given object becomes important for efficient imaging [84].

In this section, objects with different types of permittivity distribution are computed by using the current refinement algorithm along with the Born and the Newton iterative techniques and the behavior of these two iterative algorithms are compared.

6.2.1 Object with Continuous Permittivity Distribution

Example 1 presented and computed in Chapter 4 is an object with continuous permittivity distribution. Seven illuminations and 28 receivers are used in illuminations and measurements as indicated in Fig. 4.1. The results obtained by using the current refinement algorithm with the Born and the Newton iterative techniques are shown in Fig. 6.1. In the numerical computation, the initial regularization parameter g changes to 6×10^{-3} from 6×10^{-4} after the first iteration. After the ninth iteration, the regularization parameter g is reduced to 2.7×10^{-3} and after the 13th iteration, it is reduced to 2.3×10^{-3}. It can be seen from Fig. 6.1 that the current refinement algorithm with the Born technique is more convergent than the one when using the Newton technique. In fact, after several iterations, the error in the object reconstruction for the algorithm with the Newton technique does not decrease any more.

6.2.2 Object with Discontinuities in Permittivity Distribution

Example 2 presented and computed in Chapter 4 is an object with discontinuities in permittivity distribution. Five illuminations and 13 receivers are used in illuminations and measurements as indicated in Fig. 4.2. The errors of reconstruction in the current refinement algorithm with the Born and the Newton iterative techniques at each iteration step is shown in Fig. 6.2. The regularization parameter is 10^{-9} except for the first iteration when the value is 6×10^{-4}. It can be seen that the algorithm with the Born technique is more convergent than the one using the Newton technique. Contrary to the results shown in 6.2.1, the results obtained by the current refinement

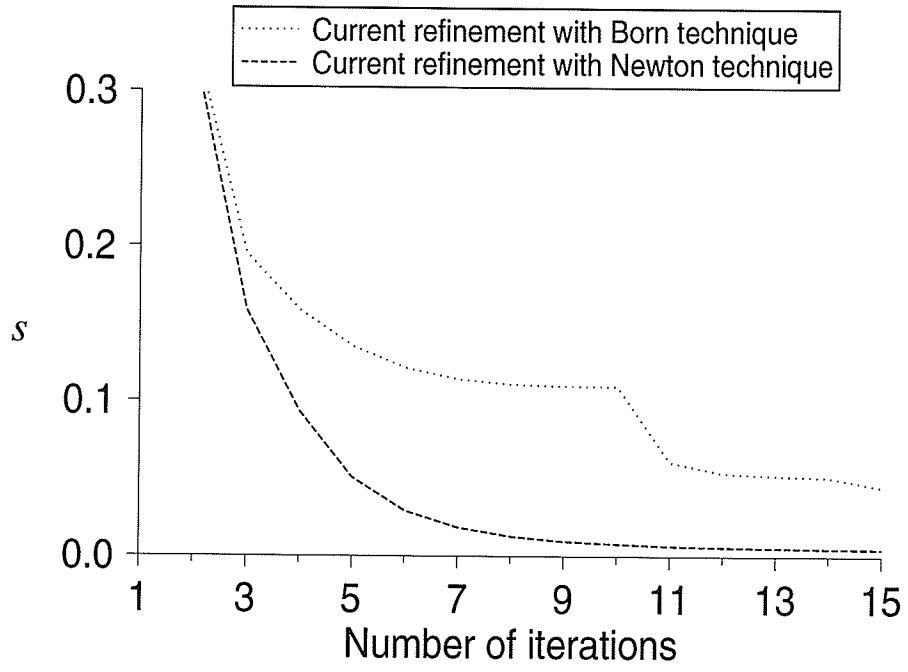

(a)

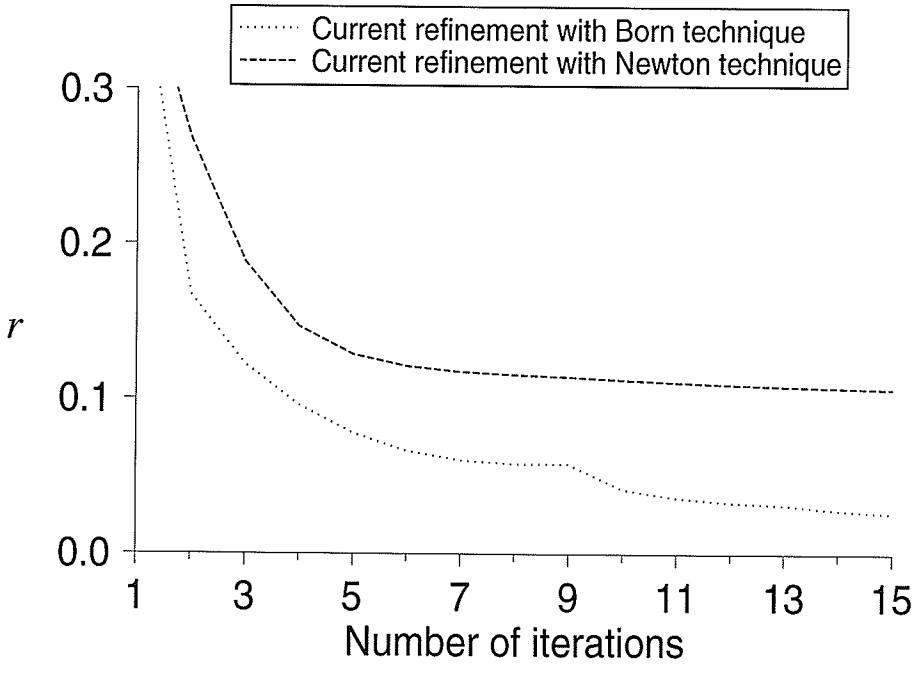

(b)

Fig. 6.1 : Errors s and r for example one by the different current refinement algorithms.

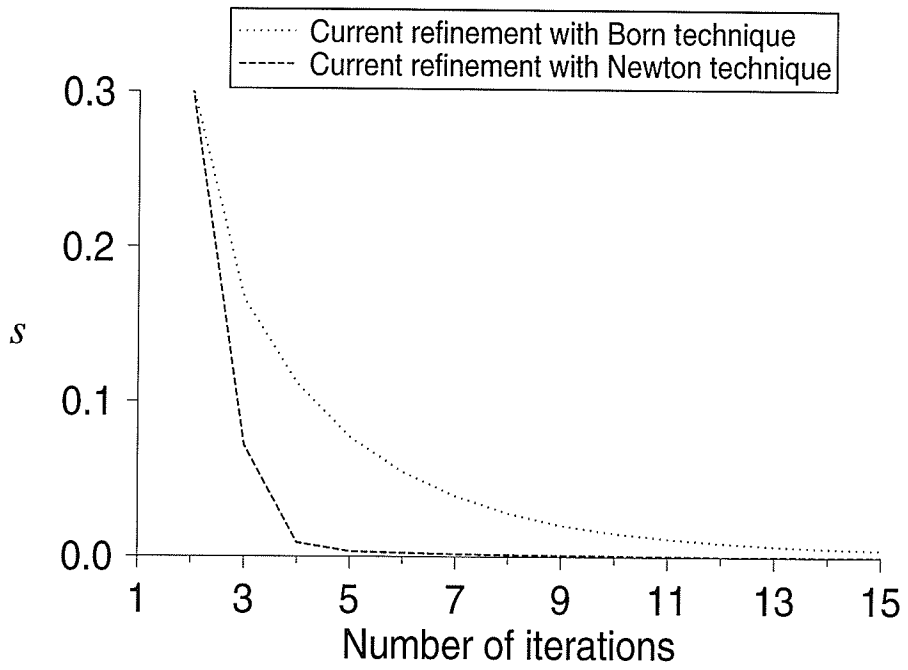

(a)

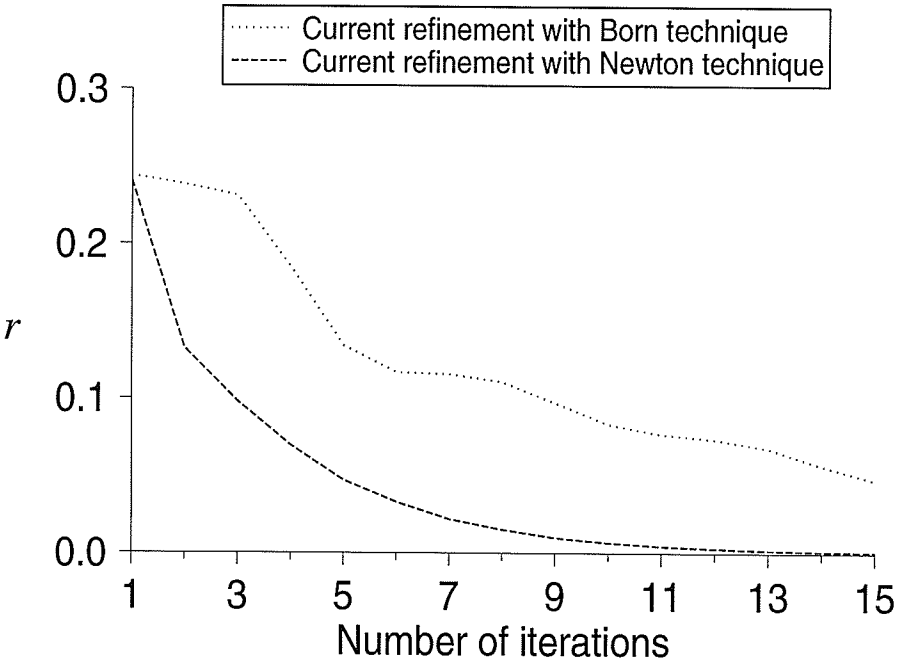

(b)

Fig. 6.2 : Errors s and r for example two by the different current refinement algorithms.

algorithm with the Newton technique is better than the one with the Born technique.

The current refinement algorithm provides better results than those corresponding to the iterative technique alone as shown in chapter 4. The convergence of the iterative process when employing the current refinement algorithm along with the Born or the Newton iterative technique appears to be quite different in different situations. Therefore, in solving a specific inverse scattering problem, the optimum iterative method has to be carefully determined in order to make the iterative process converge faster and get a good reconstruction. Numerical results presented in this section show that the Born iterative technique seems more advantageous for the continuous profile considered, while the Newton iterative technique is more suitable for the profile with discontinuities.

6.3 Adaptive Algorithm

In the above section, the different behavior of the equivalent current refinement algorithms with the Born and the Newton iterative techniques are compared by numerical simulations. These numeral results show the differences of their performances in different situations. However, it is not enough to draw a clear conclusion from these numerical results. This is because the effectiveness of different algorithms is also affected by factors such as the illumination and measurement arrangements, the selection of regularization parameters, and the matrix inversion techniques used. The convergence of an iterative process depends on many factors such as the initial estimate of the object function, the permittivity distribution of the object, the regularization parameter and the numerical technique for matrix inversion. Only when these effects on different algorithms are known, can a reliable comparison of different algorithms be made. At present, a rigorous mathematical analysis of the performance of such algorithms is not available. Repeated numerical simulations must be applied to obtain the information and determine the most suitable algorithm for the given object. From the engineering point of view, it is important to be able to determine a suitable algorithm for a given type of object. On the other hand, at a specified stage or step of an iterative process, the suitable algorithm may be different. For example, the simulated annealing algorithm

[53] at the final stage of an iterative process is effective in allowing the iterative process to escape from local minima but at the beginning of the iteration process this escape is not as important as ensuring a better convergence. Therefore, the selection of the appropriate algorithm to optimize the iterative process is important in the numerical computation.

To further optimize the iterative process, an adaptive algorithm is proposed. In this algorithm, different iterative algorithms are used selectively. The results obtained from those algorithms are compared and the appropriate algorithm is applied for subsequent iterations in the iterative process.

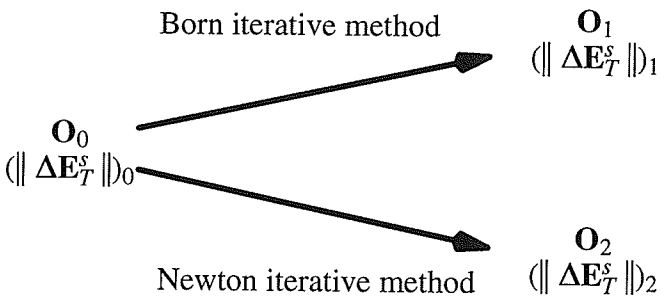

(a) The $\Delta \mathbf{E}_T^s$ obtained by using the same initial estimate of the object function.

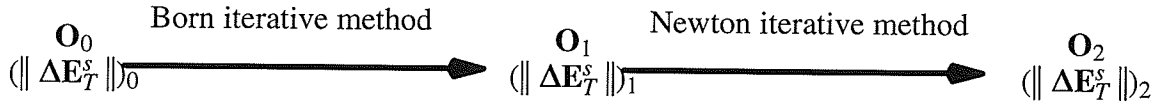

(b) The $\Delta \mathbf{E}_T^s$ obtained by using different initial estimates of the object function.

Fig. 6.3 : The computation of the $\Delta \mathbf{E}_T^s$ for different algorithms.

In order to find the suitable algorithm in the iterative process, we have to determine the criterion for comparing the performance of all applied algorithms and determine how to obtain the criteria for all algorithms. An immediate quantity that can be used as a criterion is $\|\Delta \mathbf{E}_T^s\|$ where the column vector, $\Delta \mathbf{E}_T^s$, represents the difference between the measured and computed scattered field. The better algorithm should provide smaller $\|\Delta \mathbf{E}_T^s\|$ in the same situation. The next problem is how to obtain those $\|\Delta \mathbf{E}_T^s\|$ for different algorithms. For example, consider the case when the Born

iterative technique and the Newton iterative technique are applied in iterations. One manner to obtain the data for comparison is applying all of them with the same initial estimate of the object function as illustrated in Fig. 6.3(a). The other way is using the results obtained at different iteration steps as illustrated in Fig. 6.3(b). For comparison, assume that the iteration results obtained in these two manners, shown in Fig. 6.3, satisfy

$$(\| \Delta \mathbf{E}_T^s \|)_0 > (\| \Delta \mathbf{E}_T^s \|)_1 > (\| \Delta \mathbf{E}_T^s \|)_2 . \tag{6–1}$$

From the results obtained by the first manner, one can conclude that the Newton iterative method is better than Born iterative method with respect to the same initial estimate of the object function and associated errors in the computed scattered field. However, it is not numerically efficient, because for comparison all algorithms must be used in computation with the same estimate of the object function. For the second manner, the main advantage is it is much more numerically efficient. The problem for the second manner is that the conclusion obtained by this criterion is questionable. Since the initial situations, $\mathbf{O}$ and $\|\Delta E_T^s\|$, for different algorithms are different, one can not conclude that the Newton iterative method has a better performance than the one for the Born iterative method from (6–1). Without consideration of the difference in the initial condition, the comparison using the data obtained in the second manner is a biased comparison. Therefore, a new criterion has to be found to deal with the results obtained in the second manner.

Here, we define a ratio of decrease of errors in the computed scattered electric field

$$R_j = \frac{\| \Delta \mathbf{E}_{Tj}^s \|_a}{\| \Delta \mathbf{E}_{Tj}^s \|_b} \tag{6–2}$$

as the criterion for the comparison of different algorithms where the subscript j stands for the j–th algorithm and $\| \Delta \mathbf{E}_{Tj}^s \|_b$ and $\| \Delta \mathbf{E}_{Tj}^s \|_a$ represent the errors in the computed scattered field determined from the estimate of the object function available before an iteration and from the estimate of the object function available after the iteration, respectively. This criterion, which uses the ratio of the error norms, is more effective than that using the error norm itself. It selects the algorithm that yields the greatest rate of decrease of the error, rather than the algorithm with the

smallest error as illustrated in Fig. 6.4. In this criterion, the effect from different initial estimates

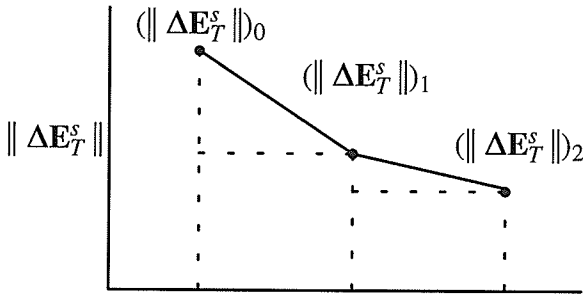

Fig. 6.4 : The illustration of the criterion for algorithm selection.

of the object function is also suppressed by the introduction of $\| \Delta \mathbf{E}_{Tj}^s \|_b$. If the criteria for different algorithms is obtained by the first manner mentioned above, $\| \Delta \mathbf{E}_{Tj}^s \|_b$ for all algorithms are the same and the performances of different algorithms are determined by their differences in $\| \Delta \mathbf{E}_{Tj}^s \|_a$. This criterion is still applicable.

In actual computation, different algorithms are selectively employed at different iteration steps. At each iteration step, only the selected algorithm is employed and its criterion is updated by using the newly obtained results.

The comparison of different algorithms is a complicated problem. Various factors affect the ratios used for the algorithm comparison. The method for the algorithm selection proposed here is a quite simple one and in some cases it may not work well. In this adaptive algorithm, the combination of different iterative technique is determined by the values of their criteria. When the criteria are obtained by using the estimates of the object function far from the one newly obtained, they may not represent the performances of the corresponding algorithms with the newly obtained estimate. The algorithm comparison fails to find the proper algorithm from those data. Consider the case that the *i*–th algorithm is efficient in the early stage of the iterative process and the *j*–th one is efficient in the final stage of the iterative process. If these two algorithms are applied in an iterative

process, a very small R_i and a very high R_j may be obtained in the early stage of the iterative process. Thus, the j–th algorithm may not be employed in the whole iterative process because of its high R_j. The iterative process fails to select the suitable algorithm for each iteration and can not provide a better image. Consider another example in which a specific algorithm is continuously applied many times in an iterative process. The differences from the newly obtained estimate of the object function to the ones used for the criteria of other algorithms become larger. These criteria do not show the behavior of the corresponding algorithms with the new estimate. The comparison based on these ratios is not reliable. Based on the above consideration, we set a maximum number N_m for which an algorithm can be continuously applied. Once any algorithm is continuously applied N_m times, all algorithms will be applied successively to update their R_j. This updating of the ratios can prevent the above situation from happening. Since the updating of all R_j requires more iterations, the updating of ratios for different algorithms consumes more computer time and reduces the efficiency of the computation. Therefore, the maximum number N_m for the continuous application of a single algorithm should be determined carefully. The prevention of the situations discussed above is not the only reason for the setup of N_m. In numerical computation, when using a single iterative algorithm, the process may be trapped at a local minimum and can not converge to the global minimum. The application of other iterative algorithms may interrupt the loop of repeated iteration around the same estimate and help the iteration process out of the trap. From this point of view, the other non–optimum algorithms may play important roles. In the simulated annealing algorithm, the prevention of the iteration trapped at a local minimum is provided by using a random change of the object functions. Here, it is done by changing the algorithm and this is more efficient. When updating all criteria, poorer estimates of the object function are obtained because of the employment of non–optimum algorithms. These poor estimates may make the iterative process divergent. Therefore, this procedure has to be applied with the prediction–correction technique in order to prevent divergence in the iterative process.

Consider an iterative process by using an adaptive algorithm. The initial values of $R_1, R_2, \ldots$

. are all taken to be equal to unity. In a first iteration we apply, say, the first algorithm and compute the new R_1, with $\| \Delta \mathbf{E}^s_{T1} \|_b$ considered to be the norm of the vector consisting of the vectors $\mathbf{E}^s_l$ corresponding to the measured scattered field for all illuminations. If the new R_1 is less than unity, then the second iteration is performed by employing the first algorithm again. In the case where the new R_1 is greater than or equal to unity, we apply the second algorithm for the second iteration and compute the new R_2, with $\| \Delta \mathbf{E}^s_{T2} \|_b$ being the same as in the previous iteration. After each iteration we update the corresponding ratio (6–2) and continue the iterative process by using the algorithm which has the smallest R_j. When some of the algorithms have the same value of R_j, the next iteration is performed by using the closest succeeding algorithm. On the other hand, if the same algorithm has been used consecutively for a chosen number N_m of iterations, then we apply in successive iterations, in turn, all of the other algorithms to update all the values of R_j, and each time the object function before an iteration is taken to be the object function computed in the preceding iteration. The updated values of all R_j are compared and the iterative process is continued by employing the algorithm with the smallest R_j. This procedure is repeated until the end of the iterative process. The usage of the same algorithm in only a fixed number N_m of consecutive iterations prevents the iterative procedure from being trapped in a local minimum of the global error in a similar manner as in the simulated annealing algorithm where a random change of the object function is used. This adaptive algorithm incorporates the positive features of the individual prediction–correction algorithms employed and performs substantially better than these algorithms when applied separately to various body reconstructions. The proposed algorithm can be summarized as follows:

(a) set all $R_j = 1$; apply the first algorithm and compute R_1 ;

(b) if $R_1 \geq 1$ select the second algorithm; otherwise take the first algorithm to be the selected algorithm;

(c) apply the selected algorithm in the next iteration and update the corresponding R_j ;

(d) when the same algorithm has been used in N_m consecutive iterations, apply in turn all the algorithms in successive iterations to update all R_j;

(e) compare all R_j and select the algorithm which has the smallest R_j (when several algorithms have the same smallest value of R_j, select the closest succeeding algorithm);

(f) if the error in the computed scattered field is acceptable, end the iterative process; otherwise go to (c).

The advantage of using the adaptive algorithm is that it optimizes the iterative process by selectively using different algorithms. In an iteration process, at a specific iteration step or at different stages such as the beginning and the final stages, the optimum algorithms are different. To find the suitable algorithm for a specific iteration step or stage, using separated numerical simulations with different combinations of different algorithms require much more computation. In this new algorithm, different algorithms are automatically combined together to get better results at different iterative steps and stages. Therefore, it is quite efficient. In the first section, it has been shown that the behavior of different algorithms in different situations are quite different and specific iteration methods are more efficient than the other methods for the reconstruction of specific objects. The adaptive algorithm combines the strengths of different algorithms. It is flexible to different objects. The employment of the adaptive algorithm is more powerful than the employment of single algorithms in dealing with complex objects.

6.4 Numerical Results

In this section, the computation results of example one, example two and a new example, example four, with its permittivity shown in Fig. 6.5, by using the adaptive algorithm are presented. In the adaptive algorithm, the algorithm comparison is carried out between the Born and Newton iterative techniques along with the prediction–correction and the current refinement techniques. The results by the adaptive algorithm and the algorithms which are used in the adaptive algorithm are discussed.

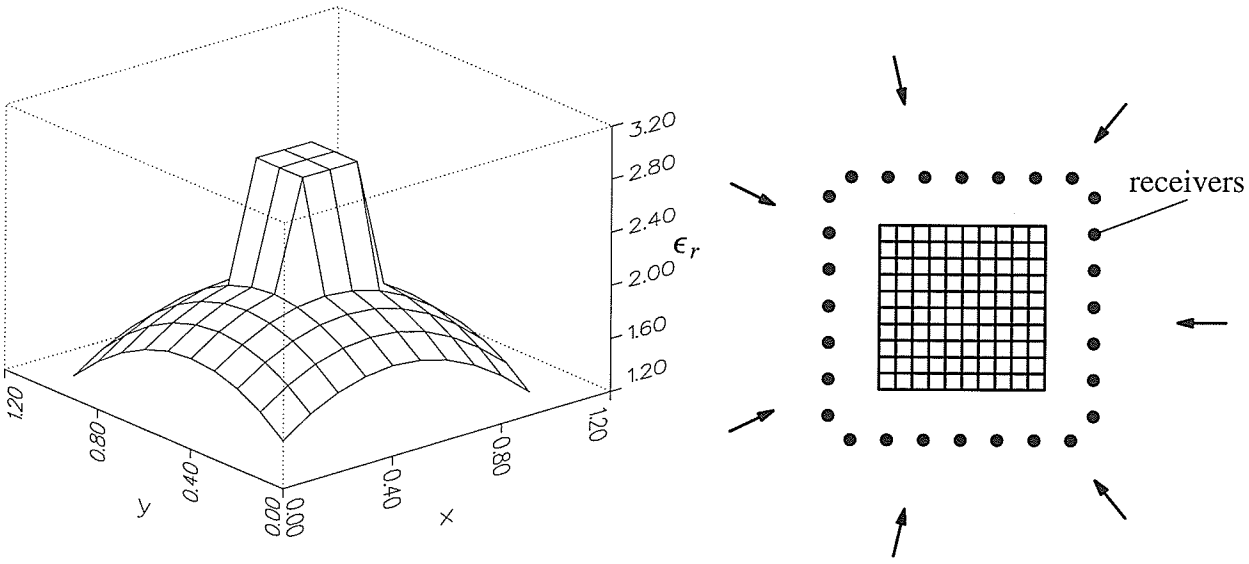

(a) permittivity profile. (b) discretization grid.

Fig. 6.5 : The grid and the permittivity distribution of example 4.

Example 4 – A lossless dielectric cylinder of square cross section with continuous permittivity distribution similar to example one except for a central square subregion on the boundary of which the permittivity has a salient discontinuity is shown in Fig. 6.5(a). The maximum and the minimum of ϵ_r are 3 and 1.2, respectively. The cross section is discretized in 100 cells (cell size $0.1\lambda \times 0.1\lambda$), as shown in Fig. 6.5(b). The illumination is provided by line sources parallel to the cylinder placed successively at different positions, equally spaced around the cylinder at a distance of six wavelengths from its center. The scattered field is measured by equidistant receivers on a $1.67\lambda \times 1.67\lambda$ square contour as indicated in Fig. 6.5(b).

For example one, 7 illuminations are applied and 28 receivers are used to measure the scattered field, the same as used in chapter 4 for the numerical experiments. The results are pres-

ented in Fig. 6.6 and Fig. 6.7. Except 6×10^{-4} for the first iteration, the regularization parameter used in the iteration process is 6×10^{-3}, and then reduced to 3×10^{-3} for Fig. 6.6 and to 3×10^{-5} for Fig. 6.7 after the 5th iteration.

The adaptive algorithm provides faster convergence. For the parameter s, representing the errors in the computed electric field, the value obtained by using the adaptive algorithm is smaller than the values obtained by other algorithms. The parameter r, representing the error in the object reconstruction, is better or equal to the values obtained by the Born iterative technique which is much better than the ones obtained by using Newton iterative technique. An interesting feature is that when using the Newton iterative technique, the error in the computed scattered field is much smaller than the one by using the Born iterative technique. In practical computation, the quantity which can be determined is the error in the computed scattered field, since the object is unknown and the error in reconstruction, r, cannot be obtained. The larger s for the Born iterative technique makes it difficult to determine if its reconstruction is good. The adaptive algorithm provides both small s and r. Therefore, the parameter s for the adaptive algorithm can be used to more accurately measure the degree of the object reconstruction.

For the second example, the results are presented in Fig. 6.8 and Fig. 6.9. Except 6×10^{-4} for the first iteration, the regularization parameter is 10^{-6} for Fig. 6.8 and 10^{-10} for Fig. 6.9. The adaptive algorithm is not as convergent as the optimal prediction–correction algorithm with Newton iterative technique, although it also provides a good reconstruction. This is because it has to compare the performance of all iterative algorithms in the whole process. However, when the optimum one is not known, one has to try other algorithms in order to find the best algorithm. The use of the adaptive algorithm is still efficient.

Example four is a more complex example and is used to check if the adaptive algorithm is able to combine the different specialties of different algorithms and reconstruct complex objects. For the results shown in Fig. 6.10, along with the prediction–correction algorithm, the regularization parameter for the Born iterative technique, which is 10^{-7} at the final stage of the iteration pro-

cess, is different from the one for the Newton iterative technique, which is 10^{-9} at the final stage of the iteration process. Nine illuminations and 28 receivers are used for Fig. 6.10. The adaptive algorithm combines these two algorithms with their own regularization parameters (After 6×10^{-4} used as the initial value, for the Born technique, g is 6×10^{-3}, 10^{-5}, 10^{-6} and 10^{-7} after the first, 9th, 40th and 55th iterations, respectively; for the Newton technique, g is 6×10^{-3}, 10^{-5}, 10^{-8} and 10^{-9} after the first, 9th, 15th and 60th iterations, respectively). The results shown in Fig. 6.10 illustrate that the adaptive algorithm has a smaller error of reconstruction than the other two algorithms. The final error of reconstruction for the adaptive algorithm is 2.06%. To see the reconstruction error with more illuminations, the case of 13 illuminations and 28 receivers is computed and the results are shown in Fig. 6.11. The adaptive algorithm provides better results than those obtained by using other algorithms. The final error of reconstruction for the adaptive algorithm is 2.64%. Although the illuminations used for Fig. 6.11 are almost one half more than the one for Fig. 6.10, the reconstruction is worse than the one in Fig. 6.10. From these two cases, it can be seen that the reconstruction is very closely related to the illumination and receiving arrangement in data measurement. In these two numerical experiments, the difference between the CPU time for the adaptive and the prediction–correction algorithms is less than 2%, although the reconstruction error for the adaptive algorithm is about one half of that for the corresponding algorithms.

Next 20dB noise is added to the measured data and the different objects are computed by the adaptive algorithm. For example one, with the same physical situation as in Fig. 5.6, the results are shown in Fig. 6.12. For Fig. 6.12, except 6×10^{-4} for the first iteration, the regularization parameter is 9×10^{-3}. For example two, with the same situation as the one in Fig. 5.13, the results are shown in Fig. 6.13. For example four, the results are shown in Fig. 6.14 and 6.15. In the computation, 8 illuminations and 28 receivers are used in the measurement. The regularization used in the iteration process is 3×10^{-2} for Fig. 6.14 and 6×10^{-3} for Fig. 6.15 after an initial value of 6×10^{-4} used in the first iteration. The performance of the adaptive algorithm is

not as good as the one in the case of no noise present in the measured data. When noise is present in the measured data, the difference between the computed scattered field obtained from the actual object function and measured data is not zero. The reason is the effect of the noise not being considered in the criterion for the algorithm selection. Now the criterion in (6–2) is not as efficient as for the case when the noise is not present.

6.5 Conclusion

The adaptive algorithm is an efficient and flexible algorithm. It optimizes the iterative process by selectively using different algorithms. In this algorithm, the performances of different iterative techniques are compared within the iterative process in order to determine the more appropriate choice for subsequent iterations. The flexibility of this algorithm is that it can incorporate various available techniques and is capable of dealing with a wider range of objects than the other methods. In the algorithm comparison, as shown in Section 6.2, the ratio of decrease of the error in the computed scattered electric field is used as the the criterion for the algorithm selection. Because of the complexity, a maximum number for continuous application of a single algorithm is set up for updating the criteria for all algorithms. Numerical results show that this algorithm works well in the reconstruction of quite different objects when no noise is present in the measured data.

The algorithm proposed in this chapter is a primary work and more investigation of the algorithm performance, especially for the case when noise is present in the measured data, must be done in the future.

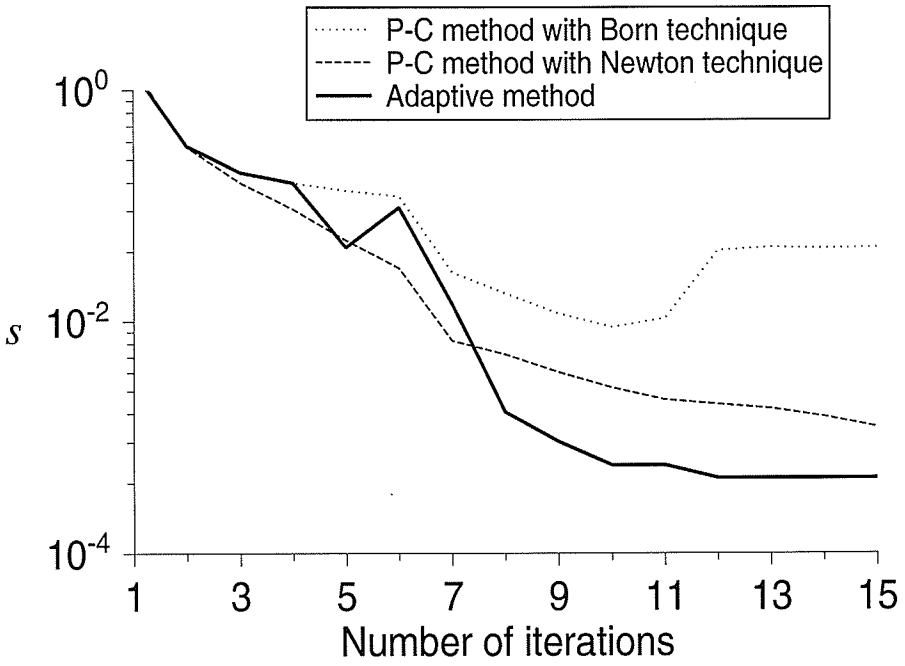

(a)

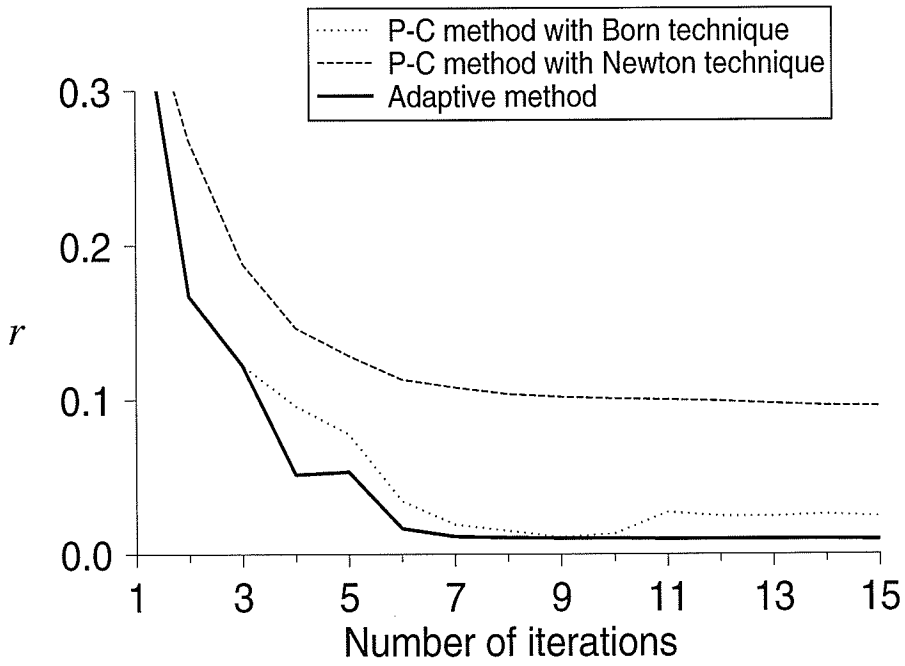

(b)

Fig. 6.6 : Errors s and r for example one with $g = 3 \times 10^{-3}$ after the 5th iteration.

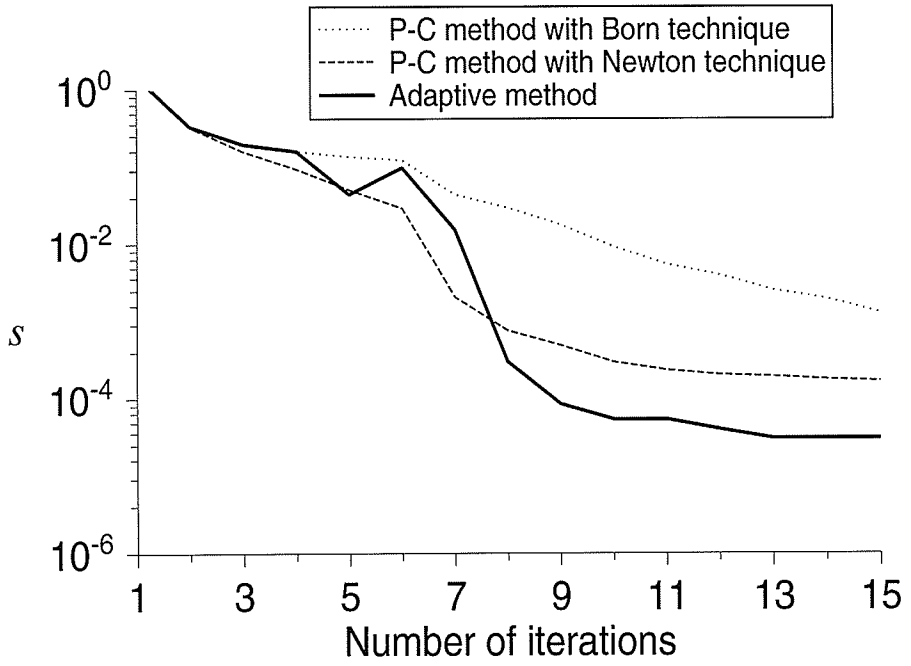

(a)

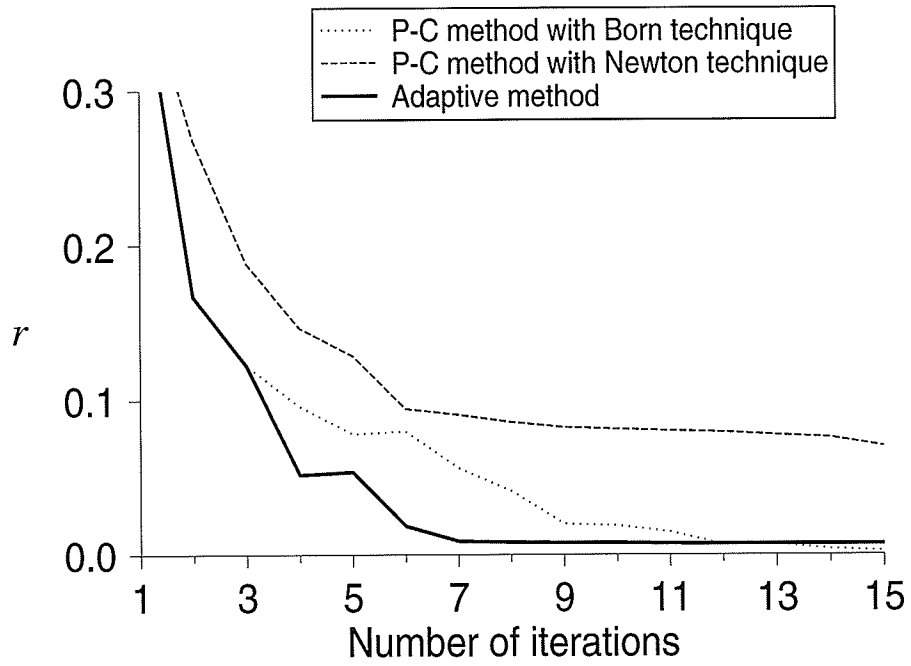

(b)

Fig. 6.7 : Errors s and r for example one with $g = 3 \times 10^{-5}$ after the 5th iteration.

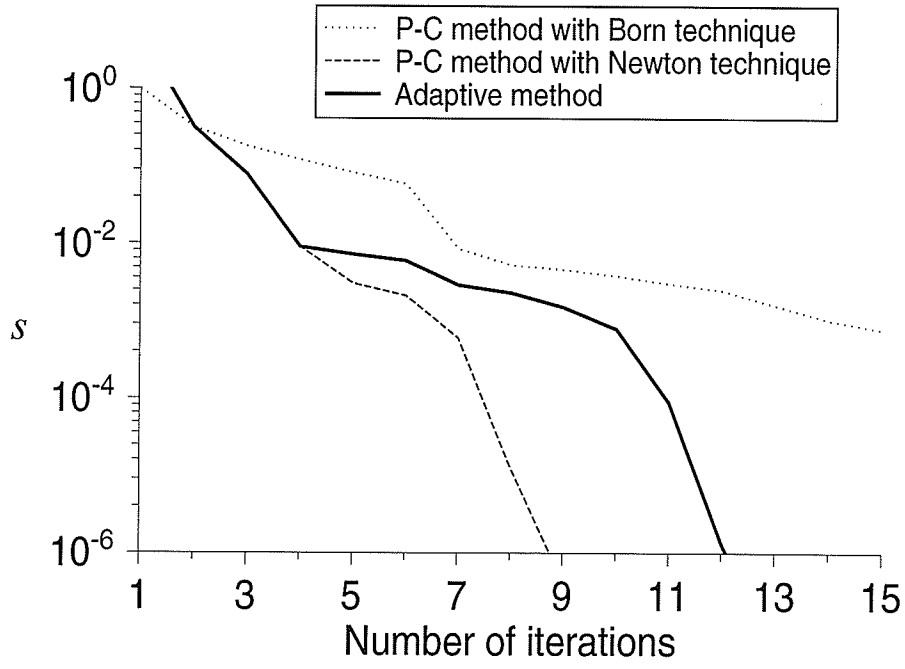

(a)

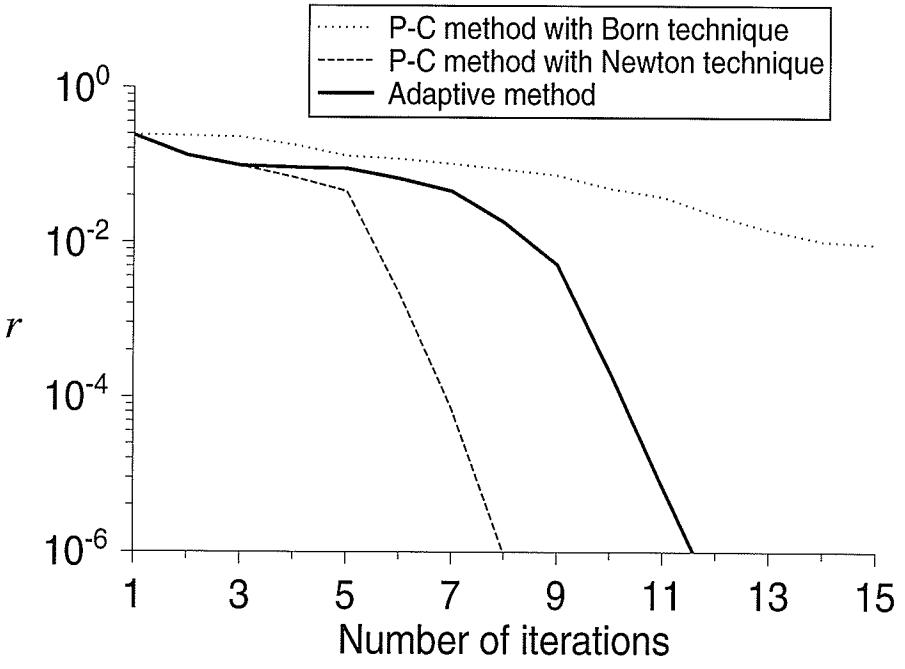

(b)

Fig. 6.8 : Errors s and r for example two with $g = 10^{-6}$ after first iteration.

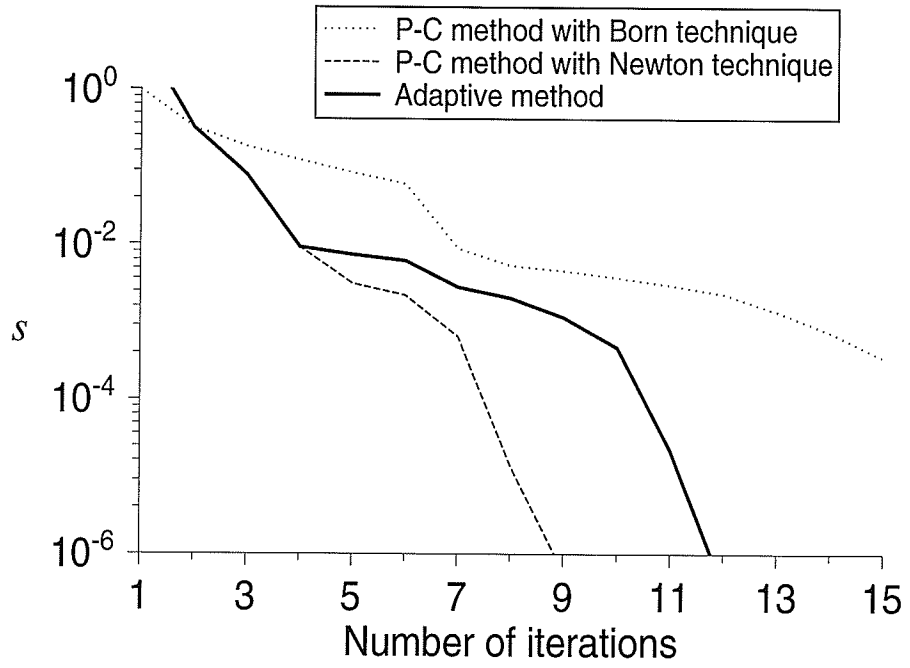

(a)

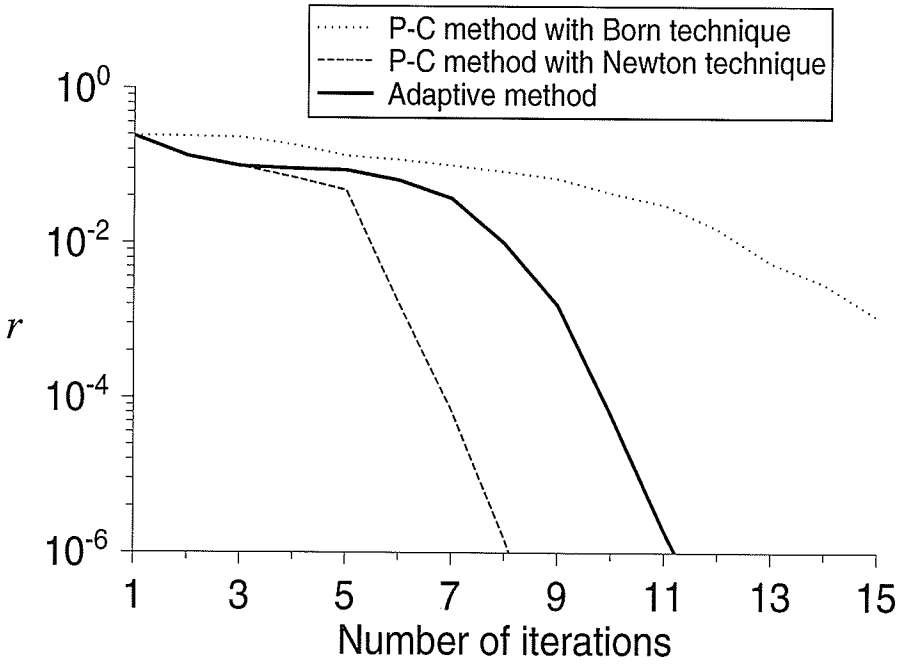

(b)

Fig. 6.9 : Errors s and r for example two with $g = 10^{-10}$ after first iteration.

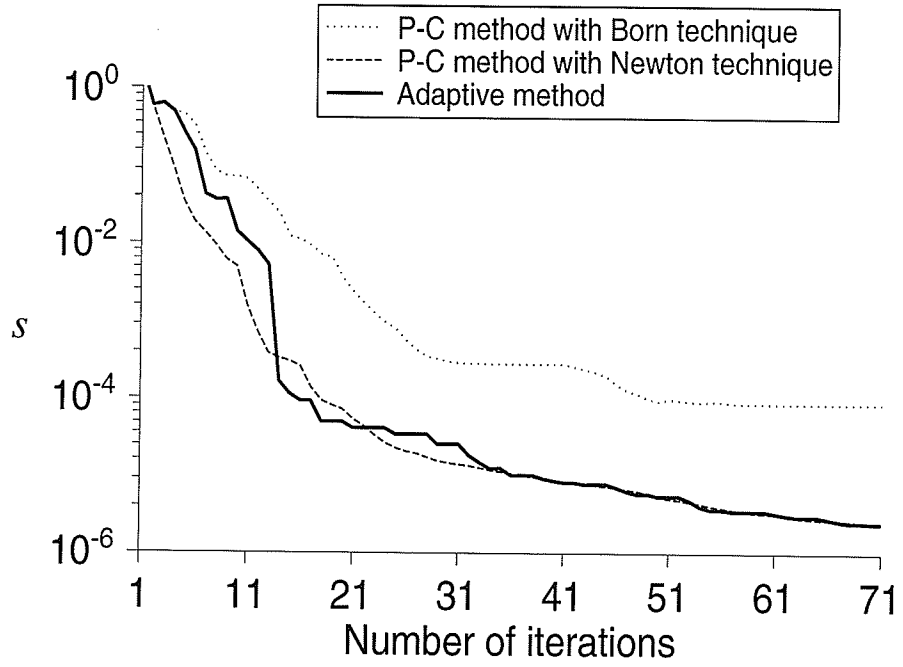

(a)

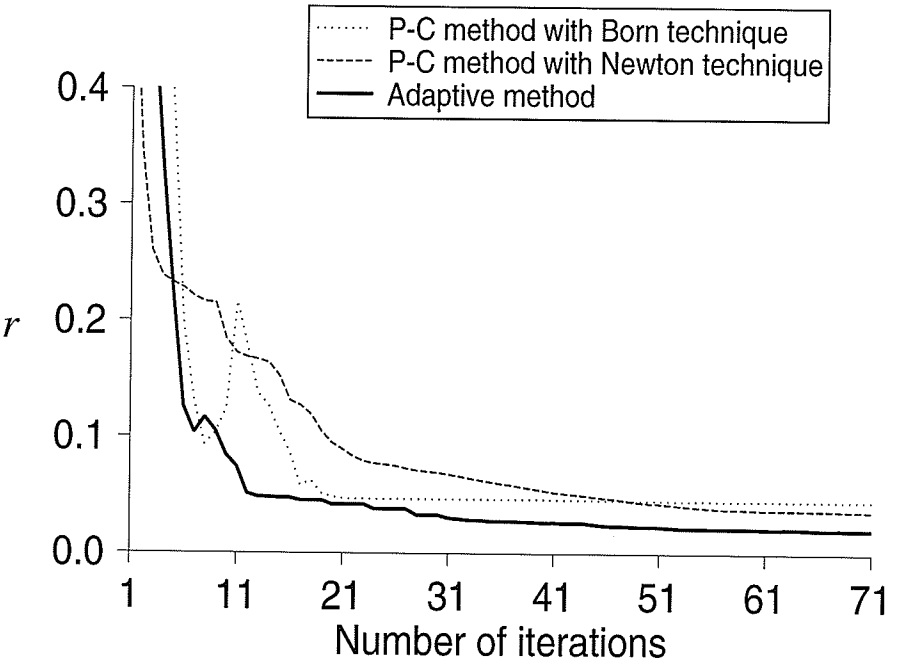

(b)

Fig. 6.10 : Errors s and r for example four with 9 illuminations used.

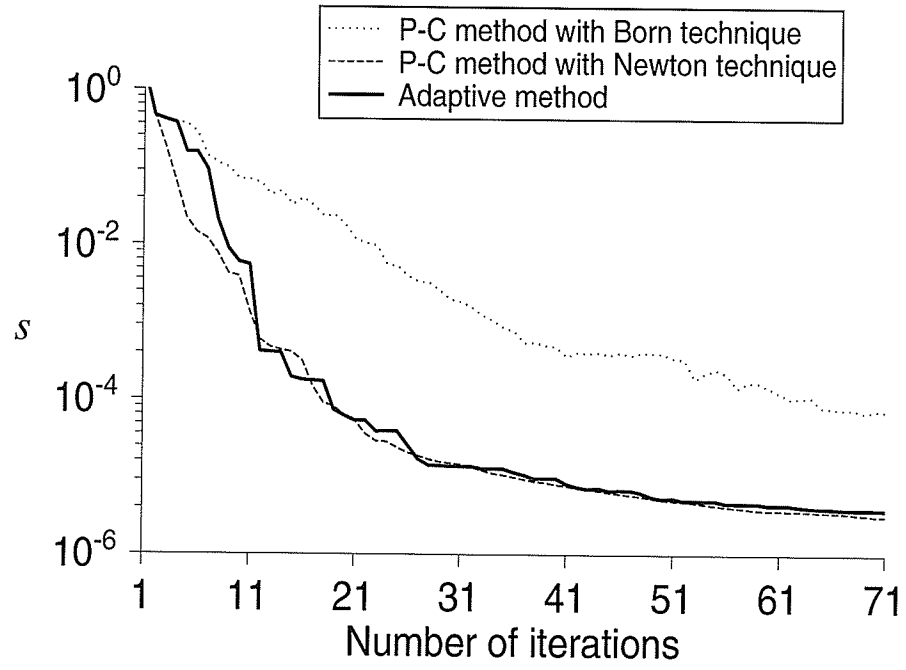

(a)

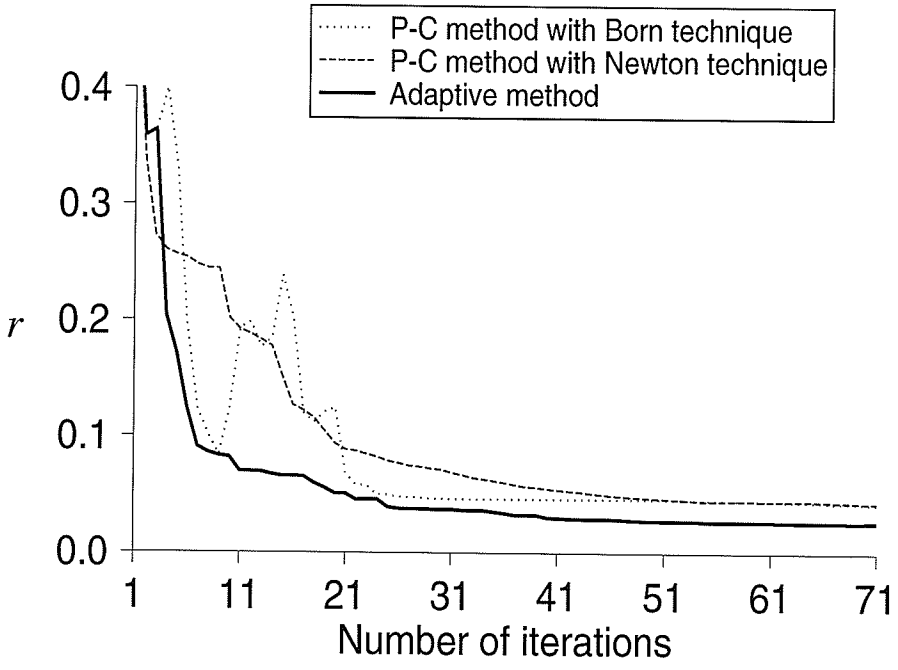

(b)

Fig. 6.11 : Errors s and r for example four with 13 illuminations used.

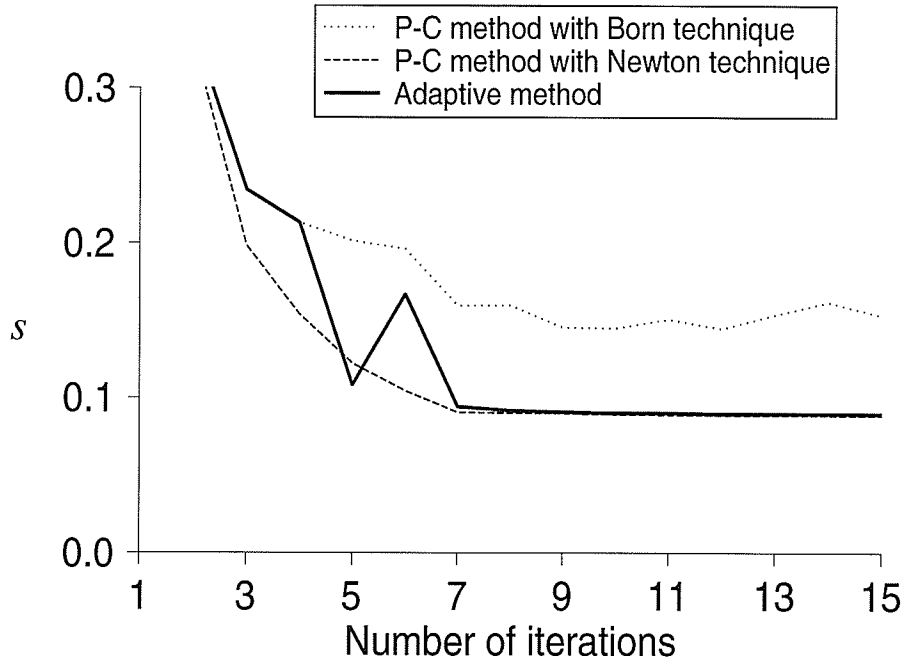

(a)

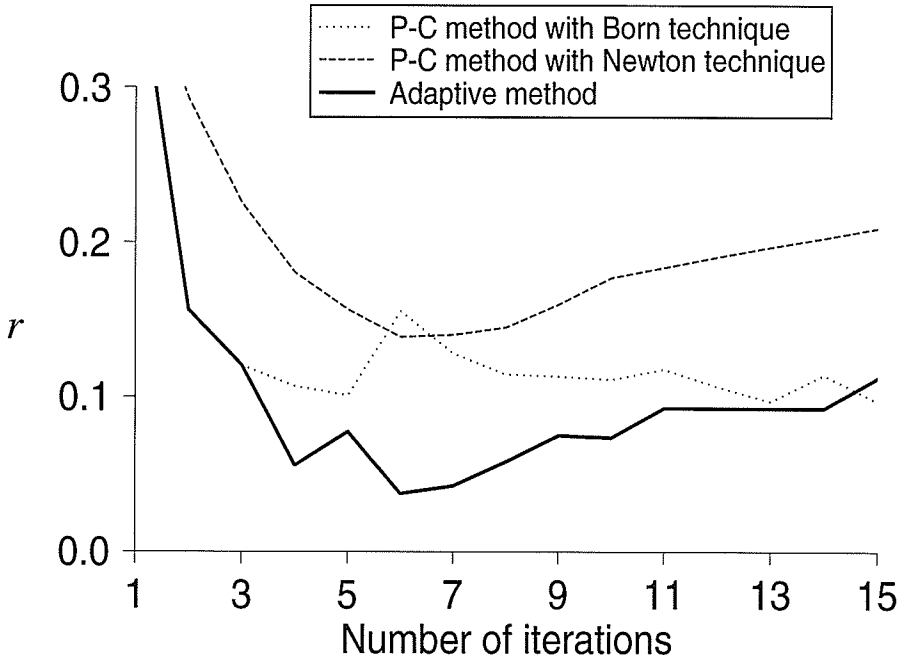

(b)

Fig. 6.12 : Errors s and r for example one in the presence of noise in the measured data, $g = 9 \times 10^{-3}$ after the first iteration.

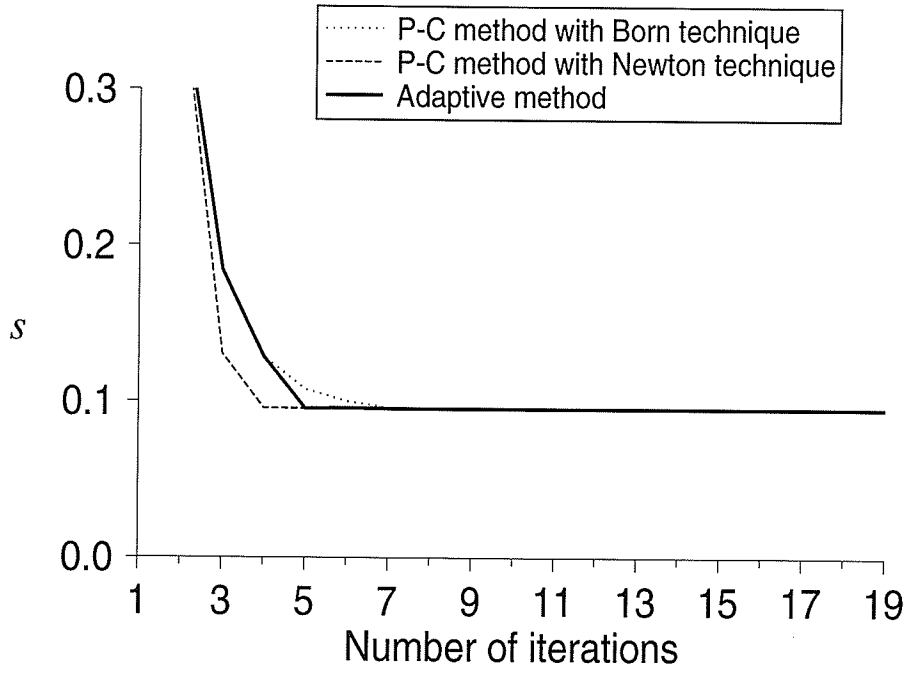

(a)

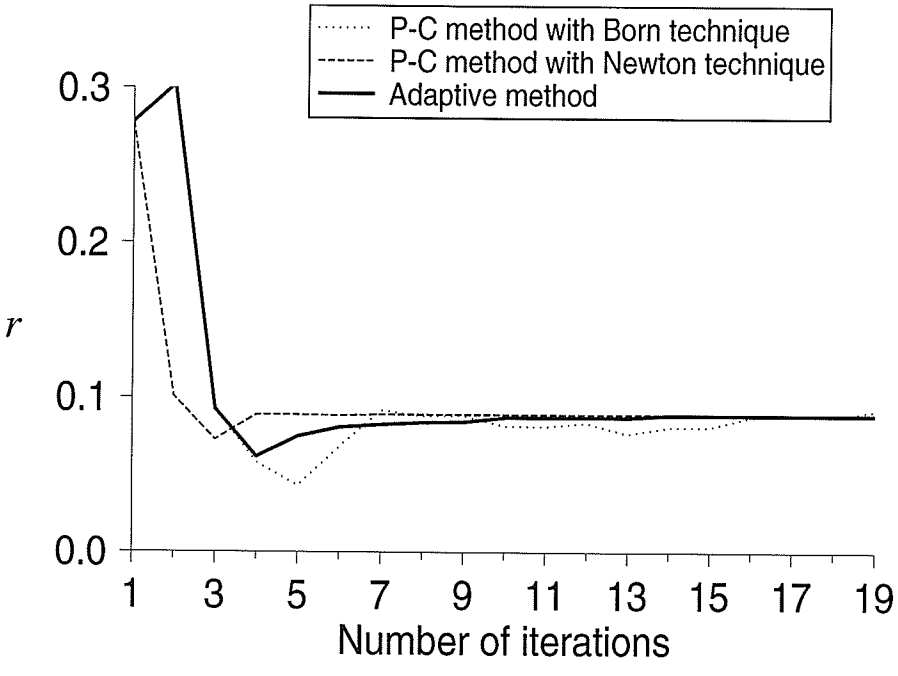

(b)

Fig. 6.13 : Errors s and r for example two in the presence of noise in the measured data, in the same situation for Fig. 5.13.

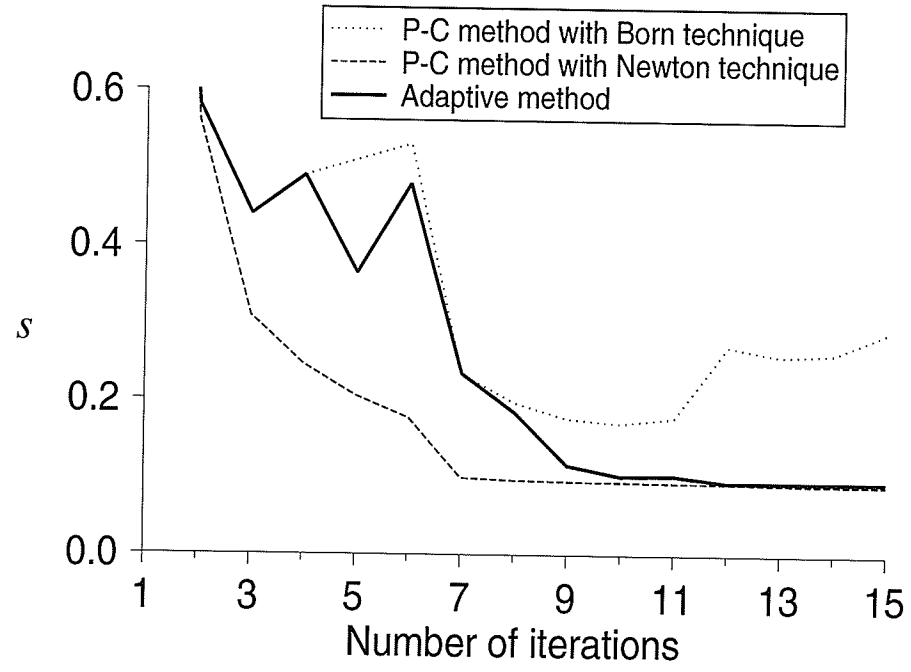

(a)

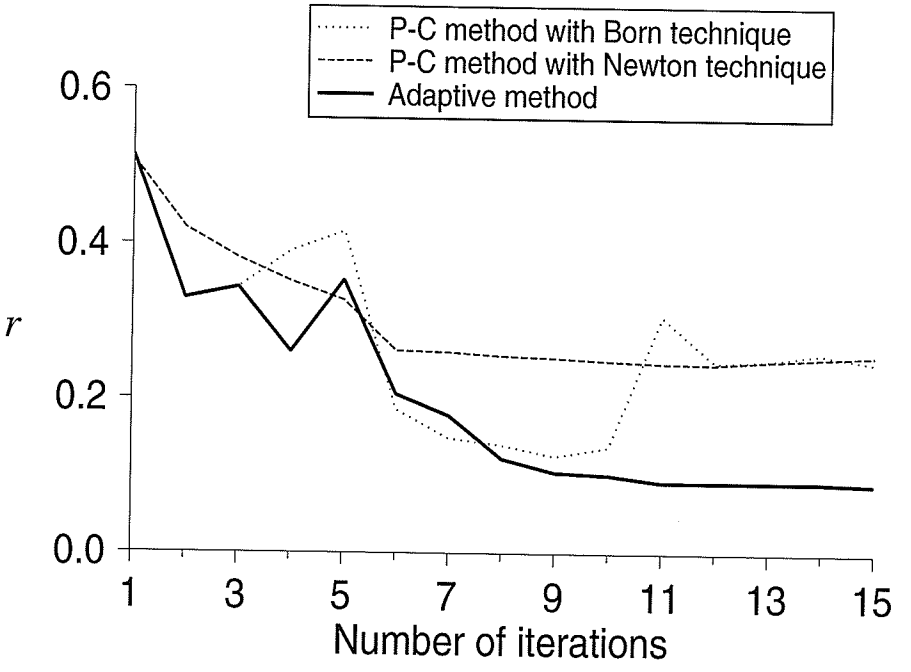

(b)

Fig. 6.14 : Errors s and r for example four in the presence of noise in the measured data, $g = 3 \times 10^{-2}$ after the first iteration.

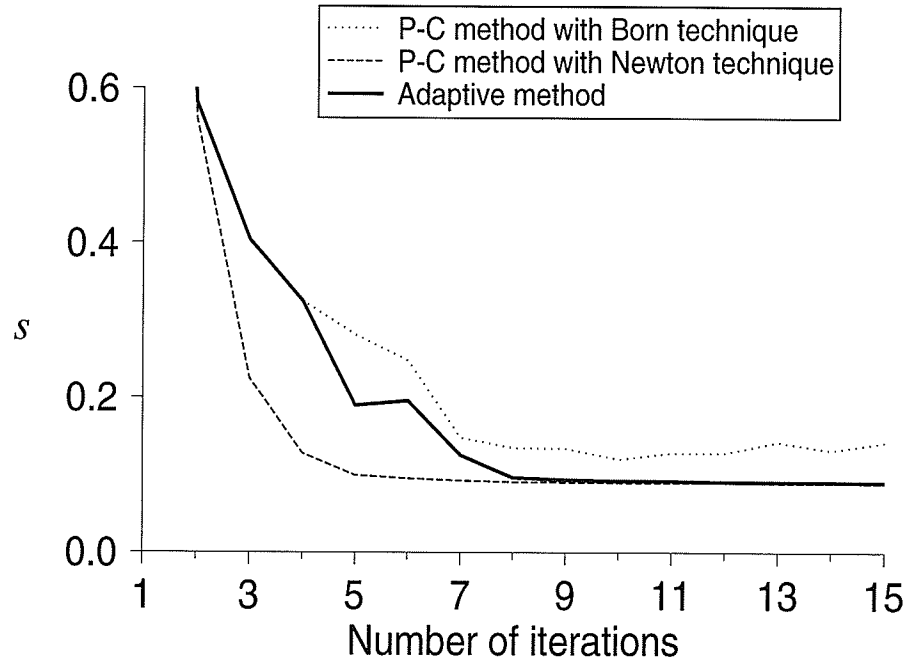

(a)

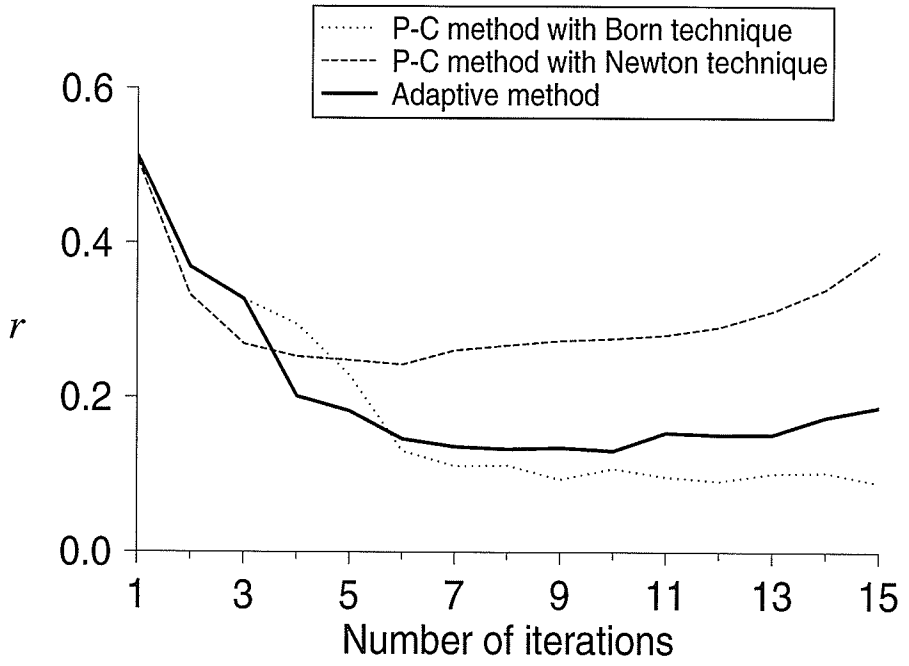

(b)

Fig. 6.15 : Errors s and r for example four in the presence of noise in the measured data, $g = 6 \times 10^{-3}$ after the first iteration.

Chapter 7
Three–Dimensional Object Reconstruction

7.1 Introduction

This chapter is an extension of the discussion about the iterative techniques presented in previous chapters to the three–dimensional case. In the 3–D case, more components of electric field have to be considered in the integral equations for the direct and inverse problems. The electric field integral equations become more complex. After the application of the moment method, the electric field integral equations for three–dimensional problems are transformed into matrix equations. These matrix equations can be expressed in the same form as the ones for two–dimensional problems. Thus, the discussion of the numerical computation is quite similar to the previous discussion for the problems in 2–D case. The main difference between three–dimensional and two–dimensional problems is that more information is available and the amount of numerical computation is larger. The adaptive iteration method is used in the numerical computation of the reconstruction of three–dimensional dielectric objects.

7.2 Matrix Formulation for Iterative Methods

Consider the object divided into N cells and the moment method described in chapter 2 used in the discretization of the integral equations. The matrix equation for the direct problem in the three–dimensional case is

$$\left\{\begin{bmatrix}[I] & [0] & [0]\\ [0] & [I] & [0]\\ [0] & [0] & [I]\end{bmatrix}-\begin{bmatrix}[G^i_{xx}] & [G^i_{xy}] & [G^i_{xz}]\\ [G^i_{yx}] & [G^i_{yy}] & [G^i_{yz}]\\ [G^i_{zx}] & [G^i_{zy}] & [G^i_{zz}]\end{bmatrix}\begin{bmatrix}[O] & [0] & [0]\\ [0] & [O] & [0]\\ [0] & [0] & [O]\end{bmatrix}\right\}\begin{bmatrix}\mathbf{E}^t_x\\ \mathbf{E}^t_y\\ \mathbf{E}^t_z\end{bmatrix}=\begin{bmatrix}\mathbf{E}^i_x\\ \mathbf{E}^i_y\\ \mathbf{E}^i_z\end{bmatrix} \qquad (7\text{–}1)$$

where the dimension of all submatrices is $N \times N$ and the dimension of the vectors for different polarization components of electric field is N. Symbolically, equation (7–1) can be rewritten as

$$\mathbf{E}^i = ([I_3] - [G^i][O_3])\mathbf{E}^t \tag{7–2}$$

where

$$\mathbf{E}^t = \begin{bmatrix} \mathbf{E}_x^t \\ \mathbf{E}_y^t \\ \mathbf{E}_z^t \end{bmatrix}, \qquad \mathbf{E}^i = \begin{bmatrix} \mathbf{E}_x^i \\ \mathbf{E}_y^i \\ \mathbf{E}_z^i \end{bmatrix} \tag{7–3}$$

and

$$[I_3] = \begin{bmatrix} [[I]\,[0]\,[0] \\ [0]\,[I]\,[0] \\ [0]\,[0]\,[I] \end{bmatrix}, \qquad [O_3] = \begin{bmatrix} [O]\,[0]\,[0] \\ [0]\,[O]\,[0] \\ [0]\,[0]\,[O] \end{bmatrix}. \tag{7–4}$$

The matrix equation for the inverse problem in the three–dimensional case is

$$\begin{bmatrix} [G_{xx}^o]\,[G_{xy}^o]\,[G_{xz}^o] \\ [G_{yx}^o]\,[G_{yy}^o]\,[G_{yz}^o] \\ [G_{zx}^o]\,[G_{zy}^o]\,[G_{zz}^o] \end{bmatrix} \begin{bmatrix} [E_x^t]\,[0]\,[0] \\ [0]\,[E_y^t]\,[0] \\ [0]\,[0]\,[E_z^t] \end{bmatrix} \begin{bmatrix} \mathbf{O} \\ \mathbf{O} \\ \mathbf{O} \end{bmatrix} = \begin{bmatrix} \mathbf{E}_x^s \\ \mathbf{E}_y^s \\ \mathbf{E}_z^s \end{bmatrix} \tag{7–5}$$

or

$$[G^o][E^t]\mathbf{O}_3 = \mathbf{E}^s \tag{7–6}$$

where

$$\mathbf{O}_3 = \begin{bmatrix} \mathbf{O} \\ \mathbf{O} \\ \mathbf{O} \end{bmatrix}, \qquad \mathbf{E}^s = \begin{bmatrix} \mathbf{E}_x^i \\ \mathbf{E}_y^i \\ \mathbf{E}_z^i \end{bmatrix}. \tag{7–7}$$

and $[E^t]$ is a diagonal matrix consisting of the elements of $\mathbf{E}^t$.

When applying the Born iterative method, the submatrices in (7–5), $[E_x^t]$, $[E_y^t]$ and $[E_z^t]$, are known from the solution of the direct problem. The matrix equation for the Born iterative method can be written as

$$\mathbf{E}^s = [D]\mathbf{O} \tag{7–8}$$

where

$$\mathbf{E}^s = \begin{bmatrix} \mathbf{E}_x^s \\ \mathbf{E}_y^s \\ \mathbf{E}_z^s \end{bmatrix}, \quad [D] = \begin{bmatrix} [G_{xx}^o][E_x^t] + [G_{xy}^o][E_y^t] + [G_{xz}^o][E_z^t] \\ [G_{yx}^o][E_x^t] + [G_{yy}^o][E_y^t] + [G_{yz}^o][E_z^t] \\ [G_{zx}^o][E_x^t] + [G_{zy}^o][E_y^t] + [G_{zz}^o][E_z^t] \end{bmatrix}. \tag{7–9}$$

For the Newton iterative method, following a similar procedure for the two–dimensional case, the obtained matrix equation is

$$\Delta \mathbf{E}^s = [G^o]([I_3] - [O_3][G^i])^{-1}[E^t]\Delta \mathbf{O}_3 \tag{7–10}$$

where

$$\Delta \mathbf{O}_3 = \begin{bmatrix} \Delta \mathbf{O} \\ \Delta \mathbf{O} \\ \Delta \mathbf{O} \end{bmatrix} \tag{7–11}$$

and $\Delta \mathbf{O}$ is the variation of $\mathbf{O}$. To simplify the matrix equation in (7–10), the following matrix division is defined

$$([I_3] - [O_3][G^i])^{-1}[E^t] = \left[[W_x] \ [W_y] \ [W_z] \right] \tag{7–12}$$

where, $[W_x], [W_y]$ and $[W_z]$ are three $3N \times N$ matrices. The matrix equation in (7–10) can be rewritten as

$$\Delta \mathbf{E}^s = [D]\Delta \mathbf{O} \tag{7–13}$$

with

$$[D] = [G^o]([W_x] + [W_y] + [W_z]) \ . \tag{7–14}$$

When multiple illuminations are used, the matrix equation for the direct problem is

$$\mathbf{E}_l^i = ([I_3] - [G^i][O_3])\mathbf{E}_l^t \qquad l = 1, 2, \ . \ . \ . \ , L \ . \tag{7–15}$$

In the Born iterative method, the matrix equation for the inverse problem is

$$\mathbf{E}_l^s = [D_l]\mathbf{O} \ . \tag{7–16}$$

In the Newton iterative method, the matrix equation for the inverse problem is

$$\Delta \mathbf{E}_l^s = [D_l]\Delta \mathbf{O} \ . \tag{7–17}$$

The global equation of (7–16) or (7–17) for all illuminations with regularization is

$$[D]^H \mathbf{B} = ([D]^H[D] + g[I])\mathbf{X} \tag{7–18}$$

with

$$[D] = \begin{bmatrix} [D_1] \\ [D_2] \\ \cdot \\ \cdot \\ \cdot \\ [D_L] \end{bmatrix} \tag{7–19}$$

For the Born iterative method, $\mathbf{X}$ is $\mathbf{O}$, $[D]$ consists of matrices in (7–9) and $\mathbf{B}$ consists of column vectors $\mathbf{E}_l^s$ for all illuminations, respectively. For the Newton iterative method, $\mathbf{X}$ is $\Delta\mathbf{O}$, and $[D]$ and $\mathbf{B}$ consist of the matrices $[G_l^o]([W_x] + [W_y] + [W_z])_l$ and the column vector $\Delta\mathbf{E}_l^s$ for all illuminations, respectively. The matrix equations are expressed in the same form as the ones for the two–dimension cases. For the direct problem, (7–2) is similar to (4–1). For the inverse problem, (7–8) is similar to (4–2), and (7–10) to (4–14). At each iteration, the total electric field is updated by solving (7–15). Then, (7–18) is solved to update $\mathbf{O}$ for the Born iterative method or $\Delta\mathbf{O}$ for the Newton iterative method.

When the current refinement algorithm is used, the current refinement procedure is applied after solving (7–15) and (7–18) at each iteration. With the total electric field and the object function obtained from (7–15) and (7–18), respectively, the equivalent current is refined from

$$\mathbf{J}_l = [E_l^t]\mathbf{O} \ . \tag{7–20}$$

Then, the total electric field is refined from

$$\mathbf{E}_l^t = [G^i]\mathbf{J}_l + \mathbf{E}_l^i \ . \tag{7–21}$$

The new object function is computed from least square solution of (7–20) for all illuminations by using the refined equivalent current and the total electric field.

In the prediction–correction algorithm, $\Delta\mathbf{E}_{lk}^s$ and $\mathbf{J}_{lk}$ include all the involved polarization components and are used in the computation of $\Delta\mathbf{E}_{Tk}^s$ and $\mathbf{J}_{Tk}$ for making prediction, respectively.

In the adaptive algorithm, each $\Delta\mathbf{E}_l^s$ consists of all involved polarization components and are used in the computation of $\Delta\mathbf{E}_T^s$. At each iteration, $\Delta\mathbf{E}_T^s$ computed from the initial estimate of

the object function and the updated one are used to update the value of the criterion for the algorithm applied. The criteria of different algorithms are compared to determine the more suitable algorithm for the next iteration.

7.3 Numerical Results

In the numerical simulation, a fifth example, a cubic region is considered.

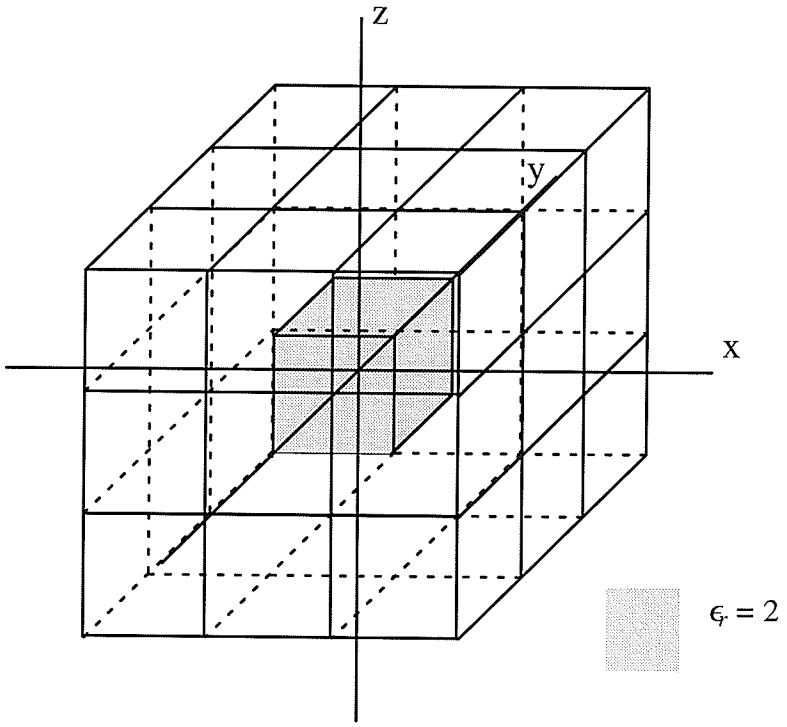

Fig. 7.1 : The grid for the investigated region and permittivity distribution.

Example 5 – The region of investigation is divided into 27 cells (cell size $0.3\lambda \times 0.3\lambda$) and a dielectric cube with permittivity $\epsilon_r = 2$ and size $0.3\lambda \times 0.3\lambda$ is placed at the center of the region as shown in Fig. 7.1. The region is successively illuminated by four plane waves with the electric field parallel to the z direction as indicated in Fig. 7.2. Sixteen receivers are placed in two planes at $z = \mp 0.75\lambda$. In each plane, 8 receivers are equally spaced on the contour of a square of size $3\lambda \times 3\lambda$ as shown in Fig. 7.2.

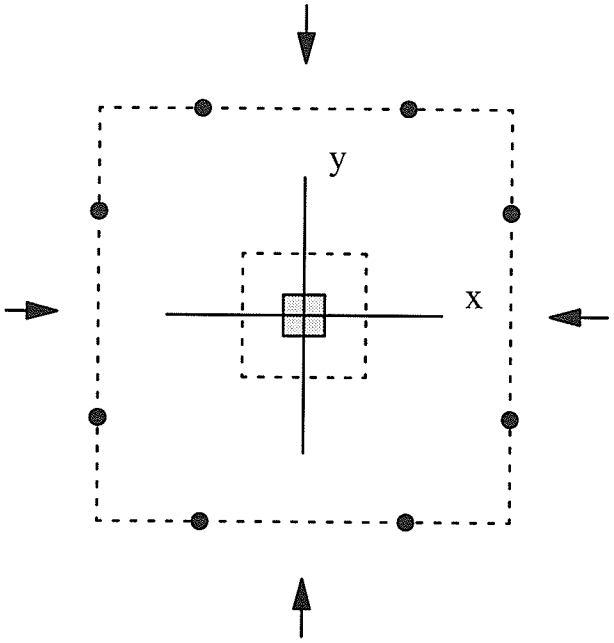

(a) Top view of the experiment arrangement.

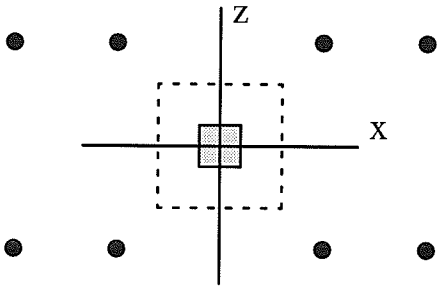

(b) Side view of the experiment arrangement.

Fig. 7.2 : The arrangement of illumination and measurement.

The computation is carried out by using the adaptive algorithm presented in chapter 6. The object is reconstructed by first using only E_z, then only E_x and E_y, and finally all three polarization components of the measured scattered field. The results for different regularization are shown in Figs. 7.3, 7.4 and 7.5. The regularization parameters are 5×10^{-2} for Fig. 7.3, 10^{-4} for Fig. 7.4, and 10^{-6} for Fig. 7.5, except 6×10^{-4} for the first iteration. When only E_z com-

ponent of the measured scattered field is used in the reconstruction, the reconstruction is an under–determined problem. Because the number of measurement location is less than the number of cells. From the curves shown in those figures, it can be seen that, when using only the E_z component, the results for the errors in the object function reconstruction is divergent. In the contrast, the results for the errors in the computed electric field E_z is convergent with a rate faster than other ones by using E_x and E_y and by using all components. Although the difference between the computed scattered field and the measured data is very small, the lack of information makes the reconstruction error quite large. In the cases of Figs. 7.3, 7.4 and 7.5, the reconstruction errors reach up to 100%. The results obtained from the measured E_x and E_y are good but the corresponding curve in Fig. 7.4 shows that the process of reconstruction is not numerically stable. The reconstruction by using the data of all three polarization components is better than the other ones. However, in practice, the measurement of all three components is not convenient. When using only a part of the polarization components of the scattered field in the object reconstruction, the numerical stability is still very important.

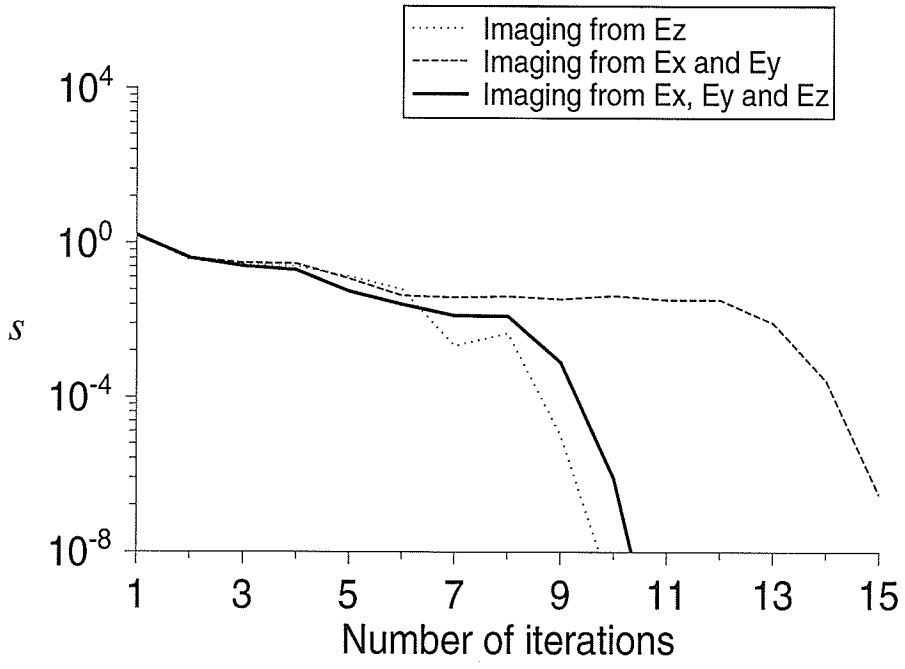

(a)

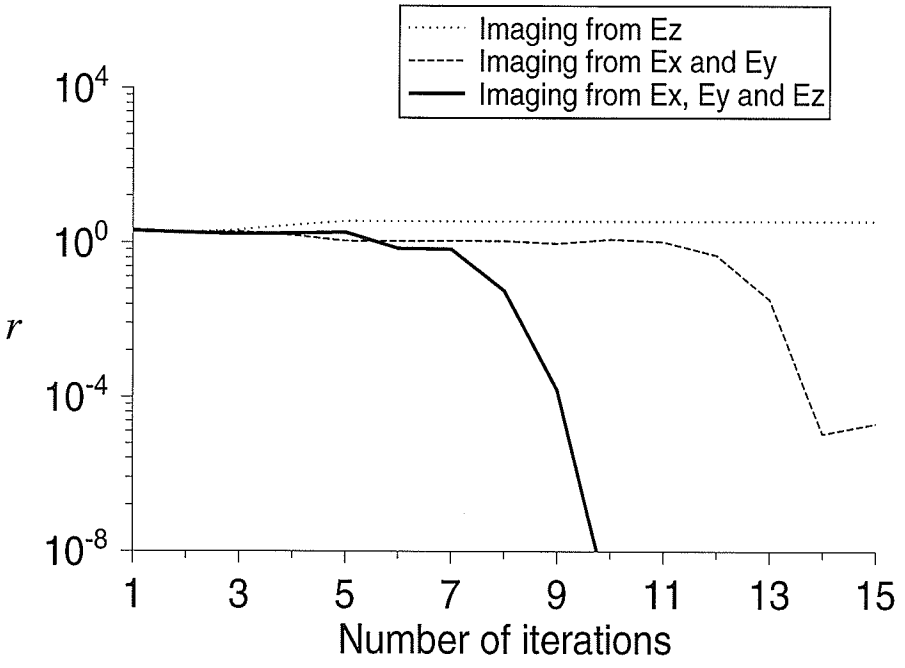

(b)

Fig. 7.3 : Errors s and r for example five with $g = 5 \times 10^{-2}$ after the first iteration.

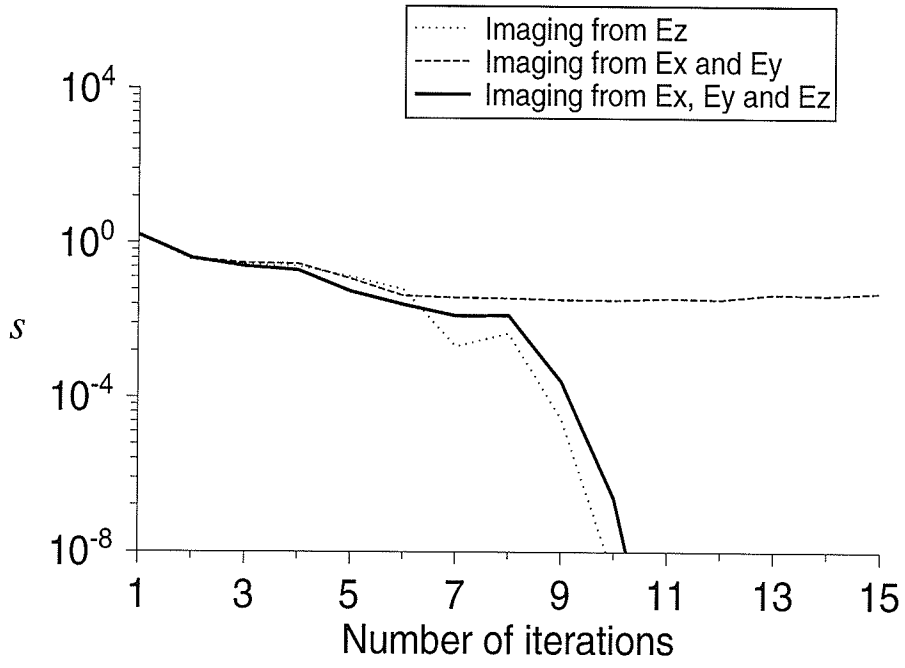

(a)

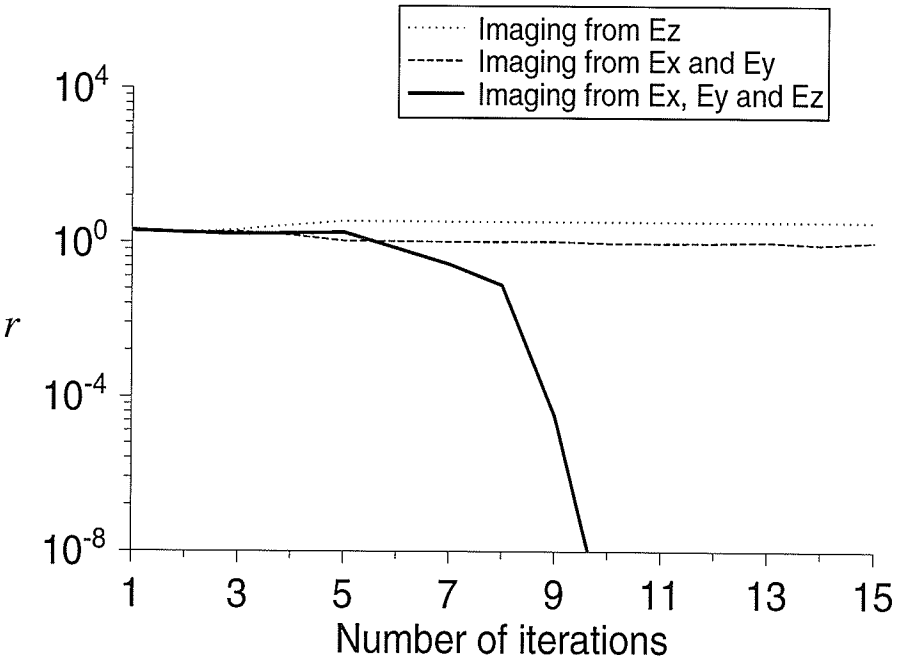

(b)

Fig. 7.4 : Errors s and r for example five with $g = 10^{-4}$ after the first iteration.

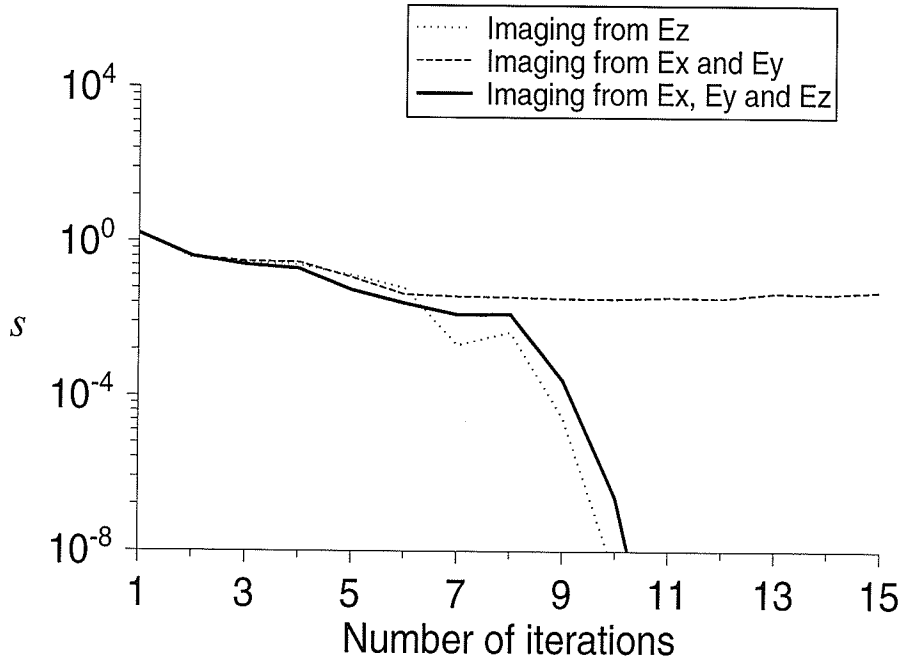

(a)

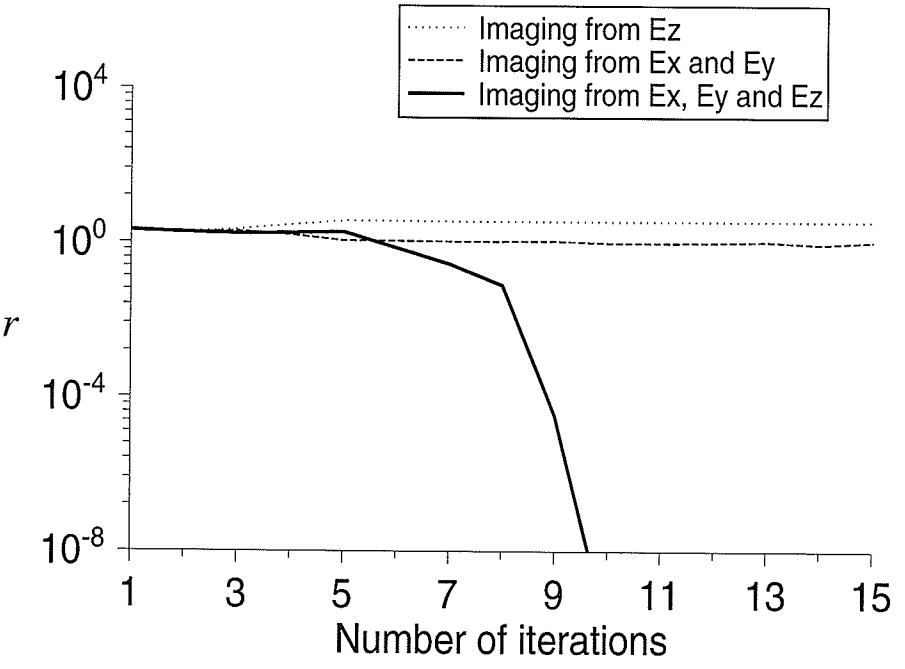

(b)

Fig. 7.5 : Errors s and r for example five with $g = 10^{-6}$ after the first iteration.

7.4 Conclusion

The three–dimensional problem of electromagnetic imaging is discussed in this chapter. The matrix equations involved are expressed in forms quite similar to the ones for the two–dimensional case. The techniques developed in previous chapters can be easily applied in the three–dimensional case. For the object function reconstruction, the iterative process is fast and numerically stable when the measured data include all three components. In the application of iterative methods, the under–determined problem has to be avoided. Otherwise one may obtain a very poor reconstruction even from an iterative process which is rapidly convergent.

Chapter 8

Conclusions and Suggestions

8.1 General Conclusions

Iterative methods for electromagnetic imaging of lossless and lossy dielectric objects are investigated in this thesis. The techniques of current refinement, prediction–correction and adaptive algorithm transference are presented for improving the numerical convergence, stability, robustness, and flexibility of iterative methods and discussed in detail. They can be applied with different iterative techniques such as the Born or the Newton iterative methods. Numerical tests show that the application of these techniques significantly improves the numerical convergence, stability and flexibility of the iterative process for a variety of dielectric objects.

The equivalent current refinement technique is presented in chapter 4. It improves the convergence and numerical stability of the Born or the Newton iterative methods proposed for electromagnetic imaging. This technique is based on the more precise consideration of the effect of the errors in the computed scattered electric field. In this technique, the object function is reconstructed from the better evaluated equivalent current at each iteration step. Since, at each iteration, this technique is used to refine the iteration results, it can be applied to different iterative methods. The supplementary numerical computation needed for this technique is negligible compared with the one for the solution of a dense matrix equation for the direct or the inverse problem. Numerical tests are presented to show the improvement to the Born and the Newton iterative methods.

The prediction–correction method, presented in chapter 5, is a further development of improving the numerical stability and convergence of an iterative process. It stabilizes the iterative process by providing a better initial estimate of the object function for each iteration. The method is

characterized by using all information acquired within the iteration process itself to make the prediction for the next iteration. It is numerically more stable and faster than other iterative methods. The prediction of the object function consists of a linear prediction of the equivalent current by minimizing the error in the computed scattered field and a nonlinear estimation of the object function from the predicted equivalent current. The prediction of the equivalent current is a prediction for a linear ill–posed problem and the prediction of the object function is the one for a nonlinear well–posed problem. This method avoids the difficulty of the direct prediction for an ill–posed nonlinear problem. In the selection of the iteration results used for making a prediction, the worst iteration results are discarded. Even when results from the preceding iteration is poor, the application of this method can still provide a comparatively good estimate of the object function for the next iteration. The iteration process is not divergent. Numerical tests show that this algorithm is not as sensitive to a change in the regularization parameter as other iterative algorithms. As shown in Figs. 5.5, 5.6, 5.12, 5.13, 5.17 and 5.18, in the presence of noise in the measured data, this technique still provides better reconstruction results and is robust.

The adaptive algorithm is presented in chapter 6. If the algorithm presented in chapter 5 is considered as an improvement on providing a better estimate of the object function, the adaptive algorithm is an improvement on providing a better algorithm for solving the inverse problem. In solving a nonlinear ill–posed problem, specific iteration methods are more efficient than other methods for the reconstruction of specific objects. Different algorithms have different numerical specialities and at the same time, they also are differently affected by factors such as the illumination and receiving arrangements, the regularization parameter or the permittivity profile of the objects. In this algorithm, we introduce a decreasing ratio of the computed scattered field and use it as the criterion for the selection of the optimum algorithm. The main characteristic of this algorithm is that different algorithms are combined in one iteration process. The first advantage of this algorithm is that the appropriate algorithm for the given object is applied in the iterative process. The iterative process is optimized by using this algorithm. The second advantage is there are no repeated numerical computations in the search of the suitable algorithm. It is numerically efficient. The third

advantage is this algorithm combines the strengths of different algorithms, which makes it able to deal with more complex objects. Since the algorithm comparison is a complex problem, the error ratios for different algorithms have to be updated at specific iteration stages. The updating of all ratios used for algorithm comparison also has the advantage it prevents the iterative process from being trapped at local minima. The ratio updating is discussed in detail.

In chapter 7, the computation for a three–dimensional electromagnetic problem is considered. The matrix formulation is presented and the numerical results are discussed.

The combination of the techniques presented in Chapter 4, 5 and 6 can be illustrated in Fig. 8.1.

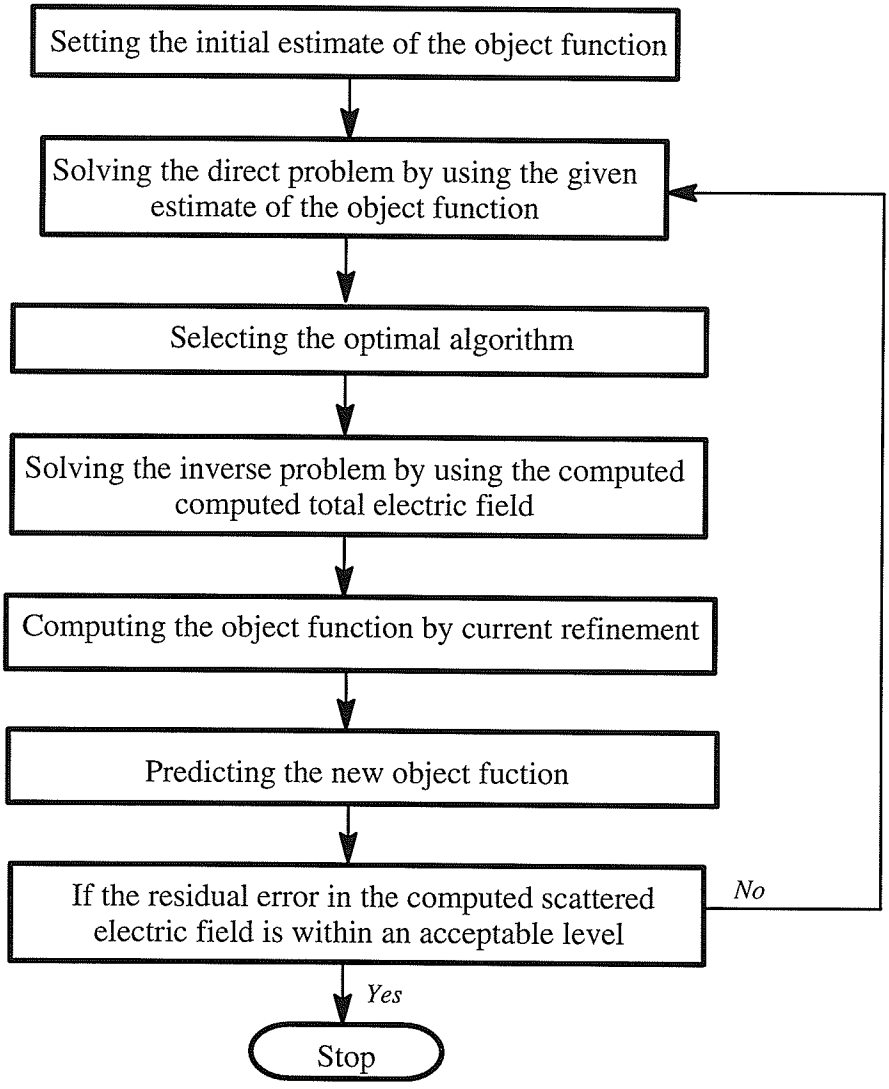

Fig. 8.1 : The diagram of the combined algorithm.

8.2 Suggestions for the Further Research

The following recommendations are made for future work on the iterative methods applied to electromagnetic imaging:

1. Incorporate transient incident waves in electromagnetic imaging. By employing the Fourier Transform technique, more information can be obtained from the transient scattered field. This makes the imaging problem not as ill–posed as the one with single frequency illumination and this reduces the difficulty in the numerical computation.
2. Incorporate special illumination and receiving arrangements in the iterative methods. The choice of the illumination scheme and of the scattered field measurement scheme has a strong effect on the reconstruction results. The optimum choice reduces the ill–posedness of the electromagnetic imaging problem, but this choice varies with the shape and the materials composition of the object. The optimum can be approached from the knowledge of a priori information about the object.
3. Further develop the adaptive algorithm. For instance, other algorithms such as the Simulated Annealing method, the Markov Random Field method, or the Maximum Entropy method can be applied with the Born and the Newton iterative methods into the adaptive algorithm. The optimization of the regularization can also be incorporated into the adaptive algorithm. The optimization of the regularization includes the selection of the regularization parameter and of the stabilization function. Not only does the optimum algorithm for solving the inverse problem and the optimum regularization method have to be considered but also their combination in the optimization. Therefore the optimization problem becomes more complex. An artificial intelligence method such as the Neural Network method may be a powerful tool to deal with this complex problem.
4. A further study of the discretization process of objects in order to treat objects with irregular shape and irregular distribution of electric parameters. For such objects, more complex basis functions have to be used to simulate more precisely the distributions of the equivalent current and of the permittivity.

5. In order to further optimize the imaging system, a study of the reconstruction from different types of data, such as polarization, receiving and illumination arrangements, should be performed.
6. Although there is no special requirement in the case of the algorithm for imaging lossy media, more information is needed in reconstruction due to the attenuation of the incident wave. The study is now to be focused on how to efficiently obtain the necessary information.

References

[1] A.G. Nekut and B.R. Spies "Petroleum exploration using controlled source electromagnetic methods," *Proc. IEEE,* 1989, 77, (2), pp. 338–362.

[2] R. Zorgati, B. Duchene, D. Lesselier, and F. Pons, "Eddy current testing of anomalies in conductive materials, Part I: Qualitative imaging via diffraction tomography techniques," *IEEE Trans. Magn.*, vol. 27, no. 6, pp. 4416–4437, 1991.

[3] R. Zorgati, D. Lesselier, B. Duchene, and F. Pons, "Eddy current testing of anomalies in conductive materials, Part II: quantitative imaging via deterministic and stochastic inversion techniques," *IEEE Trans. Magn.,* vol. 28, no. 3, pp. 1850–1862, 1992.

[4] K.A. Davis, and R. J. Lytle, "Computerized geophisical tomography," *Proc. IEEE,* vol. 67, no. 7, pp. 981–990, July 1979.

[5] R. J. Lytle, J.T. Okada, and E.E. Laine, " Geotomography applied to nuclear wast repositionary site assessment," *International Union of Radio Science Syposium*, Quebec, Canada, June 2–6, 1980

[6] D.J. Gjessing, *Remote Surveillance by Electromagnetic Waves.* Ann Arbor, MI: Ann Arbor Science, 1978.

[7] A. J. Devaney, "A computer simulation study of diffraction tomography," *IEEE Trans. Biomed. Eng.*, vol. BME–30, pp. 377–386, 1983.

[8] S.X. Pan and A.C. Kak, "A computational study of reconstruction algorithms for diffraction tomography: interpolation versus filtered backpropagation," *IEEE Trans. Acoust., Speech and Signal Processing,* vol. ASSP–31, no. 5, pp. 1262–1275, 1983.

[9] P. Hua, E.J. Woo, J.G. Webster, and W. J. Tompkins, "Iterative reconstruction methods using regularization and optimal current patterns in electrical impedance tomography," *IEEE Trans. Med. Imaging*, vol. MI–10, pp. 621–628, 1991.

[10] J.H. Jacobi, L.E. Larsen, and C.T. Hast, "Water immersed microwave antennas and their applications to microwave interrogation of biological targets," *IEEE Trans. Microwave Theory Tech.,* vol. MTT–27, no. 1, pp. 860–873, 1979.

[11] F.M. Adams, and A.P. Anderson, "Synthetic aperture tomography (SAT) imaging for microwave diagnostics," *IEE Proc.,* H, vol. 129, pp. 83–88, 1982.

[12] M. Slaney, A.C. Kak, and L.E. Larsen, "Limitation of imaging with first–order diffraction tomography," *IEEE Trans. Microwave Theory Tech.,* vol. MTT–32, pp. 860–873, 1984.

[13] C. Pichot, L. Jofre, G. Peronnet, and J.C. Bolomey, "Active microwave imaging of inhomogeneous bodies," *IEEE Trans. Antennas Propagat.,* vol. AP–33, no. 4, pp. 416–425, 1985.

[14] N.N. Bojarski, "Inverse scattering inverse source theory," *Math. Phys.,* vol. 22, no. 8, pp. 1647–1650, 1981.

[15] E. Wolf and A.J. Devaney, "On the physical contents of some integral equations for inverse scattering from inhomogeneous objects," *Rad. Sci.,* vol. 21, pp. 627–634, 1986.

[16] R.M. Lewis, "Physical optics inverse diffraction," *IEEE Trans. Antennas Propagat.,* vol. AP–17, pp. 308–314, 1986.

[17] R.P. Porter and A.J. Devaney, "Holography and the inverse source problem," *J. Opt. Soc. Am.,* vol. 72, pp. 327–330, 1982.

[18] E. Wolf and A.J. Devaney, "On the physical contents of some integral equations for inverse scattering from inhomogeneous objects," *Rad. Sci.*, vol. 21, pp. 627–634, 1986.

[19] W.R. Stone, "An exact theory for cohereant acoustic probing," *11th International Symposium on Acoustic Imaging and Acoustic Holography*, J.P. Powers, Ed., pp.365–384, Plenum, New York, 1982.

[20] S. Caorsi, G.L. Gragnani, and M. Pastorino, "Numerical solution to three–dimensional inverse scattering for dielectric reconstruction purposes," *IEE Proc., H,* vol. 129, pp. 45–52, 1992.

[21] M.M. Ney, A.M. Smith, and S.S. Stuchly, "A solution of electromagnetic imaging using pseudoinverse transformation," *IEEE Trans. Med. Imaging,* vol. MI–3, pp. 155–162, 1984.

[22] S. Caorsi, G.L. Gragnani, and M. Pastorino, "Two–dimensional microwave imaging by a numerical inverse scattering solution," *IEEE Trans. Microwave Theory Tech.,* vol. MTT–38, no. 8, pp. 981–989, 1990.

[23] N. Joachimowicz, C. Pichot, and J. Hugonin, "Inverse scattering : An iterative numerical method for electromagnetic imaging," *IEEE Trans. Antennas Propagat.*, vol. AP–39, no. 12, pp. 1742–1752, 1991.

[24] A.N. Tikhonov, and V. Y. Arsenine, *Solutions fo Ill–Posed Problems.* V. H. Winston & Sons, 1977.

[25] H. Wright, "Impulse response function corresponding to reflection from a region of continuous impedance change," *J. Acoust. Soc. of Am.* vol. 53, 1973.

[26] P.L., Goupillaud, "An approach to inverse filtering of near–surface layer effects from seismic records," *Geophysics* vol. 24, no. 6, pp. 754–760, 1961.

[27] J.R. Wait, *Electromagnetic waves in Straitified Media*, Pergamon, New York, 1970.

[28] C.Coen, K. Mei and D.J. Angelakos, " Inverse scattering techniques apllied to remote sensing of layered media," *IEEE Trans. Antennas and Propagation*, vol. AP–29, pp. 298–306, 1981.

[29] E.A. Robinson, "Wave Propagation in Layered Media," Chap. 3 in *Multichannel Time Series Analysis*, Holden Day, San Francisco, 1967.

[30] E.A. Robinson, "Spectral approach to geophysical inversion by Lorentz, Dourier, and Radon transforms," *Proc. IEEE*, vol. 70, no.2, pp.1039–1055, 1982.

[31] P.S. Rao, K. Santosh, and E.G. Gregg, "Computed tomography with microwaves," *Radiol.,* vol. 135, pp.767–770, 1980.

[32] R.D. Radicliff and C.A. Balanis, "Reconstruction algorithms for geophysical applications in noisy enveroments," *Ultrasonic Imaging*, vol. 1, pp.154–184, 1979.

[33] N.N. Bojarski, "Inverse scattering, inverse field, and inverse source theory," in the *11th International symposium on Accoustic Imaging and Accoustic Holography*, pp. 399–408, J.P.Powers, Ed., Plenum, New York, 1982.

[34] N. Bleistein and J. Cohen, "Nonuniqueness in the inverse source problem in accoustics and electromagnetics," *J.Math Phys.*, vol. 18, pp. 194–201, 1977.

[35] N. Bleistein and N.N. Bojarski, "Recently developed formulations of the inverse problem in acoustics and electromagnetics," Report MS–R–7501, Denver Research Institute, University of Denver, Colorado, 1974.

[36] M. Slaney, N. Azimi, A.C. Kak, and L.E. Larsen, "Microwave imaging with first order diffraction tomography," *Medical Applications of Microwave Imaging*, pp.184–213, L.E. Larsen et al. Ed., IEEE Press, 1986.

[37] M. Azimi and A.C. Kak, "Distortionin diffraction imaging caused by multiple scattering," *IEEE TRans. Medical Imaging*, vol. MI–2, pp. 176–195, 1983.

[38] J.–M. Lee, S.–Y. Kim, and J.–W. Ra, "Spectral inverse technique for reconstruction of complex permittivity profiles," *Electron. lett.*, vol. 24, no. 9, pp. 556–558, 1988.

[39] S.–Y. Kim, H.–C. Choi, J.–W. Ra, and S.–Y. Lee, "Electromagnetic imaging of 2–D inhomogeneous dielectric objects by an improved spectral inverse technique," *IEEE Trans. Magnetics*, vol. 26, no. 2, pp. 634–637, 1990.

[40] J.H. Richmond, "Scattering by a dielectric cylinder of arbitrary cross section shape," *IEEE Trans. Antennas Propagat.*, vol. AP–13, no. 3, pp. 334–341, 1965.

[41] M.M. Ney, "Method of moments as applied to electromagnetic problems," *IEEE Trans. Microwave Theory Tech.*, vol. MTT–33, pp. 972–980, 1985.

[42] S. Caorsi, G.L. Gragnani, and M. Pastorino, "Equivalent current density reconstruction for microwave imaging purposes," *IEEE Trans. Microwave Theory Tech.*, vol. MTT–37, no. 5, pp. 910–916, May 1989.

[43] S. Caorsi, G.L. Gragnani, and M. Pastorino, "Redundant electromagnetic data for microwave imaging of three–dimensional dielectric objects," *IEEE Trans. Antennas Propagat.,* vol. AP–42, no. 5, pp. 581–589, May 1994.

[44] M.J. Hagmann, and R.L. Levin, "Procedures for noninvasive electromagnetic property and dosimetry measurement," *IEEE Trans. Antennas Propagat.*, vol. AP–38, no. 1, pp. 99–106, Jan. 1990.

[45] W. Weiyan, and Z. Shourong, "Unrelated illumination method for electromagnetic inverse scattering of inhomogeneous lossy dielectric bodies," *IEEE Trans. Antennas Propagat.*, vol. AP–40, pp. 1292–1296, Nov., 1992.

[46] Y.M Wang, and W.C. Chew, "An iterative solution of two–dimensional electromagnetic inverse scattering problem," *Int. J. Imaging Syst. Technol.*, vol. 1, no. 1, pp. 100–108, 1989.

[47] W.C. Chew, and Y.M. Wang, "Reconstruction of two–dimensional permittivity using the Distorted Born iterative method," *IEEE Trans. Med. Imaging,* vol. MI–9, pp. 218–225, 1990.

[48] M.A. Djafari and G. Demoment "Maximum entropy fourier synthesis with application to diffraction tomography" *Applied Optics* vol. 26, no. 9, pp. 1745–1754, May 1987.

[49] M. Baribaud, "Microwave imagery: analytical method and maximum entropy method" *J. Phys. D.: Appi. Phys.* pp. 269–288, 1990.

[50] D.T.T. Lan and B. Michel, "Maximum Entropy Method for Electromagnetic Imaging," *Proc. Int. Geoscience and Remote Sensing Syp.,* pp.278–280. Tokyo, Japan, Aug. 18–21, 1993.

[51] E.T. Jaynes "On the rationale of maximum–entropy methods" *Proceeding of IEEE*, vol. 70, no. 9, pp. 939–952, September 1982.

[52] Z. Nashed "Operator–theoretic and computational approaches to ill–posed problems with applications to antenna theory" *IEEE Trans. Antennas and Propagation*, vol. AP–29, No. 2, pp. 220 –231, Mar. 1981.

[53] L. Garners, A. Franchois, J.–P. Hugonin, C. Pichot, and N. Joachimowicz, "Microwave imaging–complex permittivity reconstruction by simulated annealing," *IEEE Trans. Microwave Theory Tech.*, vol. MTT–39, no. 11, pp. 1801–1807, 1991.

[54] S. Caorsi, G. L. Gragnani, S. Medicina, M. Pastorino, and G. Zunino, " Microwave imaging method using a simulated annealing approach," *IEEE Microwave and Guided Wave Letters,* vol. MGWL–1, pp. 331–333, 1991.

[55] S. Caorsi, G. L. Gragnani, S. Medicina, M. Pastorino, and G. Zunino, " Microwave imaging based on a Markov random field model," *IEEE Trans. Antennas Propagat,* vol. AP–42, no. 3, pp. 293–303, Mar. 1994.

[56] A. Tijhuis, "Iterative determination of permittivity and conductivity profile of a dielectric slab in the time domain," *IEEE Trans. Antennas and Propagation*, vol. AP–29, No. 3, pp. 239 –245, Mar. 1981.

[57] M. Moghaddam and W.C. Chew, "Nonlinear two–dimensional velocity profile inversion using time domain data," *IEEE Trans. Geosci. Remote Sensing,* vol. 30, no. 1, pp. 147–156, Jan. 1992.

[58] D.O. Batrakov ans N.P. Zhuk "An iterative solution to th inverse problem of remote sensing of nonuniform media based on values of the polarization parameters" *Journal of Communications Technology and Electronics*, vol. 38, no.12, pp. 108–115, 1993.

[59] D.O. Batrakov and N.P. Zhuk "Solution of a general inverse scattering problem using the distorted Born approximation and iterative technique" *Inverse Problems* vol. 10, pp.39–54, 1994.

[60] J.H. Jacobi, and L.E. Larsen, "Linear FM pulse compression radar techniques applied to biological imaging," *Medical Applications of Microwave Imaging,* L.E. Larsen , Ed., IEEE Press, New York, pp. 138–147, 1986.

[61] G.A. Burrel and L. Peters, Jr., "Pulse propagation in lossy media using the low–frequency window for video radar application," *Proc. IEEE,* vol. 67, no. 7, pp. 981–990, July 1979.

[62] L.E. Larsen and J.H. Jacobi, "Microwave scattering parameter imaginary of an isolated canine kidney," *Med. Phys.*, vol.6 , no. 5, pp. 395–403, 1979.

[63] J.H. Jacobi and L.E. Larsen, " Microwave time delay spectroscopic imaginary of isolated canine kidney," *Med. Phys.*, vol. 7, no. 1, pp. 1–7, 1980.

[64] J.D. Young, and L. Pters, Jr., " Examination of video pulse system as potensial biological exploratory tools," *Medical Applications of Microwave Imaging,* L.E. Larsen , Ed., IEEE Press, New York, pp. 82–105, 1986.

[65] Y. Kim, and J.G. Webster, "Medical imaging using electrical impedance," *Medical Applications of Microwave Imaging,* L.E. Larsen , Ed., IEEE Press, New York, pp. 107–117, 1986.

[66] D. Isaacson, "Distinguishability of conductivities by electric current computed tomography," *IEEE Trans. Med. Imaging,* vol. MI–5, pp. 91–95, 1986.

[67] C.T. Tai *Dyadic Green's Function in Electromagnetic Theory.* Scranton. PA: Intext Educational, 1971.

[68] J. Van Bladel, "Some remarks on Green's dyadic for infinite space," *IRE Trans. Antennas Propagat.*, vol. AP–9, pp. 563–566, Nov. 1961.

[69] D.E. Livesay, and K.–M. Chen, "Electromagnetic fields induced inside arbitrary shaped biological bodies," *IEEE Trans. Microwave Theory Tech.*, vol. MTT–22, no. 12, pp. 1273–1280, 1974.

[70] T.M. Habashy, and R. Mittra, "On some inverse methods in electromagnetics," *J. EM Wave and applications,* vol. 1, pp.25–58, 1987.

[71] M. Fisher, and K.–J. Lahgenberg, "Limitations and defects of certain inverse scattering theories," *IEEE Trans. Antennas Propagat.*, vol. AP–32, pp. 1080–1088, 1984.

[72] J.N. Franklin, *Matrix Theory.* Prentice–Hall, Inc., Englewood Cliffs, N.J., pp. 174–177, 1968.

[73] B.A. Barry, *Errors in practical measurement in science, engineering, and technology.* Wiley, New York, 1978.

[74] V.V. Jory, "Approximation schema for generalized inverse spectral results and regularization of ill–posed problems" in *Inverse Methods in Electromagnetic Imaging* D. Reidel Pub. Co., Dordrecht, Holland, 1985, pp. 365–374.

[75] V.A. Morozov, *Regularization methods for ill–posed problems.* CRC Press Inc., Boca Raton, Florida, 1993.

[76] Y. Liu and I.R. Ciric, "A More Convergent Iterative Algorithm for Electromagnetic Imaging," *IEEE Trans. Magnetics*, vol. 31, May 1995.

[77] Y. Liu and I.R. Ciric, "Refined equivalent current reconstruction for electromagnetic imaging," *Electron. Lett.* vol. 30, no. 25, pp. 2122–2144, December 1994.

[78] Y. Liu and I.R. Ciric, "An Improved Iterative Method for Inverse Scattering", *IEEE AP–S Int. Symp.*, Seattle, U.S.A., June 1994, pp. 1656–1659.

[79] B. Wendroff, *Theoretical Numerical Analysis.* New York: Academic Press, pp. 84–86, 1966.

[80] J.S. Vandergraft, *Introduction to Numerical Computations.* New York: Academic Press, pp. 329–332, 349–350, 1983.

[81] I.J. Gupta, M.J. Beals, and A. Moghaddar, "Data extrapolation for high resolution radar imaging," *IEEE Trans. Antennas Propagat.*, vol. AP–42, no. 11, pp. 1540–1545, Nov. 1994.

[82] Y. Liu and I.R. Ciric, "A Prediction–Correction Iterative Method for Inverse Scattering", *1994 PIERS Symposium*, Noordwijk, The Netherlands, July, 1994.

[83] Y. Liu and I.R. Ciric, "Prediction–correction Algorithm for Electromagnetic Imaging", *IEEE AP–S Symposium*, Newport Beach, California, June 1995.

[84] Y. Liu and I.R. Ciric, "A Comparison of Two New Iterative Procedures for Microwave Imaging", *Symp. Antenna Technol. Appl Electromagn., ANTEM*, Ottawa, Canada, Aug. 1994, pp. 45–50.